VNIVERSITAT^ŸⒺVALÈNCIA

Departament de Física Teòrica

Phenomenology of two-Higgs-doublet models in the LHC era

TESIS DOCTORAL

Alejandro Celis

Director: Antonio Pich Zardoya

Valencia, 2014

Antonio Pich Zardoya, Catedrático del Departamento de Física Teórica de la Universitat de València

Certifica:

Que la presente memoria, "Phenomenology of two-Higgs-doublet models in the LHC era" ha sido realizada bajo su dirección en el Instituto de Física Corpuscular de València por *Alejandro Celis*, y constituye su Tesis para optar al grado de Doctor en Ciencias Físicas.

Y para que así conste, en cumplimiento de la legislación vigente, presenta en la Universitat de València la referida Tesis Doctoral, y firma el presente certificado, en

Burjassot, 5 de Mayo de 2014

Antonio Pich Zardoya

Resumen de la tesis

El 4 de Julio del año 2012, las colaboraciones experimentales ATLAS y CMS del gran acelerador de hadrones (LHC, por sus siglas en inglés) han descubierto un nuevo bosón en la naturaleza con una masa cercana a 126 GeV, unas ciento veintiseis veces más pesado que un átomo de hidrógeno. Esta nueva partícula no fue encontrada por azar, por el contrario, es el resultado de una larga búsqueda para entender el origen de la masa de las partículas elementales. La masa de las partículas elementales está intrínsicamente relacionada a la interacción electrodébil, la cual, junto con la gravedad y la interacción fuerte constituyen las fuerzas fundamentales conocidas en la Naturaleza.

La teoría de la interacción electrodébil describe fenómenos tan dispares como la desintegración radiactiva de ciertos núcleos, la estabilidad de los átomos y moléculas, las ondas electromagnéticas, la desintegración del muón, entre una infinidad más. De alguna manera, el tratar de entender la física fundamental subyacente en estos fenómenos nos ha llevado hasta el descubrimiento del 4 de Julio de 2012. La interacción electrodébil está determinada de forma elegante por el principio de la simetría de gauge. Sin embargo, el hecho de que las partículas tienen masa solo se puede explicar si la simetría de gauge está rota de manera espontánea. La manera más sencilla de explicar dicha ruptura es asumiendo la existencia de un sector escalar en la Naturaleza cuyo estado en el vacío rompe la simetría electrodébil, dando lugar a un bosón neutro masivo de espín cero y tres bosones de Goldstone que proveen masa a los bosones $W^{\pm}, Z$. El modelo estándar de la interacción electrodébil es la teoría científica que se ha probado experimentalmente con mayor precisión. Sin embargo, a pesar de la gran cantidad de mediciones experimentales que comprueban la teoría, no se había podido encontrar dicho bosón neutro de espín cero.

El bosón recién descubierto en el LHC, podría ser entonces la primera evidencia directa que tenemos del mecanismo que causa la ruptura de la simetría de gauge electrodébil y, por ende, del origen de la masa de las partículas elementales.

En esta tesis se analiza la posibilidad de que el bosón recién descubierto pertenezca a un sector escalar extendido conocido como modelo de dos dobletes de Higgs, teniendo en cuenta experimentos en la frontera de intensidad (factorías de mesones B) y de energía (LHC). Hay varias razones para estudiar la fenomenología de sectores escalares extendidos. Por un lado, ningún principio fundamental de la teoría electrodébil explica la ruptura espontánea de la simetría de gauge electrodébil, uno más bien tiene que asumir que este fenómeno ocurre. Muchos modelos o teorías que tratan de explicar el rompimiento de la simetría electrodébil involucran sectores escalares más complejos que el del modelo estándar. Sectores escalares extendidos son una interesante posibilidad también dado que pueden proporcionar: nuevas fuentes de violación de CP, necesarias para entender la asimetría entre la materia y la antimateria en el Universo; candidatos para explicar la materia oscura en el Universo, entre otras.

This thesis is based on the following publications:

I Celis, A., Li, X-Q., Jung, M., Pich, A. (2013): **Sensitivity to charged scalars in $\mathbf{B} \to \mathbf{D}^{(*)}\tau\nu_\tau$ and $\mathbf{B} \to \tau\nu_\tau$ decays**. Journal of High Energy Physics, 1301 (2013) 054.

II Celis, A., Cirigliano, V., Passemar, E. (2013): **Lepton flavour violation in the Higgs sector and the role of hadronic τ-lepton decays**. Physical Review D 89 (2014) 013008.

III Celis, A., Ilisie, V., Pich, A. (2013): **LHC constraints on two-Higgs-doublet models**. Journal of High Energy Physics, 1307 (2013) 053.

IV Celis, A., Ilisie, V., Pich, A. (2013): **Towards a general analysis of LHC data within two-Higgs-doublet models**. Journal of High Energy Physics, 1312 (2013) 095.

During my time as a PhD student, I have co-authored the following proceedings:

P.I Celis, A. (2013): **Effects of a charged Higgs boson in $\mathbf{B} \to \mathbf{D}^{(*)}\tau\nu$ decays**. Proceedings of the 2013 European Physical Society Conference on High Energy Physics, Stockholm, Sweden, 18-24 July, 2013.

P.II Celis, A., Li, X-Q., Jung, M., Pich, A. (2013): **$\mathbf{B} \to \mathbf{D}^{(*)}\tau\nu$ decays in two-Higgs-doublet models**. Proceedings for 3rd Symposium on Prospects in the Physics of Discrete Symmetries (DISCRETE 2012), Lisbon, Portugal, 3-6 December 2012.

I have also co-authored the following preprint (to be published in Phys. Rev. D.)

P.III Celis, A., Cirigliano, V., Passemar, E. (2014): **The model-discriminating power of lepton flavor violating tau decays**. arXiv:1403.5781 [hep-ph].

Contents

Chapter 1

Introduction

Particle physics as a branch of physics is interested in a very simple question: What are the elementary building blocks of matter and how these interact? The word "atom" was coined by the Greek philosopher Democritus around the year 465BC and literally means "uncuttable" or "indivisible". Currently, we know that the atoms which form all the basis of Chemistry (Hydrogen, Helium, Oxygen, . . .) are not elementary or fundamental but are composed of smaller constituents. Our present understanding of the elementary particles that build up the matter around us and the fundamental interactions in Nature is encoded in what we know as the Standard Model of elementary particle physics, see figure 1.1. Gravity is not included in this framework and in the rest of this manuscript we will not discuss effects related to this force. It is however worth stressing that gravitational effects have in general no impact at the energy scales and experiments we will be interested. Apart from Gravity, we know of the electromagnetic interaction which unifies electric and magnetic forces, the weak interaction which is behind the radioactive decay of certain nuclei, and, the strong force responsible for the formation of hadrons like the proton and the neutron. The electromagnetic and weak forces are nowadays seen as different manifestations of the electroweak interaction, see figure 1.2. The different elementary particles can be classified according to their spin as fermions (spin 1/2) and bosons (spin 0 or 1). Forces associated with a symmetry of the Lagrangian are mediated by the exchange of spin one bosons (γ, $W^{\pm}$, Z, g).

Figure 1.1: *Interactions among the elementary particles discovered in Nature so far are well described by the Standard Model of elementary particle physics. The particles are divided in this table as spin $1/2$ fermions (leptons and quarks) and spin 1 bosons (force carriers). We now have strong evidence that the spin 0 Higgs boson has been discovered, having a mass around 126 GeV.*

One of the most mysterious aspects of the Standard Model is that the gauge symmetry which describes particle interactions with such great success cannot explain elementary particle masses, in other words, the vacuum state breaks the electroweak gauge symmetry. By enlarging the particle content of the theory to include a $\mathrm{SU}(2)_L$ doublet complex scalar, one can account for the breaking of the electroweak symmetry if the vacuum expectation value of the scalar field is non-vanishing. This can be regarded as a minimal and simple way to account for the breaking of the electroweak gauge symmetry. It is however unsatisfactory from the point of view that it really does not explain why the electroweak symmetry is broken, one can say that it just parametrizes the phenomenon. In any case, this hypothesis leads to a very clear and testable prediction: the existence of a spin zero boson in Nature whose properties are completely specified once its mass is known. The mass of such particle is a free parameter of the theory and searches for

such particle were carried over the years covering a large mass range, having no clue where could it lie. On July 4 of 2012, the ATLAS and CMS collaborations at the Large Hadron Collider (LHC) have discovered a new boson in Nature with characteristics so far in remarkable agreement with those predicted by the Standard Model. Even though the data are still in early stages and experimental uncertainties on many measurements of the properties of this boson are large, it seems that the simple Standard Model picture of electroweak symmetry breaking is on the right path. The discovery of such boson is a milestone in our understanding of Nature, a new era in particle physics has started with the objective of achieving a better understanding of the phenomenon of electroweak symmetry breaking.
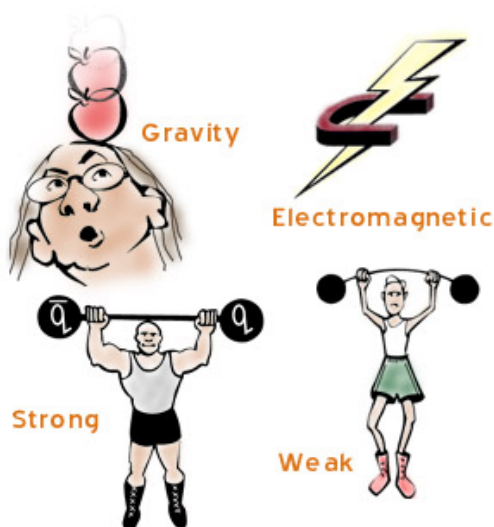
Figure 1.2:   *The known fundamental interactions in Nature. The electromagnetic and weak interactions are understood nowadays as manifestations of the same force, "the electroweak interaction".* Figure taken from www.particleadventure.org.

Our hope is that by understanding at a deeper level the mechanism of electroweak symmetry breaking we will also obtain answers to many of the remaining big questions of particle physics as: Why are there 3 generations of fermions and why their masses are so hierarchical? What is the origin of the Baryon Asymmetry of the Universe? What forms the observed Dark Matter content of the Universe? Is there some unknown dynamics behind the Strong CP-problem? Many extensions of the electroweak sector of the Stan-

dard Model addressing these questions often lead one to consider richer scalar sectors that involve several Higgs bosons. Searching for additional scalar bosons in Nature is therefore one of the main tasks of the particle physics community in the following years. In this thesis we perform a phenomenological analysis of a simple extension of the Standard Model in which the scalar sector contains two complex scalar doublets instead of just one.

The thesis is divided as follows: In chapter 2 we discuss the basic features of the Standard Model of electroweak interactions. In chapter 3 we present the two-Higgs-doublet model. The different papers constituting the bulk of the thesis are introduced in chapter 4 and are presented afterwards in separate chapters 5, 6, 7 and 8. General conclusions are given in chapter 9.

The standard model of electroweak interactions

2.1 The gauge symmetry principle

Our modern understanding of the fundamental interactions in Nature, with the exception of Gravity, is based on the gauge symmetry principle. The simplest example of a gauge theory that we know in Nature is that of quantum electrodynamics. Consider a free Dirac field ψ_e. The Lagrangian for a free Dirac fermion is given by

$$\mathcal{L} = \bar{\psi}_e(i\gamma^\mu\partial_\mu - m_e)\psi_e\,. \tag{2.1}$$

Here $\bar{\psi}_e$ is the conjugate field. This Lagrangian posses an invariance under a global phase transformation of the fermion fields

$$\psi_e \to \psi'_e = e^{iQ\theta}\psi_e\,, \qquad \bar{\psi}_e \to \bar{\psi}'_e = e^{-iQ\theta}\bar{\psi}_e\,. \tag{2.2}$$

This just reflects the fact that absolute phases are not observable in Quantum Mechanics. The parameter Q is going to be later identified with the electric charge while θ is an arbitrary real number. The principle of gauge invariance promotes the invariance of the Lagrangian under phase transformations of the fermions fields to a local symmetry, that is, the parameter θ is allowed to vary in every point of space $\theta \to \theta(x)$. The most general gauge invariant Lagrangian that can be built from operators of dimension $d \leq 4$ is given

in this case by

$$\mathcal{L} = -\frac{1}{4}F_{\mu\nu}F^{\mu\nu} + \bar{\psi}_e(i\gamma^\mu D_\mu - m_e)\psi_e \,, \tag{2.3}$$

where we have introduced the covariant derivative $D_\mu \equiv (\partial_\mu + ieQA_\mu)$,[1] the vector field A_μ, and, the field strength tensor $F_{\mu\nu} \equiv \partial_\mu A_\nu - \partial_\nu A_\mu$. The vector field A_μ transforms under a gauge transformation as $A_\mu \to A_\mu - (1/e)\partial_\mu\theta$ and is introduced so that the electron kinetic term is gauge invariant. Note that a mass term for the field A_μ is forbidden by the gauge symmetry. By using the equations of motion one arrives to

$$\partial_\mu F^{\mu\nu} = eQ(\bar{\psi}_e\gamma^\nu\psi_e) \,, \tag{2.4}$$

which are precisely the Maxwell equations describing the dynamics of a point-like particle with charge eQ in the presence of an electromagnetic field.

The standard model of electroweak interactions due to Weinberg, Salam and Glashow [1–3] is a renormalizable quantum field theory based on the principles of unitarity, causality, locality, Lorentz invariance and local gauge invariance under $\mathrm{SU}(2)_L \otimes \mathrm{U}(1)_Y$. Strong interactions are described by the non-abelian gauge group $\mathrm{SU}(3)_C$ and together with the electroweak sector form the standard model (SM) of elementary particle physics. Gauge interactions are mediated by bosons also known as gauge bosons, just like the photon in the previous example of quantum electrodynamics. The gauge bosons associated with the electroweak gauge symmetry $\mathrm{SU}(2)_L \otimes \mathrm{U}(1)_Y$ are the photon together with the $W^\pm$ and Z bosons. In this sense, the electroweak theory unifies the electromagnetic interactions and the weak interactions. The strong force described by the non-abelian gauge group $\mathrm{SU}(3)_C$ on the other hand is mediated by bosons called gluons.

The matter content of the theory can be classified according to its transformation properties under the gauge group $\mathrm{SU}(3)_C \otimes \mathrm{SU}(2)_L \otimes \mathrm{U}(1)_Y$ and the Lorentz group. All the fermion fields are represented by Weyl fields of definite chirality,

---

[1]We have written Q in terms of the electric charge "e".

$$L_L(1, 2, -1/2) = \begin{pmatrix} \nu_L \\ l_L \end{pmatrix}, \qquad l_R(1, 1, -1),$$

$$Q_L(3, 2, +1/6) = \begin{pmatrix} u_L \\ d_L \end{pmatrix}, \qquad u_R(3, 1, +2/3), \quad d_R(3, 1, -1/3).$$

(2.5)

There are three known families of fermions with the same quantum numbers and different masses, we say that each type of fermion comes in three flavours. These are (u, c, t) and (d, s, b) for the up and down quarks respectively, and (e, μ, τ) and their corresponding neutrino flavours for the leptons. A pedagogical introduction to the formulation of the SM as a gauge theory can be found in ref. [4].

2.2 The Brout-Englert-Higgs mechanism

The principle of gauge invariance forbids mass terms for the elementary particles so that the EW gauge symmetry must be spontaneously broken in Nature. This is achieved in the SM through the Brout-Englert-Higgs mechanism [5, 6]. A complex $SU(2)_L$-doublet $\Phi(1, 2, +1/2)$ transforming as a singlet under Lorentz transformations is introduced into the theory. The electroweak symmetry then gets spontaneously broken to the electromagnetic $U(1)_{em}$ group due to a non-vanishing vacuum expectation value of the scalar doublet. Lectures about the phenomenon of spontaneous symmetry breaking of a global symmetry and how the situation changes in the presence of a local gauge symmetry can be found in refs. [7–9].

The complex scalar doublet Φ can be parametrized in terms of four real fields $\varphi_i(x)$ $(i = 1, 2, 3)$ and $H(x)$ as

$$\Phi(x) = \begin{bmatrix} \Phi^+ \\ \Phi^0 \end{bmatrix} = \exp\left\{ \frac{i}{v} \vec{\sigma} \cdot \vec{\varphi}(x) \right\} \frac{1}{\sqrt{2}} \begin{bmatrix} 0 \\ v + H(x) \end{bmatrix}, \qquad (2.6)$$

where $\vec{\sigma} = (\sigma_1, \sigma_2, \sigma_3)$ denote the usual Pauli matrices. The most general renormalizable scalar Lagrangian can be written as

$$\mathcal{L}_\Phi = (D_\mu \Phi)^\dagger D^\mu \Phi - \lambda \left(|\Phi|^2 - \frac{v^2}{2} \right)^2 + \frac{\lambda}{4} v^4. \qquad (2.7)$$

Here $\langle 0|\Phi^0|0\rangle = v/\sqrt{2}$ is the vacuum expectation value (vev) for the neutral component of Φ, which is responsible for the electroweak symmetry breaking (EWSB). The covariant derivative acting on the scalar field is given by[2]

$$D^\mu \Phi \;=\; \left[\partial^\mu + ig\frac{\sigma_i}{2}W_i^\mu + ig' y_\Phi B^\mu\right]\Phi\,, \qquad y_\Phi = Q_\Phi - T_3 = \frac{1}{2}\,. \tag{2.8}$$

In the unitary gauge, $\vec{\varphi}(x) = \vec{0}$, one can expand the kinetic term as

$$(D_\mu \Phi)^\dagger (D^\mu \Phi) \to \frac{1}{2}\partial_\mu H \partial^\mu H + (v+H)^2 \left\{\frac{g^2}{4}W_\mu^\dagger W^\mu + \frac{g^2}{8\cos^2\theta_W}Z_\mu Z^\mu\right\}\,, \tag{2.9}$$

where $v = (\sqrt{2}G_F)^{-1/2} \simeq 246$ GeV fixes the value of the $W^\pm$ and Z masses through the relation

$$M_W = \cos\theta_W M_Z = \frac{1}{2}vg\,. \tag{2.10}$$

Of the original four real degrees of freedom contained in Φ, three have become the longitudinal polarization components of the $W^\pm, Z$ bosons while the remaining degree of freedom is the physical scalar field $H(x)$. The would-be Goldstone bosons $\vec{\varphi}$ correspond to excitations along the bottom of the scalar potential while the physical scalar corresponds to radial excitations, see figure 2.1. The photon remain massless since it is associated with the unbroken gauge symmetry $U(1)_{\text{em}}$. The classical value of the Higgs mass is given by

$$M_H^2 \;=\; 2v^2\lambda\,. \tag{2.11}$$

Tree level self-interactions of the Higgs boson H are determined uniquely in terms of the vev and the quartic coupling λ.

The Higgs boson plays a very important role in the SM regarding the ultraviolet behaviour (UV) of the theory [11, 12]. Consider the scattering of longitudinally polarized gauge bosons in the SM at high center of mass energies, $W_L^+(p_1)W_L^-(p_2) \to W_L^+(k_1)W_L^-(k_2)$. The diagrams contributing to this process at tree-level in the SM are shown in figure 2.2. Diagrams (a-c) involve pure gauge couplings while diagrams (d-e) involve the coupling of the Higgs boson with the longitudinal component of the massive vector boson $W^\pm$. In the center of mass frame of the incoming $W_L^+(p_1)W_L^-(p_2)$ bosons,

---

[2]See ref. [4] for details about the conventions used here.
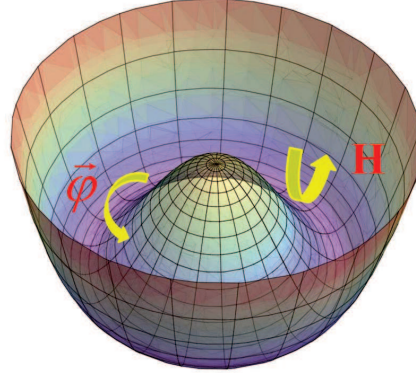
Figure 2.1: *The SM scalar potential. The Goldstone boson $\vec{\varphi}$ and Higgs field (H) parametrize fluctuations of the scalar field along the directions shown by the arrows. Figure taken from ref. [10].*
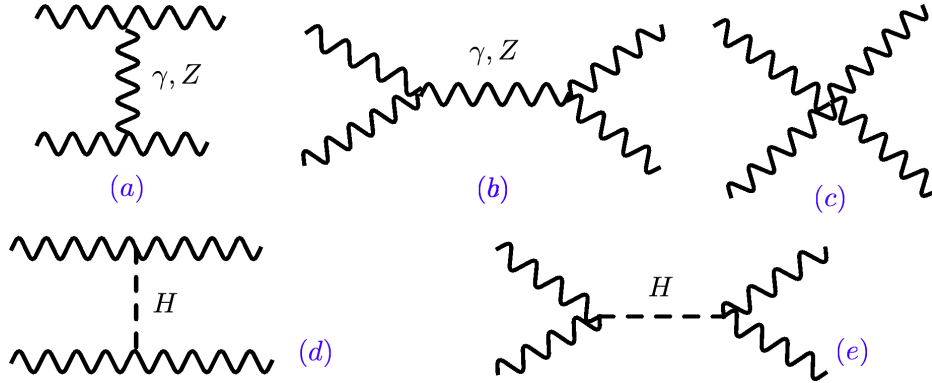
Figure 2.2: *Diagrams contributing to W^+W^- scattering at tree-level in the SM.*

we can express the longitudinal polarization vectors of the incoming bosons (at leading order in M_W/E) as

$$\epsilon_L^\mu(p_1) = \frac{p_1^\mu}{M_W} - \frac{2M_W}{s}p_2^\mu, \qquad \epsilon_L^\mu(p_2) = \frac{p_2^\mu}{M_W} - \frac{2M_W}{s}p_1^\mu. \tag{2.12}$$

The longitudinal polarization vectors for the outgoing vector bosons are given by similar expressions. Here we define the Mandelstam variables as usual $s = (p_1 + p_2)^2 = (k_1 + k_2)^2$, $u = (p_1 - k_2)^2$ and $t = 4M_W^2 - s - u$. Assuming that $s \gg M_H^2, M_W^2$ one gets that diagrams

(a), (b) and (c) contribute to the amplitude as

$$i\mathcal{M}^{\text{gauge}} \;=\; i\mathcal{M}_t^{\gamma+Z} + i\mathcal{M}_s^{\gamma+Z} + i\mathcal{M}_4 \simeq -\frac{ig^2}{4M_W^2}\,u\,. \tag{2.13}$$

Here we have neglected sub-leading terms which do not grow with the energy. Weak interactions cannot remain perturbative up to very high energies in the absence of the Higgs boson or else unitarity would be violated [11, 12]. The Higgs mediated diagrams (d) and (e) give rise to

$$i\mathcal{M}^{\text{Higgs}} \;\simeq\; \frac{ig^2}{4M_W^2}\,u\,, \tag{2.14}$$

so that the Higgs boson has the role of curing the bad high-energy behavior of the total amplitude for $W_L^+ W_L^-$ scattering, one obtains up to $O(M_W/E)$ corrections that

$$i\mathcal{M}^{\text{Higgs}} + i\mathcal{M}^{\text{gauge}} \;\simeq\; 0\,. \tag{2.15}$$

2.3   The flavour structure of the standard model

Gauge interactions corresponding to unbroken symmetries do not distinguish between the different fermion families. All the flavour dynamics in the SM, i.e. interactions that distinguish between different flavours, is then generated by the electroweak sector. In the SM electroweak theory, fermions also acquire their masses from their interaction with the Higgs field after EWSB. In the case of neutrinos, however, it is possible that the Brout-Englert-Higgs mechanism is not entirely responsible for the generation of their observed masses. The most general renormalizable Lagrangian containing the interactions of the Higgs field with SM fermions (without right-handed neutrinos) is given by

$$\begin{aligned}
\mathcal{L}_{\text{Y}} \;=\; & -\sum_{j,k=1}^{3} \left\{ \left(\bar{u}'_j, \bar{d}'_j\right)_L \left[c_{jk}^{(d)}\, \Phi\, d'_{kR} \;+\; c_{jk}^{(u)}\, \tilde{\Phi}\, u'_{kR} \right] \right. \\
& \left. \;+\; \left(\bar{\nu}'_j, \bar{l}'_j\right)_L c_{jk}^{(l)}\, \Phi\, l'_{kR} \right\} \;+\; \text{h.c.},
\end{aligned} \tag{2.16}$$

where the parameters $c_{j,k}^{(f)}$ ($f = u, d, l$) are arbitrary complex numbers and $\tilde{\Phi} = i\sigma_2 \Phi^*$. The fermionic fields have been expressed as three-dimensional vectors in flavour space and carry a prime as an upper index to emphasize that these are not physical fields at this

point. One is free to perform unitary transformations of the fermion fields under which the Lagrangian remains invariant [13]. After EWSB, the Yukawa Lagrangian $\mathcal{L}_\mathrm{Y}$ can be diagonalized giving rise to fermion masses and fermionic interactions for the physical scalar H,

$$\mathcal{L}_Y = -\left(1 + \frac{H}{v}\right)\left\{\bar{d}\,M_d\,d + \bar{u}\,M_u\,u + \bar{l}\,M_l\,l\right\}. \tag{2.17}$$

Here

$$\begin{aligned} M_u &= \mathrm{diag}(m_u, m_c, m_t)\,, \\ M_d &= \mathrm{diag}(m_d, m_s, m_b)\,, \\ M_l &= \mathrm{diag}(m_e, m_\mu, m_\tau)\,. \end{aligned} \tag{2.18}$$

In the fermion mass basis, the charged weak current is not diagonal and can be written as

$$\mathcal{L}_\mathrm{CC} = -\frac{g}{2\sqrt{2}}\left\{W_\mu^\dagger\left[\sum_{ij}\bar{u}_i\,\gamma^\mu(1-\gamma_5)\,V_{ij}\,d_j + \sum_l\bar{\nu}_l\,\gamma^\mu(1-\gamma_5)\,l\right] + \mathrm{h.c.}\right\}, \tag{2.19}$$

where V is the Cabibbo-Kobayashi-Maskawa (CKM) matrix [14, 15],

$$V = \begin{bmatrix} V_{ud} & V_{us} & V_{ub} \\ V_{cd} & V_{cs} & V_{cb} \\ V_{td} & V_{ts} & V_{tb} \end{bmatrix}. \tag{2.20}$$

The CKM matrix is unitary $VV^\dagger = V^\dagger V = 1$ [13] and its elements have to be determined experimentally. The following parametrization of the CKM matrix is used by the Particle Data Group (PDG) [16]

$$V = \begin{bmatrix} c_{12}\,c_{13} & s_{12}\,c_{13} & s_{13}\,\mathrm{e}^{-i\delta_{13}} \\ -s_{12}\,c_{23} - c_{12}\,s_{23}\,s_{13}\,\mathrm{e}^{i\delta_{13}} & c_{12}\,c_{23} - s_{12}\,s_{23}\,s_{13}\,\mathrm{e}^{i\delta_{13}} & s_{23}\,c_{13} \\ s_{12}\,s_{23} - c_{12}\,c_{23}\,s_{13}\,\mathrm{e}^{i\delta_{13}} & -c_{12}\,s_{23} - s_{12}\,c_{23}\,s_{13}\,\mathrm{e}^{i\delta_{13}} & c_{23}\,c_{13} \end{bmatrix}. \tag{2.21}$$

Here $c_{ij} = \cos\theta_{ij}$, $s_{ij} = \sin\theta_{ij}$ $(i, j = 1, 2, 3)$. By an appropriate redefinition of the quark fields, one can restrict the real angles θ_{12}, θ_{23} and θ_{13} to lie in the first quadrant so that

	λ	A	$\bar{\rho}$	$\bar{\eta}$
CKMfitter	$0.22543^{+0.00059}_{-0.00095}$	$0.812^{+0.015}_{-0.022}$	0.145 ± 0.027	0.343 ± 0.015
UTfit	0.22535 ± 0.00065	0.827 ± 0.013	0.132 ± 0.021	0.350 ± 0.014

Table 2.1: *CKMfitter [18–20] and UTfit [21, 22] results for the CKM parameters in the Wolfenstein parametrization from a global fit of the SM. We have used $(\bar{\rho}, \bar{\eta}) = (1 - \lambda^2/2)(\rho, \eta)$.*

$c_{ij} \geq 0$ and $s_{ij} \geq 0$. The CP-violating phase δ_{13} lies in the range $0 \leq \delta_{13} \leq 2\pi$. Another useful parametrization of the CKM matrix is due to Wolfenstein [17],

$$
V = \begin{bmatrix}
1 - \dfrac{\lambda^2}{2} & \lambda & A\lambda^3(\rho - i\eta) \\[2mm]
-\lambda & 1 - \dfrac{\lambda^2}{2} & A\lambda^2 \\[2mm]
A\lambda^3(1 - \rho - i\eta) & -A\lambda^2 & 1
\end{bmatrix} + O\left(\lambda^4\right), \tag{2.22}
$$

which exploits the strong hierarchy between the CKM matrix elements and performs a perturbative expansion in terms of $\lambda \equiv s_{12} \simeq 0.22$. Both parametrizations are related by the following relations:

$$
\begin{aligned}
s_{12} &= \lambda = |V_{us}|/\sqrt{|V_{ud}|^2 + |V_{us}|^2}, \\
s_{23} &= A\lambda^2 = \lambda|V_{cb}/V_{us}|, \\
s_{13}e^{i\delta} &= A\lambda(\rho + i\eta) = V_{ub}^*.
\end{aligned} \tag{2.23}
$$

The current values for the Wolfenstein parameters, as obtained by a global fit to flavour observables within the SM by the CKMfitter [18–20] and UTfit [21, 22] groups, are given in table 2.1.

The unitarity of the CKM matrix implies the following identities

$$
\sum_i V_{ij}\, V_{il}^* = \delta_{jl}, \qquad \sum_j V_{ij}\, V_{kj}^* = \delta_{ik}, \tag{2.24}
$$

which can be represented as triangles in the complex plane. The area of these triangles is independent of the phase conventions for the fermion fields, it is equal to half of the Jarlskog invariant [23], $\mathcal{J}$, defined by

$$
\mathrm{Im}\left[V_{ij}V_{ik}^*V_{lk}V_{lj}^*\right] = \mathcal{J} \sum_{mn=1}^{3} \epsilon_{ilm}\epsilon_{jkn}. \tag{2.25}
$$
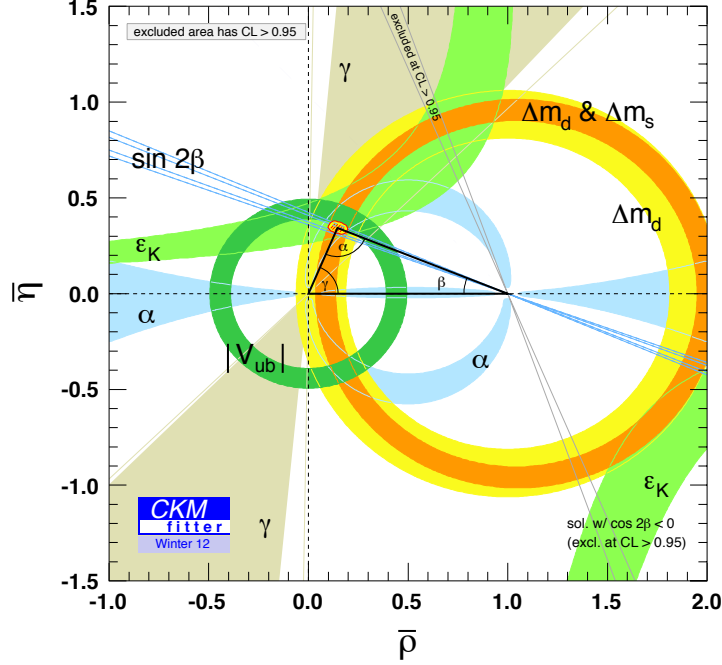
Figure 2.3:   *State-of-the-Art constraints on the $(\bar{\rho}, \bar{\eta})$ plane from the CKMfitter [18–20].*

The Jarlskog invariant is explicitly given by

$$\mathcal{J} \;=\; c_{12}\, c_{23}\, c_{13}^2\, s_{12}\, s_{23}\, s_{13}\, \sin \delta_{13} \simeq A^2 \lambda^6 \eta < 10^{-4}\,, \tag{2.26}$$

and it measures the strength of CP violation in the SM [23]. The unitarity relations in eq. (2.24) give rise to the identities

$$
\begin{aligned}
V_{ud}^* V_{us} + V_{cd}^* V_{cs} + V_{td}^* V_{ts} &= 0\,, \\
V_{us}^* V_{ub} + V_{cs}^* V_{cb} + V_{ts}^* V_{tb} &= 0\,, \\
V_{ub}^* V_{ud} + V_{cb}^* V_{cd} + V_{tb}^* V_{td} &= 0\,.
\end{aligned}
\tag{2.27}
$$

The first two of these relations describe triangles for which one side is much shorter than the others. The relations between the sides of the triangle described by the first and second lines are $\lambda : \lambda : \lambda^5$ and $\lambda^4 : \lambda^2 : \lambda^2$ respectively. The last identity in eq. (2.27) describes a triangle with all sides of a similar size $\sim \lambda^3$. Normalizing the last line of eq. (2.27) by

$V_{cb}^* V_{cd}$ one arrives to a triangle with sides of length $\{1, |V_{ud}V_{ub}^*/(V_{cd}V_{cb}^*)|, |V_{td}V_{tb}^*/(V_{cd}V_{cb}^*)|\}$ and with internal angles $\{\alpha, \beta, \gamma\}$ given by:

$$\alpha \equiv -\arg\left(\frac{V_{td}\,V_{tb}^*}{V_{ud}V_{ub}^*}\right), \qquad \beta \equiv -\arg\left(\frac{V_{cd}\,V_{cb}^*}{V_{td}V_{tb}^*}\right), \qquad \gamma \equiv -\arg\left(\frac{V_{ud}\,V_{ub}^*}{V_{cd}V_{cb}^*}\right). \qquad (2.28)$$

It is common to display the determination of the CKM matrix elements from experimental data in the $(\bar{\rho}, \bar{\eta})$ plane as shown in figure 2.3, where $(\bar{\rho}, \bar{\eta}) = (1 - \lambda^2/2)(\rho, \eta)$.

2.4 The discovery of a new boson

Despite the remarkable success of the SM model of EW interactions, the Brout-Englert-Higgs (BEH) mechanism of EWSB predicted a neutral scalar boson which had not been observed experimentally. The properties of the Higgs boson are completely specified once its mass is known but in the SM the Higgs mass is a free parameter. The Large Hadron Collider (LHC) was built with the purpose of discovering the Higgs boson, or alternatively, the mechanism responsible for restoring unitarity in WW scattering.

At the LHC, the dominant Higgs production mechanisms involve the Higgs coupling with massive gauge bosons or with the top quark. Gluon fusion ($pp \to H$) which occurs at the loop level due to intermediate heavy quarks has the largest cross section, followed by vector boson fusion ($pp \to qqH$), Higgs-strahlung ($pp \to VH$), and top-quark fusion ($pp \to t\bar{t}H$), see figure 2.4. The decay modes of the Higgs on the other hand depend considerably on the Higgs boson mass. For a light Higgs boson the decay width is dominated by the Higgs decaying into a $b\bar{b}$ pair, though many other decay modes have relevant branching fractions also. A heavy Higgs on the other hand would decay dominantly into massive gauge bosons as shown in figure 2.5.

The LEP experiment was able to exclude the SM Higgs boson up to ~ 114 GeV. It took only a small amount of time for the LHC to rule out the SM Higgs up to masses of ~ 600 GeV [25], leaving only a very small window around 125 GeV where a light SM Higgs could still be hiding. These were very exciting times, the possibility of a light Higgs boson within the SM was very close to be excluded once and for all after many years of experimental efforts. Things however were going to change drastically.

On the 4th of July 2012, the ATLAS and CMS collaborations at the LHC announced the discovery of a new boson with mass close to 126 GeV which properties so far compat-
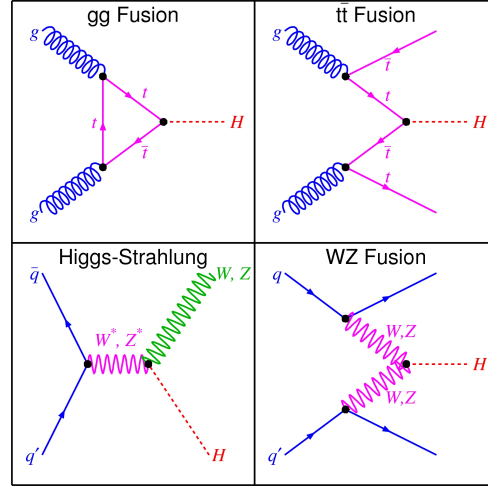
Figure 2.4:   *Feynman diagrams contributing to the dominant Higgs production modes at the LHC.*

ible with those of the SM Higgs boson [26, 27]. The masses of the new boson measured by ATLAS ($125.5 \pm 0.2 \, ^{+0.5}_{-0.6}$ GeV) [28] and CMS ($125.7 \pm 0.3 \pm 0.3$ GeV) [27] are well compatible with each other and agree nicely with fits to electroweak precision data, see figure 2.6. For such value of the Higgs mass the quartic scalar coupling is determined to be $\lambda \simeq 0.13$ and weak interactions among all particles in the SM are perturbative up to very high energy [11, 12].

A first insight into the properties of the new boson can be obtained from the Higgs signal strengths measured by the ATLAS and CMS collaborations in different channels. Higgs signal strengths are defined as Higgs cross sections normalized by the SM prediction

$$\mu_F = \frac{\sigma(pp \to H \to F)}{\sigma(pp \to H \to F)_{\rm SM}} \, . \tag{2.29}$$

The most accessible final states at the LHC for a 126 GeV Higgs are $\gamma\gamma$, W^+W^{-*}, ZZ^*, $\bar{b}b$ and $\tau^+\tau^-$. Measurements of the Higgs signal strengths by the ATLAS and CMS collaborations in different channels are shown in figure 2.7 and are well compatible with a SM Higgs. It is also important to note that the sensitivity is still very low in many channels and sizable deviations from the SM predictions are still possible in principle.

To get an idea of how SM-like the discovered new boson is, lets consider a simple fit
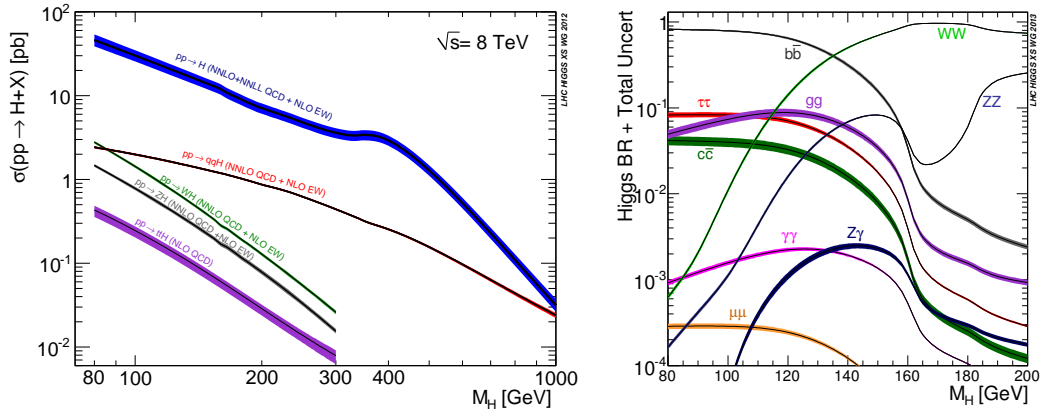
Figure 2.5: *Left: Production cross section for the Higgs boson at the LHC in the dominant modes as a function of the Higgs mass. Right: Branching fractions for the Higgs boson as a function of the Higgs mass. See ref. [24] for details.*

of the Higgs couplings to current data. We assume that the Higgs couplings scale with respect with the SM as $(\kappa_F^H = g_{HF\bar{F}}/g_{HF\bar{F}}^{\mathrm{SM}})$

$$\kappa_V^H = a\,, \qquad \kappa_f^H = c\,. \qquad\qquad (2.30)$$

Here a and c are real parameters to be determined from experimental data; $V = W, Z$ while f denotes any fermion. The SM corresponds to $(a, c) = (1, 1)$ by definition. The relevant production cross-sections and partial decay widths will scale as functions of a and c, for example $\Gamma(H \to \bar{b}b) = c^2\Gamma(H \to \bar{b}b)^{\mathrm{SM}}$ at leading order. By fitting the Higgs signal strengths to the experimental measurements one can then extract the free parameters. A fit of current experimental data done by J. Ellis and T. You gives [31]

$$a = 1.03 \pm 0.06\,, \qquad c = 0.84 \pm 0.15\,. \qquad\qquad (2.31)$$

Fits of Higgs data performed by other groups obtain similar values. This results suggest that the observed boson is remarkably close to what we expected from the Brout-Englert-Higgs mechanism of electroweak symmetry breaking in the SM.
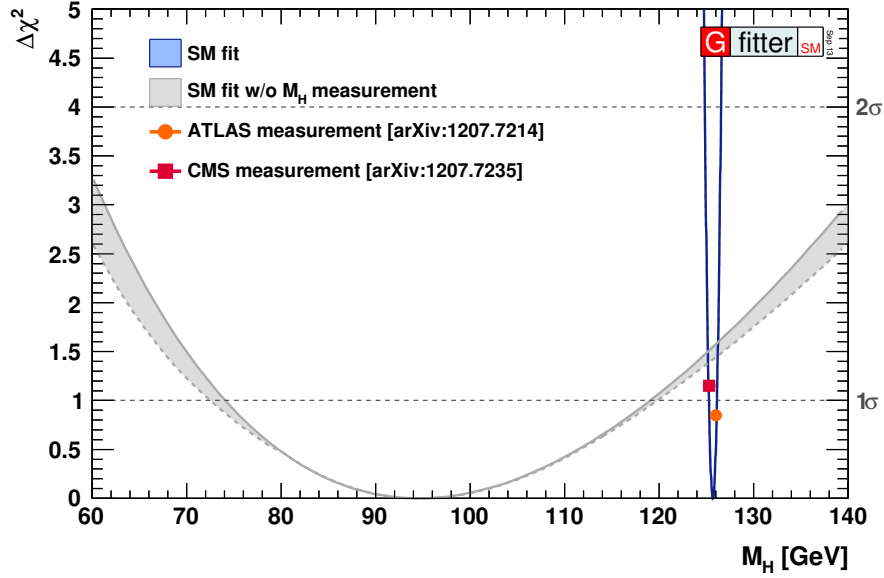
Figure 2.6: *Results of a global fit of the SM Higgs boson mass to electroweak precision data from the Gfitter collaboration [29]. The figure shows Δ^2_χ as a function of Higgs boson mass M_H, blue band. Also shown is the result of the fit without the M_H measurements (grey band). The solid and dashed lines give the results when including and ignoring theoretical errors, respectively.*
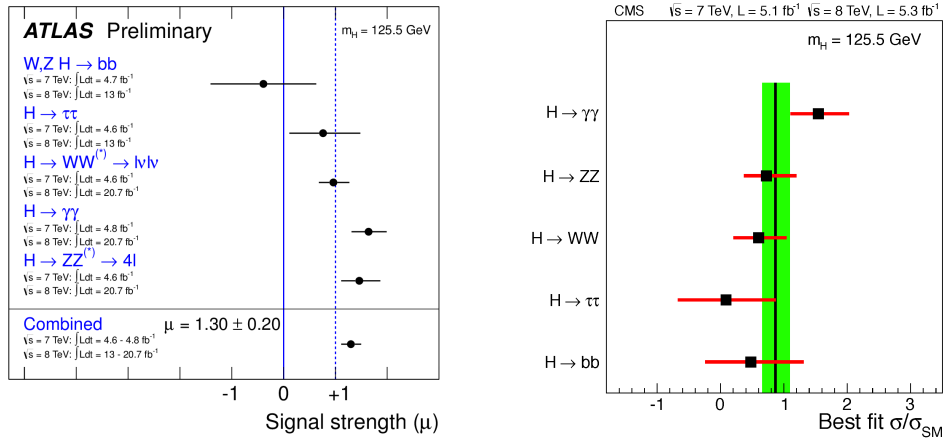
Figure 2.7: *Measurement of Higgs signal strengths in several channels by the ATLAS [30] (left) and CMS [27] (right) collaborations. The vertical line at $\mu \equiv \sigma/\sigma_{SM} = 1$ corresponds to a SM Higgs boson.*

Bibliography

[1] S. L. Glashow, Nucl. Phys. **22** (1961) 579.

[2] S. Weinberg, Phys. Rev. Lett. **19** (1967) 1264.

[3] A. Salam, Conf. Proc. C **680519** (1968) 367.

[4] A. Pich, arXiv:0705.4264 [hep-ph].

[5] F. Englert and R. Brout, Phys. Rev. Lett. **13** (1964) 321.

[6] P. W. Higgs, Phys. Rev. Lett. **13** (1964) 508.

[7] R. Brout, hep-th/0203096.

[8] F. Englert, hep-th/0203097.

[9] F. Englert, arXiv:1204.5382 [hep-th].

[10] A. Pich, EPJ Web Conf. **60** (2013) 02006 [arXiv:1307.7700].

[11] B. W. Lee, C. Quigg and H. B. Thacker, Phys. Rev. Lett. **38** (1977) 883.

[12] B. W. Lee, C. Quigg and H. B. Thacker, Phys. Rev. D **16** (1977) 1519.

[13] G. C. Branco, L. Lavoura and J. P. Silva, Int. Ser. Monogr. Phys. **103** (1999) 1.

[14] N. Cabibbo, Phys. Rev. Lett. **10** (1963) 531.

[15] M. Kobayashi and T. Maskawa, Prog. Theor. Phys. **49** (1973) 652.

[16] J. Beringer *et al.* [Particle Data Group Collaboration], Phys. Rev. D **86** (2012) 010001.

[17] L. Wolfenstein, Phys. Rev. Lett. **51** (1983) 1945.

[18] J. Charles *et al.* [CKMfitter Group Collaboration], Eur. Phys. J. C **41** (2005) 1 [hep-ph/0406184].

[19] A. Hocker, H. Lacker, S. Laplace and F. Le Diberder, Eur. Phys. J. C **21** (2001) 225 [hep-ph/0104062].

[20] G. P. Dubois-Felsmann, D. G. Hitlin, F. C. Porter and G. Eigen, hep-ph/0308262.

[21] M. Bona *et al.* [UTfit Collaboration], JHEP **0507** (2005) 028 [hep-ph/0501199].

[22] M. Bona *et al.* [UTfit Collaboration], JHEP **0803** (2008) 049 [arXiv:0707.0636 [hep-ph]].

[23] C. Jarlskog, Phys. Rev. Lett. **55** (1985) 1039.

[24] S. Heinemeyer *et al.* [LHC Higgs Cross Section Working Group Collaboration], arXiv:1307.1347 [hep-ph].

[25] R. Barate *et al.* [LEP Working Group for Higgs boson searches and ALEPH and DELPHI and L3 and OPAL Collaborations], Phys. Lett. B **565** (2003) 61 [hep-ex/0306033].

[26] G. Aad *et al.* [ATLAS Collaboration], Phys. Lett. B **716** (2012) 1 [arXiv:1207.7214 [hep-ex]].

[27] S. Chatrchyan *et al.* [CMS Collaboration], Phys. Lett. B **716** (2012) 30 [arXiv:1207.7235 [hep-ex]].

[28] [ATLAS Collaboration], ATLAS-CONF-2013-014.

[29] M. Baak, M. Goebel, J. Haller, A. Hoecker, D. Kennedy, R. Kogler, K. Moenig and M. Schott *et al.*, Eur. Phys. J. C **72** (2012) 2205 [arXiv:1209.2716 [hep-ph]].

[30] [ATLAS Collaboration], ATLAS-CONF-2013-034.

[31] J. Ellis and T. You, JHEP **1306** (2013) 103 [arXiv:1303.3879 [hep-ph]].

Chapter 3

The two-Higgs-doublet model

3.1 Introduction

Extensions of the SM scalar sector have been extensively studied in the past [1,2]. From the theoretical point of view, there are many motivations to enlarge the scalar sector of the standard model electroweak sector. Solutions to the hierarchy problem like supersymmetry [3], explaining the Dark Matter in the Universe [4,5], theories of spontaneous CP-violation [6], the strong CP problem [7,8], the baryon asymmetry of the Universe (BAU) and electroweak Baryogenesis [9–16]; often require extending the scalar sector of the SM. Having observed a neutral boson around 126 GeV with properties so far compatible with the SM Higgs, one of the main tasks in particle physics will be to address whether this particle pertains to a richer scalar sector.

Of all the types of scalar multiplets that can be part of the electroweak symmetry breaking sector, scalar singlets and doublets under $SU(2)_L$ are particularly interesting because they do not spoil the relation $M_W = \cos\theta_W M_Z$ at the classical level [1,13]. While adding additional scalar singlets to the SM scalar sector does not introduce modifications in the flavour structure of the theory (scalar singlets do not couple to fermions due to gauge invariance), adding additional doublets gives rise to a completely different flavour structure. We are interested in this thesis in the two-Higgs-doublet model (2HDM), a minimal extension of the SM scalar sector with an additional scalar doublet. In section 3.2 we describe the Lagrangian of the 2HDM. In section 3.3 we explain the phenomenological complications that arise due to tree-level flavour-changing neutral currents (FCNCs)

present in the model and discuss different ways to suppress these dangerous terms. In section 3.4 we provide a brief description of the different constraints that have to be imposed on the scalar potential in order to have a viable model.

3.2   The two-Higgs-doublet model Lagrangian

The scalar sector of the two-Higgs-doublet model contains two complex scalar doublets $\phi_a(x)$ $(a = 1, 2)$ under $SU(2)_L$ with hypercharge $Y = 1/2$,

$$\phi_a = \begin{bmatrix} \varphi_a^+ \\ \varphi_a^{(0)} \end{bmatrix} . \tag{3.1}$$

The corresponding charged conjugated fields $\tilde{\phi}_a = i\sigma_2\phi_a^*$ are also $SU(2)_L$ doublets with hypercharge $Y = -1/2$. In general, both scalar doublets can acquire vacuum expectation values that break spontaneously the electroweak gauge symmetry, $\langle 0|\phi_a^T(x)|0\rangle = \frac{1}{\sqrt{2}}(0, v_a e^{i\theta_a})$, while preserving invariance under $U(1)_{\text{em}}$. Through an appropriate $U(1)_Y$ transformation we can enforce $\theta_1 = 0$ without loss of generality, only the relative phase $\theta \equiv \theta_2 - \theta_1$ is observable. The 2HDM is then described by the most general renormalizable and gauge invariant Lagrangian that can be built with the same gauge symmetry than in the SM,

$$\mathcal{L}_{\text{2HDM}} = \mathcal{L}_{\text{scalar}} + \mathcal{L}_{\text{gauge-kinetic}} + \mathcal{L}_{\text{GF}} + \mathcal{L}_{\text{Y}} . \tag{3.2}$$

The scalar part of the Lagrangian can be written as

$$\mathcal{L}_{\text{scalar}} = \sum_{a=1}^{2} c_{aa}(D^\mu\phi_a)^\dagger(D_\mu\phi_a) + \left[c_{12}(D^\mu\phi_1)^\dagger(D_\mu\phi_2) + \text{h.c.}\right] - V(\phi_1, \phi_2) . \tag{3.3}$$

Here c_{11} and c_{22} are arbitrary real parameters while c_{12} can be complex. The covariant derivative associated with the $SU(2)_L \times U(1)_Y$ gauge symmetry is the same than in the SM and is given by

$$D_\mu = \partial_\mu + ieQA_\mu + i\frac{g}{\cos\theta_W} Z_\mu(T_3 - Q\sin^2\theta_W) + ig\left[T_+W_\mu^\dagger + T_-W_\mu\right] . \tag{3.4}$$

The weak mixing angle θ_W is defined through the relation $g\sin\theta_W = g'\cos\theta_W = e$ and the operators $T_\pm = \frac{1}{\sqrt{2}}(T_1 \pm i\,T_2)$ and T_3 can be expressed in terms of the Pauli matrices

by $T_i = \dfrac{\sigma_i}{2}$. The hermitian scalar potential V contains all possible quadratic and quartic couplings among the scalar doublets compatible with the electroweak gauge symmetry.

The scalar Lagrangian retains its form (is invariant) after an arbitrary non-singular complex transformation in the scalar space, $\phi_a \to \phi'_a = \mathcal{T}_{ab}\phi_b$, where the complex matrix $\mathcal{T}_{ab}$ is parametrized by eight real parameters [17–20]. Four degrees of freedom in $\mathcal{T}_{ab}$ can be used to bring the scalar sector into canonical form ($c_{11} = c_{22} = 1$ and $c_{12} = 0$).[1] The most general redefinition of the scalar fields, which leaves invariant the form of the canonical kinetic term, corresponds then to a global U(2) transformation, $\phi_a \to \phi'_a = \mathcal{U}_{ab}\phi_b$, parametrized by four real parameters [17]. A U(2) transformation in the scalar space is nothing more than a change of basis. Any physical prediction within the general 2HDM should be independent of the chosen scalar basis, in the same way than physical predictions within the SM are independent of weak-basis transformations of the fermions fields.

Working in a scalar basis in which only one of the scalar doublets acquires a vev is particularly useful, one can always arrive to such basis from a generic one (ϕ_1, ϕ_2) by means of a U(2) transformation

$$\begin{pmatrix} \Phi_1 \\ -\Phi_2 \end{pmatrix} \equiv \begin{bmatrix} \cos\beta & \sin\beta \\ \sin\beta & -\cos\beta \end{bmatrix} \begin{pmatrix} \phi_1 \\ e^{-i\theta}\phi_2 \end{pmatrix}, \qquad (3.5)$$

with $\tan\beta = v_2/v_1$, $\langle\Phi_1^0\rangle = \frac{1}{\sqrt{2}}\sqrt{v_1^2 + v_2^2}$ and $\langle\Phi_2^0\rangle = 0$. The basis (Φ_1, Φ_2) is known as the Higgs basis and is closely related to physical quantities (invariants under basis transformations) [17–20]. The Higgs basis however is not unique, an overall rephasing transformation $\Phi_2 \to e^{i\chi}\Phi_2$ does not alter the fact that $\langle\Phi_2^0\rangle = 0$.

3.2.1 The scalar potential

In general one can parametrize the scalar doublets in the Higgs basis as

$$\Phi_1 = \begin{bmatrix} G^+ \\ \frac{1}{\sqrt{2}}\left(v + S_1 + iG^0\right) \end{bmatrix}, \qquad \Phi_2 = \begin{bmatrix} H^+ \\ \frac{1}{\sqrt{2}}\left(S_2 + iS_3\right) \end{bmatrix}, \qquad (3.6)$$

---

[1]When a theory contains several fields with the same quantum numbers one can always write the kinetic part of the Lagrangian in the canonical form as shown in refs. [21, 22] within the context of lepton flavour violating μ to e transitions.

with $v = \sqrt{v_1^2 + v_2^2}$. The fields $\{G_0, S_1, S_2, S_3\}$ are hermitian Klein-Gordon fields, while G^+ and H^+ are complex Klein-Gordon fields. In the Higgs basis the Goldstone bosons $G^{0,\pm}$ and the physical charged scalar $H^\pm$ appear explicitly. The scalar potential in the Higgs basis takes the form

$$
\begin{aligned}
V \;=\;& \mu_1\, \Phi_1^\dagger \Phi_1 \;+\; \mu_2\, \Phi_2^\dagger \Phi_2 \;+\; \left[\mu_3\, \Phi_1^\dagger \Phi_2 \;+\; \mu_3^*\, \Phi_2^\dagger \Phi_1 \right] \\
&+\; \lambda_1 \left(\Phi_1^\dagger \Phi_1 \right)^2 + \lambda_2 \left(\Phi_2^\dagger \Phi_2 \right)^2 + \lambda_3 \left(\Phi_1^\dagger \Phi_1 \right) \left(\Phi_2^\dagger \Phi_2 \right) + \lambda_4 \left(\Phi_1^\dagger \Phi_2 \right) \left(\Phi_2^\dagger \Phi_1 \right) \\
&+\; \left[\left(\lambda_5\, \Phi_1^\dagger \Phi_2 + \lambda_6\, \Phi_1^\dagger \Phi_1 + \lambda_7\, \Phi_2^\dagger \Phi_2 \right) \left(\Phi_1^\dagger \Phi_2 \right) + \text{h.c.} \right] .
\end{aligned}
\tag{3.7}
$$

The Hermiticity of the potential requires all parameters to be real except $\mu_3, \lambda_5, \lambda_6$ and λ_7. The tree-level potential stationary conditions read

$$
\left. \frac{\partial V(\Phi_1, \Phi_2)}{\partial \Phi_i^\dagger} \right|_{\langle \Phi_1^0 \rangle = v/\sqrt{2}} = 0 \;, \qquad \text{for } i = 1, 2.
\tag{3.8}
$$

These conditions give rise to the following relations among the scalar potential parameters

$$
\mu_1 = -\lambda_1 v^2 \,, \qquad\qquad \mu_3 = -\frac{1}{2} \lambda_6 v^2 \,.
\tag{3.9}
$$

Note that μ_1 can be used to fix the value of the vev from the first of these relations. After imposing the potential stationary conditions in the Higgs basis, there are twelve free real parameters in the scalar potential $\{\mu_1, \mu_2, \lambda_1, \ldots, \lambda_7\}$. Since the Higgs basis is not unique, only the relative phases of the complex parameters $\{\lambda_5, \lambda_6, \lambda_7\}$ are physical, leaving a total of eleven physical degrees of freedom [23].

   The scalar potential can be decomposed into a quadratic term plus cubic and quartic interactions

$$
V \;=\; -\frac{1}{4} \lambda_1\, v^4 \;+\; V_2 \;+\; V_3 \;+\; V_4 \,.
\tag{3.10}
$$

The mass terms take the form

$$
\begin{aligned}
V_2 \;=\;& M_{H^\pm}^2\, H^+ H^- \;+\; \frac{1}{2}\, (S_1, S_2, S_3)\, \mathcal{M} \begin{pmatrix} S_1 \\ S_2 \\ S_3 \end{pmatrix} \\
\\
=\;& M_{H^\pm}^2\, H^+ H^- \;+\; \frac{1}{2} M_h^2\, h^2 \;+\; \frac{1}{2} M_H^2\, H^2 \;+\; \frac{1}{2} M_A^2\, A^2 \,,
\end{aligned}
\tag{3.11}
$$

where the charged Higgs mass is given by

$$M_{H^\pm}^2 = \mu_2 + \frac{1}{2}\lambda_3 v^2 \,. \tag{3.12}$$

The neutral scalar mass matrix $\mathcal{M}$ reads

$$\mathcal{M} = \begin{pmatrix} 2\lambda_1 v^2 & v^2 \lambda_6^{\rm R} & -v^2 \lambda_6^{\rm I} \\ v^2 \lambda_6^{\rm R} & M_{H^\pm}^2 + v^2\left(\frac{\lambda_4}{2} + \lambda_5^{\rm R}\right) & -v^2 \lambda_5^{\rm I} \\ -v^2 \lambda_6^{\rm I} & -v^2 \lambda_5^{\rm I} & M_{H^\pm}^2 + v^2\left(\frac{\lambda_4}{2} - \lambda_5^{\rm R}\right) \end{pmatrix}, \tag{3.13}$$

where $\lambda_i^{\rm R} \equiv \mathrm{Re}(\lambda_i)$ and $\lambda_i^{\rm I} \equiv \mathrm{Im}(\lambda_i)$. The physical states $\varphi_i^0 = \{h, H, A\}$ are obtained by means of an orthogonal transformation $\varphi_i^0 = \mathcal{R}_{ij} S_j$ that diagonalizes the mass matrix $\mathcal{M}$. Assuming that the CP-violating terms in the scalar potential are very small, the mixing matrix can be written conveniently as

$$\begin{pmatrix} h \\ H \\ A \end{pmatrix} = \begin{pmatrix} \cos\tilde{\alpha} & \sin\tilde{\alpha} & \epsilon_{13} \\ -\sin\tilde{\alpha} & \cos\tilde{\alpha} & \epsilon_{23} \\ \epsilon_{31} & \epsilon_{32} & 1 \end{pmatrix} \begin{pmatrix} S_1 \\ S_2 \\ S_3 \end{pmatrix}. \tag{3.14}$$

At first order in the CP-violating terms $\lambda_{5,6}^{\rm I}$, the elements ϵ_{ij} are found to be

$$\epsilon_{13} = \frac{v^2}{\left(\bar{M}_A^2 - \bar{M}_h^2\right)} \left(\sin\tilde{\alpha}\,\lambda_5^{\rm I} + \cos\tilde{\alpha}\,\lambda_6^{\rm I}\right),$$

$$\epsilon_{23} = \frac{v^2}{\left(\bar{M}_A^2 - \bar{M}_H^2\right)} \left(\cos\tilde{\alpha}\,\lambda_5^{\rm I} - \sin\tilde{\alpha}\,\lambda_6^{\rm I}\right),$$

$$\epsilon_{31} = -\frac{1}{2v^2} \left(\alpha_3^A\,\lambda_5^{\rm I} + 2\,\alpha_2^A\,\lambda_6^{\rm I}\right),$$

$$\epsilon_{32} = -\frac{1}{2v^2} \left(2\,\alpha_1^A\,\lambda_5^{\rm I} + \alpha_3^A\,\lambda_6^{\rm I}\right), \tag{3.15}$$

where

$$\bar{M}_h^2 = \frac{1}{2}\left(\Sigma - \Delta\right), \qquad \bar{M}_H^2 = \frac{1}{2}\left(\Sigma + \Delta\right), \qquad \bar{M}_A^2 = M_{H^\pm}^2 + v^2\left(\frac{\lambda_4}{2} - \lambda_5^{\rm R}\right), \tag{3.16}$$

and

$$\Sigma = M_{H^\pm}^2 + v^2\left(2\,\lambda_1 + \frac{\lambda_4}{2} + \lambda_5^{\rm R}\right), \tag{3.17}$$

$$\Delta = \sqrt{\left[M_{H^\pm}^2 + v^2\left(-2\,\lambda_1 + \frac{\lambda_4}{2} + \lambda_5^{\rm R}\right)\right]^2 + 4v^4(\lambda_6^{\rm R})^2} \,. \tag{3.18}$$

The mixing angle $\tilde{\alpha}$ is determined through

$$\tan \tilde{\alpha} \;=\; \frac{\bar{M}_h^2 - 2\lambda_1 v^2}{v^2 \lambda_6^{\mathrm{R}}}\,. \tag{3.19}$$

The physical scalar masses can be written, at leading order in the CP-violating parameters $\lambda_{5,6}^{\mathrm{I}}$, as

$$M_{\varphi_i^0}^2 \;=\; \bar{M}_{\varphi_i^0}^2 + \alpha_1^{\varphi_i^0}\,(\lambda_5^I)^2 + \alpha_2^{\varphi_i^0}\,(\lambda_6^I)^2 + \alpha_3^{\varphi_i^0}\,(\lambda_5^I \lambda_6^I)\,, \tag{3.20}$$

where $\bar{M}_{\varphi_i^0}$ are given in (3.16) and

$$\alpha_1^{\varphi_i^0} \;=\; \frac{v^4 \left(\bar{M}_{\varphi_i^0}^2 - 2\lambda_1 v^2 \right)}{\prod_{j \neq i} \left(\bar{M}_{\varphi_j^0}^2 - \bar{M}_{\varphi_i^0}^2 \right)}\,,$$

$$\alpha_2^{\varphi_i^0} \;=\; \frac{v^4 \left(2\lambda_1 v^2 + \bar{M}_{\varphi_i^0}^2 - \bar{M}_H^2 - \bar{M}_h^2 \right)}{\prod_{j \neq i} \left(\bar{M}_{\varphi_j^0}^2 - \bar{M}_{\varphi_i^0}^2 \right)}\,,$$

$$\alpha_3^{\varphi_i^0} \;=\; \frac{2v^6 \lambda_6^R}{\prod_{j \neq i} \left(\bar{M}_{\varphi_j^0}^2 - \bar{M}_{\varphi_i^0}^2 \right)}\,. \tag{3.21}$$

In the CP conserving limit, $\lambda_{5,6,7}^I = 0$, the physical states $\varphi_i^0 = \{h, H, A\}$ have definite CP quantum numbers. The matrix $\mathcal{R}$ becomes block-diagonal ($\epsilon_{ij} = 0$) and the physical masses reduce to $M_{\varphi_i^0} = \bar{M}_{\varphi_i^0}$. Cubic and quartic Higgs self interactions are described in chapter 7.

3.2.2   Scalar couplings with gauge bosons

The scalar coupling with gauge bosons are determined by the kinetic term for the scalar fields and the gauge fixing Lagrangian. The scalar kinetic term can be decomposed according to the number of scalar (ϕ) and vector (V) fields as,

$$\sum_{a=1}^{2} (D^\mu \Phi_a)^\dagger (D_\mu \Phi_a) = \mathcal{L}_{V^2} + \mathcal{L}_{\phi^2} + \mathcal{L}_{\phi V} + \mathcal{L}_{\phi^2 V} + \mathcal{L}_{\phi V^2} + \mathcal{L}_{\phi^2 V^2}\,. \tag{3.22}$$

The term $\mathcal{L}_{V^2}$ is given by

$$\mathcal{L}_{V^2} \;=\; -\frac{1}{2}\,(\partial_\mu A^\mu)^2 - \frac{1}{2}\,(\partial_\mu Z^\mu)^2 + \frac{1}{2}\,M_Z^2\, Z_\mu Z^\mu - \left(\partial^\mu W_\mu^\dagger \right)(\partial_\nu W^\nu) + M_W^2\, W_\mu^\dagger W^\mu\,, \tag{3.23}$$

with $M_W = gv/2$ and $M_Z = M_W/\cos\theta_W$. The vev of Φ_1 is then fixed to $v = (\sqrt{2}G_F)^{-1/2} \simeq$ 246 GeV in order to accommodate the gauge boson masses. It is convenient to adopt the Feynman-'t Hooft R_ξ gauge ($\xi = 1$) for the gauge fixing Lagrangian $\mathcal{L}_{\text{GF}}$, given by

$$\mathcal{L}_{\text{GF}} = -\frac{1}{2}\left(\partial_\mu A^\mu\right)^2 - \frac{1}{2}\left(\partial_\mu Z^\mu + M_Z G^0\right)^2 - \left(\partial^\mu W_\mu^\dagger + iM_W G^+\right)\left(\partial_\nu W^\nu - iM_W G^-\right), \tag{3.24}$$

where the specific choice of gauge has been done to cancel exactly all terms in $\mathcal{L}_{\phi V}$, which mix gauge and Goldstone bosons. The part of the Lagrangian $\mathcal{L}_{\phi^2}$ takes the form

$$\begin{aligned}
\mathcal{L}_{\phi^2} &= \frac{1}{2}\left[\partial_\mu h\,\partial^\mu h + \partial_\mu H\,\partial^\mu H + \partial_\mu A\,\partial^\mu A\right] + \partial_\mu H^+ \partial^\mu H^- \\
&+ \frac{1}{2}\partial_\mu G^0\,\partial^\mu G^0 - \frac{1}{2}M_Z^2\,(G^0)^2 + \partial_\mu G^+ \partial^\mu G^- - M_W^2\,G^+ G^-\,.
\end{aligned} \tag{3.25}$$

The cubic interactions terms between the scalar and gauge bosons in $\mathcal{L}_{\phi V^2}$ are given by:

$$\begin{aligned}
\mathcal{L}_{\phi V^2} &= \frac{2}{v}\,S_1\left[\frac{1}{2}M_Z^2\,Z_\mu Z^\mu + M_W^2\,W_\mu^\dagger W^\mu\right] \\
&+ \left(eM_W A^\mu - gM_Z \sin^2\theta_W\,Z^\mu\right)\left(G^+ W_\mu + G^- W_\mu^\dagger\right).
\end{aligned} \tag{3.26}$$

In the CP-conserving limit, the scaling of the lightest CP-even Higgs coupling with a gauge boson pair is then given by

$$\kappa_V^h = \cos\tilde{\alpha}\,, \qquad\qquad \kappa_V^H = -\sin\tilde{\alpha}\,, \qquad\qquad \kappa_V^A = 0\,, \tag{3.27}$$

with $\kappa_V^{\varphi_i^0} \equiv g_{\varphi_i^0 VV}/g_{hVV}^{\text{SM}}$, $V = W, Z$. The rest of cubic and quartic interaction terms between the scalar fields and the gauge vector bosons are discussed in chapter 7.

3.2.3 Yukawa interactions

The interactions of the Higgs fields with fermions are contained in the Yukawa Lagrangian, which includes all renormalizable and gauge invariant interaction terms between the scalar fields and the fermions. In the Higgs basis, the Yukawa Lagrangian is given by,

$$\begin{aligned}
\mathcal{L}_Y &= -\frac{\sqrt{2}}{v}\Big\{\bar{L}_L'\left(M_\ell'\,\Phi_1 + \Pi_\ell'\,\Phi_2\right)\ell_R' \\
&+ \bar{Q}_L'\left(M_d'\,\Phi_1 + \Pi_d'\,\Phi_2\right)d_R' + \bar{Q}_L'\left(M_u'\,\tilde{\Phi}_1 + \Pi_u'\,\tilde{\Phi}_2\right)u_R'\Big\} + \text{h.c.}\,, \tag{3.28}
\end{aligned}$$

where the mass M'_f and Yukawa matrices Π'_f are arbitrary complex matrices in flavour space at this point, the primes indicate that we are in a generic weak basis. After EWSB, the mass terms can be diagonalized as in the SM by means of a bi-unitary transformation in flavour space, one arrives then at

$$
\begin{aligned}
\mathcal{L}_Y \;=\; & -\sum_{\varphi_k, f=u,d,\ell} \varphi_k\, \bar{f}\, Y_f^{\varphi_k}\, P_R\, f \\
& -\frac{\sqrt{2}}{v}\, H^+ \left\{ \bar{u} \left[V\, \Pi_d\, P_R - \Pi_u^\dagger\, V\, P_L \right] d + \bar{\nu}\, \Pi_\ell\, P_R\, \ell \right\} + \text{ h.c.} .
\end{aligned}
\tag{3.29}
$$

Here V represents the CKM matrix, $P_{L,R} = (1 \mp \gamma_5)/2$ are the usual chirality projectors and

$$
\begin{aligned}
v\, Y_{d,\ell}^{\varphi_k} &= M_{d,\ell}\, \mathcal{R}_{k1} + \Pi_{d,\ell}\, (\mathcal{R}_{k2} + i\, \mathcal{R}_{k3}) \;, \\
v\, Y_u^{\varphi_k} &= M_u\, \mathcal{R}_{k1} + \Pi_u\, (\mathcal{R}_{k2} - i\, \mathcal{R}_{k3}) \;,
\end{aligned}
\tag{3.30}
$$

where $\varphi_i^0 = \mathcal{R}_{ij} S_j$, $M_{f=u,d,l}$ being diagonal fermion mass matrices and $\Pi_{f=u,d,l}$ remaining arbitrary complex matrices in flavour space. Since the two matrices M'_f and Π'_f are in general independent, it is not possible to diagonalize both of them simultaneously with the same bi-unitary transformation. The non-diagonal matrices $\Pi_{f=u,d,l}$ lead to tree-level flavour-changing neutral currents (FCNCs) in the Higgs sector as well as to new sources of CP violation beyond the SM.

3.3 Avoiding large flavour-changing neutral currents

New sources of CP violation and tree-level flavour changing neutral currents are strongly constrained by experimental data [22, 24]. If it is the case that Nature posses an scalar sector composed of two complex Higgs doublets, the discovery of a Higgs boson around 126 GeV implies that some mechanism should be operating suppressing these phenomenologically dangerous terms to acceptable levels [25, 26]. One possibility is that the 2HDM is near the decoupling limit, leaving an SM-like Higgs at the electroweak scale while the other scalars are very heavy and quasi-degenerate. The non-diagonal couplings of the light Higgs boson are suppressed by the heavy mass scale in this case, see section 3.3.1. Another possibility is that the flavour structure of the 2HDM is determined by some underlying symmetry or an unknown flavour dynamics associated with an UV completion of the model, this will be discussed in section 3.3.2.

3.3.1   The decoupling limit of the 2HDM

In a special limit of the 2HDM, two disparate mass scales arise in the scalar sector. The lightest CP-even Higgs boson remains around the electroweak scale while the other scalars $H, A, H^\pm$ become very heavy and quasi-degenerate, this is called the large-mass decoupling limit [27, 28]. In the Higgs basis, the large-mass decoupling limit occurs for $\mu_2 \gg v^2$, where μ_2 is the coefficient of the quadratic $\Phi_2^\dagger \Phi_2$ term in the scalar potential, while keeping perturbative quartic scalar couplings $|\lambda_i/4\pi| \lesssim 1$. The scalar masses are given in this limit by

$$M_h^2 \simeq 2\lambda_1 v^2 + \mathcal{O}\left(\frac{v^4}{M_{H^\pm}^2}\right), \qquad\qquad M_H^2 \simeq M_A^2 \simeq M_{H^\pm}^2 = \mu_2 + \mathcal{O}(v^2). \qquad (3.31)$$

The mixing between the two Higgs doublets approaches zero, $\tan\tilde{\alpha} \simeq \mathcal{O}(v^2/M_{H^\pm}^2)$, and as a consequence, the couplings of the lightest CP-even Higgs boson with vector bosons and fermions approach the SM values

$$\cos\tilde{\alpha} = (1 + \tan^2\tilde{\alpha})^{-1/2} \simeq 1 + \mathcal{O}\left(\frac{v^4}{M_{H^\pm}^4}\right), \qquad\qquad Y_f^h \simeq \frac{M_f}{v} + \mathcal{O}\left(\frac{v^2}{M_{H^\pm}^2}\right). \qquad (3.32)$$

In the large-mass decoupling limit of the 2HDM, dangerous contributions due to tree-level FCNCs and new sources of CP-violation are naturally suppressed by the heavy mass scale $M_{H^\pm}^2 \simeq \mu_2 \gg v^2$.

An SM-like CP-even Higgs can also arise when $\mu_3, \lambda_6 \to 0$; i.e., for vanishing $\Phi_1^\dagger \Phi_2$ and $\Phi_1^\dagger \Phi_1 \Phi_1^\dagger \Phi_2$ terms [27]. This is known as the weak-coupling decoupling limit. For a recent discussion see also refs. [28–32]. In this limit the scalar mass matrix $\mathcal{M}$ becomes diagonal and there is no mixing between the CP-even fields. The masses of the CP-even Higgs bosons take a simple form in this limit

$$M_h^2 \simeq 2\lambda_1 v^2, \qquad\qquad M_H^2 \simeq M_{H^\pm}^2 + v^2\left(\frac{\lambda_4}{2} + \lambda_5\right), \qquad (3.33)$$

while the masses of the CP-odd Higgs and the charged Higgs remain the same than in the general 2HDM. Unlike for the large-mass decoupling scenario, the SM-like scalar field S_1 in this case can correspond to either the lightest CP-even Higgs h or the heaviest one H. The two kinds of decoupling of the 2HDM are depicted in figure 3.1.
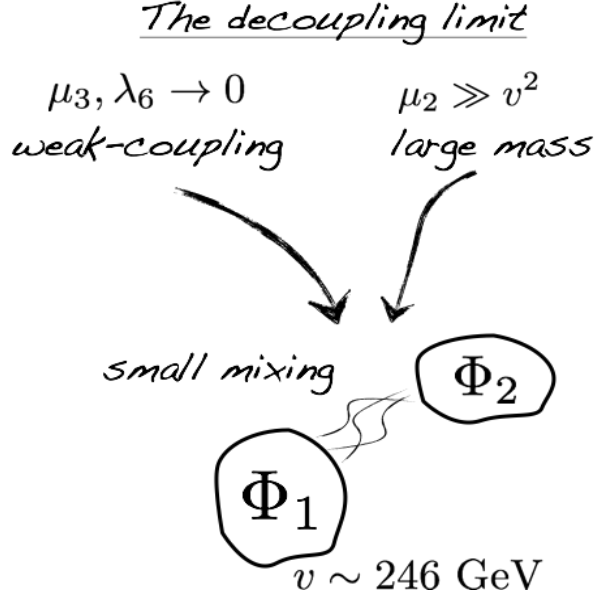
Figure 3.1: *Decoupling limits of the 2HDM, denoted as weak-coupling and large-mass decoupling after ref. [28].*

3.3.2   Yukawa alignment and natural flavour conservation

In the aligned two-Higgs doublet model (A2HDM) one assumes that due to some unknown dynamics of flavour, probably related with an UV completion of the model, the Yukawa matrices for each type of fermion are aligned in flavour space. Explicit models that can lead to a low energy A2HDM structure have been discussed in refs. [33–35]. The Yukawa alignment hypothesis [36, 37] eliminates tree-level FCNCs while allowing for new sources of CP-violation beyond the CKM-phase at the same time. In the Higgs basis this implies that one can write the matrices Π_f in eq. (3.29) as

$$\Pi_{d,l} = \varsigma_{d,l} M_{d,l} \,, \qquad \Pi_u = \varsigma_u^* M_u \,, \tag{3.34}$$

where the flavour universal alignment parameters $\varsigma_{f=u,d,l}$ are arbitrary complex numbers. Another approach that can be found in the literature, is to assume that the flavour sector is governed by a minimal flavour violating principle which then suppresses non-diagonal couplings by fermion masses and small elements of the CKM matrix [38–42].

Model	ς_d	ς_u	ς_l
Type I	$\cot \beta$	$\cot \beta$	$\cot \beta$
Type II	$-\tan \beta$	$\cot \beta$	$-\tan \beta$
Type X	$\cot \beta$	$\cot \beta$	$-\tan \beta$
Type Y	$-\tan \beta$	$\cot \beta$	$\cot \beta$
Inert	0	0	0

Table 3.1: *CP-conserving 2HDMs with natural flavour conservation.*

In the CP-conserving limit of the A2HDM, the fermionic couplings of the neutral scalar fields are then given, in units of the SM Higgs couplings, by

$$y_f^h = \cos \tilde{\alpha} + \varsigma_f \sin \tilde{\alpha} \,, \qquad\qquad y_{d,l}^A = i \, \varsigma_{d,l} \,,$$
$$y_f^H = - \sin \tilde{\alpha} + \varsigma_f \cos \tilde{\alpha} \,, \qquad\qquad y_u^A \;=\; -i \, \varsigma_u \,. \qquad (3.35)$$

Loop corrections introduce misalignment between the Yukawa matrices at the quantum level, giving rise to FCNCs with the following structure [37, 43–45]

$$
\begin{aligned}
\mathcal{L}_{\text{FCNC}} \;=\; & \frac{C(\mu)}{4\pi^2 v^3} \left(1 + \varsigma_u^* \varsigma_d \right) \\
& \sum_i \varphi_i^0(x) \left\{ \left(\mathcal{R}_{i2} + i\,\mathcal{R}_{i3}\right) \left(\varsigma_d - \varsigma_u\right) \left[\bar{d}_L \, V^\dagger M_u M_u^\dagger V M_d \, d_R \right] - \right. \\
& \left. - \left(\mathcal{R}_{i2} - i\,\mathcal{R}_{i3}\right) \left(\varsigma_d^* - \varsigma_u^*\right) \left[\bar{u}_L \, V M_d M_d^\dagger V^\dagger M_u \, u_R \right] \right\} \;+\; \text{h.c.}
\end{aligned}
$$
$$(3.36)$$

where $C(\mu) = C(\mu_0) - \log \left(\mu / \mu_0 \right)$. However, the generated non-diagonal terms are suppressed by quark masses and quark-mixing factors in such a way that the stringent bounds from light-quark systems can be avoided. The loop generated FCNCs in eq. (3.36) vanish exactly in special limits corresponding to the different versions of the 2HDM with natural flavour conservation (NFC) [37, 43–45], see table 3.1.

The NFC hypothesis was formulated independently in refs. [46, 47] were it was noted that if only one Higgs doublet couples to each type of fermion, the couplings of the neutral scalars are flavour diagonal in the fermion mass basis. It is possible to arrive to such a Yukawa structure by imposing a discrete $\mathcal{Z}_2$ symmetry in the Lagrangian. The $\mathcal{Z}_2$
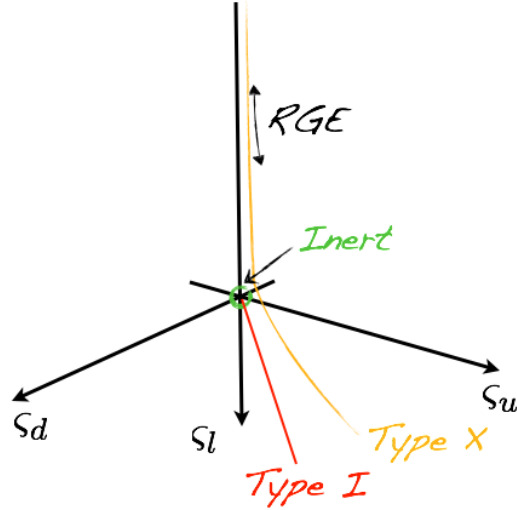
Figure 3.2: *Evolution of the 2HDM Yukawa structure under the renormalization group equations (RGE) in the CP-conserving A2HDM. 2HDMs with NFC appear as stable solutions to the RGE (the Yukawa structure remains flavour diagonal).*

symmetry can be imposed in a generic scalar basis (3.1), were both doublets acquire a vev. Defining the following charge assignments for the scalar fields $\phi_1 \rightarrow \phi_1$, $\phi_2 \rightarrow -\phi_2$ and the left-handed fermion doublets $Q_L \rightarrow Q_L$, $L_L \rightarrow L_L$, four different versions of 2HDM with NFC appear according to how the right handed fermions transform:

Type I: $f_R \rightarrow -f_R$ $(f = u, d, l)$.

Type II: $u_R \rightarrow -u_R$, $d_R \rightarrow d_R$, $l_R \rightarrow l_R$.

Type X (lepton-specific): $u_R \rightarrow -u_R$, $d_R \rightarrow -d_R$, $l_R \rightarrow l_R$.

Type Y (flipped): $u_R \rightarrow -u_R$, $d_R \rightarrow d_R$, $l_R \rightarrow -l_R$.

Terms with an odd number of ϕ_2 fields in the scalar potential are be forbidden in this case by the $\mathcal{Z}_2$ symmetry in all of these models. For the type II model, for example, the Yukawa Lagrangian in a generic scalar basis takes the form

$$\mathcal{L}_Y = -\bar{Q}'_L \, \Delta'_2 \, \tilde{\phi}_2 \, u'_R - \bar{Q}'_L \, \Gamma'_1 \, \phi_1 \, d'_R - \bar{L}'_L \, \Pi'_1 \, \phi_1 \, \ell'_R + \text{h.c.} \qquad (3.37)$$

Notice that each type of fermion couples only with one Higgs doublet and as a result there are no tree-level FCNCs.

The $\mathcal{Z}_2$ symmetry can also be imposed in the Higgs basis so that all SM fields and Φ_1 are even under this symmetry while $\Phi_2 \to -\Phi_2$, this is the Inert 2HDM. Terms with an odd number of Φ_2 fields in the scalar potential are forbidden in this case ($\mu_3 = \lambda_{6,7} = 0$), therefore there is no mixing between the CP-even neutral Higgs bosons h and H.

3.4   Constraints on the scalar potential

The 2HDM posses a large freedom in the scalar sector, coming from the many free parameters of the scalar potential. There are certain theoretical restrictions on the scalar potential that have to be imposed in order to obtain a viable model. In general one is interested in the 2HDM as a weakly coupled theory so that one needs to impose perturbativity and perturbative unitarity bounds. One needs to ensure also that the vacuum of the theory is not unstable. Oblique corrections to gauge boson two-point functions will restrict the mass-splitting between the physical scalars of the theory. Furthermore, LHC data for the 126 GeV boson put direct constraints on the structure of the scalar sector. Lets describe briefly these constraints:

Vacuum stability: For the vacuum configuration to be stable, the Higgs potential must be positive in all field space directions for asymptotically large values of the fields [48–52]. Following ref. [52] and references therein we parametrize the Higgs doublets as (we work in the Higgs basis)

$$\Phi_1 = |\Phi_1|\hat{\Phi}_1\,, \qquad \Phi_2 = |\Phi_2|\hat{\Phi}_2\,. \tag{3.38}$$

Here $|\Phi_1|$ represents the norm of Φ_i and $\hat{\Phi}_i$ is a unit spinor. Due to $\mathrm{SU}(2)_L$ invariance only four combinations of fields are relevant,

$$\Phi_1^\dagger\Phi_1 = |\Phi_1|^2\,, \qquad \Phi_2^\dagger\Phi_2 = |\Phi_2|^2\,, \qquad \Phi_2^\dagger\Phi_1 = |\Phi_2||\Phi_1|\hat{\Phi}_2^\dagger\cdot\hat{\Phi}_1\,, \qquad \Phi_1^\dagger\Phi_2 = [\Phi_2^\dagger\Phi_1]^*\,. \tag{3.39}$$

We parametrize the norms of the Higgs fields and the product $\hat{\Phi}_2^\dagger \cdot \hat{\Phi}_1$ as

$$|\Phi_1| = r\cos\gamma\,, \qquad |\Phi_2| = r\sin\gamma\,, \qquad \hat{\Phi}_2^\dagger \cdot \hat{\Phi}_1 = \frac{\Phi_2^\dagger\Phi_1}{|\Phi_1||\Phi_2|} = \rho\,e^{i\theta}\,. \tag{3.40}$$

Here $\gamma \in [0, \pi/2]$, $r \geq 0$, $\rho \in [0, 1]$ and $\theta \in [0, 2\pi)$. The scalar potential in eq. (3.7) can then be decomposed as

$$V = r^2 \, \mathcal{V}_2 + r^4 \, \mathcal{V}_4 \,, \tag{3.41}$$

where we have factored out the common factor r. The quartic part of the potential $\mathcal{V}_4$ is given by

$$
\begin{aligned}
\mathcal{V}_4 \;=\;& \lambda_1 \cos^4 \gamma + \lambda_2 \sin^4 \gamma + \lambda_3 \cos^2 \gamma \sin^2 \gamma + \lambda_4 \, \rho^2 \cos^2 \gamma \sin^2 \gamma \\
&+ 2\lambda_5 \, \rho^2 \cos(2\theta) \cos^2 \gamma \sin^2 \gamma + 2\lambda_6 \, \rho \cos \theta \cos^3 \gamma \sin \gamma + 2\lambda_7 \, \rho \cos \theta \cos \gamma \sin^3 \gamma \,.
\end{aligned}
\tag{3.42}
$$

For the stability condition to be satisfied we require that the quartic part must be positive $\mathcal{V}_4 > 0$ for all allowed values of $\{\gamma, \rho, \theta\}$. Some special points give particularly simple conditions

$$\mathcal{V}_4(\gamma = 0) = \lambda_1 \,, \qquad \mathcal{V}_4(\gamma = \pi/2) = \lambda_2 \,, \tag{3.43}$$

so that our first two stability conditions are

$$\lambda_1 > 0 \,, \qquad \lambda_2 > 0 \,. \tag{3.44}$$

Another point is $\rho = 0$ for which

$$\mathcal{V}_4(\rho = 0) = \lambda_1 \cos^4 \gamma + \lambda_2 \sin^4 \gamma + \lambda_3 \cos^2 \gamma \sin^2 \gamma \,. \tag{3.45}$$

This implies that

$$\lambda_3 > -\left(\frac{\lambda_1}{\tan^2 \gamma} + \lambda_2 \tan^2 \gamma \right) \,. \tag{3.46}$$

The right-hand side takes its minimum value at $\tan^2 \gamma = \sqrt{\lambda_1/\lambda_2}$ so that our third stability condition arises

$$\lambda_3 > -2\sqrt{\lambda_1 \lambda_2} \,. \tag{3.47}$$

Similarly, setting $\theta = \pi/2$ and $\rho = 1$ we get an additional condition

$$\lambda_3 + \lambda_4 - \lambda_5 > -2\sqrt{\lambda_1 \lambda_2} \,. \tag{3.48}$$

We can get another necessary condition by considering $\rho = 1$, $\cos\theta = \pm 1$ and $\gamma = \pi/4$, giving

$$2|\lambda_6 + \lambda_7| < \lambda_1 + \lambda_2 + \lambda_3 + \lambda_4 + 2\lambda_5 \,. \tag{3.49}$$

In summary, necessary conditions for the stability of the scalar potential are given in eqs. (3.44), (3.47), (3.48) and (3.49). Sufficient conditions for the stability of the CP-conserving 2HDM potential have been derived in refs. [53, 54] but these do not take a simple form.

Perturbativity: A usual requirement on the quartic coefficients of the scalar potential is that these are small $|\lambda_i| \lesssim \mathcal{O}(1)$, to avoid that the Higgs sector becomes strongly coupled and perturbation theory is no longer valid. Though the exact upper bound imposed on $|\lambda_i|$ is somewhat arbitrary, we attach to 4π being a common choice in the literature,

$$|\lambda_i| \leq 4\pi \,, \tag{3.50}$$

for $i = 1, \ldots, 7$.

Perturbative unitarity: Arguments about the perturbative unitarity in $W_L W_L \to W_L W_L$ elastic scattering within the SM as derived in ref. [11, 12], can also be extended to the 2HDM. The scalar-scalar scattering matrix at high energies contains only s-wave amplitudes which are described by the quartic part of the Higgs potential, tree-level unitarity constraints put an upper bound on the eigenvalues of the scattering matrix. The full scattering matrix $S_{Y,\sigma}$ in the 2HDM have been worked out in refs. [55–59], see for example eqs. (7a)-(7d) of ref. [58]. The perturbative unitarity bound on the eigenvalues Λ_j of the matrices $8\pi S_{Y,\sigma}$ read

$$|\Lambda_j| < \frac{1}{8\pi} \,. \tag{3.51}$$

Analytical expressions for the Λ_j in terms of the quartic-couplings λ_j can be found when a $\mathcal{Z}_2$ symmetry is imposed in the Lagrangian [58].

Oblique Parameters: The S, T and U parameters, introduced in refs. [60, 61], are ultraviolet-finite combinations of radiative corrections to gauge bosons two-point functions also known as oblique corrections. The oblique parameters are expressed

in terms of the transverse part of the gauge boson two-point functions as

$$\bar{\alpha}\, T \equiv \frac{\Pi_{WW}^{\text{new}}(0)}{M_W^2} - \frac{\Pi_{ZZ}^{\text{new}}(0)}{M_Z^2}\,,$$

$$\frac{\bar{\alpha}}{4\bar{s}_Z^2\bar{c}_Z^2}\, S \equiv \frac{\Pi_{ZZ}^{\text{new}}(M_Z^2) - \Pi_{ZZ}^{\text{new}}(0)}{M_Z^2}$$
$$- \left(\frac{\bar{c}_W^2 - \bar{s}_W^2}{\bar{c}_W \bar{s}_W}\right) \frac{\Pi_{Z\gamma}^{\text{new}}(M_Z^2)}{M_Z^2} - \frac{\Pi_{\gamma\gamma}^{\text{new}}(M_Z^2)}{M_Z^2}\,,$$

$$\frac{\bar{\alpha}}{4\bar{s}_W^2\bar{c}_Z^2}\, (S+U) \equiv \frac{\Pi_{WW}^{\text{new}}(M_W^2) - \Pi_{WW}^{\text{new}}(0)}{M_W^2} - \frac{\bar{c}_W}{\bar{s}_W}\frac{\Pi_{Z\gamma}^{\text{new}}(M_W)}{M_W^2} - \frac{\Pi_{\gamma\gamma}^{\text{new}}(M_W)}{M_W^2}\,. \quad (3.52)$$

Here $\bar{s}_W \equiv \sin\theta_W(M_Z)$, $\bar{c}_W \equiv \cos\theta_W(M_Z)$, and $\bar{\alpha} \equiv \bar{g}^2 \bar{s}_Z^2/(4\pi)$ are defined in the $\overline{\text{MS}}$ scheme and are evaluated at M_Z. The $\Pi_{V_a V_b}^{\text{new}}$ denote the new physics contributions to the one-loop $V_a - V_b$ vacuum polarization functions. The new physics contributions are defined relative to the SM with a particular choice for the Higgs mass, so that $S = T = U = 0$ corresponds to the SM with the reference Higgs mass. The 2HDM contributions to the oblique parameters S, T and U have been calculated in refs. [62]. Constraints from the oblique parameters bound the mass splitting between the physical Higgs bosons, which then translate into constraints on the scalar potential parameters [63].

A 126 GeV SM-like Higgs boson: The fact that we have discovered a Higgs boson around 126 GeV with a coupling to massive vector bosons that is well compatible with the SM prediction puts strong constraints on the 2HDM scalar sector. To accommodate the 126 GeV boson data within the 2HDM, at least one of the neutral bosons of the model should have a mass around 126 GeV. A pure CP-odd Higgs is excluded as the 126 GeV boson since it does not couple to massive vector bosons at tree-level, it is possible though that the 126 GeV Higgs contains some CP-odd admixture. Neglecting the exotic possibility of quasi-degenerate Higgs bosons around 126 GeV, we therefore know that the 126 GeV state must me mostly CP-even. The simplest way to accommodate the data is then is to assume a CP-conserving scalar sector where the Higgs-like boson corresponds to one of the CP-even states, h or H. To obtain a Higgs coupling to vector bosons similar in magnitude to the SM, the scalar sector is pushed towards one of the decoupling limits: weak-coupling or large-mass. If one assumes that the lightest CP-even state h is the 126 GeV boson

then both types of decoupling limits are possible. If on the other hand one assumes that the 126 GeV state corresponds to the heavy CP-even Higgs H, then only the weak-coupling decoupling limit is possible and all the scalars lie at the electroweak scale.

Bibliography

[1] J. F. Gunion, H. E. Haber, G. L. Kane and S. Dawson, Front. Phys. **80** (2000) 1.

[2] G. C. Branco, P. M. Ferreira, L. Lavoura, M. N. Rebelo, M. Sher and J. P. Silva, Phys. Rept. **516** (2012) 1 [arXiv:1106.0034 [hep-ph]].

[3] H. P. Nilles, Phys. Rept. **110** (1984) 1.

[4] E. Ma, Phys. Rev. D **73** (2006) 077301 [hep-ph/0601225].

[5] R. Barbieri, L. J. Hall and V. S. Rychkov, Phys. Rev. D **74** (2006) 015007 [hep-ph/0603188].

[6] T. D. Lee, Phys. Rev. D **8** (1973) 1226.

[7] R. D. Peccei and H. R. Quinn, Phys. Rev. D **16** (1977) 1791.

[8] R. D. Peccei and H. R. Quinn, Phys. Rev. Lett. **38** (1977) 1440.

[9] A. D. Sakharov, Pisma Zh. Eksp. Teor. Fiz. **5** (1967) 32 [JETP Lett. **5** (1967) 24] [Sov. Phys. Usp. **34** (1991) 392] [Usp. Fiz. Nauk **161** (1991) 61].

[10] G. W. Anderson and L. J. Hall, Phys. Rev. D **45** (1992) 2685.

[11] W. Buchmuller, Z. Fodor, T. Helbig and D. Walliser, Annals Phys. **234** (1994) 260 [hep-ph/9303251].

[12] M. B. Gavela, M. Lozano, J. Orloff and O. Pene, Nucl. Phys. B **430** (1994) 345 [hep-ph/9406288].

[13] M. B. Gavela, P. Hernandez, J. Orloff, O. Pene and C. Quimbay, Nucl. Phys. B **430** (1994) 382 [hep-ph/9406289].

[14] P. Huet and E. Sather, Phys. Rev. D **51** (1995) 379 [hep-ph/9404302].

[15] K. Kajantie, M. Laine, K. Rummukainen and M. E. Shaposhnikov, Nucl. Phys. B **466** (1996) 189 [hep-lat/9510020].

[16] J. M. Cline, K. Kainulainen and M. Trott, JHEP **1111** (2011) 089 [arXiv:1107.3559 [hep-ph]].

[17] F. J. Botella and J. P. Silva, Phys. Rev. D **51** (1995) 3870 [hep-ph/9411288].

[18] I. F. Ginzburg and M. Krawczyk, Phys. Rev. D **72** (2005) 115013 [hep-ph/0408011].

[19] S. Davidson and H. E. Haber, Phys. Rev. D **72** (2005) 035004 [Erratum-ibid. D **72** (2005) 099902] [hep-ph/0504050].

[20] H. E. Haber and D. O'Neil, Phys. Rev. D **74** (2006) 015018 [hep-ph/0602242].

[21] G. Feinberg, P. Kabir and S. Weinberg, Phys. Rev. Lett. **3** (1959) 527.

[22] N. Cabibbo and R. Gatto, Phys. Rev. Lett. **5** (1960) 114.

[23] L. Lavoura, Phys. Rev. D **50** (1994) 7089 [hep-ph/9405307].

[24] G. Isidori, Y. Nir and G. Perez, Ann. Rev. Nucl. Part. Sci. **60** (2010) 355 [arXiv:1002.0900 [hep-ph]].

[25] G. Blankenburg, J. Ellis and G. Isidori, Phys. Lett. B **712** (2012) 386 [arXiv:1202.5704 [hep-ph]].

[26] R. Harnik, J. Kopp and J. Zupan, JHEP **1303** (2013) 026 [arXiv:1209.1397 [hep-ph]].

[27] J. F. Gunion and H. E. Haber, Phys. Rev. D **67** (2003) 075019 [hep-ph/0207010].

[28] H. E. Haber, arXiv:1401.0152 [hep-ph].

[29] D. Lopez-Val, T. Plehn and M. Rauch, JHEP **1310** (2013) 134 [arXiv:1308.1979 [hep-ph]].

[30] D. M. Asner, T. Barklow, C. Calancha, K. Fujii, N. Graf, H. E. Haber, A. Ishikawa and S. Kanemura *et al.*, arXiv:1310.0763 [hep-ph].

[31] M. Carena, I. Low, N. R. Shah and C. E. M. Wagner, arXiv:1310.2248 [hep-ph].

[32] A. Celis, V. Ilisie and A. Pich, JHEP **1312** (2013) 095 [arXiv:1310.7941 [hep-ph]].

[33] H. Serodio, Phys. Lett. B **700** (2011) 133 [arXiv:1104.2545 [hep-ph]].

[34] I. de Medeiros Varzielas, Phys. Lett. B **701** (2011) 597 [arXiv:1104.2601 [hep-ph]].

[35] G. Cree and H. E. Logan, Phys. Rev. D **84** (2011) 055021 [arXiv:1106.4039 [hep-ph]].

[36] A. Pich and P. Tuzon, Phys. Rev. D **80** (2009) 091702 [arXiv:0908.1554 [hep-ph]].

[37] A. Pich, Nucl. Phys. Proc. Suppl. **209** (2010) 182 [arXiv:1010.5217 [hep-ph]].

[38] G. C. Branco, W. Grimus and L. Lavoura, Phys. Lett. B **380** (1996) 119 [hep-ph/9601383].

[39] G. D'Ambrosio, G. F. Giudice, G. Isidori and A. Strumia, Nucl. Phys. B **645** (2002) 155 [hep-ph/0207036].

[40] F. J. Botella, G. C. Branco and M. N. Rebelo, Phys. Lett. B **687** (2010) 194 [arXiv:0911.1753 [hep-ph]].

[41] A. J. Buras, M. V. Carlucci, S. Gori and G. Isidori, JHEP **1010** (2010) 009 [arXiv:1005.5310 [hep-ph]].

[42] A. Dery, A. Efrati, G. Hiller, Y. Hochberg and Y. Nir, JHEP **1308** (2013) 006 [arXiv:1304.6727, arXiv:1304.6727 [hep-ph]].

[43] M. Jung, A. Pich and P. Tuzon, JHEP **1011** (2010) 003 [arXiv:1006.0470 [hep-ph]].

[44] C. B. Braeuninger, A. Ibarra and C. Simonetto, Phys. Lett. B **692** (2010) 189 [arXiv:1005.5706 [hep-ph]].

[45] P. M. Ferreira, L. Lavoura and J. P. Silva, Phys. Lett. B **688** (2010) 341 [arXiv:1001.2561 [hep-ph]].

[46] S. L. Glashow and S. Weinberg, Phys. Rev. D **15** (1977) 1958.

[47] E. A. Paschos, Phys. Rev. D **15** (1977) 1966.

[48] N. G. Deshpande and E. Ma, Phys. Rev. D **18** (1978) 2574.

[49] S. Nie and M. Sher, Phys. Lett. B **449** (1999) 89 [hep-ph/9811234].

[50] S. Kanemura, T. Kasai and Y. Okada, Phys. Lett. B **471** (1999) 182 [hep-ph/9903289].

[51] P. M. Ferreira, R. Santos and A. Barroso, Phys. Lett. B **603** (2004) 219 [Erratum-ibid. B **629** (2005) 114] [hep-ph/0406231].

[52] A. W. El Kaffas, W. Khater, O. M. Ogreid and P. Osland, Nucl. Phys. B **775** (2007) 45 [hep-ph/0605142].

[53] I. P. Ivanov, Phys. Rev. D **75** (2007) 035001 [Erratum-ibid. D **76** (2007) 039902] [hep-ph/0609018].

[54] M. Maniatis, A. von Manteuffel, O. Nachtmann and F. Nagel, Eur. Phys. J. C **48** (2006) 805 [hep-ph/0605184].

[55] J. Maalampi, J. Sirkka and I. Vilja, Phys. Lett. B **265** (1991) 371.

[56] S. Kanemura, T. Kubota and E. Takasugi, Phys. Lett. B **313** (1993) 155 [hep-ph/9303263].

[57] A. G. Akeroyd, A. Arhrib and E. -M. Naimi, Phys. Lett. B **490** (2000) 119 [hep-ph/0006035].

[58] I. F. Ginzburg and I. P. Ivanov, Phys. Rev. D **72** (2005) 115010 [hep-ph/0508020].

[59] P. Osland, P. N. Pandita and L. Selbuz, Phys. Rev. D **78** (2008) 015003 [arXiv:0802.0060 [hep-ph]].

[60] M. E. Peskin and T. Takeuchi, Phys. Rev. Lett. **65** (1990) 964.

[61] M. E. Peskin and T. Takeuchi, Phys. Rev. D **46** (1992) 381.

[62] H. -J. He, N. Polonsky and S. -f. Su, Phys. Rev. D **64** (2001) 053004 [hep-ph/0102144]; W. Grimus, L. Lavoura, O. M. Ogreid and P. Osland, Nucl. Phys. B **801** (2008) 81 [arXiv:0802.4353 [hep-ph]]; H. E. Haber and D. O'Neil, Phys. Rev. D **83** (2011) 055017 [arXiv:1011.6188 [hep-ph]].

[63] A. Pomarol and R. Vega, Nucl. Phys. B **413** (1994) 3 [hep-ph/9305272].

Chapter 4

Preliminaries and motivations

This thesis consists of a phenomenological analysis of the two-Higgs-doublet model in three different areas. One part of the work focuses on the possibility to observe indirectly the effects of a charged Higgs boson in low-energy flavour experiments involving B and D meson decays. Semileptonic and leptonic meson decays which are mediated by the charged weak current at tree-level can also receive contributions from a charged scalar at the same level. If there is a light charged scalar which couples to fermions, it would give rise to modifications of the decay rates and angular correlations for this kind of meson decays.

Another part of the thesis, focuses on a phenomenological analysis of possible Higgs mediated lepton flavour violating (LFV) transitions among charged leptons. In the general 2HDM, unsuppressed FCNCs can appear both in the quark and lepton sectors. Flavour changing couplings of the Higgs boson with quarks are currently strongly constrained while there is still room for sizable LFV Higgs couplings with the heaviest leptons. We explore the complementarity between low energy flavour experiments and searches at the LHC to probe possible LFV effects associated with the Higgs sector.

The third part of this thesis discusses the constraints that can be extracted on the 2HDM parameter space from LHC and Tevatron data for the 126 GeV boson, considering also the most relevant constraints from low energy flavour experiments, electroweak precision data and searches for additional scalars at colliders.

The calculations/programming in the different works have been done by me and my collaborators in an independent manner and sometimes using different strategies. The

main idea behind paper II was borne from discussions with Vincenzo Cirigliano and Emilie Passemar during a short research stay I did on the Theory Division of Los Alamos National Laboratory. I have not carried out the determination of the hadronic form factors via dispersive methods for paper II, this was done by Emilie Passemar. I however carried a comparison of the results found by E. Passemar for the form factors with previous results in the literature, finding a reasonably good agreement. In the following subsections I will describe in more detail the motivations behind the different works that form this thesis.

4.1   Paper I

One of the distinctive features of the 2HDM is the appearance of a charged Higgs boson in the particle spectrum. A charged Higgs can induce a violation of lepton flavour universality (LFU) in semileptonic and leptonic meson decays where it enters at the same level than the SM contribution, see figure 4.1. Decays of the B or $D_{(s)}$ meson into a final state with a τ lepton are particularly sensitive to charged scalar contributions in models where the couplings of such particle are proportional to fermion masses. The BaBar collaboration has reported an excess in $b \to c\tau\nu_\tau$ exclusive semileptonic transitions [1, 2] which could be pointing to such scenario, see figure 4.2. The measured quantity by BaBar is a ratio between the $B \to D^{(*)}\tau\nu$ decay mode and that with light leptons in the final state.

$$
R(D) \equiv \frac{\mathrm{Br}(\bar{B} \to D\tau^-\bar{\nu}_\tau)}{\mathrm{Br}(\bar{B} \to D\ell^-\bar{\nu}_\ell)} \overset{\mathrm{BaBar}}{=} 0.440 \pm 0.058 \pm 0.042 \overset{\mathrm{avg}}{=} 0.438 \pm 0.056 \,,
$$

$$
R(D^*) \equiv \frac{\mathrm{Br}(\bar{B} \to D^*\tau^-\bar{\nu}_\tau)}{\mathrm{Br}(\bar{B} \to D^*\ell^-\bar{\nu}_\ell)} \overset{\mathrm{BaBar}}{=} 0.332 \pm 0.024 \pm 0.018 \overset{\mathrm{avg}}{=} 0.354 \pm 0.026 \,,
$$

$$(4.1)$$

which are larger than the corresponding SM prediction for these quantities [3–6]. By taking this ratio, some important sources of uncertainty as $|V_{cb}|$ cancel allowing to make a more precise theory prediction. The main source of uncertainty in the theoretical prediction comes then from our ability to estimate the relevant hadronic from factors in all the kinematical regime. Our determination of the form factors relies on Heavy Quark Effective Theory [7–9] , Lattice QCD [10–12] and experimental data for $B \to D^{(*)}\mu\nu$ [13].
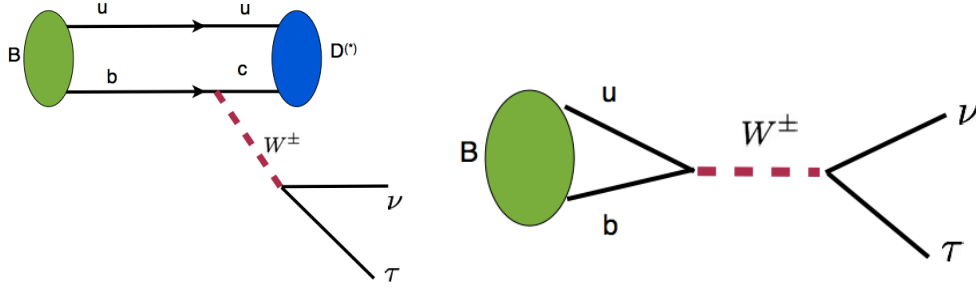
Figure 4.1: *Semileptonic and leptonic B meson decays mediated by the weak charged current at tree-level. Left: diagram contributing to $B \to D^{(*)}\tau\nu$ decays. Right: Diagram contributing to $B^- \to \tau^-\nu$ decay.*

A charged Higgs contributing to $B \to D^{(*)}\tau\nu$ decays is also expected to enter in leptonic $B^- \to \tau^-\bar{\nu}_\tau$ decays as well as in $D_{(s)}$ leptonic decays. The SM prediction $(0.733 ^{+0.121}_{-0.073}) \times 10^{-4}$ [14] (taking the modulus of the CKM matrix element $|V_{ub}|$ from a global CKM fit) is well compatible with the current experimental average $\mathrm{Br}(B^- \to \tau^-\bar{\nu}_\tau) = (1.15 \pm 0.23) \times 10^{-4}$, the same occurs for leptonic $D_{(s)}$ decays. We are interested then in trying to explain an excess on $B \to D^{(*)}\tau\nu$ decays while at the same having SM-like rates for the leptonic B and $D_{(s)}$ decays within the framework of 2HDMs. We will show how using the hypothesis of Yukawa alignment one is able to derive generic conclusions about the possibility to explain such excess as due to charged Higgs contributions. We also explore different observables that can be built based on the rich kinematical structure of the three-body decays $B \to D^{(*)}\tau\nu$. Some of these observables are particularly sensitive to charged scalar contributions and their measurement could provide a powerful way to discriminate among the different NP candidates for such excess in the future.
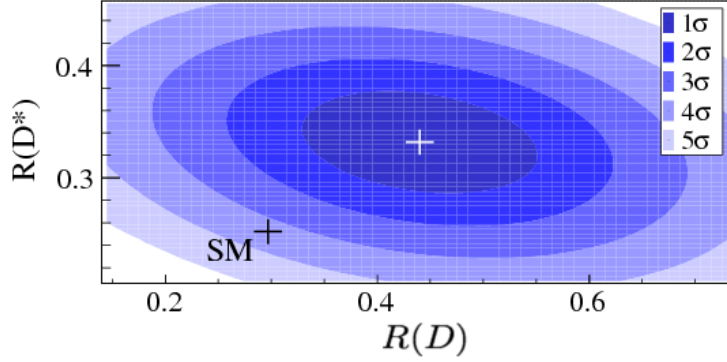
Figure 4.2:   *Excess observed by the Babar collaboration in the measurement of $R(D)$ and $R(D^*)$ [1, 2]. The white cross denotes the mean value observed experimentally while the black cross corresponds to the SM prediction.*

4.2   Paper II

It has been pointed out recently that flavour constraints still allow for large decay rates of the 126 GeV Higgs into $H \to \tau\ell$ (with $\ell = e, \mu$) [15, 16]. Branching ratios for $H \to \tau\ell$ as large as ten percent are in principle allowed by the constraints coming from radiative $\tau \to \ell\gamma$ and leptonic $\tau \to 3\ell$ decays [15, 16]. It is important to note however that these results were known well before the Higgs discovery, see for example refs. [17, 18]. The main motivation to carry out this analysis was to study the role of LFV semileptonic decays ($\tau \to \ell\pi\pi$, $\tau \to \ell\eta^{(\prime)}$) to constrain possible LFV Higgs couplings of the 126 GeV Higgs, which was not being discussed in the literature. The main obstacle or problem we encountered in this analysis was that previous treatments of the relevant hadronic matrix elements in the literature were far from adequate.

Previous treatments about Higgs mediated $\tau \to \ell\pi\pi$ decays were only taking into account the hadronic matrix element for $\langle \pi\pi | m_u \bar{u}u + m_d \bar{d}d | 0 \rangle$ within leading order chiral perturbation theory (LO-ChPT), see for example refs. [19, 20]. A description of $\tau \to \ell\pi\pi$ decays within the language of effective field theory was also done recently in ref. [21]

considering also LO-ChPT predictions for the hadronic matrix elements. This treatment of the hadronic matrix elements has two serious problems. First, Higgs interactions with hadronic systems at low energy are expected to be dominated by the effective Higgs-gluon interaction as was realized many years ago in ref. [22], the coupling of the Higgs with strange quarks is also expected to provide important contributions as is well known from studies of μ to e conversion in nuclei [23, 24]. The other important point is that for $\tau \to \ell\pi\pi$ decays the momentum transfer to the pion pair can be as large as ~ 1 GeV, it is well known that ChPT is only valid at energies below the ρ mass. Recently, it was shown in ref. [25] that a proper treatment of the scalar form factors in $\tau \to \ell\pi\pi$ decays lead to significant modifications of the decay rate and thus on the bounds extracted.

In the late eighties and nineties, physicists were looking for a SM Higgs boson with a mass around 1 GeV, see ref. [26] for a review. One of the theoretical challenges at that time was to calculate the decay rate $H \to \pi\pi$ which was expected to be one of the dominant decay channels for such low mass Higgs, together with $H \to \mu^+\mu^-$. A full calculation of the $H \to \pi\pi$ decay rate was obtained in ref. [27]. The use of chiral perturbation theory together with dispersive methods allowed a robust determination of the relevant hadronic matrix elements [27],

$$\langle \pi^i(p)\pi^k(p')|\theta^\mu_\mu|0\rangle = \theta_\pi(s)\,\delta^{ik}\,,$$
$$\langle \pi^i(p)\pi^k(p')|m_u\bar{u}u + m_d\bar{d}d|0\rangle = \Gamma_\pi(s)\,\delta^{ik}\,,$$
$$\langle \pi^i(p)\pi^k(p')|m_s\bar{s}s|0\rangle = \Delta_\pi(s)\,\delta^{ik}\,. \tag{4.2}$$

Here we have expressed the matrix element of the gluonic operator $G^a_{\mu\nu}G^{\mu\nu}_a$ via the trace anomaly relation of the energy momentum tensor

$$\theta^\mu_\mu = -9\frac{\alpha_s}{8\pi}\,G^a_{\mu\nu}G^{\mu\nu}_a + \sum_{q=u,d,s} m_q\,\bar{q}q\,. \tag{4.3}$$

In the case of the on-shell Higgs decay, the invariant mass of the pion pair is given by $s = M_H^2$ while for $\tau \to \ell\pi\pi$ decays we have

$$4m_\pi^2 \le s \le (m_\tau - m_\ell)^2\,, \qquad s = (p_{\pi^+} + p_{\pi^-})^2\,. \tag{4.4}$$

For this project, the required form factors in eq. (4.2) were determined by Emilie Passemar following the methods developed in ref. [27] and using the latest experimental data. I

verified that the form factors obtained by E. Passemar were in good agreement with the results of ref. [27]. It is instructive to review the determination of the relevant form factors within ChPT as we will discuss later the impact of a proper determination of the form factors. The leading order chiral Lagrangian in the formulation of Gasser and Leutwyler [28, 29] can be written in terms of the following building blocks

- $u_\mu = i\{u^\dagger(\partial_\mu - i r_\mu)u - u(\partial_\mu - i l_\mu)u^\dagger\}$

- $\chi_\pm = u^\dagger \chi u^\dagger \pm u \chi^\dagger u$

where

$$\chi = 2B(s + ip),$$

$$\phi = \begin{pmatrix} \pi^0 & \sqrt{2}\pi^+ \\ \sqrt{2}\pi^- & -\pi^0 \end{pmatrix},$$

$$u = e^{i\phi/2F} \approx \mathbf{1} + \left(i\phi/2F\right) + \frac{1}{2}\left(i\phi/2F\right)^2 + \frac{1}{3!}\left(i\phi/2F\right)^3 + \cdots . \tag{4.5}$$

The fields s, p, l_μ, r_μ are external hermitian matrix fields. The notation used for the basic building blocks is the one used in refs. [30, 31]. The mass term is introduced via the external field s, which in the isospin limit is equal to

$$s = \hat{m}\begin{pmatrix} 1 & 0 \\ 0 & 1 \end{pmatrix}. \tag{4.6}$$

The other external fields are not needed in the following and are set to zero $l_\mu = r_\mu = p = 0$. The leading order chiral Lagrangian is given by

$$\mathcal{L}_{\pi\pi}^{(2)} = \frac{F^2}{4}(\langle u_\mu u^\mu \rangle + \langle \chi_+ \rangle),$$

where $\langle A \rangle$ stands for the trace of A. The low energy constant F corresponds to the pion decay constant $F \equiv f_\pi/\sqrt{2} \simeq 93$ MeV and can be determined from the $\pi^+ \to \mu^+ \nu_\mu$ decay rate. Expanding the chiral Lagrangian in the pion fields one obtains

$$\mathcal{L}_{\pi\pi}^{(2)} = \frac{1}{2}\partial_\mu\pi^0\partial^\mu\pi^0 + \partial_\mu\pi^+\partial^\mu\pi^- - M^2\pi^+\pi^- - \frac{1}{2}M^2(\pi^0)^2 + \cdots . \tag{4.7}$$

To lowest order the pion mass is then given by $m_\pi^2 \equiv M^2 = 2B\hat{m}$. Matching the light-quark scalar current to the effective Lagrangian,

$$(m_u\bar{u}u + m_d\bar{d}d)^{\mathrm{eff}} = -\frac{F^2}{4}\langle \chi_+ \rangle = \frac{1}{2}m_\pi^2(\pi^0)^2 + m_\pi^2\pi^+\pi^- + \cdots , \tag{4.8}$$

so that within LO-ChPT we obtain

$$\Gamma_\pi = m_\pi^2 + \mathcal{O}(p^4)\,. \tag{4.9}$$

One also gets for the form factor associated with the energy-momentum tensor

$$\theta_\pi(s) = s + 2m_\pi^2 + \mathcal{O}(p^4)\,. \tag{4.10}$$

This result was obtained for the first time by Voloshin [32]. The determination of the remaining scalar form factor $\Delta_\pi(s)$ within ChPT has been discussed in ref. [27].

4.3   Paper III

In this paper we assume that the discovered 126 GeV boson is one of the neutral scalars of the 2HDM and analyze the implications of Tevatron and LHC data within this framework. We analyze the CP-conserving limit as well as the more general CP-violating scenario. Different possibilities for the scalar spectrum are also considered, including: the 126 GeV boson as the lightest or the heaviest CP-even Higgs boson, and, the 126 GeV observed resonance as a result of two quasi degenerate neutral Higgs bosons. By the time our work was made public, a large number of analyses of LHC data within 2HDMs had already been done by other authors. Two main aspects distinguished our work from previous analyses:

- We work in the Higgs basis and express bounds in terms of quantities that are invariant under scalar basis transformations.

- We assume a general Yukawa structure without FCNCs as provided by the hypothesis of Yukawa alignment. The different models with NFC can be recovered as particular limits of the parametrization we use.

These two points are closely related. Indeed, in the A2HDM there is no special choice of basis since one does not impose any $\mathcal{Z}_2$ discrete symmetry. By performing a basis transformation in the scalar space one can always arrive to the Higgs basis, where only one doublet has a non-vanishing vev. Working in the Higgs basis has the advantage that the parameters of the scalar sector are closely related to physical quantities (invariants

under basis transformations). Before our work appeared, there were already previous works which were using general parametrizations analogous to that of the A2HDM to analyze the data. These analyses however were performed in a generic scalar basis in which the unphysical parameter $\tan\beta$ appears explicitly.

By performing the analysis of experimental data within the A2HDM, one allows experiments to determine whether there is a 2HDM with NFC realized in Nature, see figure 4.3. On the other hand, by using a general Yukawa structure the analysis involves more free parameters and one is less predictive. In the next paper we showed how unitarity sum-rules among the scalar couplings of the 2HDM provide a powerful way to analyze LHC data for the 126 GeV Higgs and searches for additional scalars while at the same time keeping a generic Yukawa structure as provided by the A2HDM.
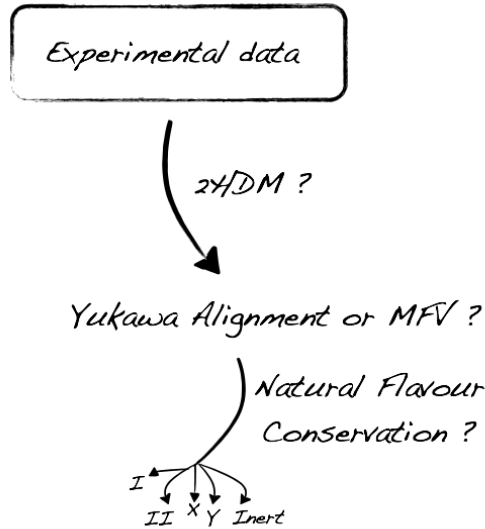

Figure 4.3: *Scheme for the determination of the 2HDM Yukawa structure.*

4.4   Paper IV

In this paper we put forward a general and powerful way to analyze LHC data within the framework of 2HDMs which exploits the use of tree-level unitarity sum-rules governing the

scalar couplings. Such tree-level unitarity sum-rules had been discussed in several works prior to the Higgs discovery and also mentioned in some analyses of LHC Higgs data. The full power of these sum-rules to analyze LHC data however was not being exploited and this work can be considered a first step along this direction. We know already from LHC data that the 126 GeV Higgs has a coupling with massive vector bosons that is close to the SM value in magnitude and that it is a spin zero boson. The 126 GeV boson should therefore be playing a major role in the restoration of perturbative unitarity in longitudinal WW boson scattering. If there is an extended scalar sector in Nature which remains perturbative up to very high energies, perturbative unitarity conditions give rise to specific sum-rules among the couplings of the different physical scalar fields. These sum-rules provide a very compact way to frame our studies of LHC and Tevatron data for the 126 GeV boson as well as searches for additional scalars within the framework of 2HDMs.

Another advantage of the use of unitarity sum-rules when analyzing the data comes from the more practical task of comparing results from different groups. Currently, there is a large amount of works analyzing LHC data within 2HDMs and one can find many different parametrizations or conventions being used for the scalar couplings, this makes it very difficult to perform even a simple comparison of the constraints extracted from the same data. Since the unitarity sum-rules are expressed in terms of physical quantities, they provide a common setting to compare analyses by different groups in a straightforward way. Independently of which parametrization one prefers for the scalar couplings of the 2HDM or the choice of scalar basis, one can always express the results in terms of the unitarity sum-rules and provide a concise result that can be interpreted by other groups without problems.

There is still room for improvement in the analyses we have performed and points that should be treated more carefully in future studies. First, one would like to perform a full scan of the 2HDM parameter space, in particular of the CP-conserving A2HDM where the number of free parameters reduces somewhat but is still more general than the 2HDMs with NFC. Studies along this direction within the A2HDM performed by different groups have assumed that the scalar potential has a softly-broken $\mathcal{Z}_2$ symmetry in a generic scalar basis, this simplifies some expressions like for example the perturbative unitarity bounds. This however is not the best way to carry such analysis since within the A2HDM there is no reason to impose such condition a priori. On the other hand, state of

the art calculations of the Higgs production cross section and Higgs decay widths within the 2HDM have been summarized recently in ref. [33]. With the advent of more data and the reduction of statistical errors, phenomenological studies of the 2HDM at the LHC will have to incorporate these developments in order to have meaningful results (taking into account properly the theoretical uncertainties). It is important to note also that we have not included in our analysis the Higgs production through b-quark fusion. This production channel becomes important to estimate the production cross-section of the missing neutral Higgs bosons for large values of the alignment parameter ς_d. Assuming for example that h is the 126 GeV Higgs boson, we know that $|y_d^h| \sim 1$ while $|y_d^{H,A}| \sim |\varsigma_d|$ (κ_V^h is bounded to be close to the SM limit) so that the b-quark fusion production mechanism can be greatly enhanced for H or A.

Bibliography

[1] J. P. Lees *et al.* [BaBar Collaboration], Phys. Rev. Lett. **109** (2012) 101802 [arXiv:1205.5442 [hep-ex]].

[2] J. P. Lees *et al.* [BaBar Collaboration], Phys. Rev. D **88** (2013) 072012 [arXiv:1303.0571 [hep-ex]].

[3] S. Fajfer, J. F. Kamenik, I. Nisandzic and J. Zupan, Phys. Rev. Lett. **109** (2012) 161801 [arXiv:1206.1872 [hep-ph]].

[4] Y. Sakaki and H. Tanaka, Phys. Rev. D **87** (2013) 5, 054002 [arXiv:1205.4908 [hep-ph]].

[5] S. Fajfer, J. F. Kamenik and I. Nisandzic, Phys. Rev. D **85** (2012) 094025 [arXiv:1203.2654 [hep-ph]].

[6] D. Becirevic, N. Kosnik and A. Tayduganov, Phys. Lett. B **716** (2012) 208 [arXiv:1206.4977 [hep-ph]].

[7] A. F. Falk and M. Neubert, Phys. Rev. D **47** (1993) 2965 [hep-ph/9209268].

[8] A. F. Falk and M. Neubert, Phys. Rev. D **47** (1993) 2982 [hep-ph/9209269].

[9] M. Neubert, Phys. Rev. D **46** (1992) 2212.

[10] G. M. de Divitiis, R. Petronzio and N. Tantalo, JHEP **0710** (2007) 062 [arXiv:0707.0587 [hep-lat]].

[11] G. M. de Divitiis, E. Molinaro, R. Petronzio and N. Tantalo, Phys. Lett. B **655** (2007) 45 [arXiv:0707.0582 [hep-lat]].

[12] J. A. Bailey, A. Bazavov, C. Bernard, C. M. Bouchard, C. DeTar, D. Du, A. X. El-Khadra and J. Foley *et al.*, Phys. Rev. Lett. **109** (2012) 071802 [arXiv:1206.4992 [hep-ph]].

[13] Y. Amhis *et al.* [Heavy Flavor Averaging Group Collaboration], arXiv:1207.1158 [hep-ex].

[14] J. Charles *et al.* [CKMfitter Group Collaboration], Eur. Phys. J. C **41** (2005) 1 [hep-ph/0406184].

[15] G. Blankenburg, J. Ellis and G. Isidori, Phys. Lett. B **712** (2012) 386 [arXiv:1202.5704 [hep-ph]].

[16] R. Harnik, J. Kopp and J. Zupan, JHEP **1303** (2013) 026 [arXiv:1209.1397 [hep-ph]].

[17] J. L. Diaz-Cruz and J. J. Toscano, Phys. Rev. D **62** (2000) 116005 [hep-ph/9910233].

[18] A. Goudelis, O. Lebedev and J. -h. Park, Phys. Lett. B **707** (2012) 369 [arXiv:1111.1715 [hep-ph]].

[19] D. Black, T. Han, H. -J. He and M. Sher, Phys. Rev. D **66** (2002) 053002 [hep-ph/0206056].

[20] S. Kanemura, T. Ota and K. Tsumura, Phys. Rev. D **73** (2006) 016006 [hep-ph/0505191].

[21] A. A. Petrov and D. V. Zhuridov, arXiv:1308.6561 [hep-ph].

[22] M. A. Shifman, A. I. Vainshtein and V. I. Zakharov, Phys. Lett. B **78** (1978) 443.

[23] R. Kitano, M. Koike and Y. Okada, Phys. Rev. D **66** (2002) 096002 [Erratum-ibid. D **76** (2007) 059902] [hep-ph/0203110].

[24] V. Cirigliano, R. Kitano, Y. Okada and P. Tuzon, Phys. Rev. D **80** (2009) 013002 [arXiv:0904.0957 [hep-ph]].

[25] J. T. Daub, H. K. Dreiner, C. Hanhart, B. Kubis and U. G. Meissner, JHEP **1301** (2013) 179 [arXiv:1212.4408 [hep-ph]].

[26] J. F. Gunion, H. E. Haber, G. L. Kane and S. Dawson, Front. Phys. **80** (2000) 1.

[27] J. F. Donoghue, J. Gasser and H. Leutwyler, Nucl. Phys. B **343** (1990) 341.

[28] J. Gasser and H. Leutwyler, Annals Phys. **158** (1984) 142.

[29] J. Gasser and H. Leutwyler, Nucl. Phys. B **250** (1985) 465.

[30] G. Ecker, J. Gasser, A. Pich and E. de Rafael, Nucl. Phys. B **321** (1989) 311.

[31] J. Bijnens, G. Colangelo and G. Ecker, JHEP **9902** (1999) 020 [hep-ph/9902437].

[32] M. B. Voloshin, Sov. J. Nucl. Phys. **44** (1986) 478 [Yad. Fiz. **44** (1986) 738].

[33] R. Harlander, M. Muhlleitner, J. Rathsman, M. Spira and O. Stal, arXiv:1312.5571 [hep-ph].

Sensitivity to charged scalars in $B \to D^{(*)}\tau\nu_\tau$ and $B \to \tau\nu_\tau$ decays

Alejandro Celis[1], Martin Jung[2], Xin-Qiang Li[3,1] and Antonio Pich[1]

[1]IFIC, Universitat de València – CSIC, Apt. Correus 22085, E-46071 València, Spain
[2]Institut für Physik, Technische Universität Dortmund, D-44221 Dortmund, Germany
[3]Department of Physics, Henan Normal University, Xinxiang, Henan 453007, P. R. China

We analyze the recent experimental evidence for an excess of τ-lepton production in several exclusive semileptonic B-meson decays in the context of two-Higgs-doublet models. These decay modes are sensitive to the exchange of charged scalars and constrain strongly their Yukawa interactions. While the usual Type-II scenario cannot accommodate the recent BaBar data, this is possible within more general models in which the charged-scalar couplings to up-type quarks are not as suppressed. Both the $B \to D^{(*)}\tau\nu_\tau$ and the $B \to \tau\nu_\tau$ data can be fitted within the framework of the Aligned Two-Higgs-Doublet Model, but the resulting parameter ranges are in conflict with the constraints from leptonic charm decays. This could indicate a departure from the family universality of the Yukawa couplings, beyond their characteristic fermion mass dependence. We discuss several new observables that are sensitive to a hypothetical charged-scalar contribution, demonstrating that they are well suited to distinguish between different

scenarios of new physics in the scalar sector, and also between this group and models with different Dirac structures; their experimental study would therefore shed light on the relevance of scalar exchanges in semileptonic $b \to c\,\tau^-\bar{\nu}_\tau$ transitions.

5.1   Introduction

The BaBar collaboration has recently reported an excess of events in two semileptonic transitions of the type $b \to c\,\tau^-\bar{\nu}_\tau$. More specifically, they have measured the ratios [1]

$$R(D) \equiv \frac{\mathrm{Br}(\bar{B} \to D\tau^-\bar{\nu}_\tau)}{\mathrm{Br}(\bar{B} \to D\ell^-\bar{\nu}_\ell)} \stackrel{\mathrm{BaBar}}{=} 0.440 \pm 0.058 \pm 0.042 \stackrel{\mathrm{avg}}{=} 0.438 \pm 0.056\,,$$

$$R(D^*) \equiv \frac{\mathrm{Br}(\bar{B} \to D^*\tau^-\bar{\nu}_\tau)}{\mathrm{Br}(\bar{B} \to D^*\ell^-\bar{\nu}_\ell)} \stackrel{\mathrm{BaBar}}{=} 0.332 \pm 0.024 \pm 0.018 \stackrel{\mathrm{avg}}{=} 0.354 \pm 0.026\,, \quad (5.1)$$

which are normalized to the corresponding decays into light leptons $\ell = e, \mu$. The second value given in each line is the average with the previous measurements by the Belle collaboration [2, 3], which also yield central values corresponding to an excess, but not significantly so. These relative rates can be predicted with a rather high accuracy, because many hadronic uncertainties cancel to a large extent. The Standard Model (SM) expectations [4–7] are significantly lower than the BaBar measurements. If confirmed, this could signal new physics (NP) contributions violating lepton-flavour universality.

A sizable deviation with respect to the SM prediction was previously observed in the leptonic decay $B^- \to \tau^-\bar{\nu}_\tau$, when combining the data by BaBar [8, 9] and Belle [10]. The world average $\mathrm{Br}(B^- \to \tau^-\bar{\nu}_\tau) = (1.65 \pm 0.34) \times 10^{-4}$ [11] used to be 2.5σ higher than the SM prediction $(0.733\,^{+0.121}_{-0.073}) \times 10^{-4}$ [12] (taking the modulus of the Cabibbo-Kobayashi-Maskawa (CKM) [13] matrix element $|V_{ub}|$ from a global CKM fit). However, a value closer to the SM expectation has been just reported by Belle [14], leading to the new Belle combination $\mathrm{Br}(B^- \to \tau^-\bar{\nu}_\tau)_{\mathrm{Belle}} = (0.96 \pm 0.22 \pm 0.13) \times 10^{-4}$, which we average with the combined BaBar result [9] to obtain $\mathrm{Br}(B^- \to \tau^-\bar{\nu}_\tau) = (1.15 \pm 0.23) \times 10^{-4}$.

While more experimental studies are clearly needed, these measurements are intriguing enough to trigger the theoretical interest [4–7, 15–20]. This kind of non-universal enhancement of the τ production in semileptonic B-meson decays could be generated by NP contributions with couplings proportional to fermion masses. In particular, it could be associated with the exchange of a charged scalar within two-Higgs-doublet models (2HDMs), with the expected contribution to the transition amplitude being proportional to $m_\tau m_b/M_{H^\pm}^2$. This approach offers (obviously) a solution when considering scalar NP contributions model-independently; even in this general case, however, non-trivial predictions for other observables in these decays can be obtained. More specific models

generally have difficulties in describing all the data. For example, the BaBar data on $\bar{B} \to D\,\tau^-\bar{\nu}_\tau$ and $\bar{B} \to D^*\tau^-\bar{\nu}_\tau$ cannot be explained simultaneously within the usually adopted Type-II scenario [1, 4, 15]. It is also observed that none of the four types of 2HDMs with natural flavour conservation (i.e., Type-I, Type-II, "lepton specific" and "flipped") [21] can simultaneously account for the $B \to \tau$ data [4]. We shall show, however, that they can be accommodated by the more general framework of the Aligned Two-Higgs-Doublet Model (A2HDM) [22], albeit creating a tension when including them in a global fit.

Other suggested interpretations of the observed excess within different NP scenarios include the 2HDM of Type-III, equipped with a MSSM-like Higgs potential and flavour-violation in the up-quark sector [15], a leptoquark model with renormalizable interactions to third-generation SM fermions [4], composite Higgs models where the heavier SM fermions are expected to be partially or mostly composite [4], the exchange of right-handed down-type squarks within the R-parity violating MSSM [19], as well as a non-universal left-right model where only the third generation couples to the W_R [23].

Generic multi-Higgs-doublet models give rise to unwanted flavour-changing neutral current (FCNC) interactions through non-diagonal couplings of neutral scalars to fermions [21]. The tree-level FCNCs can be eliminated by requiring the alignment in flavour space of the Yukawa matrices coupling to a given right-handed fermion [24]. This results in a very specific structure, with all fermion-scalar interactions being proportional to the corresponding fermion masses, and implies an interesting hierarchy of FCNC effects, suppressing them in light-quark systems while allowing potentially relevant signals in heavy-quark transitions. The A2HDM leads to a rich and viable phenomenology [22, 24–27]; it constitutes a very general framework which includes, for particular values of its parameters, all previously considered 2HDMs without tree-level FCNCs [21], and at the same time incorporates additional new sources of CP violation beyond the SM.

In the following, we shall consider the phenomenology of $b \to q\,\tau^-\bar{\nu}_\tau$ $(q = u, c)$ transitions within a framework with additional scalar operators, assumed to be generated by the exchange of a charged scalar. Starting from the most general parametrization of such effects, we then specialize to various more specific models to examine their capability to describe the data and the possibility to distinguish between them.

Our paper is organized as follows: In section 5.2, we briefly describe the theoretical framework adopted in our analysis. In section 5.3, we present our numerical results

and show the parameter ranges needed to explain the present data. We proceed in section 5.4 by analyzing various additional observables sensitive to scalar contributions, both integrated and differential, before concluding in section 5.5. The appendices include a discussion of the relevant input parameters and details on the calculation for the semileptonic B-meson decays.

5.2   Theoretical framework

We are going to assume that, in addition to the SM W-exchange amplitude, the quark-level transitions $b \to q\,l^-\bar{\nu}_l$ receive tree-level contributions from the exchange of a charged scalar. The effective low-energy Lagrangian describing these transitions takes then the form

$$\mathcal{L}_{\text{eff}} = -\frac{4G_F}{\sqrt{2}} \sum_{q=u,c} V_{qb} \sum_{l=e,\mu,\tau} \left\{ [\bar{q}\gamma^\mu \mathcal{P}_L b]\,[\bar{l}\gamma_\mu \mathcal{P}_L \nu_l] + \left[\bar{q}\left(g_L^{qbl}\,\mathcal{P}_L + g_R^{qbl}\,\mathcal{P}_R\right)b\right][\bar{l}\mathcal{P}_L\nu_l] \right\},$$

$$(5.2)$$

where $\mathcal{P}_{R,L} \equiv \frac{1\pm\gamma_5}{2}$ are the chirality projectors, and the effective couplings are, in the majority of 2HDMs, proportional to the fermion masses, $g_L^{q_u q_d l} \sim m_{q_u} m_l / M_{H^\pm}^2$, $g_R^{q_u q_d l} \sim m_{q_d} m_l / M_{H^\pm}^2$. These explicit fermion mass factors imply negligible effects in decays into light leptons (e, μ),[1] while decays involving the τ receive potentially large contributions. Owing to the m_q suppression, the coupling g_L^{qbl} does not play any relevant role in $b \to u\tau^-\bar{\nu}_\tau$ transitions, but it can give sizeable corrections to $b \to c\tau^-\bar{\nu}_\tau$.

We present next the key relations for including scalar NP contributions in the decays in question. When considering specific models, the main focus lies on the A2HDM, of which we give a short review. For the relevant kinematical variables, notation and derivation of the double differential decay rates, we refer the reader to the appendices.

5.2.1 $b \to q\,\tau^-\,\bar{\nu}_\tau\;(q = u, c)$ decays

Due to the helicity suppression of the SM amplitude, the leptonic decay $B^- \to \tau^-\bar{\nu}_\tau$ is particularly sensitive to the charged scalar exchange. The total decay width is given

---

[1] The obvious exception are leptonic meson decays, where the SM contribution is already suppressed by the light lepton masses, yielding a large relative contribution from the charged scalar.

by [25, 28]

$$\Gamma(B^- \to \tau^- \bar\nu_\tau) = G_F^2 m_\tau^2 f_B^2 |V_{ub}|^2 \frac{m_B}{8\pi} \left(1 - \frac{m_\tau^2}{m_B^2}\right)^2 (1 + \delta_{\text{em}}) |1 - \Delta_{ub}^\tau|^2 , \qquad (5.3)$$

where δ_{em} denotes the electromagnetic radiative contributions, and the new-physics information is encoded in the correction[2]

$$\Delta_{qb}^l = \frac{(g_L^{qbl} - g_R^{qbl}) m_B^2}{m_l (\overline{m}_b + \overline{m}_q)} \overset{q=u}{\simeq} -\frac{g_R^{ubl} m_B^2}{m_l \overline{m}_b} , \qquad (5.4)$$

absorbing in addition mass factors from the hadronic matrix elements.

Semileptonic decays receive contributions from a charged scalar as well, but in this case the leading SM amplitude is not helicity suppressed; therefore, the relative influence is smaller. In addition, they involve momentum-dependent form factors. The $\bar B \to D l \bar\nu_l$ decay amplitude is characterized by two form factors, $f_+(q^2)$ and $f_0(q^2)$, associated with the P-wave and S-wave projections of the crossed-channel matrix element $\langle 0|\bar c \gamma^\mu b|\bar B \bar D\rangle$. The scalar-exchange amplitude only contributes to the scalar form factor; it amounts to a multiplicative correction [25]

$$f_0(q^2) \to \tilde f_0(q^2) = f_0(q^2) \left[1 + \delta_{cb}^l \frac{q^2}{(m_B - m_D)^2}\right] , \qquad (5.5)$$

with

$$\delta_{cb}^l \equiv \frac{(g_L^{cbl} + g_R^{cbl})(m_B - m_D)^2}{m_l (\overline{m}_b - \overline{m}_c)} . \qquad (5.6)$$

The sensitivity to the scalar contribution can only be achieved in semileptonic decays into heavier leptons. The decays involving light leptons can, therefore, be used to extract information on the vector form factor, reducing the necessary theory input to information on the scalar form factor. Since the observables are usually normalized to the decays into light leptons, the relevant input quantity is not the scalar form factor itself, but the ratio of scalar to vector form factors, $f_0(q^2)/f_+(q^2)$; an important constraint on the latter is its normalization to unity at $q^2 = 0$. These features lead us to parametrize the different CP-conserving observables that we are going to consider in the following form:

$$O = c_0 + c_1 \,\text{Re}\,(\delta_{cb}^\tau) + c_2 \,|\delta_{cb}^\tau|^2 , \qquad (5.7)$$

---

[2]Here and in the following we suppress in the notation the scale dependence of *e.g.* the quark masses and scalar couplings.

implying a discrete symmetry $\mathrm{Im}\,(\delta^\tau_{cb}) \to -\mathrm{Im}\,(\delta^\tau_{cb})$. The coefficients c_i, which contain the dependence on the strong-interaction dynamics, are parametrized in turn in terms of the vector form-factor slope ρ^2_1 and the scalar density $\Delta(v_B \cdot v_D)$ [29, 30]. For the former we use the value extracted from $B \to D\ell\nu$ ($\ell = e, \mu$) decays. The function $\Delta(v_B \cdot v_D) \propto f_0(q^2)/f_+(q^2)$ has been studied on the lattice, in the range $v_B \cdot v_D = 1$–1.2, and found to be consistent with a constant value $\Delta = 0.46 \pm 0.02$, very close to its static-limit approximation $(m_B - m_D)/(m_B + m_D)$ [7, 17, 31]. This value is furthermore in agreement with QCD sum rule estimates [32, 33].

The decay $\bar{B} \to D^* l^- \bar{\nu}_l$ has a much richer dynamical structure, due to the vector nature of the final D^* meson. The differential decay distribution is described in terms of four helicity amplitudes, $H_{\pm\pm}$, H_{00} and H_{0t}, where the first subindex denotes the D^* helicity $(\pm, 0)$ and the second the lepton-pair helicity $(\pm, 0, t)$ in the B-meson rest frame [34, 35]. In addition to the three polarizations orthogonal to its total four-momentum q^μ, the leptonic system has a spin-zero time component (t) that is proportional to q^μ and can only contribute to the semileptonic decays for non-zero charged-lepton masses (it involves a positive helicity for the l^-). The corresponding H_{0t} amplitude is the only one receiving contributions from the scalar exchange [5]:

$$H_{0t}(q^2) \;=\; H_{0t}^{\mathrm{SM}}(q^2)\,\left(1 - \Delta^\tau_{cb}\,\frac{q^2}{m^2_B}\right)\,. \tag{5.8}$$

The observables are then given in an expansion analogous to eq. (5.7), with δ^τ_{cb} replaced by Δ^τ_{cb}, and the coefficients depend on the different form-factor normalizations $R_i(1)$ ($i = 0, 1, 2, 3$) and the slope ρ^2, see Appendix 5.D for details. Here, again, we use inputs extracted from the decays involving light leptons where possible, while for the remaining form-factor normalization $R_3(1)$ we adopt a value calculated in the framework of Heavy Quark Effective Theory (HQET) [36].

A summary of the different form-factor parameters is given in table 5.3, in the appendix.

5.2.2   Overview of the A2HDM

The 2HDMs extend the SM Higgs sector by a second scalar doublet of hypercharge $Y = \frac{1}{2}$. Thus, in addition to the three Goldstone bosons, they contain five physical scalars: two

charged fields $H^\pm$ and three neutral ones $\varphi_i^0 = \{h, H, A\}$. The most generic Yukawa Lagrangian with the SM fermionic content gives rise to tree-level FCNCs, because the Yukawa couplings of the two scalar doublets to fermions cannot be simultaneously diagonalized in flavour space. The non-diagonal neutral couplings can be eliminated by requiring the alignment in flavour space of the Yukawa matrices [22]; *i.e.*, the two Yukawa matrices coupling to a given type of right-handed fermions are assumed to be proportional to each other and can, therefore, be diagonalized simultaneously. The three proportionality parameters are arbitrary complex numbers and introduce new sources of CP violation.

In terms of the fermion mass-eigenstate fields, the Yukawa interactions of the charged scalar in the A2HDM read [22]

$$\mathcal{L}_Y^{H^\pm} = -\frac{\sqrt{2}}{v} H^+ \left\{ \bar{u} \left[\varsigma_d V M_d \mathcal{P}_R - \varsigma_u M_u V \mathcal{P}_L \right] d + \varsigma_l \bar{\nu} M_l \mathcal{P}_R l \right\} + \text{h.c.}, \qquad (5.9)$$

where ς_f $(f = u, d, l)$ are the proportionality parameters in the so-called "Higgs basis" in which only one scalar doublet acquires a non-zero vacuum expectation value. The CKM quark mixing matrix V [13] remains the only source of flavour-changing interactions. All possible freedom allowed by the alignment conditions is determined by the three family-universal complex parameters ς_f, which provide new sources of CP violation without tree-level FCNCs [22]. Comparing eqs. (5.9) and (5.2), one obtains the following relations between the A2HDM and the general scalar NP parameters:

$$g_L^{q_u q_d l} = \varsigma_u \varsigma_l^* \frac{m_{q_u} m_l}{M_{H^\pm}^2}, \qquad\qquad g_R^{q_u q_d l} = -\varsigma_d \varsigma_l^* \frac{m_{q_d} m_l}{M_{H^\pm}^2} . \qquad (5.10)$$

The usual models with natural flavour conservation (NFC), based on discrete $\mathcal{Z}_2$ symmetries, are recovered for particular (real) values of the couplings ς_f; especially $\varsigma_d = \varsigma_l = -1/\varsigma_u = -\tan\beta$ and $\varsigma_u = \varsigma_d = \varsigma_l = \cot\beta$ correspond to the Type-II and Type-I models, respectively.

Limits on the charged-scalar mass from flavour observables and direct searches depend strongly on the assumed Yukawa structure. The latest bound on the Type-II 2HDM charged Higgs from $\bar{B} \to X_s\gamma$ gives $M_{H^\pm} \geq 380$ GeV at 95% confidence level (CL) [37]. Within the A2HDM on the other hand it is still possible to have a light charged Higgs [25, 26]. Assuming that the charged scalar H^+ only decays into fermions $u_i\bar{d}_j$ and $l^+\nu_l$, LEP established the limit $M_{H^\pm} > 78.6$ GeV (95% CL) [38], which is independent of the Yukawa structure. A charged Higgs produced via top-quark decays has also been searched for

at the Tevatron [39, 40] and the LHC [41, 42]; these searches are, however, not readily translatable into constraints for the model parameters considered here. It should be noted that the charged-scalar mass enters only in combination with the other couplings and, therefore, its size does not affect directly our results at this level.

5.3   Results and discussions

In table 5.1 we summarize our predictions within the SM for the various semileptonic and leptonic decays considered in this work, using the hadronic inputs quoted in table 5.3 (parameters that do not appear in this table are taken from [11]). The rates for leptonic D, K and π decays are obtained from eq. (5.3) with appropriate replacements, while the ratio of $\tau \to K/\pi\nu_\tau$ decay widths is given by [25]

$$\frac{\Gamma(\tau \to K\nu)}{\Gamma(\tau \to \pi\nu)} = \left(\frac{1 - m_K^2/m_\tau^2}{1 - m_\pi^2/m_\tau^2}\right)^2 \left|\frac{V_{us}}{V_{ud}}\right|^2 \left(\frac{f_K}{f_\pi}\right)^2 (1 + \delta_{\text{em}}^{\tau K2/\tau\pi2}) \left|\frac{1 - \Delta_{us}}{1 - \Delta_{ud}}\right|^2. \quad (5.11)$$

One can see that, apart from $R(D)$ and $R(D^*)$, all the observables are in agreement with their SM predictions. While for the decays involving only $D_{(s)}$, K, and π mesons no large effect could be expected because of the relatively small quark masses involved, this is equally true for the influence of $g_L^{cb\tau}$. Contrary to that expectation, however, the data on $R(D)$ and $R(D^*)$ indicate a large value for this coupling. This not only renders especially models with NFC incompatible with the data, but also poses a problem in more general models.

We start by analyzing the constraints on the A2HDM parameters from the decays listed in table 5.1.[3] In contrast to the models with NFC, the observables involving B-meson decays ($R(D)$, $R(D^*)$ and $\text{Br}(B \to \tau\nu)$) can be consistently explained in the

---

[3]We do not take into account the experimental correlation between the measured values of $R(D)$ and $R(D^*)$ given in [1]. It is reduced to -19% when averaging with the Belle data and does not affect our results significantly. Moreover, the BaBar fit is sensitive to the assumed kinematical distribution, which is modified by the scalar contribution. While BaBar has already performed an explicit analysis within the Type-II 2HDM, it would be useful to analyze the experimental data in terms of the more general complex parameters Δ_{cb}^l and δ_{cb}^l, to make the inclusion of this effect possible in the future. This modification is, however, only relevant for large values of the scalar couplings, which are excluded in the scenarios 2 and 3 discussed below.

Table 5.1: *Predictions within the SM for the various semileptonic and leptonic decays discussed in this work, together with their corresponding experimental values. The first uncertainty given always corresponds to the statistical uncertainty, and the second, when present, to the theoretical one.*

Observable	SM Prediction	Exp. Value	Comment
$R(D)$	$0.296^{+0.008}_{-0.006} \pm 0.015$	0.438 ± 0.056	our average [1–3]
$R(D^*)$	$0.252 \pm 0.002 \pm 0.003$	0.354 ± 0.026	our average [1–3]
$\mathrm{Br}(B \to \tau\nu_\tau)$	$(0.79^{+0.06}_{-0.04} \pm 0.08) \times 10^{-4}$	$(1.15 \pm 0.23) \times 10^{-4}$	our average [9, 14]
$\mathrm{Br}(D_s \to \tau\nu_\tau)$	$(5.18 \pm 0.08 \pm 0.17) \times 10^{-2}$	$(5.54 \pm 0.24) \times 10^{-2}$	our average [11, 43]
$\mathrm{Br}(D_s \to \mu\nu)$	$(5.31 \pm 0.09 \pm 0.17) \times 10^{-3}$	$(5.54 \pm 0.24) \times 10^{-3}$	our average [11, 43]
$\mathrm{Br}(D \to \mu\nu)$	$(4.11^{+0.06}_{-0.05} \pm 0.27) \times 10^{-4}$	$(3.76 \pm 0.18) \times 10^{-4}$	[44]
$\Gamma(K \to \mu\nu)/\Gamma(\pi \to \mu\nu)$	$1.333 \pm 0.004 \pm 0.026$	1.337 ± 0.003	[11]
$\Gamma(\tau \to K\nu_\tau)/\Gamma(\tau \to \pi\nu_\tau)$	$(6.56 \pm 0.02 \pm 0.15) \times 10^{-2}$	$(6.46 \pm 0.10) \times 10^{-2}$	[11]

A2HDM. However, the resulting parameter region excludes the one selected by the leptonic $D_{(s)}$-meson decays. More generally speaking, models fulfilling the relations

$$(a) \quad g_L^{q_u q_d l}/g_L^{q'_u q'_d l'} = m_{q_u} m_l/(m_{q'_u} m_{l'}) \qquad \text{and} \qquad (b) \quad g_R^{q_u q_d l}/g_R^{q'_u q'_d l'} = m_{q_d} m_l/(m_{q'_d} m_{l'}) \tag{5.12}$$

are in conflict with the data. Removing $R(D^*)$ from the fit leads to a consistent picture in the A2HDM; in this case, however, the SM is also globally consistent with the data, as the tension in $R(D)$ is "distributed" over the remaining observables. Models with NFC remain disfavoured compared to the SM. These observations lead us to consider the following scenarios:

- Scenario 1 (Sc.1) is a model-independent approach where all couplings $g_{L,R}^{q_u q_d l}$ are assumed to be independent. One possible realization is the 2HDM of Type III. This implies that the effective couplings δ_{cb}^l and Δ_{cb}^l in the two semileptonic processes can be regarded as independent. Therefore, predictions for the additional observables in $B \to D(D^*)\tau\nu$ follow in this case *only* from $R(D)$ ($R(D^*)$).

- In scenario 2 we assume the relations in eq. (5.12) to hold for $q_d = b$, while processes involving only the first two generations are regarded as independent. When

considering only the constraints from $R(D)$, $R(D^*)$ and $\mathrm{Br}(B \to \tau\nu)$, the couplings in the A2HDM fulfill this condition; we will assume this form in the following for definiteness.

- For scenario 3 we discard the measurement of $R(D^*)$ as being due to a statistical fluctuation and/or an underestimated systematic effect, leaving us with a viable A2HDM. From a global fit to all the other measurements we then obtain predictions for the new observables in $B \to D^{(*)}\tau\nu$ as well as $R(D^*)$.

The ratios in eq. (5.12) might of course also be changed for $l = \tau$ or $l = \mu$. However, because of the smallness of m_μ, this would not be visible in any of the observables considered here. A way to test this option is to consider the ratio $\mathrm{Br}(B^- \to \tau^- \bar{\nu}_\tau)/\mathrm{Br}(B^- \to \mu^- \bar{\nu}_\mu)$, which is independent of NP in the scalar sector if eq. (5.12) is fulfilled.

In figure 5.1 we first show the allowed regions in the $R(D)$–$R(D^*)$ plane for the different scenarios. Scenario 1 is just reflecting the experimental information, while the additional constraint from $B \to \tau\nu$ already excludes part of that area in scenario 2. For the third scenario, the tension with the measurement of $R(D^*)$ is clearly visible; the allowed range includes the SM range and values even further away from the measurement, thereby predicting this effect to vanish completely in the future if this scenario is realized. The value implied by the fit reads $R(D^*)_{\mathrm{Sc.3}} = 0.241 \pm 0.003 \pm 0.007$.

In the second and third plot in this figure we show the corresponding allowed parameter regions in the complex δ^l_{cb} (left) and Δ^l_{cb} (right) planes at 95% CL. Here the strong influence of the leptonic decays becomes visible again, excluding most of the parameter space of $R(D)$ in the δ^l_{cb} plane, and driving the fit far away from the region indicated by the $R(D^*)$ measurement in the Δ^l_{cb} plane. To examine this effect further, we plot the individual constraints in the $\varsigma_l^* \varsigma_{u,d}/M_{H^\pm}^2$ planes in figure 5.2. Here it is seen explicitly that the conflict lies mainly between the leptonic charm decays and $R(D^*)$. It is also noted that, in order to accommodate the data in scenarios 1 and 2, a large value for $|\varsigma_u \varsigma_l^*|/M_{H^\pm}^2 \sim O(10^{-1})$ GeV^{-2} is needed. This is not a direct problem in these scenarios, as the different couplings are not related. It would however point to a very strong hierarchy between the charm and the top couplings or a very large value of the leptonic coupling, as the constraints from observables involving loops like $\mathrm{Br}(Z \to \bar{b}b)$ imply $|\varsigma_u| \lesssim 1$ for the top coupling [25]. In the A2HDM, the combined constraints from leptonic τ decays and these processes require a small value for $|\varsigma_u \varsigma_l^*|/M_{H^\pm}^2$: under the assumptions
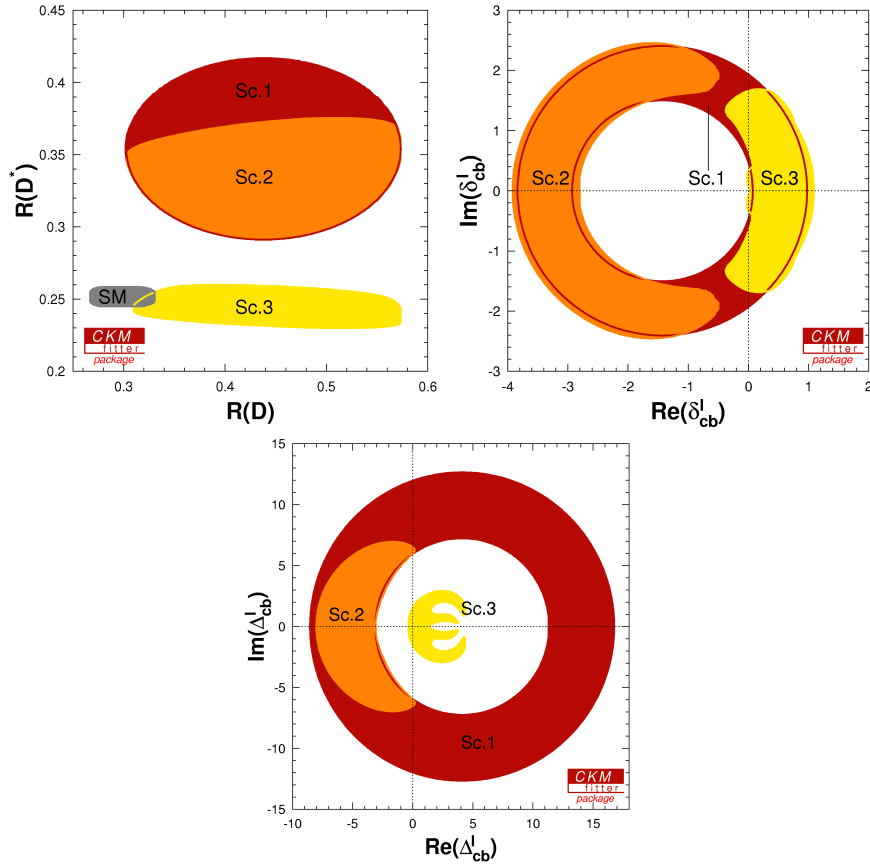
Figure 5.1: *Allowed regions in the $R(D)$–$R(D^*)$ (left), complex δ^l_{cb} (center) and Δ^l_{cb} (right) planes at 95% CL, corresponding to the three different scenarios. See text for details.*

that $|\varsigma_d| < 50$ and the charged-scalar effects dominate the NP contributions to $Z \to b\bar{b}$, $|\varsigma_u\varsigma_l^*|/M_{H^\pm}^2 < 0.005$ GeV^{-2} was obtained in [25]. Similar bounds also arise from considering the CP-violating parameter ϵ_K in K^0–$\bar{K}^0$ mixing and the mass difference Δm_{B^0} in B^0–$\bar{B}^0$ mixing [25]. This is however compatible with our results above, see figure 5.2. As the focus in this article lies on tree-level contributions, and loop induced quantities have a higher UV sensitivity, we refrain from including these constraints explicitly here.

Having in mind the above scenarios, our main concern is whether they can be differentiated with forthcoming data. In addition, the basic assumption of only scalar NP contributions in these decays can be questioned. We identify several combinations of observables which will signal the presence of additional contributions. In the following
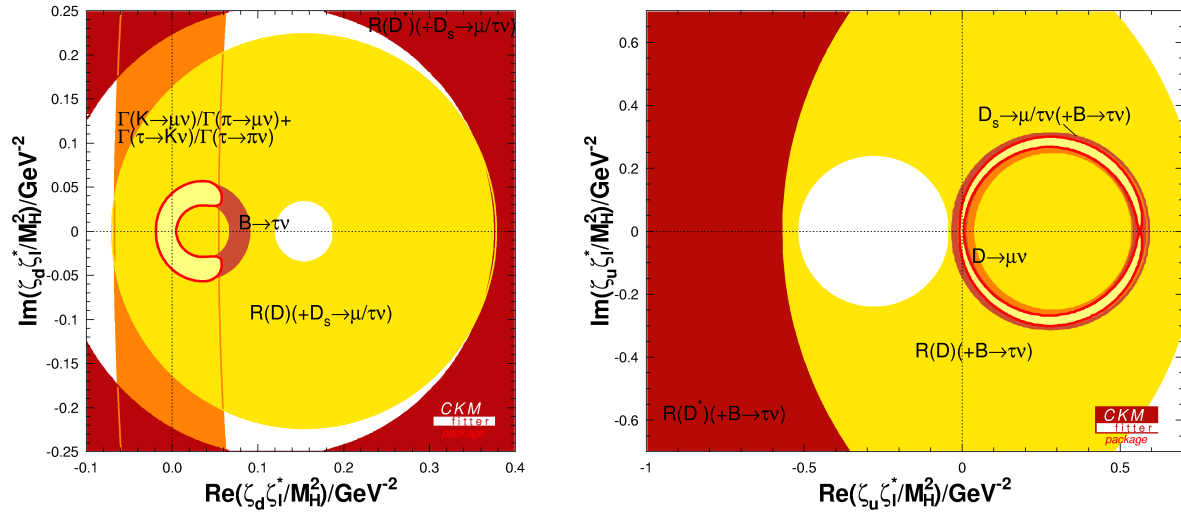
Figure 5.2:   *Constraints in the complex $\varsigma_d\varsigma_l^*/M_{H^\pm}^2$ (left) and $\varsigma_u\varsigma_l^*/M_{H^\pm}^2$ (right) planes, in units of GeV^{-2}, from the various semileptonic and leptonic decays. Allowed regions are shown at 95% CL for different combinations of the observables.*

section we discuss how future measurements of additional observables in $B \to D^{(*)}\tau\nu$ decays, especially their differential distributions, will provide useful information to address these questions.

5.4   Observables sensitive to scalar contributions

We now proceed to analyze the additional observables in $B \to D^{(*)}\tau\nu_\tau$ decays that provide an enhanced sensitivity to scalar NP contributions. Apart from the differential rates, these are the forward-backward and τ-spin asymmetries in the considered decays, and for $B \to D^*\tau\nu$ additionally the longitudinal polarization fraction of the D^*. These observables have been considered in the past by various authors [5, 6, 16, 34, 35, 45–49], addressing their sensitivity to NP contributions.

Experimentally, while one expects more information on $B \to D^{(*)}\tau\nu_\tau$ decays in the near future from Belle, BaBar, and also LHCb, most of these observables will be accessible only at a Super-Flavour factory (SFF) [50,51], as their study requires more statistics than the branching ratios and the inclusion of the information from the correlated B meson. The precise sensitivity of future experiments to the different observables has, however,

Table 5.2: *Predictions for the q^2-integrated observables both within the SM and in the different scenarios. The observables have been integrated from $q^2_{min} = m^2_\tau$ to $q^2_{max} = (m_B - m_{D^{(*)}})^2$. The first error given corresponds to the statistical uncertainty, and the second, when given, to the theoretical one.*

Observable	SM Prediction	Scenario 1	Scenario 2	Scenario 3
$R_L(D^*)$	$0.115 \pm 0.001 \pm 0.003$	0.217 ± 0.026	$0.223^{+0.013}_{-0.026} \pm 0.006$	$0.104^{+0.006}_{-0.003} \pm 0.003$
$A_\lambda(D)$	$-0.304 \pm 0.001 \pm 0.035$	$-0.55^{+0.10}_{-0.04}$	$-0.55^{+0.09}_{-0.04}$	$-0.55^{+0.09}_{-0.04} \pm 0.01$
$A_\lambda(D^*)$	$0.502^{+0.005}_{-0.006} \pm 0.017$	$0.06^{+0.10}_{-0.06}$	$0.04^{+0.10}_{-0.03} \pm 0.01$	$0.57^{+0.04}_{-0.02} \pm 0.02$
$A_\theta(D)$	$0.3602^{+0.0006}_{-0.0007} \pm 0.0022$	$0.03^{+0.01}_{-0.00} \pm 0.30$	$-0.21^{+0.13}_{-0.00} \pm 0.06$	$0.36^{+0.01\,\dagger}_{-0.09}$
$A_\theta(D^*)$	$-0.066 \pm 0.006 \pm 0.009$	$-0.136^{+0.012}_{-0.003} \pm 0.222$	$0.081^{+0.008}_{-0.059} \pm 0.009$	$-0.146^{+0.039}_{-0.017} \pm 0.021$

† Note that the lower tail is rather long, due to a suppressed local maximum.

not yet been determined.

For simplicity, we discuss below these additional observables without considering the subsequent decays of the final τ and D^*. While studying the q^2 spectra of the observables has the advantage in identifying potential NP contributions and their Dirac structure, this generally requires very high statistics, which might not be available even in the early stages of a SFF. Therefore, we shall analyze both the q^2 spectra and the q^2-integrated observables. Our predictions for the latter are given in table 5.2, both within the SM and in the three different scenarios defined before. Note that we do not consider isospin breaking; the observables shown are always isospin-averaged. Note furthermore that model-independent analyses similar to our scenario 1 have been performed in refs. [5,6,16].

5.4.1   The differential decay rates

First, we obtain the singly differential rates by summing in eqs. (5.36) and (5.43) over the τ helicities, $\lambda_\tau = \pm 1/2$, and performing the integration over $\cos\theta$:

$$\frac{d\Gamma(\bar{B} \to D\tau^-\bar{\nu}_\tau)}{dq^2} = \frac{G_F^2 |V_{cb}|^2 |\vec{p}| q^2}{96\pi^3 m_B^2} \left(1 - \frac{m_\tau^2}{q^2}\right)^2 \left[|H_0|^2 \left(1 + \frac{m_\tau^2}{2q^2}\right) + \frac{3m_\tau^2}{2q^2} |H_t|^2 \right] ,$$

$$(5.13)$$

$$\frac{d\Gamma(\bar{B} \to D^*\tau^-\bar{\nu}_\tau)}{dq^2} = \frac{G_F^2 |V_{cb}|^2 |\vec{p}| q^2}{96\pi^3 m_B^2} \left(1 - \frac{m_\tau^2}{q^2}\right)^2 \left[\left(|H_{++}|^2 + |H_{--}|^2 + |H_{00}|^2\right) \left(1 + \frac{m_\tau^2}{2q^2}\right) \right.$$
$$\left. + \frac{3m_\tau^2}{2q^2} |H_{0t}|^2 \right] .$$

$$(5.14)$$

Again, normalizing to the decays with light leptons reduces the theoretical error:

$$R_{D^{(*)}}(q^2) = \frac{d\Gamma(\bar{B} \to D^{(*)}\tau^-\bar{\nu}_\tau)/dq^2}{d\Gamma(\bar{B} \to D^{(*)}\ell^-\bar{\nu}_\ell)/dq^2} .$$

$$(5.15)$$

Note that in order to obtain the expression for $R_{D^{(*)}}$ from this, numerator and denominator have to be integrated separately. This should be kept in mind as well for the other quantities.

Our predictions for these observables, within the SM and in the three different scenarios, are shown in figure 5.3. For $R_D(q^2)$, we show in addition the binned distribution in five equidistant q^2 bins, as the ratio does diverge at the endpoint, where however both rates vanish. From these plots, we make the following observations:

- As expected, the uncertainty due to the hadronic form factors (the grey shaded band) in $R_{D^{(*)}}(q^2)$ is significantly reduced compared to that in the differential branching ratio.

- In scenario 2, relatively large deviations from the SM are predicted for almost the full range in $R_{D^*}(q^2)$ and for high q^2 in $R_D(q^2)$. The predicted q^2 spectra in scenario 3 are close to those of the SM, especially for the D^* decay mode. However, there is still room for differences, especially in $R_D(q^2)$, and furthermore in this scenario the distribution in $R_{D^*}(q^2)$ lies preferably *below* the SM one, which should differentiate this scenario clearly from the first two.
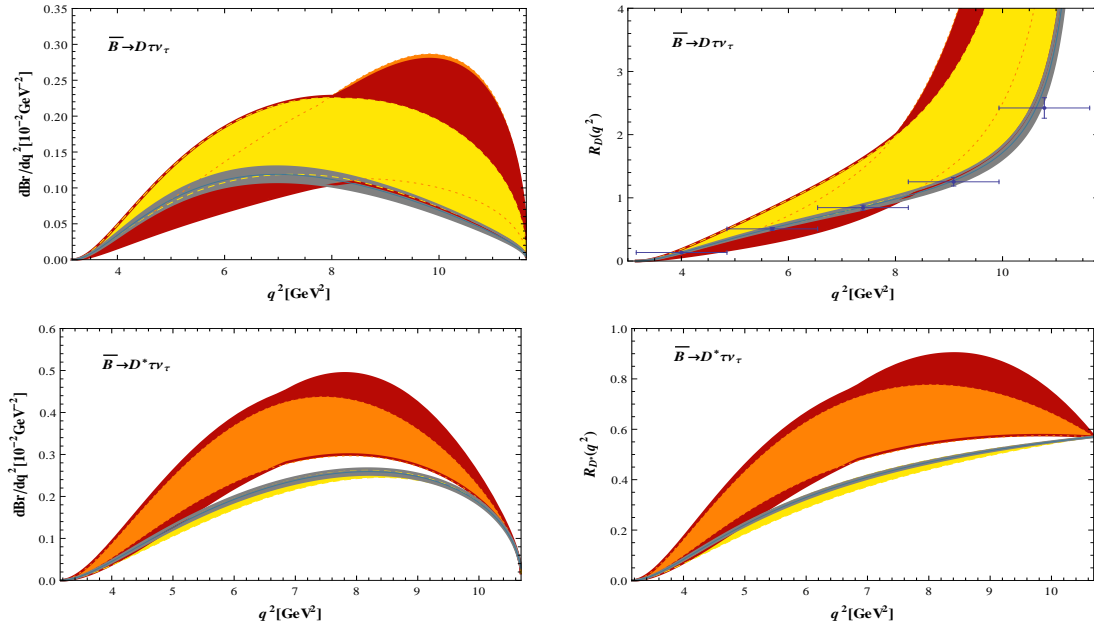
Figure 5.3: *The q^2 dependence of the differential branching ratios (left) and $R_{D^{(*)}}(q^2)$ (right), both within the SM (grey) as well as in scenario 1 (red), scenario 2 (orange), and scenario 3 (yellow). The binned distribution for $R_D(q^2)$ is also shown.*

- Compared to the SM prediction, the peak of the differential branching ratio in the NP scenarios (especially in scenario 2) is shifted to higher and lower values in q^2 for the D and the D^* decay mode, respectively. This is characteristic of scalar NP contributions and should allow for a separation from models with different Dirac structure. The reason for that is the following: while both of them are explicitly proportional to q^2 (see eqs. (5.32) and (5.39)), the charged-scalar contribution to $R_{D^*}(q^2)$ is in addition proportional to the D^* momentum $|\vec{\mathbf{p}}|$, which vanishes at the endpoint $q^2_{\max} = (m_B - m_{D^*})^2$, rendering its relative contribution maximal for intermediate values of q^2, while the one to $R_D(q^2)$ continuously increases with q^2. The relative suppression of the terms proportional to the τ mass by the D^* momentum furthermore renders $R_{D^*}(q^2)$ finite everywhere, while $R_D(q^2)$ diverges at the endpoint.[4] However, as both the rates for the τ and the light lepton modes vanish there, this does not influence the experimental extraction: when calculating

---

[4]In fact, this behavior is an artifact of setting $m_\ell \equiv 0$. The actual value is $\sim m_\tau^2/m_\ell^2$.

the contributions to different bins, all integrals remain finite. These characteristic features are illustrated by the right two plots.

As the charged scalar only contributes to the helicity amplitude H_{0t} in $B \to D^*\tau\nu_\tau$ decays, an increased sensitivity is expected by studying the case with a longitudinally polarized D^* meson in the final state, where the transverse helicity amplitudes are no longer relevant. For this purpose, we define a singly differential longitudinal decay rate [5]:

$$\frac{d\Gamma_\tau^L}{dq^2} = \frac{G_F^2 |V_{cb}| |\vec{\mathbf{p}}| q^2}{96\pi^3 m_B^2} \left(1 - \frac{m_\tau^2}{q^2}\right)^2 \left[|H_{00}|^2 \left(1 + \frac{m_\tau^2}{2q^2}\right) + \frac{3m_\tau^2}{2q^2} |H_{0t}|^2\right]. \tag{5.16}$$

In analogy to $R_{D^*}(q^2)$, it is again advantageous to consider the ratio with the τ mode normalized to the light lepton mode:

$$R_L^*(q^2) = \frac{d\Gamma_\tau^L/dq^2}{d\Gamma_\ell^L/dq^2}. \tag{5.17}$$

It is important, however, to note that within our NP framework this is not an independent observable. As long as we consider only additional scalar operators, the difference

$$X_1(q^2) \equiv R_{D^*}(q^2) - R_L^*(q^2) \tag{5.18}$$

is independent of NP effects. A measurement of this observable serves, therefore, as a cross-check for the effect in R_{D^*} and gives us information on whether scalar NP operators are sufficient to describe the data. This observation is reflected in table 5.2 and in figure 5.4, where we show the predictions for $R_L(D^*)$ and $R_L^*(q^2)$ both within the SM and in the three different scenarios; the results are analogous to the ones for $R(D^*)$ and $R_{D^*}(q^2)$ discussed above, but clearly exhibit an increased sensitivity to the scalar NP effect.

5.4.2   The τ spin asymmetry

Information on the τ spin in semileptonic B-meson decays can be inferred from its distinctive decay patterns [5, 16, 45, 49]. Therefore, we consider here the τ spin asymmetry defined in the τ-$\bar{\nu}_\tau$ center-of-mass frame:

$$A_\lambda^{D^{(*)}}(q^2) = \frac{d\Gamma^{D^{(*)}}[\lambda_\tau = -1/2]/dq^2 - d\Gamma^{D^{(*)}}[\lambda_\tau = +1/2]/dq^2}{d\Gamma^{D^{(*)}}[\lambda_\tau = -1/2]/dq^2 + d\Gamma^{D^{(*)}}[\lambda_\tau = +1/2]/dq^2}, \tag{5.19}$$
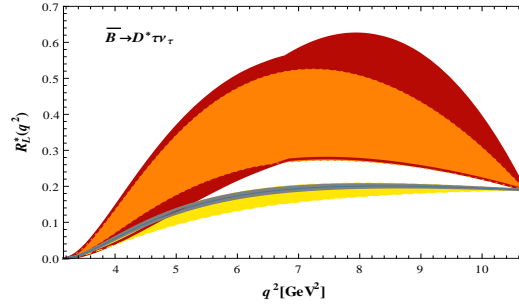
Figure 5.4: *Predictions for $R_L^*(q^2)$ both within the SM and in the three different scenarios. The other captions are the same as in figure 5.3.*

where the polarized differential decay rates are obtained after integration over $\cos\theta$ of the doubly-differential ones given by eqs. (5.36) and (5.43). Using the formulae presented in appendices 5.C and 5.D, we obtain explicitly

$$A_\lambda^D(q^2) = \frac{|H_0|^2 \left(1 - \frac{m_\tau^2}{2q^2}\right) - \frac{3m_\tau^2}{2q^2}|H_t|^2}{|H_0|^2 \left(1 + \frac{m_\tau^2}{2q^2}\right) + \frac{3m_\tau^2}{2q^2}|H_t|^2},$$

$$A_\lambda^{D^*}(q^2) = \frac{\left(|H_{00}|^2 + |H_{++}|^2 + |H_{--}|^2\right)\left(1 - \frac{m_\tau^2}{2q^2}\right) - \frac{3m_\tau^2}{2q^2}|H_{0t}|^2}{\left(|H_{00}|^2 + |H_{++}|^2 + |H_{--}|^2\right)\left(1 + \frac{m_\tau^2}{2q^2}\right) + \frac{3m_\tau^2}{2q^2}|H_{0t}|^2}. \tag{5.20}$$

Again, these two observables have the same dependence on scalar NP contributions as the differential rates; this observation follows from the combinations

$$X_2^D(q^2) \equiv R_D(q^2)\left(A_\lambda^D(q^2) + 1\right) \quad \text{and} \quad X_2^{D^*}(q^2) \equiv R_{D^*}(q^2)\left(A_\lambda^{D^*}(q^2) + 1\right) \tag{5.21}$$

being independent of δ_{cb}^τ and Δ_{cb}^τ, respectively. However, because of the different normalization and systematics in this case, a future measurement would give important information on the size and nature of NP in $B \to D^{(*)}\tau\nu$ decays: like for $X_1(q^2)$, any deviation from the SM value of these combinations would indicate non-scalar NP. Our predictions for the two asymmetries when integrated over q^2 are given again in table 5.2; the predicted ranges for the differential distributions are shown in figure 5.5. The correlation between $A_\lambda(D^*)$ and $R_L(D^*)$, following from eqs. (5.18) and (5.21), is furthermore illustrated in figure 5.6, where we show the predicted values for the two observables for the SM and the three scenarios, yielding in every case a very small band, corresponding to the hadronic uncertainties.
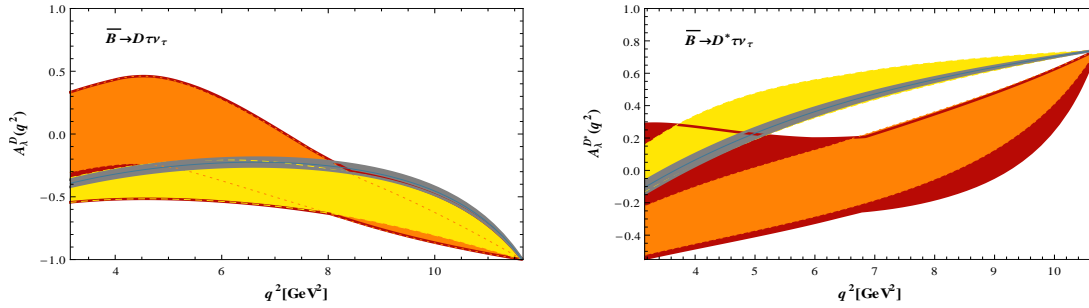
Figure 5.5:   *The q^2 dependence of the τ spin asymmetries $A_\lambda^D(q^2)$ (left) and $A_\lambda^{D^*}(q^2)$ (right). The other captions are the same as in figure 5.3.*
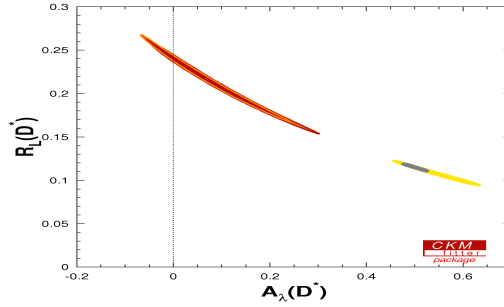

Figure 5.6:   *Predictions for $A_\lambda(D^*)$ vs. $R_L(D^*)$ both within the SM (grey) and in the three scenarios ((1)-red, (2)-orange, (3)-yellow), from a global fit including the appropriate observables.*

The integrated asymmetries span a rather large range. For $A_\lambda(D)$, due to the common input, a differentiation between the different scenarios seems very difficult, while for $A_\lambda(D^*)$ at least the separation of the SM and scenario 3 on the one hand and scenarios 1 and 2 on the other hand is very clear. Importantly, the predictions for $A_\lambda(D)$ in all scenarios are clearly negative, providing another option to potentially exclude the SM and only scalar NP at the same time. Also largely negative values for $A_\lambda(D^*)$ are excluded in all scenarios.

The separation of the different models improves, once differential distributions are considered: from figure 5.5 we observe very distinct patterns for the different scenarios, especially for scenario 2. This scenario will be clearly distinguishable from the SM and scenario 3, once the necessary experimental precision is reached. Scenario 1, on the other hand, has again possibly very large effects, but might be close to any of the other scenarios,

including the SM. A characteristic feature of this observable is the zero-crossing point: for $A_\lambda^D(q^2)$, it is absent for the SM and scenario 3, while it appears likely for scenario 2 to have one, and also scenario 1 has that option. Within the SM, the observable $A_\lambda^{D^*}(q^2)$ crosses the zero at $q^2 = 3.66 \pm 0.04$ GeV^2; compared to the SM case, the zero-crossing point occurs at significantly higher values of q^2 for scenario 2, while most likely at lower values of q^2 for scenario 3. This indicates that measuring the zero-crossing point of the τ spin asymmetries can be a useful probe of the flavour structure of the charged scalar interaction.

5.4.3   The forward-backward asymmetries

Finally, we discuss the forward-backward asymmetries defined as the relative difference between the partial decay rates where the angle θ between the $D^{(*)}$ and τ three-momenta in the τ-$\bar{\nu}_\tau$ center-of-mass frame is greater or smaller than $\pi/2$:

$$A_\theta^{D^{(*)}}(q^2) = \frac{\int_{-1}^0 d\cos\theta \, (d^2\Gamma_\tau^{D^{(*)}}/dq^2 d\cos\theta) - \int_0^1 d\cos\theta \, (d^2\Gamma_\tau^{D^{(*)}}/dq^2 d\cos\theta)}{d\Gamma_\tau^{D^{(*)}}/dq^2} \, . \quad (5.22)$$

Using eqs. (5.36) and (5.43), we arrive at the following explicit expressions:

$$A_\theta^D(q^2) = \frac{3m_\tau^2}{2q^2} \frac{\mathrm{Re}(H_0 H_t^*)}{|H_0|^2 \left(1 + \frac{m_\tau^2}{2q^2}\right) + \frac{3m_\tau^2}{2q^2}|H_t|^2} \, ,$$

$$A_\theta^{D^*}(q^2) = \frac{3}{4} \frac{|H_{++}|^2 - |H_{--}|^2 + 2\frac{m_\tau^2}{q^2}\mathrm{Re}(H_{00}H_{0t}^*)}{(|H_{++}|^2 + |H_{--}|^2 + |H_{00}|^2)\left(1 + \frac{m_\tau^2}{2q^2}\right) + \frac{3m_\tau^2}{2q^2}|H_{0t}|^2} \, . \quad (5.23)$$

In terms of a model-independent determination of NP parameters, *i.e.* scenario 1, this is the key observable to determine Δ_{cb}^τ and δ_{cb}^τ. The reason, as mentioned before, is that the observables $R_L^*(q^2)$, $R_{D^{(*)}}(q^2)$ and $A_\lambda^{D^{(*)}}(q^2)$ do not give independent information, see eqs. (5.18) and (5.21). The forward-backward asymmetry $A_\theta^{D^{(*)}}(q^2)$ is therefore the *only* independent constraint in the complex δ_{cb}^τ (Δ_{cb}^τ) plane. Our predictions for this observable are given in table 5.2 and shown in figure 5.7. Furthermore, its correlation with the τ spin asymmetry for the two modes is shown in the first two panels in figure 5.8. It is clearly seen that the correlation is much weaker in this case, especially in scenario 1, where the only influence stems from the restriction on $|\delta_{cb}^\tau|$ and $|\Delta_{cb}^\tau|$. However, the pattern of a

more SM-like A2HDM prediction and strongly shifted predictions from scenarios 1 and 2 is repeated. Regarding the differential distributions, within the SM, the observable $A_\theta^D(q^2)$ does not cross zero, while this becomes possible for scenarios 1 and 2. $A_\theta^{D^*}(q^2)$ has a zero-crossing point at $q^2 = 5.67 \pm 0.02 \text{ GeV}^2$ in the SM, for which again large shifts are possible with NP, and it might even vanish in scenario 3. Large deviations from the SM expectations, especially in scenario 2, are therefore still possible for this observable.
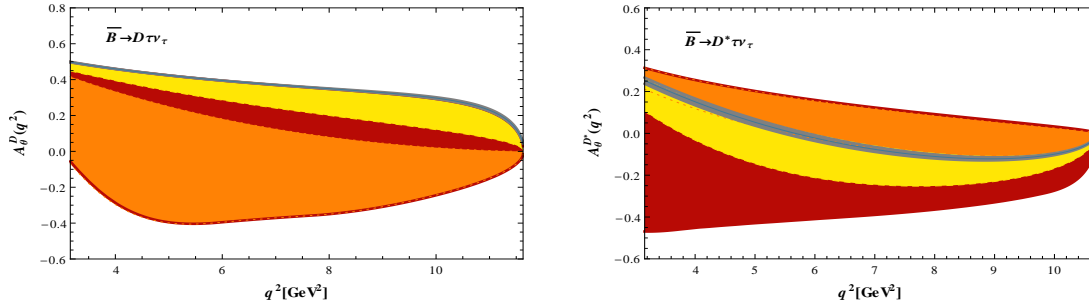

Figure 5.7:   The q^2 dependence of the forward-backward asymmetries $A_\theta^D(q^2)$ (left) and $A_\theta^{D^*}(q^2)$ (right). The other captions are the same as in figure 5.3.

In order to illustrate the impact of a possible future measurement of this observable, we exemplarily show in the right panel in figure 5.8 the resulting constraint in the Δ_{cb}^τ plane, together with the one from $R(D^*)$ as measured at the moment. The $A_\theta(D^*)$ constraints drawn in lighter colours correspond to an uncertainty of 10%. For the darker constraints, an improvement by a factor of 2 has been assumed compared to the lighter ones. Furthermore, an index 'SM' indicates the measurement chosen to be compatible with the SM, while the index 'NP' corresponds to measurements excluding the SM, but compatible with scenario 1. As can be seen, such a measurement would allow to exclude a large part of the parameter space in the model-independent scenario 1, as well as constrain the other scenarios further. Furthermore, as mentioned before, the two constraints could also miss each other in that plane, indicating NP with a different Dirac structure. This possibility exists of course also for the other observables discussed above.

Additional information on Δ_{cb}^τ could obviously be obtained from a measurement of the $B_c^- \to \tau^- \bar\nu_\tau$ rate. With the NP influence being determined by Δ_{cb}^τ, this rate is clearly predicted to be different from the SM in scenarios 1 and 2, while close to the SM in scenario 3. However, this mode is extremely hard to be measured experimentally.
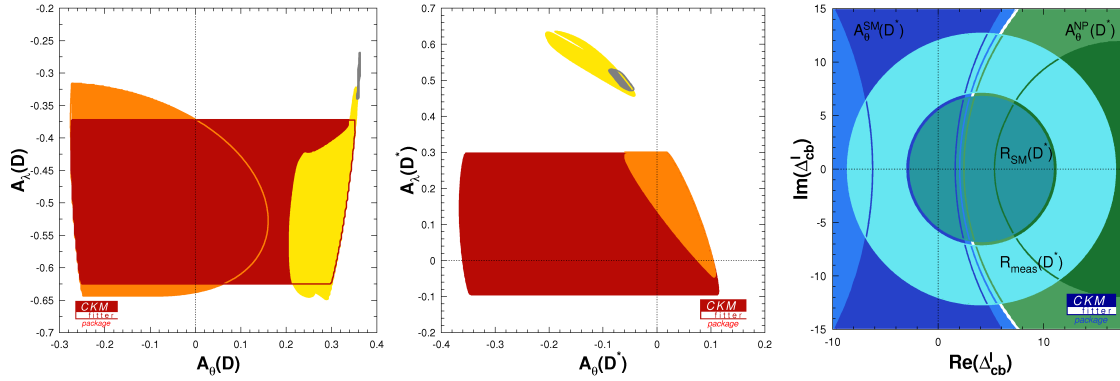
Figure 5.8: *Prediction for $A_\theta(D^{(*)})$ vs. $A_\lambda(D^{(*)})$ for the SM (grey), and the three scenarios ((1)-red, (2)-orange, (3)-yellow), from a global fit including all appropriate observables. The right plot shows the possible impact of future measurements on the complex Δ_{cb}^τ plane (see text).*

5.5   Summary

In this paper, motivated by the recent experimental evidence for an excess of τ-lepton production in exclusive semileptonic B-meson decays, we have performed a detailed phenomenological analysis of $b \to q\,\tau^-\bar\nu_\tau$ ($q = u, c$) transitions within a framework with additional scalar operators, assumed to be generated by the exchange of a charged scalar in the context of 2HDMs.

While the usual Type-II scenario cannot accommodate the recent BaBar data on $\bar B \to D^{(*)}\tau^-\bar\nu_\tau$ decays, this is possible within more general models, in which the charged-scalar couplings to up-type quarks are not as suppressed. An explicit example is given by the A2HDM, in which the $\bar B \to D^{(*)}\tau^-\nu_\tau$ as well as the $B^- \to \tau^-\bar\nu_\tau$ data can be fitted. However, the resulting parameter ranges are in conflict with the constraints from leptonic charm decays, which could indicate a departure from the family universality of the Yukawa couplings ς_f ($f = u, d, l$).

These observations led us to define three scenarios for scalar NP, in which we incorporated information from $R(D^{(*)})$ (Sc.1), B decays (Sc.2), and all available data from leptonic and semileptonic decays apart from $R(D^*)$ (Sc.3). We showed that these scenarios can be differentiated by coming data, using information e.g. from differential decay rates and/or spin and angular asymmetries. These observables therefore allow to verify this hint for NP in semileptonic decays, and gather additional information on its precise

nature. Furthermore we pointed out several combinations of observables independent of this kind of NP, as well as common characteristics, which will allow additionally to test for the presence of NP with other Dirac structures. The coming experimental analyses for these modes will therefore be an important step in our quest for NP.

Acknowledgements

Appendix

5.A   Input parameters and statistical treatment

Bounds on the parameter space are obtained using the statistical treatment based on frequentist statistics and Rfit for the theoretical uncertainties [52], which has been implemented in the CKMfitter package [12]. To fix the values of the relevant CKM entries, we only use determinations that are not sensitive to the scalar NP contributions [12,53–55]. Explicitly, we use the V_{ud} value extracted from super-allowed nuclear β decays and the CKM unitarity to determine $V_{us} \equiv \lambda$. The values of $|V_{ub}|$ and $|V_{cb}|$ are determined from exclusive and inclusive $b \to u\ell\bar{\nu}_\ell$ and $b \to c\ell\bar{\nu}_\ell$ transitions, respectively. Relevant hadronic input parameters are collected in table 5.3, while quark and meson masses as well as any other relevant parameters that do not appear in this table are taken from [11].

Table 5.3: *Input values for the hadronic parameters, obtained as described in the text. The first error denotes the statistical uncertainty, and the second the systematic/theoretical.* [†]*This value includes the correction to the isospin limit usually assumed in lattice calculations [56,69].*

Parameter	Value	Comment
f_{B_s}	$(0.228 \pm 0.001 \pm 0.006)$ GeV	[57–59]
f_{B_s}/f_{B_d}	$1.198 \pm 0.009 \pm 0.025$	[57, 58, 60]
f_{D_s}	$(0.249 \pm 0.001 \pm 0.004)$ GeV	[57, 58, 60, 61]
f_{D_s}/f_{D_d}	$1.169 \pm 0.006 \pm 0.02$	[57, 58, 60–62]
f_K/f_π	$1.1908 \pm 0.0016 \pm 0.0104^\dagger$	[62–64]
$\delta_{\text{em}}^{K\ell2/\pi\ell2}$	-0.0069 ± 0.0017	[65–69]
$\delta_{\text{em}}^{\tau K2/\tau\pi2}$	0.0005 ± 0.0053	[70–72]
λ	0.2254 ± 0.0010	[73]
$|V_{ub}|$	$(3.51 \pm 0.11 \pm 0.02) \times 10^{-3}$	[55]
$|V_{cb}|$	$(40.9 \pm 1.1) \times 10^{-3}$	[55]
ρ_1^2	$1.186 \pm 0.036 \pm 0.041$	[55]
$G_1(1)|V_{cb}|$	$(42.64 \pm 1.53) \times 10^{-3}$	[55]
$\Delta|_{B \to Dl\nu}$	0.46 ± 0.02	[7, 17, 31]
$h_{A_1}(1)|V_{cb}|$	$(35.90 \pm 0.45) \times 10^{-3}$	[55]
$R_1(1)$	1.403 ± 0.033	[55]
$R_2(1)$	0.854 ± 0.020	[55]
$R_3(1)$	0.97 ± 0.10	[36]
ρ^2	1.207 ± 0.026	[55]

The plots for the differential observables are obtained using the allowed NP parameter ranges from a different fit. As the latter already include uncertainties from the hadronic input parameters, we do not vary them again additionally.

5.B   Kinematics for semileptonic decays

Within the SM, the squared matrix element for the decay $\bar{B}(p_B) \to D^{(*)}(p_{D^{(*)}}, \lambda_{D^{(*)}})l(k_l, \lambda_l)\bar{\nu}(k_{\bar{\nu}})$ can be written as [34, 35]

$$|\mathcal{M}(\bar{B} \to D^{(*)}l\bar{\nu})|^2 = |\langle D^{(*)}l\bar{\nu}|\mathcal{L}_{\text{eff}}|\bar{B}\rangle|^2 = L_{\mu\nu}H^{\mu\nu} , \qquad (5.24)$$

where the leptonic ($L_{\mu\nu}$) and hadronic ($H^{\mu\nu}$) tensors are built from the respective tensor products of the lepton and hadron currents. Using the completeness relation for the virtual W^* polarization vectors $\bar{\epsilon}_\mu(\pm, 0, t)$, one can further express eq. (5.24) as

$$|\mathcal{M}(\bar{B} \to D^{(*)}l\bar{\nu})|^2 = \sum_{m,m',n,n'} L(m,n)H(m',n')\, g_{mm'}g_{nn'} , \qquad (5.25)$$

where $g_{mm'} = \text{diag}(+1, -1, -1, -1)$, $L(m,n) = L^{\mu\nu}\,\bar{\epsilon}_\mu(m)\bar{\epsilon}^*_\nu(n)$ and $H(m,n) = H^{\mu\nu}\,\bar{\epsilon}^*_\mu(m)\bar{\epsilon}_\nu(n)$. The two quantities $L(m,n)$ and $H(m,n)$ are Lorentz invariant and can, therefore, be evaluated in different reference frames. For convenience, the hadronic part $H(m,n)$ is usually evaluated in the B-meson rest frame with the z axis along the $D^{(*)}$ trajectory, and $L(m,n)$ in the l-$\bar{\nu}$ center-of-mass frame (*i.e.* in the virtual W^* rest frame) [34, 35].

In the B-meson rest frame with the z axis along the $D^{(*)}$ trajectory, a suitable basis for the virtual W^* polarization vectors $\bar{\epsilon}_\mu(\pm, 0, t)$ can be chosen as [34]

$$\bar{\epsilon}_\mu(\pm) = \frac{1}{\sqrt{2}}\,(0, \pm 1, -i, 0), \qquad \bar{\epsilon}_\mu(0) = \frac{1}{\sqrt{q^2}}\,(|\vec{\mathbf{p}}|, 0, 0, -q_0),$$

$$\bar{\epsilon}_\mu(t) = \frac{1}{\sqrt{q^2}}\,(q_0, 0, 0, -|\vec{\mathbf{p}}|), \qquad (5.26)$$

where $q_0 = (m_B^2 - m_{D^{(*)}}^2 + q^2)/2m_B$ and $|\vec{\mathbf{p}}| = \lambda^{1/2}(m_B^2, m_{D^{(*)}}^2, q^2)/2m_B$ are the energy and momentum of the virtual W^*, with $q^2 = (p_B - p_{D^{(*)}})^2$ being the momentum transfer squared, bounded at $m_l^2 \leq q^2 \leq (m_B - m_{D^{(*)}})^2$, and $\lambda(a, b, c) = a^2 + b^2 + c^2 - 2(ab + bc + ca)$. Similarly, a convenient basis for the D^* polarization vectors is

$$\epsilon_\alpha(\pm) = \mp\frac{1}{\sqrt{2}}\,(0, 1, \pm i, 0), \qquad \epsilon_\alpha(0) = \frac{1}{m_{D^*}}\,(|\vec{\mathbf{p}}|, 0, 0, E_{D^*}), \qquad (5.27)$$

where $E_{D^{(*)}} = (m_B^2 + m_{D^{(*)}}^2 - q^2)/2m_B$ is the $D^{(*)}$ energy in the B-meson rest frame.

In the l-$\bar{\nu}$ center-of-mass frame, which can be obtained by a simple boost from the B-meson rest frame, the lepton and antineutrino four-momenta are given, respectively, as

$$k_l = (E_l, p_l \sin\theta, 0, p_l \cos\theta)\,, \qquad k_{\bar{\nu}} = (p_l, -p_l \sin\theta, 0, -p_l \cos\theta)\,, \tag{5.28}$$

where $E_l = (q^2 + m_l^2)/2\sqrt{q^2}$, $p_l = (q^2 - m_l^2)/2\sqrt{q^2}$, and θ is the angle between the $D^{(*)}$ and l three-momenta in this frame. The virtual W^* polarization vectors $\bar{\epsilon}_\mu(\pm, 0, t)$ reduce to [34, 35]

$$\bar{\epsilon}_\mu(\pm) = \frac{1}{\sqrt{2}}(0, \pm 1, -i, 0)\,, \qquad \bar{\epsilon}_\mu(0) = (0, 0, 0, -1)\,,$$

$$\bar{\epsilon}_\mu(t) = \frac{1}{\sqrt{q^2}}q_\mu = (1, 0, 0, 0)\,. \tag{5.29}$$

With the above specified kinematics, the explicit expression for $L_{\mu\nu}H^{\mu\nu}$ in terms of the q^2 dependent helicity amplitudes can be found in refs. [5, 34]. Using the equations of motion, the hadronic and leptonic amplitudes of the scalar and the pseudoscalar current can be related to those of the vector and the axial-vector current, respectively. Therefore, the scalar NP contributions can be considered together with the spin-zero component ($\lambda_{W^*} = t$) of the virtual W^* exchange.

5.C   Formulae for $\bar{B} \to Dl\bar{\nu}$

In the presence of NP of the form (5.2), the non-zero hadronic matrix elements of the $\bar{B} \to D$ transition can be parametrized as

$$\langle D(p_D)|\bar{c}\gamma^\mu b|\bar{B}(p_B)\rangle = f_+(q^2)\left[(p_B + p_D)^\mu - \frac{m_B^2 - m_D^2}{q^2}q^\mu\right] + f_0(q^2)\frac{m_B^2 - m_D^2}{q^2}q^\mu\,,$$

$$\tag{5.30}$$

$$\langle D(p_D)|\bar{c}\,b|\bar{B}(p_B)\rangle = \frac{q_\mu}{\overline{m}_b - \overline{m}_c}\langle D(p_D)|\bar{c}\gamma^\mu b|\bar{B}(p_B)\rangle = \frac{m_B^2 - m_D^2}{\overline{m}_b - \overline{m}_c}f_0(q^2)\,, \tag{5.31}$$

where $\overline{m}_q$ are the running quark masses and the two QCD form factors $f_+(q^2)$ and $f_0(q^2)$ encode the strong-interaction dynamics. Contracting the above matrix elements with the virtual W^* polarization vectors (5.26) in the B-meson rest frame, we obtain the two non-vanishing helicity amplitudes [5, 34]:

$$H_0(q^2) = \frac{2m_B|\vec{\mathbf{p}}|}{\sqrt{q^2}}f_+(q^2)\,,$$

$$H_t(q^2) = \frac{m_B^2 - m_D^2}{\sqrt{q^2}}f_0(q^2)\left[1 + \delta_{cb}^l \frac{q^2}{(m_B - m_D)^2}\right]\,, \tag{5.32}$$

where δ^l_{cb}, defined by eq. (5.6), accounts for the contribution from the charged scalar.

It is customary to relate the QCD form factors $f_+(q^2)$ and $f_0(q^2)$ to the quantities $G_1(w)$ and $\Delta(w)$ in the HQET [36]

$$f_+(q^2) \; = \; \frac{G_1(w)}{R_D} \,, \qquad f_0(q^2) \; = \; R_D \, \frac{(1+w)}{2} \, G_1(w) \, \frac{1+r}{1-r} \, \Delta(w) \,, \qquad (5.33)$$

where $R_{D^{(*)}} \; = \; 2\sqrt{m_B m_{D^{(*)}}}/(m_B + m_{D^{(*)}})$, $r \; = \; m_{D^{(*)}}/m_B$, and the new kinematical variable w is defined as

$$w \; = \; v_B \cdot v_{D^{(*)}} \; = \; \frac{m_B^2 + m_{D^{(*)}}^2 - q^2}{2m_B m_{D^{(*)}}} \,, \qquad (5.34)$$

with v_B and $v_{D^{(*)}}$ being the four-velocities of the B and $D^{(*)}$ mesons, respectively. We approximate the scalar density $\Delta(w)$ by a constant value $\Delta(w) = 0.46 \pm 0.02$ [7, 17, 31] and $G(w)$ is parametrized in terms of the normalization $G_1(1)$ and the slope ρ_1^2 as [74]

$$G_1(w) \; = \; G_1(1) \left[1 - 8\rho_1^2 \, z(w) + (51\rho_1^2 - 10) \, z(w)^2 - (252\rho_1^2 - 84) \, z(w)^3 \right] \,, \qquad (5.35)$$

with $z(w) = (\sqrt{w+1} - \sqrt{2})/(\sqrt{w+1} + \sqrt{2})$.

Equipped with the above information, the double differential decay rates for $\bar{B} \to Dl\bar{\nu}$, with l in a given helicity state ($\lambda_l = \pm 1/2$), can be written as

$$\frac{d^2\Gamma^D[\lambda_l = -1/2]}{dq^2 d\cos\theta} \; = \; \frac{G_F^2 |V_{cb}|^2 q^2}{128\pi^3 m_B^2} \left(1 - \frac{m_l^2}{q^2} \right)^2 |\vec{p}| \, |H_0(q^2)|^2 \, \sin^2\theta \,,$$

$$\frac{d^2\Gamma^D[\lambda_l = +1/2]}{dq^2 d\cos\theta} \; = \; \frac{G_F^2 |V_{cb}|^2 q^2}{128\pi^3 m_B^2} \left(1 - \frac{m_l^2}{q^2} \right)^2 |\vec{p}| \, \frac{m_l^2}{q^2} \, |H_0(q^2)\cos\theta - H_t(q^2)|^2 \, (5.36)$$

from which the total decay rate and the various q^2-dependent observables can be obtained via summation over λ_l and/or integration over $\cos\theta$. Owing to its lepton-mass suppression, the $\lambda_l = +1/2$ helicity amplitude is only relevant for the τ decay mode.

5.D   Formulae for $\bar{B} \to D^* l \bar{\nu}$

For the $\bar{B} \to D^*$ transition, the hadronic matrix elements of the vector and axial-vector currents are described by four QCD form factors $V(q^2)$ and $A_{0,1,2}(q^2)$ via

$$\langle D^*(p_{D^*}, \epsilon^*)|\bar{c}\gamma_\mu b|\bar{B}(p_B)\rangle = \frac{2iV(q^2)}{m_B + m_{D^*}} \epsilon_{\mu\nu\alpha\beta} \epsilon^{*\nu} p_B^\alpha p_{D^*}^\beta,$$

$$\langle D^*(p_{D^*}, \epsilon^*)|\bar{c}\gamma_\mu\gamma_5 b|\bar{B}(p_B)\rangle = 2m_{D^*} A_0(q^2) \frac{\epsilon^* \cdot q}{q^2} q_\mu + (m_B + m_{D^*}) A_1(q^2) \left(\epsilon_\mu^* - \frac{\epsilon^* \cdot q}{q^2} q_\mu \right)$$

$$- A_2(q^2) \frac{\epsilon^* \cdot q}{m_B + m_{D^*}} \left[(p_B + p_{D^*})_\mu - \frac{m_B^2 - m_{D^*}^2}{q^2} q_\mu \right],$$

$$(5.37)$$

from which one can show that, using the equations of motion, the $\bar{B} \to D^*$ matrix element for the scalar current vanishes while the pseudoscalar one reduces to

$$\langle D^*(p_{D^*}, \epsilon^*)|\bar{c}\gamma_5 b|\bar{B}(p_B)\rangle = -\frac{q_\mu}{\overline{m}_b + \overline{m}_c} \langle D^*(p_{D^*}, \epsilon^*)|\bar{c}\gamma^\mu\gamma_5 b|\bar{B}(p_B)\rangle$$

$$= -\frac{2m_{D^*}}{\overline{m}_b + \overline{m}_c} A_0(q^2) \epsilon^* \cdot q. \qquad (5.38)$$

Contracting the above matrix elements with the W^* and D^* polarization vectors in eqs. (5.26) and (5.27), we obtain the four non-vanishing helicity amplitudes [5,34]:

$$H_{\pm\pm}(q^2) = (m_B + m_{D^*}) A_1(q^2) \mp \frac{2m_B}{m_B + m_{D^*}} |\vec{p}| V(q^2),$$

$$H_{00}(q^2) = \frac{1}{2m_{D^*}\sqrt{q^2}} \left[(m_B^2 - m_{D^*}^2 - q^2)(m_B + m_{D^*}) A_1(q^2) - \frac{4m_B^2 |\vec{p}|^2}{m_B + m_{D^*}} A_2(q^2) \right],$$

$$H_{0t}(q^2) = \frac{2m_B|\vec{p}|}{\sqrt{q^2}} A_0(q^2) \left(1 - \Delta_{cb}^l \frac{q^2}{m_B^2} \right), \qquad (5.39)$$

where Δ_{cb}^l, defined by eq. (5.4), accounts for the contribution from the charged scalar.

In the heavy-quark limit for the b and c quarks, the four QCD form factors $V(q^2)$

and $A_{0,1,2}(q^2)$ are related to the universal HQET form factor $h_{A_1}(w)$ via [74]

$$
\begin{aligned}
V(q^2) &= \frac{R_1(w)}{R_{D^*}} h_{A_1}(w)\,, \\
A_0(q^2) &= \frac{R_0(w)}{R_{D^*}} h_{A_1}(w)\,, \\
A_1(q^2) &= R_{D^*} \frac{w+1}{2} h_{A_1}(w)\,, \\
A_2(q^2) &= \frac{R_2(w)}{R_{D^*}} h_{A_1}(w)\,,
\end{aligned}
\tag{5.40}
$$

where the w dependence of $h_{A_1}(w)$ and the three ratios $R_{0,1,2}(w)$ reads [74]

$$
\begin{aligned}
h_{A_1}(w) &= h_{A_1}(1)\left[1 - 8\rho^2 z(w) + (53\rho^2 - 15)\, z(w)^2 - (231\rho^2 - 91)\, z(w)^3\right], \\
R_0(w) &= R_0(1) - 0.11(w-1) + 0.01(w-1)^2\,, \\
R_1(w) &= R_1(1) - 0.12(w-1) + 0.05(w-1)^2\,, \\
R_2(w) &= R_2(1) - 0.11(w-1) - 0.06(w-1)^2\,.
\end{aligned}
\tag{5.41}
$$

The free parameters ρ^2, $R_1(1)$ and $R_2(1)$ are determined from the well-measured $\bar{B} \to D^*\ell\bar\nu$ decay distributions [55] ($\ell = e, \mu$), whereas for the parameter $R_0(1)$, that appears only in the helicity-suppressed amplitude H_{0t}, we have to rely on the HQET prediction for the linear combination [36],

$$
R_3(1) = \frac{R_2(1)(1-r) + r\left[R_0(1)(1+r) - 2\right]}{(1-r)^2} = 0.97 \pm 0.10\,,
\tag{5.42}
$$

which includes the leading-order perturbative (in α_s) and power ($1/m_{b,c}$) corrections to the heavy-quark limit, plus a conservative 10% uncertainty to account for higher-order contributions [5].

Finally, the double differential decay rates for $\bar{B} \to D^*l\bar\nu$, with l in a given helicity state ($\lambda_l = \pm 1/2$), can be written as

$$
\begin{aligned}
\frac{d^2\Gamma^{D^*}[\lambda_l = -1/2]}{dq^2\, d\cos\theta} &= \frac{G_F^2 |V_{cb}|^2 |\vec{\mathbf{p}}| q^2}{256\pi^3 m_B^2}\left(1 - \frac{m_l^2}{q^2}\right)^2 \\
&\quad \times \left[(1 - \cos\theta)^2 |H_{++}|^2 + (1 + \cos\theta)^2 |H_{--}|^2 + 2\sin^2\theta\, |H_{00}|^2\right]\,, \\[2mm]
\frac{d^2\Gamma^{D^*}[\lambda_l = +1/2]}{dq^2\, d\cos\theta} &= \frac{G_F^2 |V_{cb}|^2 |\vec{\mathbf{p}}| q^2}{256\pi^3 m_B^2}\left(1 - \frac{m_l^2}{q^2}\right)^2 \frac{m_l^2}{q^2} \\
&\quad \times \left[\sin^2\theta\, (|H_{++}|^2 + |H_{--}|^2) + 2\,|H_{0t} - H_{00}\cos\theta|^2\right]\,,
\end{aligned}
\tag{5.43}
$$

which are the starting point for the total decay rate, as well as the additional observables considered.

Bibliography

[1] J. P. Lees *et al.* [BaBar Collaboration], Phys. Rev. Lett. **109** (2012) 101802 [arXiv:1205.5442 [hep-ex]].

[2] I. Adachi *et al.* [Belle Collaboration], arXiv:0910.4301 [hep-ex].

[3] A. Bozek *et al.* [Belle Collaboration], Phys. Rev. D **82** (2010) 072005 [arXiv:1005.2302 [hep-ex]].

[4] S. Fajfer, J. F. Kamenik, I. Nisandzic and J. Zupan, Phys. Rev. Lett. **109** (2012) 161801 [arXiv:1206.1872 [hep-ph]].

[5] S. Fajfer, J. F. Kamenik and I. Nisandzic, Phys. Rev. D **85** (2012) 094025 [arXiv:1203.2654 [hep-ph]].

[6] Y. Sakaki and H. Tanaka, arXiv:1205.4908 [hep-ph].

[7] D. Becirevic, N. Kosnik and A. Tayduganov, Phys. Lett. B **716** (2012) 208 [arXiv:1206.4977 [hep-ph]].

[8] B. Aubert *et al.* [BABAR Collaboration], Phys. Rev. D **81** (2010) 051101 [arXiv:0912.2453 [hep-ex]].

[9] J. P. Lees *et al.* [BABAR Collaboration], arXiv:1207.0698 [hep-ex].

[10] K. Hara *et al.* [Belle Collaboration], Phys. Rev. D **82** (2010) 071101 [arXiv:1006.4201 [hep-ex]].

[11] J. Beringer *et al.* [Particle Data Group Collaboration], Phys. Rev. D **86** (2012) 010001.

[12] J. Charles *et al.* [CKMfitter Group Collaboration], Eur. Phys. J. C **41** (2005) 1 [hep-ph/0406184], updated results and plots available at: http://ckmfitter.in2p3.fr.

[13] N. Cabibbo, Phys. Rev. Lett. **10** (1963) 531; M. Kobayashi, T. Maskawa, Prog. Theor. Phys. **49** (1973) 652.

[14] I. Adachi *et al.* [Belle Collaboration], arXiv:1208.4678 [hep-ex].

[15] A. Crivellin, C. Greub and A. Kokulu, Phys. Rev. D **86** (2012) 054014 [arXiv:1206.2634 [hep-ph]].

[16] A. Datta, M. Duraisamy and D. Ghosh, Phys. Rev. D **86** (2012) 034027 [arXiv:1206.3760 [hep-ph]].

[17] J. A. Bailey, A. Bazavov, C. Bernard, C. M. Bouchard, C. DeTar, D. Du, A. X. El-Khadra and J. Foley *et al.*, Phys. Rev. Lett. **109** (2012) 071802 [arXiv:1206.4992 [hep-ph]].

[18] R. N. Faustov and V. O. Galkin, Mod. Phys. Lett. **A27** (2012) 1250183 [arXiv:1207.5973 [hep-ph]].

[19] N. G. Deshpande and A. Menon, arXiv:1208.4134 [hep-ph].

[20] D. Choudhury, D. K. Ghosh and A. Kundu, arXiv:1210.5076 [hep-ph].

[21] For a review, see for example: G. C. Branco, P. M. Ferreira, L. Lavoura, M. N. Rebelo, M. Sher, J. P. Silva, Phys. Rept. **516** (2012) 1 [arXiv:1106.0034 [hep-ph]]; J. F. Gunion, H. E. Haber, G. L. Kane, S. Dawson, Front. Phys. **80** (2000) 1.

[22] A. Pich, P. Tuzón, Phys. Rev. D **80** (2009) 091702 [arXiv:0908.1554 [hep-ph]].

[23] X. -G. He and G. Valencia, arXiv:1211.0348 [hep-ph].

[24] A. Pich, Nucl. Phys. Proc. Suppl. **209** (2010) 182 [arXiv:1010.5217 [hep-ph]].

[25] M. Jung, A. Pich, P. Tuzón, JHEP **1011** (2010) 003 [arXiv:1006.0470 [hep-ph]].

[26] M. Jung, A. Pich, P. Tuzón, Phys. Rev. D **83** (2011) 074011 [arXiv:1011.5154 [hep-ph]].

[27] M. Jung, X. -Q. Li and A. Pich, JHEP **1210** (2012) 063 [arXiv:1208.1251 [hep-ph]].

[28] W. -S. Hou, Phys. Rev. D **48** (1993) 2342.

[29] J. F. Kamenik and F. Mescia, Phys. Rev. D **78** (2008) 014003 [arXiv:0802.3790 [hep-ph]].

[30] O. Deschamps, S. Descotes-Genon, S. Monteil, V. Niess, S. T'Jampens and V. Tisserand, Phys. Rev. D **82** (2010) 073012 [arXiv:0907.5135 [hep-ph]].

[31] G. M. de Divitiis, R. Petronzio and N. Tantalo, JHEP **0710** (2007) 062 [arXiv:0707.0587 [hep-lat]].

[32] K. Azizi, Nucl. Phys. B **801** (2008) 70 [arXiv:0805.2802 [hep-ph]].

[33] S. Faller, A. Khodjamirian, C. Klein and T. Mannel, Eur. Phys. J. C **60** (2009) 603 [arXiv:0809.0222 [hep-ph]].

[34] J. G. Korner and G. A. Schuler, Z. Phys. C **46** (1990) 93, ibid. C **38** (1988) 511 [Erratum-ibid. C **41** (1989) 690].

[35] K. Hagiwara, A. D. Martin and M. F. Wade, Phys. Lett. B **228** (1989) 144, Nucl. Phys. B **327** (1989) 569.

[36] A. F. Falk and M. Neubert, Phys. Rev. D **47** (1993) 2965 [hep-ph/9209268], Phys. Rev. D **47** (1993) 2982 [hep-ph/9209269], M. Neubert, Phys. Rev. D **46** (1992) 2212.

[37] T. Hermann, M. Misiak and M. Steinhauser, arXiv:1208.2788 [hep-ph].

[38] [LEP Higgs Working Group for Higgs boson searches and ALEPH and DELPHI and L3 and OPAL Collaborations], hep-ex/0107031.

[39] A. Abulencia *et al.* [CDF Collaboration], Phys. Rev. Lett. **96** (2006) 042003 [hep-ex/0510065].

[40] V. M. Abazov *et al.* [D0 Collaboration], Phys. Lett. B **682** (2009) 278 [arXiv:0908.1811 [hep-ex]].

[41] G. Aad *et al.* [ATLAS Collaboration], JHEP **1206** (2012) 039 [arXiv:1204.2760 [hep-ex]].

[42] S. Chatrchyan *et al.* [CMS Collaboration], JHEP **1207** (2012) 143 [arXiv:1205.5736 [hep-ex]].

[43] M. -Z. Wang [Belle Collaboration], "Charm Decays at Belle", talk given at ICHEP 2012, Melbourne, Australia, July 4-11th, 2012.

[44] G. Rong, arXiv:1209.0085 [hep-ex].

[45] M. Tanaka, Z. Phys. C **67** (1995) 321 [hep-ph/9411405].

[46] C. -H. Chen and C. -Q. Geng, Phys. Rev. D **71** (2005) 077501 [hep-ph/0503123].

[47] C. -H. Chen and C. -Q. Geng, JHEP **0610** (2006) 053 [hep-ph/0608166].

[48] U. Nierste, S. Trine and S. Westhoff, Phys. Rev. D **78** (2008) 015006 [arXiv:0801.4938 [hep-ph]].

[49] M. Tanaka and R. Watanabe, Phys. Rev. D **82** (2010) 034027 [arXiv:1005.4306 [hep-ph]].

[50] T. Aushev *et al.*, arXiv:1002.5012 [hep-ex].

[51] B. O'Leary *et al.* [SuperB Collaboration], arXiv:1008.1541 [hep-ex].

[52] A. Hocker, H. Lacker, S. Laplace and F. Le Diberder, Eur. Phys. J. C **21** (2001) 225 [hep-ph/0104062].

[53] M. Bona *et al.* [UTfit Collaboration], JHEP **0507** (2005) 028 [hep-ph/0501199].

[54] M. Antonelli *et al.*, Phys. Rept. **494** (2010) 197 [arXiv:0907.5386 [hep-ph]].

[55] Y. Amhis *et al.* [Heavy Flavor Averaging Group Collaboration], arXiv:1207.1158 [hep-ex], and online update at http://www.slac.stanford.edu/xorg/hfag.

[56] V. Cirigliano and H. Neufeld, Phys. Lett. B **700** (2011) 7 [arXiv:1102.0563 [hep-ph]].

[57] A. Bazavov *et al.* [Fermilab Lattice and MILC Collaboration], Phys. Rev. D **85** (2012) 114506 [arXiv:1112.3051 [hep-lat]].

[58] H. Na, C. J. Monahan, C. T. H. Davies, R. Horgan, G. P. Lepage and J. Shigemitsu, Phys. Rev. **D86** (2012) 034506 [arXiv:1202.4914 [hep-lat]].

[59] C. McNeile, C. T. H. Davies, E. Follana, K. Hornbostel and G. P. Lepage, Phys. Rev. D **85** (2012) 031503 [arXiv:1110.4510 [hep-lat]].

[60] C. Albertus *et al.*, Phys. Rev. D **82** (2010) 014505 [arXiv:1001.2023 [hep-lat]].

[61] C. T. H. Davies, C. McNeile, E. Follana, G. P. Lepage, H. Na and J. Shigemitsu, Phys. Rev. D **82** (2010) 114504 [arXiv:1008.4018 [hep-lat]].

[62] E. Follana *et al.* [HPQCD and UKQCD Collaborations], Phys. Rev. Lett. **100** (2008) 062002 [arXiv:0706.1726 [hep-lat]].

[63] C. Bernard, C. E. DeTar, L. Levkova, S. Gottlieb, U. M. Heller, J. E. Hetrick, J. Osborn and D. B. Renner *et al.*, PoS LAT **2007** (2007) 090 [arXiv:0710.1118 [hep-lat]].

[64] S. Durr, Z. Fodor, C. Hoelbling, S. D. Katz, S. Krieg, T. Kurth, L. Lellouch and T. Lippert *et al.*, Phys. Rev. D **81** (2010) 054507 [arXiv:1001.4692 [hep-lat]].

[65] W. J. Marciano, Phys. Rev. Lett. **93** (2004) 231803 [hep-ph/0402299].

[66] V. Cirigliano and I. Rosell, JHEP **0710** (2007) 005 [arXiv:0707.4464 [hep-ph]].

[67] V. Cirigliano and I. Rosell, Phys. Rev. Lett. **99** (2007) 231801 [arXiv:0707.3439 [hep-ph]].

[68] M. Antonelli, V. Cirigliano, G. Isidori, F. Mescia, M. Moulson, H. Neufeld, E. Passemar and M. Palutan *et al.*, Eur. Phys. J. C **69** (2010) 399 [arXiv:1005.2323 [hep-ph]].

[69] V. Cirigliano, G. Ecker, H. Neufeld, A. Pich and J. Portoles, Rev. Mod. Phys. **84** (2012) 399 [arXiv:1107.6001 [hep-ph]].

[70] W. J. Marciano and A. Sirlin, Phys. Rev. Lett. **71** (1993) 3629.

[71] R. Decker and M. Finkemeier, Nucl. Phys. B **438** (1995) 17 [hep-ph/9403385].

[72] R. Decker and M. Finkemeier, Nucl. Phys. Proc. Suppl. **40** (1995) 453 [hep-ph/9411316].

[73] J. C. Hardy and I. S. Towner, Phys. Rev. C **79** (2009) 055502 [arXiv:0812.1202 [nucl-ex]].

[74] I. Caprini, L. Lellouch and M. Neubert, Nucl. Phys. B **530** (1998) 153 [hep-ph/9712417].

Chapter 6

Lepton flavour violation in the Higgs sector and the role of hadronic τ-lepton decays

Alejandro Celis[1], Vincenzo Cirigliano[2] and Emilie Passemar[2]

[1]IFIC, Universitat de València – CSIC, Apt. Correus 22085, E-46071 València, Spain
[2]Theoretical Division, Los Alamos National Laboratory, Los Alamos, NM 87545, USA

It has been pointed out recently that current low-energy constraints still allow for sizable flavour-changing decay rates of the 125 GeV boson into leptons, $h \to \tau\ell$ ($\ell = e, \mu$). In this work we discuss the role of hadronic tau-lepton decays in probing lepton flavour violating couplings in the Higgs sector. At low energy, the effective Higgs coupling to gluons induced by heavy quarks contributes to hadronic tau decays, establishing a direct connection with the relevant process at the LHC, $pp(gg) \to h \to \tau\ell$. Semileptonic transitions like $\tau \to \ell\pi\pi$ are sensitive to flavour-changing scalar couplings while decays such as $\tau \to \ell\eta^{(\prime)}$ probe pseudoscalar couplings, thus providing a useful low-energy handle to disentangle possible Higgs flavour violating signals at the LHC. As part of our analysis, we provide an appropriate description of all the relevant hadronic matrix elements needed to describe Higgs-mediated $\tau \to \ell\pi\pi$ transitions, improving over previous treatments in the literature.

6.1 Introduction

With the discovery of a new boson with mass close to 125 GeV, here referred as $h(125)$, a new era in the understanding of the electroweak symmetry breaking (EWSB) mechanism has started. Current experimental data already indicate that this boson is related to the origin of particle masses and its properties are so far in good agreement with those of the standard model (SM) Higgs boson [1,2]. The spin-parity of the new particle are consistent with the assignment $J^P = 0^+$, other possibilities being strongly disfavoured. Global fits of the ATLAS, CMS and Tevatron data also find that the couplings of this boson to the gauge vector bosons $(\gamma, g, W^\pm, Z)$ and the third family of fermions (t, b, τ) are compatible with the SM expectation [3–6].

Searches for lepton flavour violating (LFV) Higgs decays at the LHC offer an interesting possibility to test for new physics effects that could have escaped current experimental low-energy constraints [7]. LFV effects associated with the scalar sector have been studied considerably in the past [8–17]. The recent discovery of the $h(125)$ boson at the LHC has naturally caused renewed interest in this possibility [7, 18–23]. In this work we address several questions related to LFV in the Higgs sector:

- How robust a connection can be made between the LFV Higgs decays and LFV τ decays?

- What is the role of hadronic τ decays $(\tau \rightarrow \ell\pi\pi, \ell\eta^{(\prime)}, \ldots)$ compared to other τ decays $(\tau \rightarrow \ell\gamma, \ldots)$ in probing LFV couplings of the Higgs sector?

- What can be said about LFV phenomena within the general two-Higgs-doublet model based on our current knowledge of the $h(125)$ properties?

Along the way we provide an appropriate treatment of the form factors needed to study hadronic LFV τ decays. These will be useful for any analysis of LFV τ decays, beyond the specific framework adopted here. In this work we will not attempt to perform a study of all the available LFV hadronic decay modes. Indeed, just for semileptonic transitions the experimental collaborations have considered at the moment a great variety of hadronic final states $\tau \rightarrow \ell(\pi\pi, \pi K, KK, \eta\pi, \eta\eta)$. Instead, we focus here on $\tau \rightarrow \ell\pi\pi$ semileptonic transitions for which a better control of the relevant hadronic matrix elements can be achieved. Concerning the $\tau \rightarrow \ell P$ decays, we restrict the discussion to a few modes

$P = \pi, \eta, \eta'$ for clarity. The richness of hadronic τ decay modes could certainly be extremely useful in the future to corroborate any possible LFV signal at the LHC, providing complementary information to scrutinize its origin.

6.1.1   Motivation

Flavour violating couplings of the Higgs boson to leptons arise in many extensions of the SM. If the new physics originates at a scale Λ well above the EW scale, then an effective theory treatment is justifiable. Details of the ultraviolet completion of the SM can then be encoded in effective operators containing only the SM degrees of freedom and which can give rise to LFV effects [24, 25]. It is however possible that the new physics (NP) enters at a scale not much higher than the electroweak scale, so that these new degrees of freedom cannot be integrated out. One possibility is to consider an extended Higgs sector with several scalar fields below the TeV scale and non-diagonal Yukawa couplings in flavour space. Indeed, it is the case that a simple extension of the SM scalar sector by an additional Higgs doublet, a two-Higgs-doublet model (2HDM), gives rise to flavour-changing neutral currents (FCNCs) at tree-level in the quark and lepton sectors. Usually a symmetry principle is assumed that forbids such effects [26, 27] and allows to evade the stringent bounds coming from the Kaon and B-meson precision experiments. While such an approach is well justified or needed for the quark sector, one can be less restrictive in the lepton sector, while being consistent with flavour constraints.

The strongest bound on possible LFV Higgs couplings to $\tau - \ell$ ($\ell = e, \mu$) are currently obtained from $\tau \to \ell\gamma$ decays. It was first noticed in ref. [7] that present bounds still allow for very large LFV Higgs decay rates $\mathrm{BR}(h \to \tau\ell) \lesssim 10\%$. It was later shown in refs. [18, 19] that the LHC prospects in constraining such LFV Higgs couplings are very promising, even with present accumulated data. Constraining LFV couplings of the 125 GeV Higgs directly at the LHC, or finding additional low-energy handles, becomes even more relevant when one considers the nature of the bound that can be extracted from $\tau \to \ell\gamma$ decays. The effective dipole operator $(\bar{\ell}\sigma^{\mu\nu}P_{L,R}\tau)F_{\mu\nu}$ giving rise to $\tau \to \ell\gamma$ decays appears at the loop-level and is very sensitive to details of the high energy dynamics. Due to the strong chirality suppression of the one-loop diagrams, the dominant contribution to the $\tau \to \ell\gamma$ decay amplitude arises from two-loop diagrams of the Barr-Zee type [28]. Additional scalars or heavy degrees of freedom belonging to the UV completion of the

theory can cause sizable interfering contributions, making it impossible to extract a model independent bound on the scalar LFV couplings. This issue is circumvented at the LHC by searching directly for LFV Higgs decays, the Higgs being produced via its coupling to $VV = W^+W^-, ZZ$ in vector-boson fusion and in associated Higgs production with a vector boson [18], or, relying on its loop-induced coupling to gluons in the gluon fusion mode [19].

At low energy, semileptonic τ decays like $\tau \to \ell\pi\pi$ $(\pi\pi = \pi^+\pi^-, \pi^0\pi^0)$ offer a unique opportunity to extract a bound on the LFV Higgs couplings which is much less sensitive to details of the high energy dynamics, thus establishing a model-independent connection with the search for LFV Higgs decays at the LHC. The same effective coupling of the Higgs to gluons that would give rise to $pp(gg) \to h \to \tau\ell$, also enters in the $\tau \to \ell\pi\pi$ mode though at a much lower energy scale where non-perturbative QCD effects play a major role, see figure 6.1. Similarly, the semileptonic decays $\tau \to \ell P$ (where P is a pseudoscalar meson) establish a connection with the search for LFV decays of a CP-odd Higgs at the LHC.
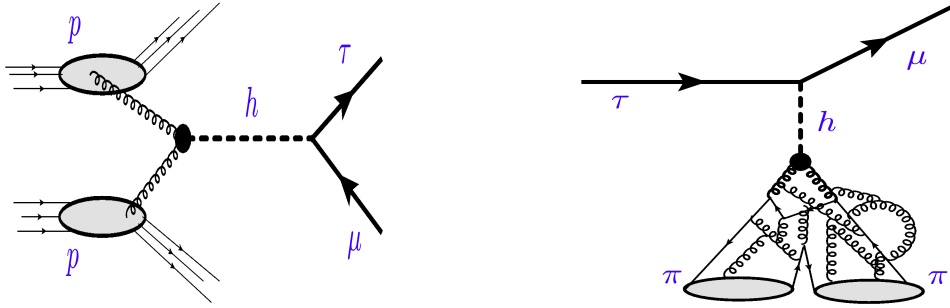
Figure 6.1: *Relation between the LHC process $pp(gg) \to h \to \tau\mu$ (left figure) and the semileptonic decay $\tau \to \mu\pi\pi$ (right figure): the effective Higgs coupling to gluons enters in both processes.*

Calculations of $\tau \to \ell\pi\pi$ mediated by a Higgs boson with LFV couplings in the literature have mostly considered the scalar-current associated with the Higgs coupling to light quarks, thus neglecting the effective coupling of the Higgs to gluons due to intermediate heavy quarks (with the exception of ref. [29], in which a more general EFT analysis including gluon operators is presented). Moreover, a description of the scalar-current hadronic matrix elements based on leading order predictions of Chiral-Perturbation Theory (ChPT) has been used in these works [9, 12, 14, 29]. Such treatment of the hadronic

matrix elements is not adequate to deal with τ decays, for which the $\pi\pi$ invariant mass can be as large as $m_\tau - m_\ell$. It was pointed out recently in ref. [30], within the context of R-parity violating supersymmetry, that by using a more appropriate description of the hadronic matrix elements of the scalar and vector currents, the bounds obtained on the R-parity-violating couplings improve considerably.

6.1.2   Overview of results

In this work we provide for the first time a complete description of the $\tau \to \ell\pi\pi$ mode in the presence of a Higgs boson with LFV couplings. A detailed discussion of the hadronic matrix elements involved is given. When relevant we also compare the form factors we obtain with those of previous work. With these tools in hand, we extract from $\tau \to \ell\pi\pi$ robust model-independent bounds on LFV couplings of the Higgs. The LFV decays $\tau \to \ell P$ and the relevant hadronic matrix elements in this case are also discussed, leading to bounds on LFV couplings of a CP-odd neutral scalar.

In the context of an extended Higgs sector, we also point out the importance of performing searches for additional Higgs bosons in the LFV decay modes $\tau - \mu$ and $\tau - e$ at the LHC. Present data constrain the $h(125)$ coupling to vector bosons to be very close to the SM value $g_{hVV} \simeq g_{hVV}^{\mathrm{SM}}$ [1–3]. In general two-Higgs-doublet models, any possible LFV coupling of the 125 GeV Higgs boson at the end turns out to be suppressed by an accompanying small or vanishing mixing factor $\left(1 - (g_{hVV}/g_{hVV}^{\mathrm{SM}})^2\right)^{1/2}$. Additional Higgs bosons which would play a minor role in the restoration of perturbative unitarity on the other hand, do not receive this suppression of their LFV couplings. The search for LFV decays associated to the scalar sector should therefore not be restricted to the 125 GeV boson.

Our paper is organized as follows: In section 6.2 we describe our framework. In section 6.3 we provide a detailed discussion of the hadronic form factors relevant for the description of $\tau \to \mu\pi\pi$ decays. In section 6.4 we describe the framework used in this work to motivate the discussion of possible LFV effects due to both CP-even and CP-odd Higgs bosons. We then consider the semileptonic LFV decay $\tau \to \mu\pi\pi$ ($\pi\pi = \pi^+\pi^-, \pi^0\pi^0$) mediated by a CP-even Higgs boson, we discuss the relevance of this process in connection to other LFV transitions accessible at B-factories ($\tau \to \mu\gamma, 3\mu, \ldots$) as well as for the LHC ($h \to \tau\mu$). The phenomenology of a CP-odd Higgs boson is also discussed along the same

lines. We give our conclusions in section 6.5.

6.2   Framework

We will consider the following phenomenological Lagrangian that describes the fermionic interactions of a generic extended scalar sector,

$$\mathcal{L} = -m_k \, \bar{f}_L^k \, f_R^k - \sum_\varphi \, Y_{ij}^\varphi \, \left(\bar{f}_L^i \, f_R^j \right) \, \varphi + \text{h.c.} \ , \tag{6.1}$$

where φ runs over the light neutral scalars of the theory, the Yukawa couplings can be complex in principle and the various physical scalar fields do not need to be CP eigenstates. A similar Lagrangian has been considered very recently in refs. [7,18] to analyze possible flavour violating effects of a CP-even Higgs of mass 125 GeV. In the SM there is only one physical CP-even scalar field, h, with Yukawa couplings given by $Y_{ij}^h = (m_i/v)\delta_{ij}$. We will parametrize the deviations from the SM diagonal couplings as $Y_{ii}^h = y_i^h \, (m_i/v)$ for convenience in the following. Since here we are not interested in CP-violating effects we will assume that CP is a good symmetry of the scalar interactions. Physical scalars are then CP-eigenstates and the couplings Y_{ij}^φ are real for a CP-even Higgs, $\varphi \equiv h$, or pure imaginary for a CP-odd Higgs, $\varphi \equiv A$.

In section 6.4.1 we will discuss how the non-standard Higgs fermion couplings of eq. (6.1) arise within the framework of the general 2HDM, or from higher dimensional gauge invariant operators. There we will also discuss in detail the phenomenological impact of LFV couplings of the CP-even and CP-odd scalars. Here, we outline in general terms the low-energy effects of the non-standard couplings of eq. (6.1) and motivate the analysis of hadronic matrix elements to be discussed in section 6.3.

At low energy, where the Higgs fields can be integrated out, the fermion couplings of eq. (6.1) generate a set of LFV operators, as depicted by representative diagrams in figure 6.2. The diagram to the left generates at one-loop the dipole operator $(\bar{\ell}\sigma^{\mu\nu}P_{L,R}\tau)F_{\mu\nu}$. Additional two-loop contributions to this operator are not shown in figure 6.2 but will be included in the calculation. The tree-level diagram in the middle generates a four-fermion operator with scalar or pseudoscalar couplings to the light quarks, $\bar{\ell}(1 \pm \gamma_5)\tau \cdot \bar{q}\{1, \gamma_5\}q$. Finally, the diagram to the right, through heavy-quarks in the loop generates gluonic operators of the type $\bar{\ell}(1 \pm \gamma_5)\tau \cdot GG$ and $\bar{\ell}(1 \pm \gamma_5)\tau \cdot G\tilde{G}$.
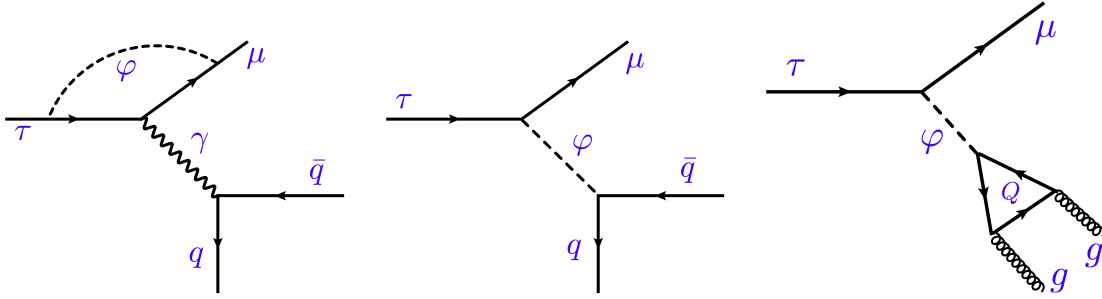
Figure 6.2: *Integrating out the Higgs field(s) generates at low-energy several LFV operator structures: dipole (left diagram), scalar four-fermion (center diagram), gluon (right diagram).*

When considering hadronic LFV decays such as $\tau \to \ell\pi\pi$ or $\tau \to \ell P$ ($P = \pi, \eta, \eta'$) one needs the matrix elements of the quark-gluon operators in the hadronic states. In particular, P-even operators will mediate the $\tau \to \ell\pi\pi$ decay and one needs to know the relevant two-pion form factors. The dipole operator requires the vector form factor related to $\langle\pi\pi|\bar{q}\gamma_\mu q|0\rangle$ (photon converting in two pions). The scalar operator requires the scalar form factors related to $\langle\pi\pi|\bar{q}q|0\rangle$. The gluon operator requires $\langle\pi\pi|GG|0\rangle$, which we will reduce to a combination of the scalar form factors and the two-pion matrix element of the trace of the energy-momentum tensor $\langle\pi\pi|\theta^\mu_\mu|0\rangle$ via the trace anomaly relation:

$$\theta^\mu_\mu = -9\frac{\alpha_s}{8\pi}G^a_{\mu\nu}G^{\mu\nu}_a + \sum_{q=u,d,s} m_q\bar{q}q \ . \tag{6.2}$$

We do not discuss in this work Z-mediated contributions to semileptonic τ decays. In general, these are expected to be much smaller than the photon-mediated contribution due to the $\mathcal{O}(q^2/M_Z^2)$ suppression factor in the amplitude coming from the Z-propagator, where q^2 is the invariant mass squared of the $\pi\pi$ system. In some new physics scenarios however, the Z-mediated contribution can be relevant and should be taken into account [31]. The Z-mediated contribution to $\tau \to \ell\pi\pi$ decays would involve the vector form factor related to $\langle\pi\pi|\bar{q}\gamma_\mu q|0\rangle$, the same as for the photon mediated contribution described in this work. The Z-mediated contribution to $\tau \to \ell P$ decays, on the other hand, would involve the hadronic matrix elements for the axial current $\bar{q}\gamma_\mu\gamma_5 q$. The latter are related to pseudoscalar $\bar{q}\gamma_5 q$ and gluonic $G\tilde{G}$ hadronic matrix elements due to the axial anomaly relation of QCD.

To impose robust bounds on LFV Higgs couplings from $\tau \to \ell\pi\pi$, we need to know

the hadronic matrix elements with a good accuracy. With this motivation in mind, we now discuss in detail the derivation of the two-pion matrix elements.

6.3 Hadronic form factors for $\tau \to \ell\pi\pi$ decays

The dipole contribution to the $\tau \to \ell\pi\pi$ decay requires the matrix element

$$\langle\pi^+(p_{\pi^+})\pi^-(p_{\pi^-})|\tfrac{1}{2}(\bar{u}\gamma^\alpha u - \bar{d}\gamma^\alpha d)|0\rangle \equiv F_V(s)(p_{\pi^+} - p_{\pi^-})^\alpha, \qquad (6.3)$$

with $F_V(s)$ the pion vector form factor. As for the scalar currents and the trace of the energy-momentum tensor θ^μ_μ, the hadronic matrix elements are given by

$$\begin{aligned}
\langle\pi^+(p_{\pi^+})\pi^-(p_{\pi^-})|m_u\bar{u}u + m_d\bar{d}d|0\rangle &\equiv \Gamma_\pi(s) \ , \\
\langle\pi^+(p_{\pi^+})\pi^-(p_{\pi^-})|m_s\bar{s}s|0\rangle &\equiv \Delta_\pi(s) \ , \\
\langle\pi^+(p_{\pi^+})\pi^-(p_{\pi^-})|\theta^\mu_\mu|0\rangle &\equiv \theta_\pi(s) \ ,
\end{aligned} \qquad (6.4)$$

with $\Gamma_\pi(s)$ and $\Delta_\pi(s)$ the pion scalar form factors and $\theta_\pi(s)$ the form factor related to θ^μ_μ. Here s is the invariant mass squared of the pion pair: $s = (p_{\pi^+} + p_{\pi^-})^2 = (p_\tau - p_\ell)^2$.

In what follows, we determine the form factors by matching a dispersive parameterization (that uses experimental data) with both the low-energy form dictated by chiral symmetry and the asymptotic behavior dictated by perturbative QCD. Numerical tables with our results are available upon request.

6.3.1 Determination of the $\pi\pi$ vector form factor

The vector form factor $F_V(s)$ has been measured both directly from $e^+e^- \to \pi^+\pi^-$ [32–36] and via an isospin rotation from $\tau \to \pi^-\pi^0\nu_\tau$ [37, 38]. It has also been determined by several theoretical studies [39–54, 56].

In the spirit of refs. [53, 57–63] we determine the vector form factor phenomenologically by fitting the invariant mass distribution of $\tau \to \pi^-\pi^0\nu_\tau$ decays using a theoretically well-motivated parametrization. To this end, we adapt the dispersive parametrizations introduced in refs. [53, 61] mimicking what has been done for $K\pi$ in refs. [58–60, 64]. Note that for our purposes, the isospin-breaking corrections can be neglected. A dispersion relation with three subtractions at $s = 0$ is written for $\ln(F_V(s))$. This leads to the following

representation for $F_V(s)$ [53, 61]

$$F_V(s) = \exp\left[\lambda'_V \frac{s}{M_\pi^2} + \frac{1}{2}\left(\lambda''_V - \lambda'^2_V\right)\left(\frac{s}{M_\pi^2}\right)^2 + \frac{s^3}{\pi}\int_{4M_\pi^2}^{\infty} \frac{ds'}{s'^3}\frac{\phi_V(s')}{(s'-s-i\epsilon)}\right] . \qquad (6.5)$$

To fix one subtraction constant, use has been made of $F_V(s=0) \equiv 1$ required by gauge invariance. λ'_V and λ''_V are the two other subtraction constants corresponding to the slope and the curvature of the form factor. They are determined from a fit to the data. $\phi_V(s)$ represents the phase of the form factor. In the elastic region $\left(s \lesssim 1 \text{ GeV}^2\right)$, according to Watson theorem [65] the phase of the form factor $\phi_V(s)$ is equal to the P wave $I = 1$ $\pi\pi$ scattering phase shift $\delta_1^1(s)$ which is known with an excellent precision from the solutions of Roy-Steiner equations [55, 66]. However for $s > 1 \text{ GeV}^2$ other channels open $(4\pi, K\bar{K})$ and $\phi_V(s)$ is not known. Taking advantage of the precise measurements of the invariant mass distribution of $\tau \to \pi^-\pi^0\nu_\tau$ decays [38], the phase of the form factor can be modeled in terms of the three resonances found in this decay region and directly determined from the data.

We write $\tan\phi_V(s) = \text{Im}\tilde{F}_V(s)/\text{Re}\tilde{F}_V(s)$ in terms of a model for the form factor $\tilde{F}_V(s)$ that includes three resonances $\rho(770)$, $\rho'(1465)$ and $\rho''(1700)$ with two mixing parameters α' and α'' measuring the relative weight between the resonances and ϕ' and ϕ'' accounting for the corresponding interferences, see ref. [61]:

$$\tilde{F}_V(s) = \frac{\tilde{M}_\rho^2 + \left(\alpha'e^{i\phi'} + \alpha''e^{i\phi''}\right)s}{\tilde{M}_\rho^2 - s + \kappa_\rho(s)\,\text{Re}\left[A_\pi(s) + \frac{1}{2}A_K(s)\right] - i\tilde{M}_\rho\tilde{\Gamma}_\rho(s)} - \frac{\alpha'e^{i\phi'}s}{D(\tilde{M}_{\rho'}, \tilde{\Gamma}_{\rho'})} - \frac{\alpha''e^{i\phi''}s}{D(\tilde{M}_{\rho''}, \tilde{\Gamma}_{\rho''})} ,$$
$$(6.6)$$

with

$$D(\tilde{M}_R, \tilde{\Gamma}_R) = \tilde{M}_R^2 - s + \kappa_R(s)\text{Re}A_\pi(s) - i\tilde{M}_R\tilde{\Gamma}_R(s) . \qquad (6.7)$$

In this equation $\tilde{M}_R$ and $\tilde{\Gamma}_R$ are model parameters. $\tilde{\Gamma}_R$ and κ_R are given by :

$$\tilde{\Gamma}_R(s) = \tilde{\Gamma}_R \frac{s}{\tilde{M}_R^2} \frac{(\sigma_\pi^3(s) + 1/2\,\sigma_K^3(s))}{\left(\sigma_\pi^3(\tilde{M}_R^2) + 1/2\,\sigma_K^3(\tilde{M}_R^2)\right)} , \quad \kappa_R(s) = \frac{\tilde{\Gamma}_R}{\tilde{M}_R} \frac{s}{\pi\left(\sigma_\pi^3(\tilde{M}_R^2) + 1/2\,\sigma_K^3(\tilde{M}_R^2)\right)} ,$$
$$(6.8)$$

if $R \equiv \rho$ and

$$\tilde{\Gamma}_R(s) = \tilde{\Gamma}_R \frac{s}{\tilde{M}_R^2} \frac{\sigma_\pi^3(s)}{\sigma_\pi^3(\tilde{M}_R^2)} , \quad \kappa_R(s) = \frac{\tilde{\Gamma}_R}{\tilde{M}_R} \frac{s}{\pi\sigma_\pi^3(\tilde{M}_R^2)} , \qquad (6.9)$$

otherwise. This parametrization is guided by Resonance Chiral Theory (RChT) [67–69]. While RChT allows one to compute the decay width $\tilde{\Gamma}_R$ and κ_R for the ρ resonance, eq. (6.8), taking into account the $\pi\pi$ and $K\bar{K}$ intermediate states [49], this is not the case anymore for ρ' and ρ''. Hence in eq. (6.9), generic $\tilde{\Gamma}_R$ and κ_R as expected for a vector resonance decaying only in $\pi\pi$ has been assumed[1] [57]. In eq. (6.6), $A_\pi(s)$ and $A_K(s)$ are the $\pi\pi$ and $K\bar{K}$ loop functions in ChPT [49,61] and σ_π and σ_K represents the velocity of the two particles in the centre-of-mass frame:

$$
\begin{aligned}
\sigma_\pi(s) &\equiv \sqrt{1 - 4M_\pi^2/s}\,\theta\left(s - 4M_\pi^2\right)\ , \\
\sigma_K(s) &\equiv \sqrt{1 - 4M_K^2/s}\,\theta\left(s - 4M_K^2\right)\ .
\end{aligned}
\tag{6.10}
$$

Here θ denotes the Heaviside step function $\theta(x) = 1$ for $x > 0$, being zero otherwise. Note that the parameter κ_R is defined such as $i\kappa_R(s)\,\mathrm{Im}A_\pi(s) = -i\tilde{M}_R\tilde{\Gamma}_R(s)$ with $\mathrm{Im}A_\pi(s) \to \mathrm{Im}[A_\pi(s) + 1/2A_\pi(s)]$ for ρ. We emphasize here that $\tilde{M}_R$ and $\tilde{\Gamma}_R$ are model parameters and do not correspond to the physical resonance mass and width. To find them one has to find the pole of each term of eq. (6.6) or equivalently the zeros of their denominator eq. (6.7) on the second Riemman sheet.

The model used to determine ϕ_V, eq. (6.6), inspired by the Gounaris-Sakurai parametrization [40] is only valid in the τ decay region and is therefore only used in eq. (6.5) for $s \le s_{\text{cut}} \sim m_\tau^2$. For the high-energy region of the dispersive integral eq. (6.5) $(s > s_{\text{cut}} \sim m_\tau^2)$ the phase is unknown and following refs. [60, 64, 70] we take a conservative interval between 0 and 2π centered at the asymptotic value of the phase of the form factor which is π. Indeed perturbative QCD dictates the asymptotic behavior of the form factor: it should vanish as $\mathcal{O}(1/s)$ up to logarithmic corrections [71] for large values of s implying that its phase should asymptotically reach π. The use of a three-time subtracted dispersion relation reduces the impact of our ignorance of the phase at relative high energies in eq. (6.5). However, in order for the form factor to have the correct asymptotic behavior two sum rules have to be satisfied:

$$
\lambda_V'^{\,\text{sr}} = \frac{m_\pi^2}{\pi} \int_{4M_\pi^2}^{\infty} ds'\, \frac{\phi_V(s')}{s'^2}\ ,
\tag{6.11}
$$

---

[1]The assumption that ρ' and ρ'' only decay in $\pi\pi$ has been made. One could improve the model by considering other decay modes as it has been done for $K\pi$ in ref. [64].

$$(\lambda_V'' - \lambda_V'^2)^{\mathrm{sr}} = \frac{2m_\pi^4}{\pi} \int_{4M_\pi^2}^\infty ds' \frac{\phi_V(s')}{s'^3} \equiv \alpha_{2v}^{\mathrm{sr}} \,. \tag{6.12}$$

They are used to constrain the fit to the data as done for $K\pi$ in refs. [60, 64].

Twelve parameters entering $F_V(s)$, eq. (6.5) are therefore determined by a fit to the data:

- λ_V' and λ_V'', the two subtraction constants

- $\tilde{M}_\rho$ and Γ_ρ, $\tilde{M}_{\rho'}$ and $\Gamma_{\rho'}$, $\tilde{M}_{\rho''}$ and $\Gamma_{\rho''}$ the mass and decay width of $\rho(770)$, $\rho'(1465)$ and $\rho''(1700)$ respectively used to model the phase

- α', α'' and their phases ϕ', ϕ'' the mixing parameters between the resonances

The following quantity is minimized :

$$\chi^2 = \sum_{i=1}^{62} \left(\frac{(|F_V(s)|^2)_i^{\mathrm{theo}} - (|F_V(s)|^2)_i^{\mathrm{exp}}}{\sigma_{(|F_V(s)|^2)_i^{\mathrm{exp}}}} \right)^2 + \left(\frac{\lambda_V' - \lambda_V'^{\,\mathrm{sr}}}{\sigma_{\lambda_V'^{\,\mathrm{sr}}}} \right)^2 + \left(\frac{\alpha_{2v} - \alpha_{2v}^{\mathrm{sr}}}{\sigma_{\alpha_{2v}^{\mathrm{sr}}}} \right)^2 , \tag{6.13}$$

with $(|F_V(s)|^2)^{\mathrm{exp}}$ and its uncertainty $\sigma_{(|F_V(s)|^2)\mathrm{exp}}$, the modulus squared of the vector form factor experimentally extracted from the measurement of the $\tau^- \to \pi^- \pi^0 \nu_\tau$ invariant decay distribution [38] and $F_V(s)^{\mathrm{theo}}$ the form factor parametrized in eq. (6.5). In addition to the first term also minimized in previous analyses [38, 61], we impose the constraints given by the two sum rules eqs. (6.11) and (6.12)[2] to guarantee the correct asymptotic behaviour of the form factor. This allows us to have a description for the form factor, eq. (6.5) that not only fulfills the properties of analyticity and unitarity but is also in agreement with perturbative QCD. This is not the case for the dispersive representations of refs. [53, 61] and for the parametrization used by Belle collaboration to fit their data [38].

The result of the fit is given in table 6.1 and shown in figure 6.3 together with the Belle data. As can been seen from the figure and the χ^2, the agreement with data is excellent. Note that we have presented here a description for the form factor that represents the state-of-the-art, in that it relies on the fewest model assumptions and is valid on a large

---

[2]$\sigma_{\lambda_V'^{\,\mathrm{sr}}}$ and $\sigma_{\alpha_{2v}^{\mathrm{sr}}}$ are given by the 2π band taken for the high energy phase.

$\lambda_V' \times 10^3$	36.7 ± 0.2
$\lambda_V'' \times 10^3$	3.12 ± 0.04
$\tilde{M}_\rho[\text{MeV}]$	833.9 ± 0.6
$\tilde{\Gamma}_\rho[\text{MeV}]$	198 ± 1
$\tilde{M}_{\rho'}[\text{MeV}]$	1497 ± 7
$\tilde{\Gamma}_{\rho'}[\text{MeV}]$	785 ± 51
$\tilde{M}_{\rho''}[\text{MeV}]$	1685 ± 30
$\tilde{\Gamma}_{\rho''}[\text{MeV}]$	800 ± 31
α'	0.173 ± 0.009
ϕ'	-0.98 ± 0.11
α''	0.23 ± 0.01
ϕ''	2.20 ± 0.05
$\chi^2/d.o.f$	$38/52$

Table 6.1: *Results for the $\pi\pi$ vector form factor parameters from a fit to $\tau \to \pi\pi\nu_\tau$ data [38]. Note that $\tilde{M}_R$ and $\tilde{\Gamma}_R$ are model parameters and do not correspond to the physical resonance mass and width.*

energy range. For the purposes of bounding LFV Higgs couplings, a parametrization a la Gounaris-Sakurai that describes well the data as the one used in ref. [38] could have been sufficient.

6.3.2   Determination of $\Gamma_\pi(s)$, $\Delta_\pi(s)$ and $\theta_\pi(s)$

The scalar form factors and $\theta_\pi(s)$ cannot be determined so directly and unambiguously from the data. However, they can be reconstructed from dispersive theory with a matching at low-energy to ChPT as pioneered in ref. [72]. As we have seen, elastic unitarity only holds at low-energy for $s \ll 1 \text{ GeV}^2$ and in the scalar case it is very well known that the elastic approximation breaks down for the $\pi\pi$ S-wave already at the $K\bar{K}$ threshold due to the strong inelastic coupling of two S-wave pions to $K\bar{K}$ in the region of $f_0(980)$. In order to describe the scalar form factors in the kinematical region needed for $\tau \to \ell\pi\pi$, one has to solve a two-channel Muskhelishvili-Omnès problem following refs. [72,74] including $\pi\pi$ and $K\bar{K}$ scattering. As s increases, a new two-body channel opens: $\eta\eta$. At some
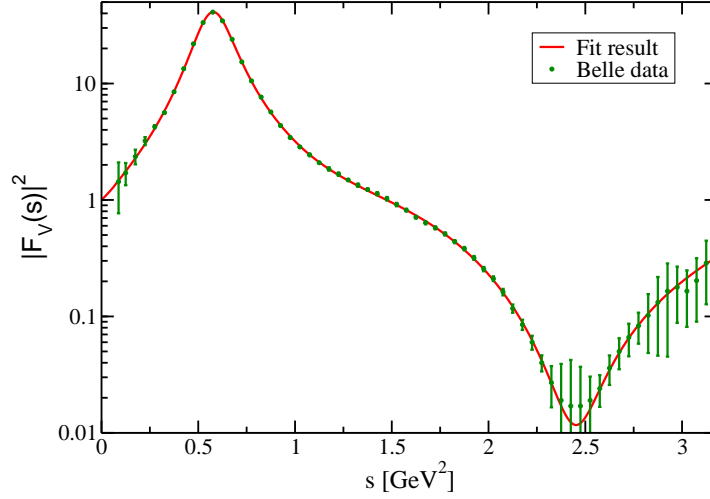
Figure 6.3:   *Fit result for the modulus squared of the pion vector form factor. The data in green are from Belle Collaboration [38]. The red line represents the result of the fit presented in table 6.1.*

point, the 4π-channel will also become important. As discussed in refs. [74, 75], below $\sqrt{s} \sim 1.4$ GeV the inelasticity is found to be saturated to a good approximation by a single channel $K\bar{K}$.

The Muskhelishvili-Omnès problem

We briefly recall below the procedure presented in ref. [72] to solve a two-channel Muskhelishvili-Omnès (MO) problem. The form factors $F_i(s)$ ($F_1 \equiv \Gamma_\pi, \Delta_\pi$, or θ_π and $\sqrt{3}/2 F_2 \equiv \Gamma_K, \Delta_K$, or θ_K) are analytic functions everywhere in the complex plane except for a right-hand cut. Under the assumptions discussed above, the discontinuity of the form factors along the cut is determined by the two-channel unitarity condition:

$$\mathrm{Im} F_n(s) = \sum_{m=1}^{2} T_{nm}^*(s)\sigma_m(s)F_m(s) \; , \tag{6.14}$$

where T_{mn} represent the T matrix elements which describe the scattering among the relevant channels ($n = \pi\pi, K\bar{K}$ with $\ell = 0$ and $I = 0$). The general solution to the

condition (6.14) that does not grow faster than a power of s at infinity can be written as [72, 73]:

$$\begin{pmatrix} F_\pi(s) \\ \frac{2}{\sqrt{3}} F_K(s) \end{pmatrix} = \begin{pmatrix} C_1(s) & D_1(s) \\ C_2(s) & D_2(s) \end{pmatrix} \begin{pmatrix} P_F(s) \\ Q_F(s) \end{pmatrix} , \qquad (6.15)$$

where $P_F(s)$ and $Q_F(s)$ are polynomials and the "canonical" solutions $C_n(s)$, $D_n(s)$ generalize the Omnès factor appearing in the solution of the one-channel unitarity condition [76].

Provided that the S-matrix satisfies certain asymptotic conditions at large s (namely that $S_{12} \to 0$ and $\text{Arg}(det(S)) \to 4\pi$), the solutions $C_n(s)$ and $D_n(s)$, generically denoted by $X_n(s)$ behave as $1/s$ for $|s| \to \infty$. Therefore, the $X_n(s)$ satisfy unsubtracted dispersion relations, which combined with the unitarity condition (6.14) lead to a set of coupled Muskhelishvili-Omnès singular integral equations [73, 76]

$$X_n(s) = \sum_{m=1}^{2} \frac{1}{\pi} \int_{4M_\pi^2}^{\infty} \frac{dt}{t-s} T_{nm}^*(t) \sigma_m(t) X_m(t) , \qquad X(s) = C(s), D(s) . \qquad (6.16)$$

So in order to find a solution to the MO problem described above, we need to specify an appropriate T matrix. The T matrix is related to the S matrix by

$$S_{mn} = \delta_{mn} + 2i \sqrt{\sigma_m \sigma_n} \, T_{mn} , \qquad (6.17)$$

where the kinematical factor $\sigma_m(s)$ represents the velocity of the two particles in the centre-of-mass frame defined in eq. (6.10) with $\sigma_1(s) = \sigma_\pi(s)$ and $\sigma_2(s) = \sigma_K(s)$. In turn, the $\ell = 0$, $I = 0$ projection of the S matrix is parameterized as follows

$$S = \begin{pmatrix} \cos\gamma \; e^{2i\delta_\pi} & i \; \sin\gamma \; e^{i(\delta_\pi + \delta_K)} \\ i \; \sin\gamma \; e^{i(\delta_\pi + \delta_K)} & \cos\gamma \; e^{2i\delta_K} \end{pmatrix} , \qquad (6.18)$$

and therefore we need three input functions, the inelasticity $\eta_0^0 \equiv \cos\gamma$, the $\pi\pi$ S-wave phase shift $\delta_\pi(s)$ and the $K\bar{K}$ phase shift $\delta_K(s)$. Up to some energy, these inputs are determined by solving the Roy-Steiner equations for $\pi\pi$ [55, 66, 77, 78] and $K\pi$ scattering [79]. Since eq. (6.14) is a reasonable approximation to the exact discontinuity only in the energy region below some cut $s_{\text{cut}} \lesssim m_\tau^2$, we use the following strategy: for $s < s_{\text{cut}}$ we use the inputs for the two phase shifts $\delta_\pi(s)$ and $\delta_K(s)$ and the inelasticity $\eta_0^0(s)$ coming

from a recent update of the solutions of Roy-Steiner equations [79] [3] provided by B. Moussallam. For $s > s_{\text{cut}}$, we drive the T matrix to zero consistently with unitarity, by forcing the three input functions to the asymptotic values $\delta_\pi = 2\pi$, $\delta_K = 0$, $\eta_0^0 = 1$, which ensure that the canonical solutions to the MO problem fall off as $1/s$ [72,74,80]. We have varied s_{cut} in the range $(1.4\ \text{GeV})^2 - (1.8\ \text{GeV})^2$, and find that the form factors are insensitive to s_{cut} for $\sqrt{s} < 1.4$ GeV.

Following ref. [72], we generate a family of solutions $\{X_1(s), X_2(s)\}$ of the unitary condition by iteration. We start with $\left\{X_1^{(1)}(s) = \Omega_\pi(s), X_2^{(1)} = \lambda\,\Omega_K(s)\right\}$ where λ is a real parameter and $\Omega_{\pi,K}(s)$ is the Omnès function [76]

$$\Omega_{\pi,K}(s) \equiv \exp\left[\frac{s}{\pi}\int_{4M_\pi^2}^{\infty}\frac{dt}{t}\frac{\delta_{\pi,K}(t)}{(t-s)}\right]\ , \tag{6.19}$$

solution of the one-channel unitary condition. We compute the iteration $(N+1)$ from iteration (N) using eq. (6.14) for the imaginary part and eq. (6.16) for the real part. The problem admits two independent solutions [73] that are linear combinations of the family of solutions labelled by the parameter λ we have found. They are chosen such that [72]

$$C_n(s)|_{s=0} = \delta_{n1},\quad D_n(s)|_{s=0} = \delta_{n2}\ . \tag{6.20}$$

Fixing the subtraction constants with chiral symmetry

The form factors $F_{\pi,K}(s)$ (with $F \in \{\Gamma, \Delta, \theta\}$) are obtained from (6.15) once the polynomials $P_F(s)$ and $Q_F(s)$ are given. The polynomials can be determined by matching the form factors to their ChPT expressions at low energy [72], as summarized below.

For $\Gamma_{\pi,K}(s)$ and $\Delta_{\pi,K}(s)$, the requirement that the form factors behave as $\mathcal{O}(1/s)$ for large values of s fixes the polynomials to be constants. The polynomials are then determined by the values of the form factors at $s = 0$, which are related to the response of the pseudoscalar masses to changes in the quark masses (Feynman-Hellmann theorem):

$$\Gamma_P(0) = \left(m_u\frac{\partial}{\partial m_u} + m_d\frac{\partial}{\partial m_d}\right)M_P^2\ ,\quad \Delta_P(0) = \left(m_s\frac{\partial}{\partial m_s}\right)M_P^2\ . \tag{6.21}$$

---

[3]The input values $M_\pi = 139.57018$ MeV and $M_K = 495.7$ MeV have been used to generate these inputs.

The above relations imply [72]:

$$P_\Gamma(s) \;=\; \Gamma_\pi(0) = M_\pi^2 + \cdots \tag{6.22}$$

$$Q_\Gamma(s) \;=\; \frac{2}{\sqrt{3}}\Gamma_K(0) = \frac{1}{\sqrt{3}}M_\pi^2 + \cdots \tag{6.23}$$

$$P_\Delta(s) \;=\; \Delta_\pi(0) = 0 + \cdots \tag{6.24}$$

$$Q_\Delta(s) \;=\; \frac{2}{\sqrt{3}}\Delta_K(0) = \frac{2}{\sqrt{3}}\left(M_K^2 - \frac{1}{2}M_\pi^2\right) + \cdots\;, \tag{6.25}$$

where in the second equality above we have given the leading chiral order result and the dots represent higher order corrections. For the pion form factors, we neglect the higher order chiral corrections expected to be of order $M_\pi^2/(4\pi F_\pi)^2$. However, for the kaon form factors the chiral corrections are not a priori negligible. They can be calculated within $SU(3)$ ChPT in terms of low-energy constants estimated from lattice QCD [81]. These corrections have also been recently evaluated from lattice data in the framework of Resumed ChPT [82]. We take the ranges $\Gamma_K(0) = (0.5 \pm 0.1)\,M_\pi^2$, $\Delta_K(0) = 1^{+0.15}_{-0.05}\,(M_K^2 - 1/2M_\pi^2)$ [30] that encompass the recent estimates.

For $\theta_{\pi,K}(s)$ requiring that $P_\theta(s)$ and $Q_\theta(s)$ be constant (to enforce $\theta_{\pi,K} \sim \mathcal{O}(1/s)$ asymptotically) is not consistent with the behavior in the chiral regime [72]. This is a signal that the unsubtracted dispersion relation for these form factors is not saturated by the two states considered in the analysis. Relaxing the requirement on the asymptotic behavior and matching to ChPT expressions implies

$$P_\theta(s) \;=\; 2M_\pi^2 + \left(\dot\theta_\pi - 2M_\pi^2 \dot C_1 - \frac{4M_K^2}{\sqrt{3}}\dot D_1\right)s \tag{6.26}$$

$$Q_\theta(s) \;=\; \frac{4}{\sqrt{3}}M_K^2 + \frac{2}{\sqrt{3}}\left(\dot\theta_K - \sqrt{3}M_\pi^2 \dot C_2 - 2M_K^2 \dot D_2\right)s\;, \tag{6.27}$$

where $\dot f \equiv (df/ds)(s=0)$. $\dot\theta_\pi = 1$ up to small chiral $SU(2)$ corrections. At leading chiral order $\dot\theta_K = 1$. An alternative procedure to estimate $\dot\theta_K$, taking into account chiral $SU(3)$ corrections, has been given in ref. [72]. The approach is based on writing an unsubtracted dispersion relation for $\theta_K(s) - \theta_\pi(s)$: this leads to $\dot\theta_K = 1.15 - 1.18$, depending on the value of $s_{\rm cut}$ adopted. Based on this, in what follows we use the range $\dot\theta_K = 1.15 \pm 0.1$.
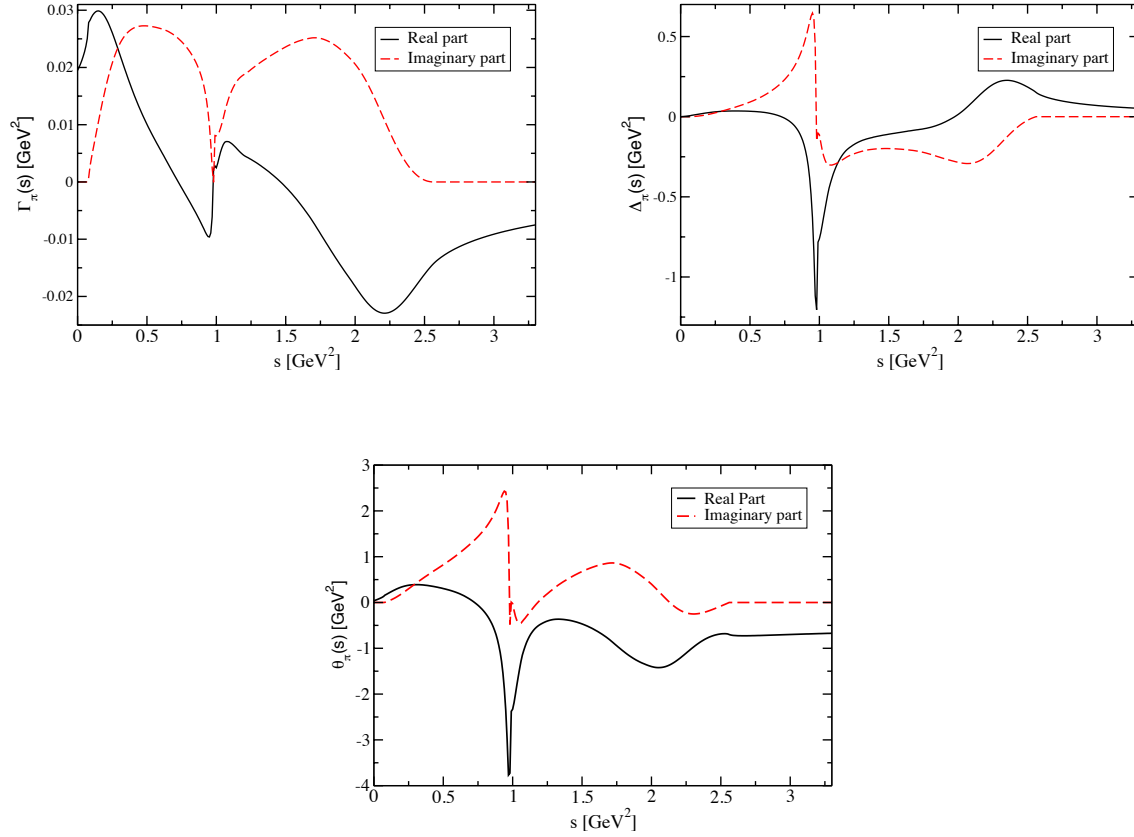
Figure 6.4:   *The form factors $\Gamma_\pi(s)$, $\Delta_\pi(s)$ and $\theta_\pi(s)$ defined in eq. (6.4) as determined by solving the two-channel unitarity condition and then by matching to ChPT, see text for details. The black solid line represents their real part and the red dashed-dotted red line stands for their imaginary part. This plot is generated using $s_{\text{cut}} = (1.4\,\text{GeV})^2$ and central values for the matching coefficients.*

Results

Using the two sets of solutions $\{C_1(s), C_2(s)\}$ and $\{D_1(s), D_2(s)\}$ and the polynomials determined in the last subsection we can construct the three form factors $\Gamma_\pi(s)$, $\Delta_\pi(s)$ and $\theta_\pi(s)$ from eq. (6.15). They are shown in figure 6.4 using $s_{\text{cut}} = (1.4\,\text{GeV})^2$ and central values for the matching coefficients. For $\sqrt{s} < 1.4$ GeV, the form factor are relatively insensitive to the choice of s_{cut}: the dependence on s_{cut} induces variations of the $\tau \to \ell\pi\pi$

phase space integrals at the $< 15\%$ level. Likewise, varying the matching polynomials in the ranges specified in the previous subsection leads to changes in the phase space integrals at the level of 10%.

Note that a similar approach to describe $\Gamma_\pi(s)$, $\Delta_\pi(s)$ to study lepton flavour violating effects within R-parity violating supersymmetry has been implemented in ref. [30] improving the hadronic treatment used in ref. [14]. Compared to previous work, we include the effective Higgs-gluon interaction induced by the Higgs coupling to heavy quarks. The influence of heavy quarks is not small and provides in general the dominant contribution to low-energy hadronic transitions mediated by scalar bosons associated to the mechanism of EWSB, the Higgs coupling to light quarks being mass suppressed. This well known fact has been discussed for example within the context of Higgs-nucleons interactions [83] and for the decay of a very light Higgs into two pions, $H \to \pi\pi$ [72]. Here we provide for the first time an adequate description of this effect for Higgs mediated semileptonic $\tau \to \ell\pi\pi$ decays.

6.4   Phenomenology

Having developed the necessary form factors to describe Higgs mediated LFV $\tau \to \ell\pi\pi$ decays in the previous section, we proceed to analyze the role of semileptonic τ decays to probe for LFV effects in the scalar sector. We discuss the robustness of the bounds obtained compared with previous treatments in the literature that rely on LO-ChPT predictions. We also analyze the connection between semileptonic τ decays and other LFV τ decays as well as with the search for LFV Higgs decays at the LHC. The phenomenology of a CP-odd Higgs boson with LFV couplings is discussed with a similar spirit. A general two-Higgs-doublet model is introduced to motivate the discussion of LFV effects in the scalar sector, however all the results in this section are expressed using the Lagrangian in eq. (6.1) and can therefore be interpreted within other new physics scenarios.

6.4.1   Phenomenological analysis within the 2HDM

Two-Higgs-doublet models (2HDM) provide a specific gauge-invariant framework where lepton flavour violating effects encoded in eq. (6.1) can occur, due to both CP-even and CP-odd Higgs bosons at tree-level. Comparing the 2HDM Lagrangian presented in chap-

ter 3 with the generic Lagrangian presented in eq. (6.1) we derive the following matching
for the CP-conserving limit,

$$
\begin{aligned}
Y_{ij}^h &= \frac{(M_f)_{ij}}{v}\cos\tilde\alpha + \frac{(\Pi_f)_{ij}}{v}\sin\tilde\alpha\,, \\
Y_{ij}^H &= -\frac{(M_f)_{ij}}{v}\sin\tilde\alpha + \frac{(\Pi_f)_{ij}}{v}\cos\tilde\alpha\,, \\
Y_{ij}^A &= \pm i\,\frac{(\Pi_f)_{ij}}{v}\,.
\end{aligned}
\tag{6.28}
$$

The plus sign in the expression for Y_{ij}^A is for $f=d,\ell$ while the minus sign is for $f=u$. In
this limit $g_{hVV}=\cos\tilde\alpha\,g_{hVV}^{\mathrm{SM}}$, $g_{HVV}=-\sin\tilde\alpha\,g_{hVV}^{\mathrm{SM}}$ and $g_{AVV}=0$. We can see that certain
relations between the LFV scalar couplings arise in this case. The fermionic couplings
of the lightest CP-even Higgs are flavour conserving in the limit $g_{hVV}=g_{hVV}^{\mathrm{SM}}$, and, in
general these are suppressed by the factor $\sin\tilde\alpha$. Flavour-changing couplings of the CP-
odd Higgs on the other hand do not receive such suppression. Considering the 2HDM
to be a low-energy effective theory, the effect of heavy degrees of freedom contained in a
UV completion will in general introduce corrections to eq. (6.28), spoiling these specific
relations. The effective Lagrangian of dimension-six for example contains the following
terms that modify the Yukawa structure of the 2HDM,

$$
\mathcal{L}_{d=6} \supset \sum_{p,r,s} \frac{1}{\Lambda^2}\left(C_\ell^{prs}\,\Phi_p^\dagger\Phi_r\,(\bar L_L\,\ell_R\,\Phi_s)+\text{h.c.}\right)+\cdots\,,
\tag{6.29}
$$

where Λ represents the scale of new physics (beyond the 2HDM) and C_ℓ^{prs} are arbitrary
coefficients with the role of dimensionless low-energy constants that encode the high-
energy dynamics. Corrections of the type (6.29) are in general very small since these are
suppressed by inverse powers of the high energy scale Λ. For the LFV couplings however
these corrections can become relevant since it is possible that these couplings vanish or
are very small in the low-energy theory.

6.4.2   A CP-even Higgs with LFV couplings

The phenomenology of a CP-even Higgs at 125 GeV with LFV couplings has been analyzed
recently in refs. [7,18,19]. It has been noticed that large branching fractions for the decay
$h\to\tau\mu$ are possible $(\mathrm{BR}(h\to\tau\mu)\lesssim 0.1)$ while being compatible with present low-energy

constraints from $\tau \to \mu\gamma$ and $\tau \to \mu\mu\mu$. Higgs decays into a $\tau - e$ pair can also have large branching fractions consistent with low-energy flavour constraints while $h \to e\mu$ is already strongly bounded by $\mu \to e\gamma$ [7]. In ref. [19] it has been estimated that the LHC can set an upper bound $\mathrm{BR}(h \to \tau\mu) \lesssim 4.5 \times 10^{-3}$ with 20 fb^{-1} of data with Higgs production occurring mainly through the dominant gluon fusion mode.

The strongest low-energy constraint on possible τ-ℓ LFV couplings of the 125 GeV Higgs is obtained from the process $\tau \to \ell\gamma$. This decay occurs at the loop-level and receives dominant contributions from two-loop diagrams of the Barr-Zee type since the one-loop diagrams are chirality suppressed [28]. The LFV radiative τ decay however is not directly related to the process $pp(gg) \to h \to \tau\ell$ observable at the LHC. Indeed, heavy degrees of freedom belonging to the UV completion of the theory or additional scalars from an extended Higgs sector could contribute also to the effective dipole operator $(\bar{\ell}\sigma^{\mu\nu}P_{L,R}\tau)F_{\mu\nu}$, making the bound extracted very model dependent. For example, in the simple scenario of a 2HDM, the additional neutral Higgs bosons A and H generate interfering contributions through diagrams similar to the ones involving h. These effects cannot be neglected in general [16, 28].

It is therefore important to consider processes that can give a more reliable bound on the LFV couplings of the 125 GeV Higgs and, also, which are more directly connected with the observables measured at the LHC. Besides light quark exchange, the same effective vertex of the Higgs to gluons responsible for the production of the Higgs via gluon fusion at the LHC, would also contribute to the semileptonic decay $\tau \to \ell\pi\pi$ ($\pi\pi = \pi^+\pi^-, \pi^0\pi^0$), see figure 6.1. The energy scale of these processes however are completely different and in opposite domains of QCD: the LHC process $gg \to h$ occurs in the perturbative domain of QCD, while the τ decays takes place at an intermediate scale where non-perturbative QCD effects play a crucial role (one has to consider the matrix element $\langle\pi\pi|G^a_{\mu\nu}G^{\mu\nu}_a|0\rangle$). At the energy scale relevant for τ decays, the effective Lagrangian describing the interactions of the Higgs with light-quarks and gluons is given by [83]

$$\mathcal{L}^h_{eff} \simeq -\frac{h}{v}\left(\sum_{q=u,d,s} y^h_q\, m_q\, \bar{q}q - \sum_{q=c,b,t} \frac{\alpha_s}{12\pi}\, y^h_q\, G^a_{\mu\nu}G^{\mu\nu}_a\right). \tag{6.30}$$

Neglecting m_ℓ, the differential decay width for the decay $\tau \to \ell\pi\pi$ mediated by the CP-even Higgs h can be written in terms of the two-pion invariant mass $\sqrt{s}$ ($s = (p_{\pi^+} +$

$p_{\pi^-})^2 = (p_\tau - p_\ell)^2)$ as

$$
\frac{d\Gamma(\tau \to \ell\pi^+\pi^-)_{\mathrm{Higgs}}}{d\sqrt{s}} = \frac{(m_\tau^2 - s)^2 \, (s - 4m_\pi^2)^{1/2}}{256 \, \pi^3 \, m_\tau^3} \cdot \frac{|Y_{\tau\ell}^h|^2 + |Y_{\ell\tau}^h|^2}{M_h^4 \, v^2}
$$

$$
\times \left| \mathcal{K}_\Delta \Delta_\pi(s) + \mathcal{K}_\Gamma \Gamma_\pi(s) + \mathcal{K}_\theta \theta_\pi(s) \right|^2 ,
$$

$$
\frac{d\Gamma(\tau \to \ell\pi^0\pi^0)_{\mathrm{Higgs}}}{d\sqrt{s}} = \frac{1}{2} \frac{d\Gamma(\tau \to \mu\pi^+\pi^-)_{\mathrm{Higgs}}}{d\sqrt{s}} , \tag{6.31}
$$

where

$$
\mathcal{K}_\theta = \frac{2}{27} \sum_{q=c,b,t} y_q^h , \qquad \mathcal{K}_\Delta = y_s^h - \mathcal{K}_\theta , \qquad \mathcal{K}_\Gamma = \frac{m_u y_u^h + m_d y_d^h}{m_u + m_d} - \mathcal{K}_\theta . \tag{6.32}
$$

The form factors $\Gamma_\pi(s)$, $\Delta_\pi(s)$, and $\theta_\pi(s)$ parametrize the hadronic matrix elements of the scalar-currents and the gluonic operators (see eqs. (6.2) and (6.4)).

At the loop-level, a LFV Higgs also generates an effective dipole operator

$$
\mathcal{L}_{\mathrm{eff}} = c_L \, Q_{L\gamma} + c_R \, Q_{R\gamma} + \mathrm{h.c.} , \tag{6.33}
$$

with

$$
Q_{L\gamma, R\gamma} = \frac{e}{8\pi^2} m_\tau \left(\bar{\ell} \, \sigma^{\alpha\beta} \, P_{L,R} \, \tau \right) F_{\alpha\beta} . \tag{6.34}
$$

For the evaluation of the Wilson coefficients $c_{L,R}$ we consider one- and two-loop contributions calculated in ref. [28] and recently discussed in ref. [18]. The effective dipole operator gives rise to $\tau \to \ell\pi^+\pi^-$ via photon exchange, the associated differential decay width is given by (neglecting small lepton mass effects)

$$
\frac{d\Gamma(\tau \to \ell\pi^+\pi^-)_{\mathrm{photon}}}{d\sqrt{s}} = \frac{\alpha^2(|c_L|^2 + |c_R|^2)}{768\pi^5 \, m_\tau} \cdot \frac{(s - 4m_\pi^2)^{3/2} \, (m_\tau^2 - s)^2 \, (s + 2m_\tau^2) \, |F_V(s)|^2}{s^2} ,
$$

$$
\frac{d\Gamma(\tau \to \ell\pi^0\pi^0)_{\mathrm{photon}}}{d\sqrt{s}} = 0 , \tag{6.35}
$$

where $F_V(s)$ is the pion vector form factor defined in eq. (6.3).

The Higgs (eq. (6.31)) and photon exchange (eq. (6.35)) contributions do not interfere so that $\Gamma_{\mathrm{total}} = \Gamma_{\mathrm{Higgs}} + \Gamma_{\mathrm{photon}}$. While the $\tau \to \ell\pi^+\pi^-$ channel can be mediated by photon exchange, the $\tau \to \ell\pi^0\pi^0$ mode does not receive any contributions from intermediate photons due to the Bose statistics of the hadronic final state. The $\tau \to \mu\pi^0\pi^0$ decays therefore do not receive any contributions from the effective dipole operator $(\bar{\ell}\sigma^{\mu\nu} P_{L,R}\tau)F_{\mu\nu}$
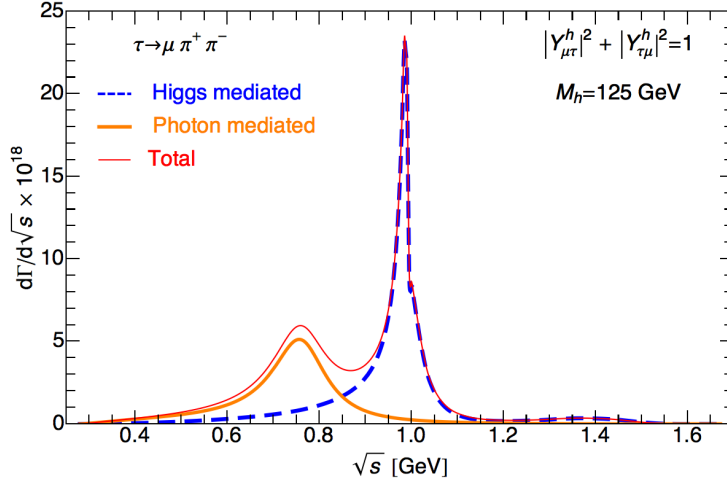
Figure 6.5: $\tau \to \mu\pi^{+}\pi^{-}$ *differential decay rate vs the di-pion invariant mass $\sqrt{s}$: dipole contribution (thick solid orange line), Higgs-mediated contribution (dashed blue line), and total rate (thin solid red line). The diagonal couplings of the Higgs are fixed to their SM values.*

and isolates the CP-even Higgs exchange contribution (a CP-odd Higgs cannot mediate $\tau \to \mu\pi\pi$ decays due to spin-parity conservation).

In figure. 6.5 we plot the $\tau \to \mu\pi^{+}\pi^{-}$ differential decay rate in the di-pion invariant mass $\sqrt{s}$, using the benchmark input values $M_h = 125$ GeV, $y_f^h = 1$, and $|Y_{\tau\ell}^h|^2 + |Y_{\ell\tau}^h|^2 = 1$. The dipole contribution is characterized by the ρ resonance peak, while the Higgs-mediated contribution (dominated by $\Delta_\pi(s)$ and $\theta_\pi(s)$) is characterized by the sharp $f_0(980)$ peak. Clearly, a measurement of the spectrum would greatly help disentangling the underlying LFV mechanism.

The branching fraction for $\tau \to \mu\pi^{+}\pi^{-}$ is shown in figure 6.6 (left-panel) as a function of the combination of LFV couplings $\sqrt{|Y_{\tau\mu}^h|^2 + |Y_{\mu\tau}^h|^2}$, the mass of the Higgs is fixed at $M_h = 125$ GeV and the diagonal fermionic Higgs couplings are taken to be SM-like ($y_f^h = 1$). We use here the form factors determined in section 6.3. The short-dashed (blue) curve shows the Higgs mediated contribution eq. (6.31) while the long-dashed (orange) curve shows the photon mediated one eq. (6.35). The total branching fraction is shown as a continuous (red) line. In figure 6.6 (right-panel) we compare our prediction for the Higgs mediated contribution to the one usually considered in the literature [9, 12, 14], which is based on leading order ChPT predictions for $\Gamma_\pi(s)$, see section 6.4.2 for a detailed
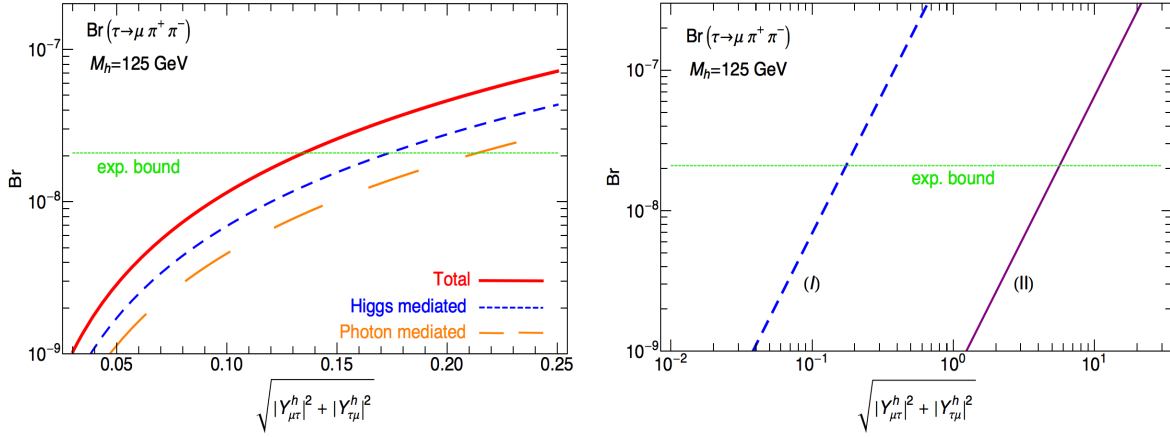
Figure 6.6:   *Left-plot: Branching fraction for $\tau \to \mu\pi^+\pi^-$ as a function of $\sqrt{|Y_{\mu\tau}^h|^2 + |Y_{\tau\mu}^h|^2}$ for $M_h = 125$ GeV and SM-like diagonal couplings (continuous red line). The effective dipole contribution is shown in orange (long-dashed) while the Higgs exchange contribution is shown in blue (short-dashed). The present experimental upper bound is shown in green (horizontal dashed line). Right-plot: Higgs mediated contribution to the branching ratio considering: (I) our prediction for the form factors $\{\Gamma_\pi(s), \Delta_\pi(s), \theta_\pi(s)\}$ using ChPT and dispersion relations, (II) estimate usually found in the literature considering only the scalar form factor $\Gamma_\pi(s)$ in LO-ChPT.*

discussion.

In table 6.2 we show the bounds that different LFV τ decays put on the combination of LFV couplings $\sqrt{|Y_{\mu\tau}^h|^2 + |Y_{\tau\mu}^h|^2}$, assuming SM-like diagonal Yukawa couplings ($y_f^h = 1$). Similar bounds for $\tau - e$ transitions are shown in table 6.3. The branching fraction for $\tau \to \mu\rho$ is obtained by a cut on the invariant mass of the pair of charged pions ($\pi^+\pi^-$), 587 MeV $< \sqrt{s} <$ 962 MeV [86]. The processes $\tau \to \mu\gamma$ and $\tau \to 3\mu$ receive the dominant contribution from two-loop diagrams of the Barr-Zee type [28]. We find our results for these processes to be in good agreement with those of ref. [18]. Even though the experimental limits for $\tau \to \mu\gamma$ and $\tau \to 3\mu$ are very similar, the extracted bound from $\tau \to 3\mu$ is weaker by an order of magnitude mainly due to the additional factor of $\alpha_{\rm em}$.

The 90% CL current upper bounds on BR($\tau \to \ell\pi^+\pi^-$) set by the Belle collaboration are at the 10^{-8} level using 854 fb^{-1} of collected data [87]. While weaker by one order

Process	(BR $\times 10^8$) 90% CL	$\sqrt{|Y_{\mu\tau}^h|^2 + |Y_{\tau\mu}^h|^2}$	Operator(s)
$\tau \to \mu\gamma$	< 4.4 [89]	< 0.016	Dipole
$\tau \to \mu\mu\mu$	< 2.1 [90]	< 0.24	Dipole
$\tau \to \mu\pi^+\pi^-$	< 2.1 [87]	< 0.13	Scalar, Gluon, Dipole
$\tau \to \mu\rho$	< 1.2 [86]	< 0.13	Scalar, Gluon, Dipole
$\tau \to \mu\pi^0\pi^0$	< 1.4 $\times 10^3$ [88]	< 6.3	Scalar, Gluon

Table 6.2: *Current experimental upper bounds on the different processes considered as well as the bounds obtained on* $\sqrt{|Y_{\mu\tau}^h|^2 + |Y_{\tau\mu}^h|^2}$ *for a CP-even Higgs at* 125 *GeV and SM-like diagonal couplings* $y_f^h = 1$*. The last column indicates the dominant operators contributing to each process.*

of magnitude compared to $\tau \to \ell\gamma$, the bounds from $\tau \to \ell\pi\pi$ are quite less sensitive to the UV detail of the theory, and thus allow one to probe more directly the Higgs LFV couplings. We observe that the Belle and BaBar collaborations have not presented results for the $\tau \to \ell\pi^0\pi^0$ mode. The current upper limit in this channel was set by the CLEO collaboration with 4.68 fb^{-1} of collected data, BR($\tau \to \mu\pi^0\pi^0$) < 1.4 $\times 10^{-5}$ and BR($\tau \to e\pi^0\pi^0$) < 6.5 $\times 10^{-6}$ at 90% CL [88].

Note from figure 6.6 that the Higgs and photon mediated contributions to $\tau \to \mu\pi^+\pi^-$ are of similar size. One can then infer that if the mode $\tau \to \mu\pi^0\pi^0$ had been updated by the Belle or BaBar collaborations, it would be possible to set a limit on $\sqrt{|Y_{\mu\tau}^h|^2 + |Y_{\tau\mu}^h|^2}$ at the 10^{-1} level from this process. This is reinforced by the fact that the upper-limit set by the CLEO collaboration on the mode $\tau \to \mu\pi^+\pi^-$ is very similar to that for $\tau \to \mu\pi^0\pi^0$ [88]. The process $\tau \to \mu\pi^0\pi^0$ has the advantage compared to $\tau \to \mu\pi^-\pi^+$, that it cannot be mediated by the photon and is therefore not affected by possible NP effects entering into the effective dipole operator. The decay $\tau \to \mu\pi^0\pi^0$ establishes the most direct connection between searches for LFV τ decays at B-factories and the search for LFV Higgs decays at the LHC: $pp(gg) \to h \to \tau\mu$. Similar arguments apply for $\tau \to e\pi^0\pi^0$. If LFV Higgs decays are observed at some point, this would imply lower bounds on the $\tau \to \ell\pi^0\pi^0$ BR. We therefore encourage the experimental collaborations to provide limits for this channel in the future.

Process	(BR $\times 10^8$) 90% CL	$\sqrt{|Y_{e\tau}^h|^2 + |Y_{\tau e}^h|^2}$	Operator(s)
$\tau \to e\gamma$	< 3.3 [89]	< 0.014	Dipole
$\tau \to eee$	< 2.7 [90]	< 0.12	Dipole
$\tau \to e\pi^+\pi^-$	< 2.3 [87]	< 0.14	Scalar, Gluon, Dipole
$\tau \to e\rho$	< 1.8 [86]	< 0.16	Scalar, Gluon, Dipole
$\tau \to e\pi^0\pi^0$	$< 6.5 \times 10^2$ [88]	< 4.3	Scalar, Gluon

Table 6.3: *Current experimental upper bounds on the different processes considered as well as the bounds obtained on $\sqrt{|Y_{e\tau}^h|^2 + |Y_{\tau e}^h|^2}$ for a CP-even Higgs at 125 GeV and SM-like diagonal couplings $y_f^h = 1$. The last column indicates the dominant operators contributing to each process.*

The impact of hadronic matrix elements

In figure 6.6 (right-panel) we show the branching ratio for $\tau \to \mu\pi^+\pi^-$ considering only the LO-ChPT prediction for the form factor $\Gamma_\pi(s)^{\text{LO-ChPT}} = m_\pi^2$ (while neglecting $\Delta_\pi(s)$ and $\theta_\pi(s)$) as done in refs. [9, 12, 14]. Our prediction considering the three form factors $\{\Gamma_\pi(s), \Delta_\pi(s), \theta_\pi(s)\}$, estimated using ChPT together with dispersion relations, is observed to be significantly larger. It is important to clarify some points regarding such comparison between our results and those that have been considered previously by other authors using LO-ChPT. First, a proper treatment of the decay $\tau \to \mu\pi^+\pi^-$ would require taking into account not only $\Gamma_\pi(s)$ as is usually done, but also $\theta_\pi(s)$ and $\Delta_\pi(s)$ which actually provide the dominant contributions to the decay rate. The LO-ChPT prediction for these form factors is [72]

$$\theta_\pi(s)^{\text{LO-ChPT}} = s + 2m_\pi^2\,, \qquad \Gamma_\pi(s)^{\text{LO-ChPT}} = m_\pi^2\,, \qquad \Delta_\pi(s)^{\text{LO-ChPT}} = d_F s + d_B m_\pi^2\,. \quad (6.36)$$

Here $d_F = 0.09$ while $d_B \simeq 0$, and we refer the reader to ref. [72] for the respective NLO-ChPT predictions. The range of validity of the ChPT form factors is about $\sqrt{s_\chi} \sim$ 0.3 GeV (LO-ChPT) or $\sqrt{s_\chi} \sim 0.5$ GeV (NLO-ChPT), see figures 6.7-6.8. The LO-ChPT form factors are always real. The absorptive contribution starts at NLO in ChPT due to the appearance of re-scattering one-loop diagrams generated by interaction terms of the leading chiral Lagrangian [72]. Above $\sqrt{s} \sim 0.5$ GeV, even the NLO-ChPT is not reliable anymore and significant departures can be observed compared with the form

factors obtained using dispersion relations, that take into account large $\pi\pi$ rescattering effects beyond one-loop.
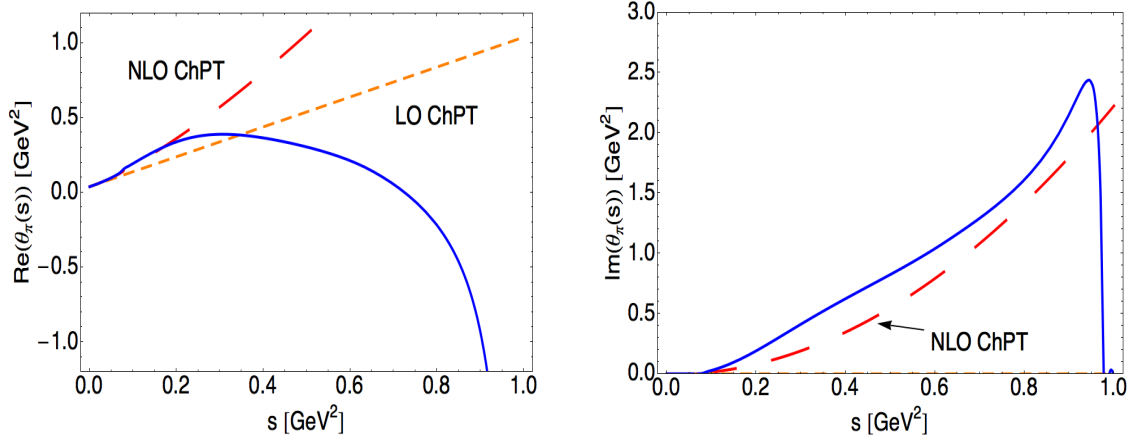

Figure 6.7: *Real (left) and imaginary (right) part of the form factor associated with the trace of the QCD energy-momentum tensor, $\theta_\pi(s)$, using different treatments: LO-ChPT (short-dashed orange), NLO-ChPT (long-dashed red), and our prediction based on ChPT and dispersion relations (continuous blue).*

In order to asses the impact of the hadronic matrix elements for the calculation of the $\tau \to \ell\pi\pi$ decay rate, we consider the ratio

$$R = \frac{\int_{s_{\min}}^{s_\chi} ds \, [d\Gamma(\tau \to \mu\pi^+\pi^-)_{\text{Higgs}}/ds]_{\text{LO-ChPT}}}{\int_{s_{\min}}^{s_{\max}} ds \, [d\Gamma(\tau \to \mu\pi^+\pi^-)_{\text{Higgs}}/ds]_{\text{ChPT + DR}}} \simeq 3.3 \times 10^{-5}. \qquad (6.37)$$

Here the numerator stands for the decay width calculated using the LO-ChPT predictions for the hadronic form factors (using the expressions in eq. (6.36)), integrated up to a cut-off $\sqrt{s_\chi} \simeq 0.3$ GeV that specifies the range of validity of the LO-ChPT treatment. The denominator represents the decay width calculated using the form factors obtained in this work using dispersion relations (DR) to extend the range of validity of the hadronic matrix elements to higher energies. The smallness of $R \simeq 3.3 \times 10^{-5}$ shows the importance of a proper treatment of the hadronic matrix elements. One may argue that by cutting the phase space integral at $\sqrt{s_\chi} = 0.3$ GeV one is throwing away most of the effect, some authors for example use the LO-ChPT estimates of the form factors over the full parameter space. If we set $s_\chi = s_{\max}$ in eq. (6.37) we get instead the much larger value
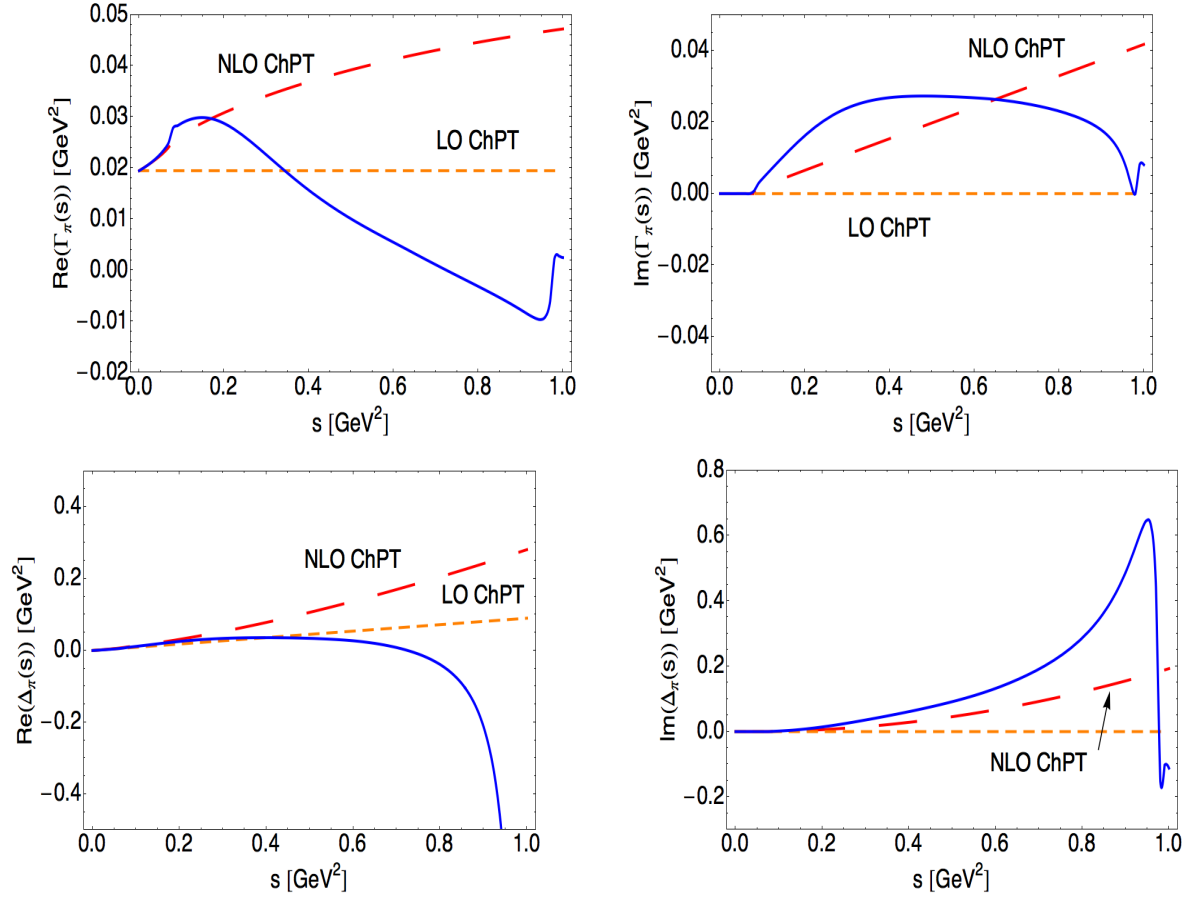
Figure 6.8: *Real (left) and imaginary (right) part for the scalar form factors $(\Gamma_\pi(s), \Delta_\pi(s))$, using different treatments: LO-ChPT (short-dashed orange), NLO-ChPT (long-dashed red), and our prediction based on ChPT and dispersion relations (continuous blue).*

$R = 0.45$. This however is a very misleading result, based on using LO-ChPT form factors in a kinematical regime where they no longer describe properly the hadronic dynamics. [4]

---

[4] The authors of ref. [29], working within an effective theory framework, set bounds on LFV gluonic operators from $\tau \to \ell\pi\pi$ using the LO-ChPT result in the chiral limit, namely $\theta_\pi(s) = s$. The claim that large departures from the LO-ChPT predictions are not to be expected [29] misses the fact that even in the chiral limit ($m_u = m_d = m_s = 0$) ChPT is inadequate to describe the hadronic dynamics for large invariant masses of the $\pi\pi$ system $\sqrt{s} \sim 1$ GeV.

6.4.3   A CP-odd Higgs with LFV couplings

The Higgs boson at 125 GeV cannot be a pure pseudoscalar state, the experimental data already constrain its coupling to vector bosons to be very close to the SM value and analyses of the angular distributions in the Higgs decay final states also disfavor this possibility [1, 2]. Assuming that the $h(125)$ boson is the lightest CP-even state of a general 2HDM, current LHC and Tevatron measurements of the $h(125)$ properties imply that $g_{hVV} \simeq g_{hVV}^{\rm SM}$ [85, 91–93]. Lepton flavour violating Yukawa couplings of h would take the form: $(\Pi_f)_{ij}/v \sin \tilde{\alpha}$ (see eq. (6.28)) and are therefore suppressed by the small factor $|\sin \tilde{\alpha}| = \left(1 - (g_{hVV}/g_{hVV}^{\rm SM})^2\right)^{1/2}$. The LFV Yukawa couplings of the heavier CP-even state H and the CP-odd Higgs A on the other hand do not receive this suppression. It is therefore interesting not only to consider searches for LFV decays of the 125 GeV boson at the LHC, but also of possible additional Higgs bosons. The question of which observables measurable at flavour factories could be related to the process $pp(gg) \to A \to \tau\mu$ relevant at the LHC then arises naturally. We argue in this section that the semileptonic decays of τ into a pseudoscalar meson P, $\tau \to \ell P$, provide a direct connection with the search for a CP-odd Higgs with LFV couplings at the LHC. In this section we focus on the CP-odd boson A, which implies a somewhat different phenomenology of τ LFV decays compared to the CP-even state already analyzed in the previous section and in refs. [7, 18, 19]. We do not consider the effect of interfering contributions of the different scalars $\varphi_k = \{h, H, A\}$ in $\tau \to \ell\gamma$ or the phenomenology of the charged Higgs, these have been discussed elsewhere [12, 16, 28].

At the relevant energy scale for τ decays, the heavy-quarks can be integrated out from the theory, the effective Lagrangian describing the interactions of the CP-odd Higgs with the light quarks is then given by [83]

$$\mathcal{L}_{eff}^A \simeq -\frac{A}{v} \left(\sum_{q=u,d,s} y_q^A \, m_q \, \bar{q} i \gamma_5 \, q - \sum_{q=c,b,t} y_q^A \, \frac{\alpha_s}{8\pi} \, G_{\mu\nu}^a \, \widetilde{G}_{\mu\nu}^a \right) , \qquad (6.38)$$

with real couplings y_q^A related to those of eq. (6.1) by $\mathrm{Im} Y_{qq}^A = (m_q/v) y_q^A$ and the dual tensor of the gluon field strength defined by $\widetilde{G}_{\rho\nu}^a = \frac{1}{2} \epsilon_{\rho\nu\alpha\beta} G_{\alpha\beta}^a$ (with $\epsilon^{0123} = 1$). Contrary to a CP-even Higgs boson, a CP-odd Higgs with LFV couplings can mediate at tree-level the semileptonic decays $\tau \to \ell P$, where $P = \pi^0, \eta, \eta'$, stands for a pseudoscalar meson. Semileptonic τ decays into a pseudoscalar meson cannot be mediated by the photon either,

so that this mode isolates the CP-odd Higgs exchange. The decays $\tau \to \ell P$ therefore establish a direct connection with the search for CP-odd Higgs decays into LFV channels at the LHC, with the Higgs being produced via gluon fusion. The relevant hadronic matrix elements can be obtained following the FKS mixing scheme [94, 95], those involving the Higgs coupling to light-quarks are parametrized by

$$
\langle \pi^0(p)|\bar{u}\,\gamma_5\,u|0\rangle \;=\; i\,\frac{m_\pi^2}{2\sqrt{2}\hat{m}}\,f_\pi\,, \qquad\qquad \langle \pi^0|\bar{d}\,\gamma_5\,d|0\rangle = -\langle \pi^0(p)|\bar{u}\,\gamma_5\,u|0\rangle\,, \qquad (6.39)
$$
$$
\langle \eta^{(\prime)}(p)|\bar{q}\,\gamma_5\,q|0\rangle \;=\; -\frac{i}{2\sqrt{2}m_q}\,h^q_{\eta^{(\prime)}}\,, \qquad\quad \langle \eta^{(\prime)}(p)|\bar{s}\,\gamma_5\,s|0\rangle \;=\; -\frac{i}{2m_s}\,h^s_{\eta^{(\prime)}}\,,
$$

while those related to the loop-induced effective operator $AG^a_{\mu\nu}\widetilde{G}^a_{\mu\nu}$ are given by

$$
\langle \eta^{(\prime)}(p)|\frac{\alpha_s}{4\pi}\,G^{\mu\nu}_a\widetilde{G}^a_{\mu\nu}|0\rangle = a_{\eta^{(\prime)}}\,. \qquad (6.40)
$$

Numerical values for the different parameters appearing in eqs. (6.39,6.40) are given in table 6.4. The contributions from the effective operator $AG^a_{\mu\nu}\widetilde{G}^a_{\mu\nu}$ to the decay $\tau \to \ell\pi$ vanishes in the isospin limit $m_u = m_d$ [96] and we do not consider it here. The total decay

Parameter	Value
f_π	130.41 ± 0.20 MeV
h^q_η	0.001 ± 0.003 GeV^3
$h^q_{\eta'}$	0.001 ± 0.002 GeV^3
h^s_η	-0.055 ± 0.003 GeV^3
$h^s_{\eta'}$	0.068 ± 0.005 GeV^3
a_η	0.022 ± 0.002 GeV^3
$a_{\eta'}$	0.056 ± 0.002 GeV^3

Table 6.4: *Numerical values for the hadronic matrix elements relevant for $\tau \to \ell P$ ($P = \pi, \eta, \eta'$) obtained in the FKS mixing scheme [94, 95].*

width for $\tau \to \ell\pi^0$, neglecting small lepton and pion mass effects, reads

$$
\Gamma(\tau \to \ell\pi^0) \;=\; \frac{f_\pi^2\,m_\pi^4\,m_\tau}{256\pi M_A^4\,v^2}\left(|Y^A_{\tau\mu}|^2 + |Y^A_{\mu\tau}|^2\right)\left(y^A_u - y^A_d\right)^2\,, \qquad (6.41)
$$

the amplitude for $\tau \to \mu\pi^0$ vanishes exactly in the limit $y_u^A = y_d^A$ since the π^0 only selects the isovector component of the amplitude. The decay width for $\tau \to \ell\eta$ can be written using the definitions of eqs. (6.39,6.40) as (neglecting small lepton mass effects)

$$\Gamma(\tau \to \ell\eta) = \frac{\bar{\beta}\,(m_\tau^2 - m_\eta^2)\,(|Y_{\mu\tau}^A|^2 + |Y_{\tau\mu}^A|^2)}{256\,\pi\,M_A^4\,v^2\,m_\tau}\left[(y_u^A + y_d^A)h_\eta^q + \sqrt{2}y_s^A h_\eta^s - \sqrt{2}a_\eta \sum_{q=c,b,t} y_q^A\right]^2 ,$$

(6.42)

with $\bar{\beta} = (1 - 2(m_\ell^2 + m_\eta^2)/m_\tau^2 + (m_\ell^2 - m_\eta^2)^2/m_\tau^4)^{1/2}$. A simple replacement of $\eta \to \eta'$ in eq. (6.42) gives the expression for $\Gamma(\tau \to \ell\eta')$.

A CP-odd Higgs boson would also give rise to an effective dipole operator at the loop-level [28], contributing then to $\tau \to \ell\gamma$, and photon-mediated $\tau \to \ell\pi^+\pi^-$, 3ℓ decays. Note that while $\tau \to 3\ell$ is also mediated at tree-level by the CP-odd Higgs, the semileptonic decay $\tau \to \ell\pi\pi$ are not due to spin-parity conservation. The CP-odd Higgs exchange contribution to $\tau \to 3\mu$ is however sub-leading compared to that coming from the two-loop diagrams of the Barr-Zee type due to the small Yukawa coupling to the muons, see the recent discussion in ref. [18]. In tables 6.5 and 6.6 we summarize the bounds on $\sqrt{|Y_{\ell\tau}^A|^2 + |Y_{\tau\ell}^A|^2}$ from the different τ decays considered fixing the diagonal couplings to $|y_f^A| = 1$. The scaling of the semileptonic $\tau \to \ell P$ decay rates with the CP-odd Higgs mass is very simple, $\propto M_A^{-4}$, while that for processes mediated by the photon is non-trivial due to loop-functions entering in the calculation of the transition dipole moment. The stringent bound coming from $\tau \to \ell\gamma$ is sensitive to possible interference effects from other scalars or heavy particles from a UV completion of the theory. The semileptonic decays $\tau \to \ell P$ on the other hand are mediated at tree-level by the CP-odd Higgs exchange and provide then a more reliable bound in this respect.

In case any LFV signal $pp \to \tau\ell + X$ is observed at the LHC, it will be crucial to determine the properties of the mediator. The complementarity between low-energy searches for LFV τ decays and the energy frontier is very important for this purpose. A CP-even Higgs with LFV couplings for example would give rise to $\tau \to \ell\gamma$ decays via loop contributions while it cannot mediate semileptonic $\tau \to \ell P$ decays. If the 125 GeV Higgs turns out to have sizable LFV couplings and $h \to \tau\ell$ decays are observed at some point at the LHC, specific patterns between all the possible LFV τ decays would then be predicted and any departure from these could be an indication of additional particles with LFV couplings for example.

Process	(BR $\times 10^8$) 90% CL	$M_A = 200$ GeV	$M_A = 500$ GeV	$M_A = 700$ GeV
$\tau \to \mu\gamma$	< 4.4 [89]	$Z < 0.018$	$Z < 0.040$	$Z < 0.055$
$\tau \to \mu\mu\mu$	< 2.1 [90]	$Z < 0.28$	$Z < 0.60$	$Z < 0.85$
$^{(*)} \tau \to \mu\pi$	< 11 [97]	$Z < 41$	$Z < 257$	$Z < 503$
$^{(*)} \tau \to \mu\eta$	< 6.5 [97]	$Z < 0.52$	$Z < 3.3$	$Z < 6.4$
$^{(*)} \tau \to \mu\eta'$	< 13 [97]	$Z < 1.1$	$Z < 7.2$	$Z < 14.1$
$\tau \to \mu\pi^+\pi^-$	< 2.1 [87]	$Z < 0.25$	$Z < 0.54$	$Z < 0.75$
$\tau \to \mu\rho$	< 1.2 [86]	$Z < 0.20$	$Z < 0.44$	$Z < 0.62$

Table 6.5: *Current experimental upper bounds on the different processes considered as well as the bounds obtained on $Z \equiv \sqrt{|Y_{\mu\tau}^A|^2 + |Y_{\tau\mu}^A|^2}$ for different values of the CP-odd Higgs mass and SM-like diagonal couplings $|y_f^A| = 1$. Neither the effective dipole operator nor the CP-even Higgs exchange contribute to the processes marked with $^{(*)}$.*

Process	(BR $\times 10^8$) 90% CL	$M_A = 200$ GeV	$M_A = 500$ GeV	$M_A = 700$ GeV
$\tau \to e\gamma$	< 3.3 [89]	$Z < 0.016$	$Z < 0.034$	$Z < 0.05$
$\tau \to eee$	< 2.7 [90]	$Z < 0.14$	$Z < 0.30$	$Z < 0.42$
$^{(*)} \tau \to e\pi$	< 8 [97]	$Z < 35$	$Z < 219$	$Z < 430$
$^{(*)} \tau \to e\eta$	< 9.2 [97]	$Z < 0.6$	$Z < 3.9$	$Z < 7.6$
$^{(*)} \tau \to e\eta'$	< 16 [97]	$Z < 1.3$	$Z < 8$	$Z < 15.6$
$\tau \to e\pi^+\pi^-$	< 2.3 [87]	$Z < 0.26$	$Z < 0.56$	$Z < 0.80$
$\tau \to e\rho$	< 1.8 [86]	$Z < 0.25$	$Z < 0.54$	$Z < 0.76$

Table 6.6: *Current experimental upper bounds on the different processes considered as well as the bounds obtained on $Z \equiv \sqrt{|Y_{e\tau}^A|^2 + |Y_{\tau e}^A|^2}$ for different values of the CP-odd Higgs mass and SM-like diagonal couplings $|y_f^A| = 1$. Neither the effective dipole operator nor the CP-even Higgs exchange contribute to the processes marked with $^{(*)}$.*

In view of the possibility to make a dedicated search for heavy scalars decaying to a $\tau - \mu$ pair, similar to the flavour conserving searches [98, 99], we estimate the total cross-section for $\sigma(pp \to A \to \tau\mu)$ at the LHC. The inclusive Higgs production cross-
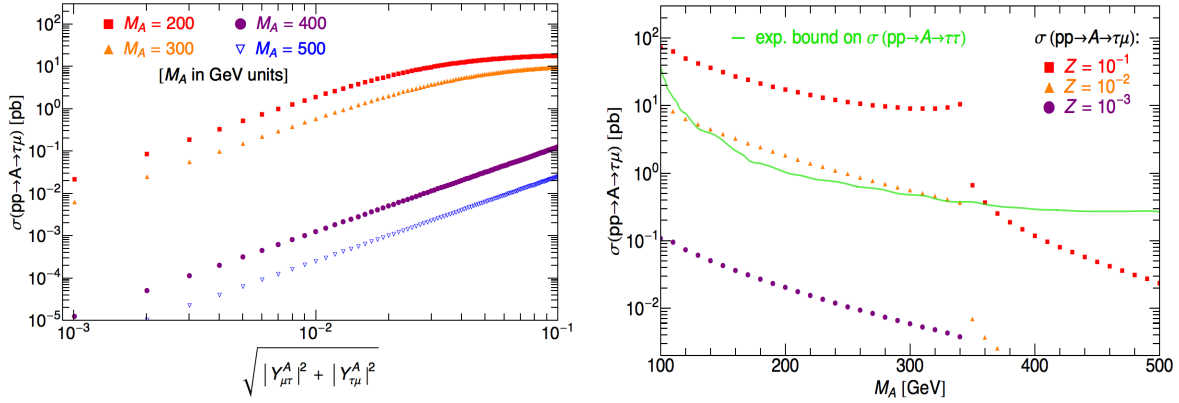
Figure 6.9: *Left-plot: Inclusive cross-section $\sigma(pp \to A \to \tau\mu)$ at $\sqrt{s} = 8$ TeV as a function of $Z \equiv \sqrt{|Y_{\mu\tau}^A|^2 + |Y_{\tau\mu}^A|^2}$ for SM-like diagonal couplings $|y_f^A| = 1$, taking different values of the CP-odd Higgs mass M_A. Right-plot: Inclusive cross-section $\sigma(pp \to A \to \tau\mu)$ at $\sqrt{s} = 8$ TeV as a function of the CP-odd Higgs mass M_A for $Z = 0.1$ (squares), 0.01 (triangles), 0.001 (circles). The continuous green line shows the upper bound at 95% CL on the cross-section $\sigma(pp \to A \to \tau\tau)$ using the full $2011 + 2012$ data set by the CMS collaboration [98].*

section $\sigma(pp \to A)$ was obtained using the *SusHi* code [100, 101], considering only the dominant gluon fusion production mode. Higgs partial decay widths were obtained using the *2HDMC* code [102]. For a CP-odd Higgs we have (neglecting small lepton mass corrections)

$$\Gamma(A \to \tau^+\mu^- + \tau^-\mu^+) \equiv \Gamma(A \to \tau\mu) = \frac{M_A \left(|Y_{\tau\mu}^A|^2 + |Y_{\mu\tau}^A|^2\right)}{8\pi} \ . \qquad (6.43)$$

We assume that besides $A \to \tau\mu$, only SM decay channels are significant ($A \to gg, \bar{c}c, \bar{b}b, \tau\tau, \ldots$) and we fix the diagonal Yukawa couplings at $|y_f^A| = 1$. Large branching ratios for the fermionic decays of a CP-odd Higgs and in particular for the $A \to \tau\mu$ mode, can be obtained since the CP-odd Higgs does not couples to $VV = W^+W^-, ZZ$ at tree-level. Here we focus on the $\tau - \mu$ mode but an analogous analysis can be carried for $\tau - e$.

In figure 6.9 we show the total cross-section $\sigma(pp \to A \to \tau\mu)$ as a function of $\sqrt{|Y_{\mu\tau}^A|^2 + |Y_{\tau\mu}^A|^2}$ for $\sqrt{s} = 8$ TeV. A large drop in the total cross section can be observed when $M_A \gtrsim 2m_t$ since $A \to \bar{t}t$ decays become kinematically open and suppress the branching ratio BR($A \to \tau\mu$). The total cross-section $\sigma(pp \to A \to \tau\mu)$ can be as large as ~ 1 pb for a CP-odd Higgs with $M_A \sim 200$ GeV and $\sqrt{|Y_{\mu\tau}^A|^2 + |Y_{\tau\mu}^A|^2} \sim 10^{-2}$, which

is allowed in principle by low-energy constraints, see table 6.5. Current upper bounds for the flavour conserving cross-section $\sigma(pp \to A \to \tau\tau)$ by the CMS collaboration, using the full $2011 + 2012$ data set [98], are also shown in figure 6.9. The bound on $\sigma(pp \to A \to \tau\tau)$ is already at the ~ 1 pb level. One can therefore expect that the sensitivity of the LHC to a plausible heavy Higgs with LFV couplings should be very good compared to flavour constraints, as previous analyses have shown for the 125 GeV boson [18, 19]. A detailed analysis of the LHC prospects to detect LFV Higgs decays of a heavy Higgs boson within the generic 2HDM was performed in ref. [103] finding promising results. Given the considerable experimental progress in the study of the Higgs sector over the last years, we encourage experimental collaborations to consider the search for heavy scalars in LFV decay modes.

6.5   Conclusions

The discovery of a new boson around 125 GeV, $h(125)$, opens a new era in our understanding of the electroweak symmetry breaking mechanism, yet to be explored in detail. Any departure from the SM Higgs properties or exotic effect associated with the $h(125)$ boson would be an indication of new physics beyond the SM. The search for LFV phenomena in the scalar sector at the LHC has a special role in this respect, given the relatively weak constraints from low-energy experiments.

While $h \to e\mu$ transitions are strongly constrained already by $\mu \to e\gamma$ decays and $\mu - e$ conversion in nuclei, the situation is completely different for $h \to \tau\ell$ ($\ell = e, \mu$) in which large decay rates are still allowed [7, 18, 19]. The strongest bound on such LFV Higgs couplings is currently extracted from the radiative $\tau \to \ell\gamma$ decays. This decay receives dominant contributions from two-loop diagrams of the Barr-Zee type due to the strong chirality suppression of the one-loop diagrams, making the bounds very sensitive to the underlying UV model.

Hadronic τ-lepton decays offer an interesting low-energy handle to constrain possible LFV effects associated with the Higgs sector and in particular the $h(125)$ boson. The bounds extracted from hadronic τ-decays are less sensitive to the UV completion of the theory and establish a more direct connection with the search for LFV Higgs decays at the LHC. We have shown in this work that the bounds obtained from semileptonic decays

$\tau \to \ell\pi\pi$ are at the same level than those from $\tau \to 3\ell$ ($\tau \to 3\ell$ decays are dominated by the same two-loop diagrams than $\tau \to \ell\gamma$ and are therefore very sensitive to the UV completion of the theory). This result was achieved thanks to an adequate description of the hadronic matrix elements involved, improving considerably over previous related works on this subject. Concerning the semileptonic $\tau \to \ell\pi\pi$ transitions we emphasize the following results found in this work:

- In section 6.3 we provide a dispersive treatment of all the hadronic matrix elements needed to describe Higgs mediated $\tau \to \ell\pi\pi$ decays. These results will be useful in analyzing $\tau \to \ell\pi\pi$ decays beyond the specific framework adopted here.

- The form factors obtained in section 6.3 were used to extract robust bounds on possible LFV couplings of the $h(125)$ boson from current experimental data. This was done in section 6.4.2, the main results being summarized in tables 6.2 and 6.3, as well as figures 6.5 and 6.6.

- We find that the dominant contributions to the Higgs mediated decay rate $\tau \to \ell\pi\pi$ arise from the effective Higgs couplings to gluons (induced by heavy quarks) and the strange component of the scalar current (Higgs coupling directly to strange quarks). Previous treatments [9, 12, 14] of these decays considering only the scalar current $m_u \bar{u}u + m_d \bar{d}d$ therefore do not capture the main contributions to the decay rate.

- LO-ChPT predictions for the hadronic matrix elements contributing to $\tau \to \ell\pi\pi$ are valid only at very low energies $\sqrt{s} \lesssim 0.3$ GeV (see section 6.4.2): if used over the whole phase space they lead to unreliable bounds on the LFV couplings.

- Contrary to $\tau \to \ell\pi^+\pi^-$, the $\tau \to \ell\pi^0\pi^0$ decays cannot be mediated by the effective dipole operator $(\bar{\ell}\sigma^{\mu\nu}P_{L,R}\tau)F_{\mu\nu}$ and isolate the CP-even Higgs exchange contribution. So $\tau \to \ell\pi^0\pi^0$ decays establish the most direct connection between searches for LFV τ decays at B-factories and the search for LFV Higgs decays at the LHC ($pp(gg) \to h \to \tau\ell$). We encourage the experimental collaborations to provide limits for these modes in the future.

Finally, we point out in section 6.4.3 that the search for LFV effects associated to the scalar sector should not be restricted to the $h(125)$ boson. Within the general 2HDM, it

is plausible that the LFV couplings of the $h(125)$ boson are too suppressed to be observed given that its coupling to vector bosons $VV = W^+W^-, ZZ$ is already constrained to be very close to the SM value. If such an LFV extended scalar sector is realized in nature, it might be possible on the other hand to detect LFV phenomena at the LHC due to the decays of additional scalars for which such strong suppression of the LFV couplings does not takes place. Current constraints from low-energy flavour experiments still allow for sizable LFV effects in this respect.

Acknowledgments

Bibliography

[1] CMS Collaboration, CMS-PAS-HIG-13-005.

[2] [ATLAS Collaboration], ATLAS-CONF-2013-034.

[3] K. Cheung, J. S. Lee and P. -Y. Tseng, JHEP **1305** (2013) 134 [arXiv:1302.3794 [hep-ph]].

[4] J. Ellis and T. You, JHEP **1306** (2013) 103 [arXiv:1303.3879 [hep-ph]].

[5] A. Falkowski, F. Riva and A. Urbano, JHEP **1311** (2013) 111 [arXiv:1303.1812 [hep-ph]].

[6] P. P. Giardino, K. Kannike, I. Masina, M. Raidal and A. Strumia, arXiv:1303.3570 [hep-ph].

[7] G. Blankenburg, J. Ellis and G. Isidori, Phys. Lett. B **712** (2012) 386 [arXiv:1202.5704 [hep-ph]].

[8] J. L. Diaz-Cruz and J. J. Toscano, Phys. Rev. D **62** (2000) 116005 [hep-ph/9910233].

[9] D. Black, T. Han, H. -J. He and M. Sher, Phys. Rev. D **66** (2002) 053002 [hep-ph/0206056].

[10] K. S. Babu and C. Kolda, Phys. Rev. Lett. **89** (2002) 241802 [hep-ph/0206310].

[11] A. Brignole and A. Rossi, Nucl. Phys. B **701** (2004) 3 [hep-ph/0404211].

[12] S. Kanemura, T. Ota and K. Tsumura, Phys. Rev. D **73** (2006) 016006 [hep-ph/0505191].

[13] P. Paradisi, JHEP **0602** (2006) 050 [hep-ph/0508054].

[14] E. Arganda, M. J. Herrero and J. Portoles, JHEP **0806** (2008) 079 [arXiv:0803.2039 [hep-ph]].

[15] M. J. Herrero, J. Portoles and A. M. Rodriguez-Sanchez, Phys. Rev. D **80** (2009) 015023 [arXiv:0903.5151 [hep-ph]].

[16] S. Davidson and G. J. Grenier, Phys. Rev. D **81** (2010) 095016 [arXiv:1001.0434 [hep-ph]].

[17] A. Goudelis, O. Lebedev and J. -h. Park, Phys. Lett. B **707** (2012) 369 [arXiv:1111.1715 [hep-ph]].

[18] R. Harnik, J. Kopp and J. Zupan, JHEP **1303** (2013) 026 [arXiv:1209.1397 [hep-ph]].

[19] S. Davidson and P. Verdier, Phys. Rev. D **86** (2012) 111701 [arXiv:1211.1248 [hep-ph]].

[20] A. Crivellin, A. Kokulu and C. Greub, Phys. Rev. D **87** (2013) 9, 094031 [arXiv:1303.5877 [hep-ph]].

[21] A. Dery, A. Efrati, Y. Hochberg and Y. Nir, JHEP **1305** (2013) 039 [arXiv:1302.3229 [hep-ph]].

[22] A. Arhrib, Y. Cheng and O. C. W. Kong, Phys. Rev. D **87** (2013) 015025 [arXiv:1210.8241 [hep-ph]].

[23] M. Arana-Catania, E. Arganda and M. J. Herrero, JHEP **1309** (2013) 160 [arXiv:1304.3371 [hep-ph]].

[24] W. Buchmuller and D. Wyler, Nucl. Phys. B **268** (1986) 621.

[25] B. Grzadkowski, M. Iskrzynski, M. Misiak and J. Rosiek, JHEP **1010** (2010) 085 [arXiv:1008.4884 [hep-ph]].

[26] J. F. Gunion, H. E. Haber, G. L. Kane and S. Dawson, Front. Phys. **80** (2000) 1.

[27] G. C. Branco, P. M. Ferreira, L. Lavoura, M. N. Rebelo, M. Sher and J. P. Silva, Phys. Rept. **516** (2012) 1 [arXiv:1106.0034 [hep-ph]].

[28] D. Chang, W. S. Hou and W. -Y. Keung, Phys. Rev. D **48** (1993) 217 [hep-ph/9302267].

[29] A. A. Petrov and D. V. Zhuridov, arXiv:1308.6561 [hep-ph].

[30] J. T. Daub, H. K. Dreiner, C. Hanhart, B. Kubis and U. G. Meissner, JHEP **1301** (2013) 179 [arXiv:1212.4408 [hep-ph]].

[31] M. Hirsch, F. Staub and A. Vicente, Phys. Rev. D **85** (2012) 113013 [arXiv:1202.1825 [hep-ph]].

[32] S. R. Amendolia *et al.* [NA7 Collaboration], Nucl. Phys. B **277** (1986) 168.

[33] A. Aloisio *et al.* [KLOE Collaboration], Phys. Lett. B **606** (2005) 12 [hep-ex/0407048].

[34] R. R. Akhmetshin *et al.* [CMD-2 Collaboration], Phys. Lett. B **648** (2007) 28 [hep-ex/0610021].

[35] B. Aubert *et al.* [BaBar Collaboration], Phys. Rev. Lett. **103** (2009) 231801 [arXiv:0908.3589 [hep-ex]].

[36] F. Ambrosino *et al.* [KLOE Collaboration], Phys. Lett. B **700** (2011) 102 [arXiv:1006.5313 [hep-ex]].

[37] S. Anderson *et al.* [CLEO Collaboration], Phys. Rev. D **61** (2000) 112002 [hep-ex/9910046].

[38] M. Fujikawa *et al.* [Belle Collaboration], Phys. Rev. D **78** (2008) 072006 [arXiv:0805.3773 [hep-ex]].

[39] R. Barate *et al.* [ALEPH Collaboration], Z. Phys. C **76** (1997) 15.

[40] G. J. Gounaris and J. J. Sakurai, Phys. Rev. Lett. **21** (1968) 244.

[41] J. Gasser and H. Leutwyler, Annals Phys. **158** (1984) 142.

[42] T. N. Truong, Phys. Rev. Lett. **61** (1988) 2526.

[43] J. H. Kuhn and A. Santamaria, Z. Phys. C **48** (1990) 445.

[44] J. Gasser and U. G. Meissner, Nucl. Phys. B **357** (1991) 90.

[45] G. Colangelo, M. Finkemeier and R. Urech, Phys. Rev. D **54** (1996) 4403 [hep-ph/9604279].

[46] L. v. Dung and T. N. Truong, hep-ph/9607378.

[47] T. Hannah, Phys. Rev. D **54** (1996) 4648 [hep-ph/9611307].

[48] T. Hannah, Phys. Rev. D **55** (1997) 5613 [hep-ph/9701389].

[49] F. Guerrero and A. Pich, Phys. Lett. B **412** (1997) 382 [hep-ph/9707347].

[50] J. Bijnens, G. Colangelo and P. Talavera, JHEP **9805** (1998) 014 [hep-ph/9805389].

[51] J. A. Oller, E. Oset and J. E. Palomar, Phys. Rev. D **63** (2001) 114009 [hep-ph/0011096].

[52] J. F. De Troconiz and F. J. Yndurain, Phys. Rev. D **65** (2002) 093001 [hep-ph/0106025].

[53] A. Pich and J. Portoles, Phys. Rev. D **63** (2001) 093005 [hep-ph/0101194].

[54] B. Ananthanarayan, I. Caprini and I. S. Imsong, Phys. Rev. D **83** (2011) 096002 [arXiv:1102.3299 [hep-ph]].

[55] I. Caprini, G. Colangelo, and H. Leutwyler (unpublished).

[56] C. Hanhart, Phys. Lett. B **715** (2012) 170 [arXiv:1203.6839 [hep-ph]].

[57] M. Jamin, A. Pich and J. Portoles, Phys. Lett. B **640** (2006) 176 [hep-ph/0605096].

[58] M. Jamin, A. Pich and J. Portoles, Phys. Lett. B **664** (2008) 78 [arXiv:0803.1786 [hep-ph]].

[59] D. R. Boito, R. Escribano and M. Jamin, JHEP **1009** (2010) 031 [arXiv:1007.1858 [hep-ph]].

[60] V. Bernard, D. R. Boito and E. Passemar, Nucl. Phys. Proc. Suppl. **218** (2011) 140 [arXiv:1103.4855 [hep-ph]].

[61] D. Gomez Dumm and P. Roig, Eur. Phys. J. C **73** (2013) 2528 [arXiv:1301.6973 [hep-ph]].

[62] S. Descotes-Genon, E. Kou and B. Moussallam, arXiv:1303.2879 [hep-ph].

[63] R. Escribano, S. Gonzalez-Solis and P. Roig, JHEP **1310** (2013) 039 [arXiv:1307.7908 [hep-ph]].

[64] V. Bernard, D. Boito, and E. Passemar (unpublished).

[65] K. M. Watson, Phys. Rev. **88** (1952) 1163.

[66] B. Ananthanarayan, G. Colangelo, J. Gasser and H. Leutwyler, Phys. Rept. **353** (2001) 207 [hep-ph/0005297].

[67] G. Ecker, J. Gasser, A. Pich and E. de Rafael, Nucl. Phys. B **321** (1989) 311.

[68] G. Ecker, J. Gasser, H. Leutwyler, A. Pich and E. de Rafael, Phys. Lett. B **223** (1989) 425.

[69] V. Cirigliano, G. Ecker, M. Eidemuller, A. Pich and J. Portoles, Phys. Lett. B **596** (2004) 96 [hep-ph/0404004].

[70] V. Bernard, M. Oertel, E. Passemar and J. Stern, Phys. Rev. D **80** (2009) 034034 [arXiv:0903.1654 [hep-ph]].

[71] G. P. Lepage and S. J. Brodsky, Phys. Rev. D **22** (1980) 2157.

[72] J. F. Donoghue, J. Gasser and H. Leutwyler, Nucl. Phys. B **343** (1990) 341.

[73] N. I. Muskhelishvili, Singular Integral Equations: Boundary Problems of Function Theory and Their Application to Mathematical Physics edited by J. R. M. Radok P. Noordhoff N.V., Groningen-Holland, 1953.

[74] B. Moussallam, Eur. Phys. J. C **14** (2000) 111 [hep-ph/9909292].

[75] K. L. Au, D. Morgan and M. R. Pennington, Phys. Rev. D **35** (1987) 1633.

[76] R. Omnes, Nuovo Cim. **8** (1958) 316.

[77] S. M. Roy, Phys. Lett. B **36** (1971) 353.

[78] R. Garcia-Martin, R. Kaminski, J. R. Pelaez, J. Ruiz de Elvira and F. J. Yndurain, Phys. Rev. D **83** (2011) 074004 [arXiv:1102.2183 [hep-ph]].

[79] P. Buettiker, S. Descotes-Genon and B. Moussallam, Eur. Phys. J. C **33** (2004) 409 [hep-ph/0310283].

[80] B. Moussallam, Eur. Phys. J. C **71** (2011) 1814 [arXiv:1110.6074 [hep-ph]].

[81] G. Colangelo, S. Durr, A. Juttner, L. Lellouch, H. Leutwyler, V. Lubicz, S. Necco and C. T. Sachrajda *et al.*, Eur. Phys. J. C **71** (2011) 1695 [arXiv:1011.4408 [hep-lat]].

[82] V. Bernard, S. Descotes-Genon and G. Toucas, JHEP **1206** (2012) 051 [arXiv:1203.0508 [hep-ph]].

[83] M. A. Shifman, A. I. Vainshtein and V. I. Zakharov, Phys. Lett. B **78** (1978) 443.

[84] T. P. Cheng and M. Sher, Phys. Rev. D **35** (1987) 3484.

[85] A. Celis, V. Ilisie and A. Pich, JHEP **1307** (2013) 053 [arXiv:1302.4022 [hep-ph]].

[86] Y. Miyazaki *et al.* [Belle Collaboration], Phys. Lett. B **699** (2011) 251 [arXiv:1101.0755 [hep-ex]].

[87] Y. Miyazaki *et al.* [Belle Collaboration], Phys. Lett. B **719** (2013) 346 [arXiv:1206.5595 [hep-ex]].

[88] G. Bonvicini *et al.* [CLEO Collaboration], Phys. Rev. Lett. **79** (1997) 1221 [hep-ex/9704010].

[89] B. Aubert *et al.* [BaBar Collaboration], Phys. Rev. Lett. **104** (2010) 021802 [arXiv:0908.2381 [hep-ex]].

[90] K. Hayasaka, K. Inami, Y. Miyazaki, K. Arinstein, V. Aulchenko, T. Aushev, A. M. Bakich and A. Bay *et al.*, Phys. Lett. B **687** (2010) 139 [arXiv:1001.3221 [hep-ex]].

[91] W. Altmannshofer, S. Gori and G. D. Kribs, Phys. Rev. D **86** (2012) 115009 [arXiv:1210.2465 [hep-ph]].

[92] V. Barger, L. L. Everett, H. E. Logan and G. Shaughnessy, Phys. Rev. D **88** (2013) 115003 [arXiv:1308.0052 [hep-ph]].

[93] D. Lopez-Val, T. Plehn and M. Rauch, JHEP **1310** (2013) 134 [arXiv:1308.1979 [hep-ph]].

[94] T. Feldmann, P. Kroll and B. Stech, Phys. Rev. D **58** (1998) 114006 [hep-ph/9802409].

[95] M. Beneke and M. Neubert, Nucl. Phys. B **651** (2003) 225 [hep-ph/0210085].

[96] D. J. Gross, S. B. Treiman and F. Wilczek, Phys. Rev. D **19** (1979) 2188.

[97] B. Aubert *et al.* [BaBar Collaboration], Phys. Rev. Lett. **98** (2007) 061803 [hep-ex/0610067].

[98] CMS Collaboration, CMS-PAS-HIG-13-021;

[99] G. Aad *et al.*, JHEP **1302** (2013) 095 [arXiv:1211.6956 [hep-ex]].

[100] R. V. Harlander, S. Liebler and H. Mantler, Computer Physics Communications **184** (2013) 1605 [arXiv:1212.3249 [hep-ph]].

[101] R. V. Harlander and W. B. Kilgore, Phys. Rev. Lett. **88** (2002) 201801 [hep-ph/0201206].

[102] D. Eriksson, J. Rathsman and O. Stal, Comput. Phys. Commun. **181** (2010) 189 [arXiv:0902.0851 [hep-ph]].

[103] K. A. Assamagan, A. Deandrea and P. -A. Delsart, Phys. Rev. D **67** (2003) 035001 [hep-ph/0207302].

LHC constraints on two-Higgs-doublet models

Alejandro Celis, Victor Ilisie and Antonio Pich

IFIC, Universitat de València – CSIC, Apt. Correus 22085, E-46071 València, Spain

A new Higgs-like boson with mass around 126 GeV has recently been discovered at the LHC. The available data on this new particle is analyzed within the context of two-Higgs doublet models without tree-level flavour-changing neutral currents. Keeping the generic Yukawa structure of the Aligned Two-Higgs Doublet Model framework, we study the implications of the LHC data on the allowed scalar spectrum. We analyze both the CP-violating and CP-conserving cases, and a few particular limits with a reduced number of free parameters, such as the usual models based on discrete $\mathcal{Z}_2$ symmetries.

7.1   Introduction

The ATLAS and CMS collaborations have recently announced the discovery of a new neutral boson, with a measured mass of $125.2 \pm 0.3 \pm 0.6$ GeV [1] and $125.8 \pm 0.4 \pm 0.4$ GeV [2], respectively. The LHC data is compatible with the expected production and decay of the Standard Model (SM) Higgs boson, the most significant decay modes being $H \to \gamma\gamma$ and $H \to ZZ^{(*)} \to \ell^+\ell^-$. The excess of events observed by ATLAS (CMS) has a (local) statistical significance of $6.1\,\sigma$ ($6.9\,\sigma$). Although the spin of the new particle has not been measured yet, the observed diphoton decay channel shows clearly that it is a boson with $J \neq 1$, making very plausible the scalar hypothesis. Preliminary analyses of $H \to ZZ \to 4\ell$ [3,4] and $H \to \gamma\gamma$ [5,6] events suggest indeed the assignment $J^P = 0^+$, though more statistics is still needed to give a definite answer.

Additional (but less significant) evidence has been reported by the CDF and DØ collaborations [7], which observe an excess of events in the mass range between 120 and 135 GeV (the largest local significance is $3.3\,\sigma$). The excess seems consistent with a SM Higgs produced in association with a $W^\pm$ or Z boson and decaying to a bottom-antibottom quark pair.

While more experimental analyses are needed to assess the actual nature of this boson, the present data give already very important clues, constraining its couplings in a quite significant way. The stringent exclusion limits set previously on a broad range of masses provide also complementary information which is very useful to establish allowed domains for alternative new-physics scenarios. A SM Higgs boson has been already excluded at 95% CL in the mass ranges 0–122.5 and 127–600 GeV [5,8–14].

The new boson appears to couple to the known gauge bosons ($W^\pm$, Z, γ, g) with the strength expected for the SM Higgs [15–24], although a slight excess of events in the 2γ decay channel, compared with the SM expectation, is observed by ATLAS and CMS [1,2]. Moreover, its fermionic couplings seem compatible with a linear dependence with the fermion mass, scaled by the electroweak scale $v \approx 246$ GeV [23]. Thus, it has the properties expected for a Higgs-like particle, related with the spontaneous breaking of the electroweak symmetry. An obvious question to address is whether it corresponds to the unique Higgs boson incorporated in the SM, or it is just the first signal of a much richer scalar sector.

The simplest modification of the SM Higgs mechanism consists in incorporating ad-

ditional scalar doublets, respecting the custodial symmetry, which can easily satisfy the electroweak precision tests. This leads to a rich spectrum of neutral and charged scalars, providing a broad range of dynamical possibilities with very interesting phenomenological implications. The minimal extension of the scalar sector with only one additional doublet contains five physical scalars: two charged fields $H^{\pm}$ and three neutral ones h, H and A; thus, there are three possible candidates for the recently discovered neutral boson. If the scalar potential preserves the CP symmetry, h and H are CP-even, while A is CP-odd; in this case there are no $AW^{+}W^{-}$ and AZZ couplings at tree level, which makes the A possibility quite unlikely.

Generic multi-Higgs doublet models give rise to unwanted flavour-changing neutral current (FCNC) interactions through non-diagonal couplings of neutral scalars to fermions. The tree-level FCNCs can be eliminated requiring the alignment in flavour space of the Yukawa matrices coupling to a given right-handed fermion [25]. The Aligned Two-Higgs Doublet Model (A2HDM) [26] results in a very specific structure, with all fermion-scalar interactions being proportional to the corresponding fermion masses. This leads to a rich and viable phenomenology [25–30] with an interesting hierarchy of FCNC effects, suppressing them in light-quark systems while allowing potentially relevant signals in heavy-quark transitions. The A2HDM constitutes a very general framework which includes, for particular values of its parameters, all previously considered two-Higgs doublet models (2HDMs) without FCNCs [31,32], and incorporates in addition new sources of CP violation.

In the following, we will analyze the recent discovery of a Higgs-like object within the A2HDM. We will study the different possible interpretations of the new boson, the corresponding experimental constraints on its couplings, and the implications for the remaining scalar spectrum. Previous analyses [33–43] have only considered more specific scenarios based on discrete $\mathcal{Z}_2$ symmetries [44], *i.e.*, the so called 2HDMs of types I [45,46], II [46, 47], X (leptophilic or lepton specific), Y (flipped) [48–51] and inert [52]. The more general A2HDM framework opens a wide range of additional possibilities, which we will try to characterize keeping in mind the high-statistics data samples that the LHC is expected to deliver in the future, at higher energies. Two very recent works have already employed the A2HDM, in the limit of CP conservation, to analyze the Higgs data [53, 54]. Another previous work has considered the CP-conserving A2HDM with a custodial symmetry imposed on the Higgs potential [55]. We will compare our results in

that limit and will also explore the consequences of allowing CP-violating phases, either in the scalar potential (mixing of the three neutral scalars) or in the Yukawa couplings. While parts of our analysis remain valid in more general 2HDM settings, the flavour constrains would necessary be different in models with tree-level FCNCs [56–58] and, therefore, the appropriate modifications should be taken into account.

Our paper is organized as follows: In section 7.2, we describe the theoretical framework adopted in our analysis, indicating the relevant couplings of the A2HDM scalars. In section 3 we define the Higgs signal strengths, which are used to make contact with the experimental measurements. Section 7.4 presents our results and shows the scalar parameter ranges needed to explain the present data. Our conclusions are given in section 7.5. The appendices include a compilation of useful formulae as well as the statistical treatment and data used in this work.

7.2   The Aligned Two-Higgs-Doublet Model

The 2HDM extends the SM with a second scalar doublet of hypercharge $Y = \frac{1}{2}$. The neutral components of the scalar doublets $\phi_a(x)$ ($a = 1, 2$) acquire vacuum expectation values that are, in general, complex: $\langle 0|\phi_a^T(x)|0\rangle = \frac{1}{\sqrt{2}}(0, v_a\, e^{i\theta_a})$. Through an appropriate $U(1)_Y$ transformation we can enforce $\theta_1 = 0$, since only the relative phase $\theta \equiv \theta_2 - \theta_1$ is observable. It is convenient to perform a global SU(2) transformation in the scalar space (ϕ_1, ϕ_2) and work in the so-called Higgs basis (Φ_1, Φ_2), where only one doublet acquires a vacuum expectation value:

$$
\begin{pmatrix} \Phi_1 \\ -\Phi_2 \end{pmatrix} \equiv \begin{bmatrix} \cos\beta & \sin\beta \\ \sin\beta & -\cos\beta \end{bmatrix} \begin{pmatrix} \phi_1 \\ e^{-i\theta}\phi_2 \end{pmatrix} , \tag{7.1}
$$

with $\tan\beta = v_2/v_1$. In this basis, the two doublets are parametrized as

$$
\Phi_1 = \begin{bmatrix} G^+ \\ \frac{1}{\sqrt{2}}(v + S_1 + iG^0) \end{bmatrix} , \qquad \Phi_2 = \begin{bmatrix} H^+ \\ \frac{1}{\sqrt{2}}(S_2 + iS_3) \end{bmatrix} , \tag{7.2}
$$

where $G^\pm$ and G^0 denote the Goldstone fields and $\langle 0|H^+|0\rangle = \langle 0|G^+|0\rangle = \langle 0|G^0|0\rangle = \langle 0|S_i|0\rangle = 0$. Thus, Φ_1 plays the role of the SM scalar doublet with $v \equiv \sqrt{v_1^2 + v_2^2} \simeq (\sqrt{2}\,G_F)^{-1/2} = 246$ GeV.

The physical scalar spectrum contains five degrees of freedom: the two charged fields $H^\pm(x)$ and three neutral scalars $\varphi_i^0(x) = \{h(x), H(x), A(x)\}$, which are related with the S_i fields through an orthogonal transformation $\varphi_i^0(x) = \mathcal{R}_{ij} S_j(x)$. The form of the $\mathcal{R}$ matrix is fixed by the scalar potential, which determines the neutral scalar mass matrix and the corresponding mass eigenstates. A detailed discussion is given in appendix 7.A. In general, the CP-odd component S_3 mixes with the CP-even fields $S_{1,2}$ and the resulting mass eigenstates do not have a definite CP quantum number. If the scalar potential is CP symmetric this admixture disappears; in this particular case, $A(x) = S_3(x)$ and[1]

$$\begin{pmatrix} h \\ H \end{pmatrix} = \begin{bmatrix} \cos\tilde{\alpha} & \sin\tilde{\alpha} \\ -\sin\tilde{\alpha} & \cos\tilde{\alpha} \end{bmatrix} \begin{pmatrix} S_1 \\ S_2 \end{pmatrix}. \tag{7.3}$$

Performing a phase redefinition of the neutral CP-even fields, we can fix the sign of $\sin\tilde{\alpha}$. In this work we adopt the conventions $M_h \leq M_H$ and $0 \leq \tilde{\alpha} \leq \pi$, so that $\sin\tilde{\alpha}$ is positive.

7.2.1   Yukawa Alignment

The most generic Yukawa Lagrangian with the SM fermionic content gives rise to FC-NCs because the fermionic couplings of the two scalar doublets cannot be simultaneously diagonalized in flavour space. The non-diagonal neutral couplings can be eliminated by requiring the alignment in flavour space of the Yukawa matrices [26]; *i.e.*, the two Yukawa matrices coupling to a given type of right-handed fermions are assumed to be proportional to each other and can, therefore, be diagonalized simultaneously. The three proportionality parameters ς_f $(f = u, d, l)$ are arbitrary complex numbers and introduce new sources of CP violation.

In terms of the fermion mass-eigenstate fields, the Yukawa interactions of the A2HDM

---

[1] In the usually adopted notation $\tilde{\alpha} = \alpha - \beta$, where α is the rotation angle expressing the two mass eigenstates h and H in terms of the CP-even neutral fields of the original scalar basis $\phi_1(x)$ and $\phi_2(x)$. Since the choice of initial basis is arbitrary, the parameters α and β are in general unphysical; their values can be changed at will through SU(2) rotations. These angles only become meaningful in particular models where a specific basis is singled out (through a symmetry for instance).

Table 7.1: *CP-conserving 2HDMs based on discrete $\mathcal{Z}_2$ symmetries.*

Model	ς_d	ς_u	ς_l
Type I	$\cot\beta$	$\cot\beta$	$\cot\beta$
Type II	$-\tan\beta$	$\cot\beta$	$-\tan\beta$
Type X	$\cot\beta$	$\cot\beta$	$-\tan\beta$
Type Y	$-\tan\beta$	$\cot\beta$	$\cot\beta$
Inert	0	0	0

read [26]

$$
\begin{aligned}
\mathcal{L}_Y \;=\; & -\frac{\sqrt{2}}{v}\, H^+ \left\{ \bar{u} \left[\varsigma_d\, V M_d \mathcal{P}_R - \varsigma_u\, M_u^\dagger V \mathcal{P}_L \right] d \, + \, \varsigma_l\, \bar{\nu} M_l \mathcal{P}_R l \right\} \\
& -\frac{1}{v} \sum_{\varphi_i^0, f} y_f^{\varphi_i^0}\, \varphi_i^0 \, \left[\bar{f}\, M_f \mathcal{P}_R f \right] \; + \; \text{h.c.}\,,
\end{aligned}
\tag{7.4}
$$

where $\mathcal{P}_{R,L} \equiv \frac{1\pm\gamma_5}{2}$ are the right-handed and left-handed chirality projectors, M_f the diagonal fermion mass matrices and the couplings of the neutral scalar fields are given by:

$$
y_{d,l}^{\varphi_i^0} = \mathcal{R}_{i1} + (\mathcal{R}_{i2} + i\,\mathcal{R}_{i3})\,\varsigma_{d,l}\,, \qquad\qquad y_u^{\varphi_i^0} = \mathcal{R}_{i1} + (\mathcal{R}_{i2} - i\,\mathcal{R}_{i3})\,\varsigma_u^*\,.
\tag{7.5}
$$

As in the SM, all scalar-fermion couplings are proportional to the corresponding fermion masses. This linear dependence on the fermion mass is characteristic of the A2HDM framework and does not hold in non-aligned 2HDMs with FCNCs. The only source of flavour-changing interactions is the Cabibbo-Kobayashi-Maskawa (CKM) quark mixing matrix V [59]. All possible freedom allowed by the alignment conditions is determined by the three family-universal complex parameters ς_f, which provide new sources of CP violation without tree-level FCNCs [26]. The usual models with natural flavour conservation, based on discrete $\mathcal{Z}_2$ symmetries, are recovered for particular (real) values of the couplings ς_f, as indicated in table 7.1.

Quantum corrections induce a misalignment of the Yukawa matrices, generating small FCNC effects suppressed by the corresponding loop factors [25–27, 60, 61]. However, the flavour symmetries of the A2HDM tightly constraint the possible FCNC structures,

keeping their effects well below the present experimental bounds [25–30].[2]

The orthogonality of the rotation matrix $\mathcal{R}$, implies the following relations among the Yukawa couplings of the three neutral scalars:

$$\sum_{i=1}^{3} (y_f^{\varphi_i^0})^2 = 1\,, \qquad \sum_{i=1}^{3} |y_f^{\varphi_i^0}|^2 = 1 + 2\,|\varsigma_f|^2\,, \qquad \sum_{i=1}^{3} y_f^{\varphi_i^0}\,\mathcal{R}_{i1} = 1\,,$$

$$\sum_{i=1}^{3} y_{d,l}^{\varphi_i^0}\,\mathcal{R}_{i2} = \varsigma_{d,l}\,, \qquad\qquad \sum_{i=1}^{3} y_u^{\varphi_i^0}\,\mathcal{R}_{i2} = \varsigma_u^*\,,$$

$$\sum_{i=1}^{3} y_{d,l}^{\varphi_i^0}\,\mathcal{R}_{i3} = i\,\varsigma_{d,l}\,, \qquad\qquad \sum_{i=1}^{3} y_u^{\varphi_i^0}\,\mathcal{R}_{i3} = -i\,\varsigma_u^*\,. \qquad (7.7)$$

7.2.2   Bosonic Couplings

The full set of interactions among the gauge and scalar bosons is given in appendix 7.B. The relevant vertices for our analysis are the ones coupling a single neutral scalar with a pair of gauge bosons. As shown in eq. (7.54), they are identical to their SM counterpart, with the field S_1 taking the role of the SM Higgs. Therefore ($VV = W^+W^-, ZZ$),

$$g_{\varphi_i^0 VV} = \mathcal{R}_{i1}\,g_{hVV}^{\mathrm{SM}}\,, \qquad (7.8)$$

which implies

$$g_{hVV}^2 + g_{HVV}^2 + g_{AVV}^2 = \left(g_{hVV}^{\mathrm{SM}}\right)^2\,. \qquad (7.9)$$

---

[2] The only FCNC structures induced at one loop take the form [25, 27]:

$$\mathcal{L}_{\mathrm{FCNC}} = \frac{C(\mu)}{4\pi^2 v^3}\,(1 + \varsigma_u^*\varsigma_d)\,\sum_i \varphi_i^0(x)\,\Big\{(\mathcal{R}_{i2} + i\,\mathcal{R}_{i3})\,(\varsigma_d - \varsigma_u)\,\left[\bar{d}_L\,V^\dagger M_u M_u^\dagger V M_d\,d_R\right] - \qquad (7.6)$$

$$-\,(\mathcal{R}_{i2} - i\,\mathcal{R}_{i3})\,(\varsigma_d^* - \varsigma_u^*)\,\left[\bar{u}_L\,V M_d M_d^\dagger V^\dagger M_u\,u_R\right]\Big\} + \mathrm{h.c.}$$

with $C(\mu) = C(\mu_0) - \log(\mu/\mu_0)$. These FCNC effects vanish identically in the $\mathcal{Z}_2$ models where the alignment condition is protected by a discrete symmetry. In the most general case, assuming the alignment to be exact at some scale μ_0, i.e. $C(\mu_0) = 0$, a non-zero value for the FCNC coupling is generated when running to a different scale. However, the numerical effect is suppressed by $m_q m_{q'}^2/v^3$ and quark-mixing factors, avoiding the stringent experimental constraints for light-quark systems. Explicit examples of symmetry-protected underlying theories leading to a low-energy A2HDM structure have been discussed in refs. [62–64].

The strength of the SM Higgs interaction is shared by the three 2HDM neutral bosons. In the CP-conserving limit, the CP-odd field decouples while the strength of the h and H interactions is governed by the corresponding $\cos\tilde{\alpha}$ and $\sin\tilde{\alpha}$ factors. Thus, a general feature of 2HDMs is that, at tree level, the couplings of the neutral scalars to vector bosons cannot be enhanced over the SM value and obey the custodial symmetry relation $g_{\varphi_i^0 ZZ} = g_{\varphi_i^0 WW}$. Observing a scalar boson with a somewhat enhanced coupling to vector bosons or a deviation from custodial symmetry [65] would therefore be in clear contradiction with the predictions of this class of models. The relations (7.7) and (7.9) establish a connection between the couplings of the observed 126 GeV resonance and searches for other neutral and charged scalars within the A2HDM.

In order to compute the two-photon decay widths of the neutral scalars, one also needs their couplings to a pair of charged scalars, generated through the scalar potential discussed in appendix 7.A. Since these couplings depend on still unknown parameters, we will parametrize the corresponding interaction as

$$\mathcal{L}_{\varphi^0 H^+ H^-} = -v \sum_{\varphi_i^0} \lambda_{\varphi_i^0 H^+ H^-} \; \varphi_i^0 \, H^+ H^- \, . \tag{7.10}$$

Explicit expressions for the cubic couplings $\lambda_{\varphi_i^0 H^+ H^-}$, in terms of the Higgs potential parameters, can be found in appendix 7.A. If CP is assumed to be an exact symmetry, $\lambda_{A H^+ H^-} = 0$.

7.3   Higgs Signal Strengths

The experimental data on Higgs searches is given in terms of the so-called signal strengths, measuring the observable cross sections in units of the corresponding SM expectations. At the LHC, the relevant production mechanisms for a SM-like Higgs particle are gluon fusion ($gg \rightarrow H$), vector boson fusion ($qq' \rightarrow qq'VV \rightarrow qq'H$), associated production with a vector boson ($q\bar{q}' \rightarrow WH/ZH$) and the associated production with a $t\bar{t}$ pair ($q\bar{q}/gg \rightarrow t\bar{t}H$). The Higgs decay channels explored so far are $\gamma\gamma$, $ZZ^{(*)}$, $WW^{(*)}$, $b\bar{b}$ and $\tau^+\tau^-$.

In order to fit the experimental measurements, we consider the ratios :

$$
\mu_{\gamma\gamma}^{\varphi_i^0} \equiv \frac{\sigma(pp \to \varphi_i^0)\,\mathrm{Br}(\varphi_i^0 \to \gamma\gamma)}{\sigma(pp \to h)_{\mathrm{SM}}\,\mathrm{Br}(h \to \gamma\gamma)_{\mathrm{SM}}} \,, \qquad
\mu_{\gamma\gamma jj}^{\varphi_i^0} \equiv \frac{\sigma(pp \to jj\varphi_i^0)\,\mathrm{Br}(\varphi_i^0 \to \gamma\gamma)}{\sigma(pp \to jjh)_{\mathrm{SM}}\,\mathrm{Br}(h \to \gamma\gamma)_{\mathrm{SM}}} \,,
$$

$$
\mu_{VV}^{\varphi_i^0} \equiv \frac{\sigma(pp \to \varphi_i^0)\,\mathrm{Br}(\varphi_i^0 \to VV)}{\sigma(pp \to h)_{\mathrm{SM}}\,\mathrm{Br}(h \to VV)_{\mathrm{SM}}} \,, \qquad
\mu_{WWjj}^{\varphi_i^0} \equiv \frac{\sigma(pp \to jj\varphi_i^0)\,\mathrm{Br}(\varphi_i^0 \to WW)}{\sigma(pp \to jjh)_{\mathrm{SM}}\,\mathrm{Br}(h \to WW)_{\mathrm{SM}}} \,,
$$

$$
\mu_{\tau\tau}^{\varphi_i^0} \equiv \frac{\sigma(pp \to \varphi_i^0)\,\mathrm{Br}(\varphi_i^0 \to \tau\tau)}{\sigma(pp \to h)_{\mathrm{SM}}\,\mathrm{Br}(h \to \tau\tau)_{\mathrm{SM}}} \,, \qquad
\mu_{bbV}^{\varphi_i^0} \equiv \frac{\sigma(pp \to V\varphi_i^0)\,\mathrm{Br}(\varphi_i^0 \to b\bar{b})}{\sigma(pp \to Vh)_{\mathrm{SM}}\,\mathrm{Br}(h \to b\bar{b})_{\mathrm{SM}}} \,,
$$

$$\tag{7.11}$$

where $V = W, Z$ and j stands for jet. QCD corrections cancel to a large extend in these ratios, provided that a single production mechanism dominates. This certainly applies to $\mu_{\gamma\gamma}^{\varphi_i^0}$, $\mu_{VV}^{\varphi_i^0}$ and $\mu_{\tau\tau}^{\varphi_i^0}$ which are governed by the dominant production channel through gluon fusion. The same would be true for $\mu_{WWjj}^{\varphi_i^0}$ and $\mu_{\gamma\gamma jj}^{\varphi_i^0}$ (gauge-boson fusion), and $\mu_{bbV}^{\varphi_i^0}$ (associated production), assuming that there is no contamination from other channels. It is convenient to express the ratio of the branching fractions as:

$$
\frac{\mathrm{Br}(\varphi_i^0 \to X)}{\mathrm{Br}(h \to X)_{\mathrm{SM}}} = \frac{1}{\rho(\varphi_i^0)} \frac{\Gamma(\varphi_i^0 \to X)}{\Gamma(h \to X)_{\mathrm{SM}}} \,, \tag{7.12}
$$

where $\rho(\varphi_i^0)$ measures the total decay width of the scalar φ_i^0 in units of the SM Higgs width,

$$
\Gamma(\varphi_i^0) = \rho(\varphi_i^0)\,\Gamma_{\mathrm{SM}}(h) \,. \tag{7.13}
$$

Particularizing to the A2HDM and assuming only one dominant production channel in each case,[3] one finds:

$$
\mu_{bbV}^{\varphi_i^0} = (\mathcal{R}_{i1})^2 \left[\mathrm{Re}(y_d^{\varphi_i^0})^2 + \mathrm{Im}(y_d^{\varphi_i^0})^2 \beta_b^{-2} \right] \rho(\varphi_i^0)^{-1}, \qquad
\mu_{WWjj}^{\varphi_i^0} = (\mathcal{R}_{i1})^4 \, \rho(\varphi_i^0)^{-1},
$$

$$
\mu_{\tau\tau}^{\varphi_i^0} = C_{gg}^{\varphi_i^0} \left[\mathrm{Re}(y_l^{\varphi_i^0})^2 + \mathrm{Im}(y_l^{\varphi_i^0})^2 \beta_\tau^{-2} \right] \rho(\varphi_i^0)^{-1}, \qquad
\mu_{VV}^{\varphi_i^0} = C_{gg}^{\varphi_i^0} (\mathcal{R}_{i1})^2 \, \rho(\varphi_i^0)^{-1},
$$

$$
\mu_{\gamma\gamma}^{\varphi_i^0} = C_{gg}^{\varphi_i^0} C_{\gamma\gamma}^{\varphi_i^0} \, \rho(\varphi_i^0)^{-1}, \qquad\qquad\qquad\qquad
\mu_{\gamma\gamma jj}^{\varphi_i^0} = (\mathcal{R}_{i1})^2 C_{\gamma\gamma}^{\varphi_i^0} \, \rho(\varphi_i^0)^{-1},
$$

$$\tag{7.14}$$

---

[3] The contamination of the different Higgs production mechanisms in $h \to \gamma\gamma(jj)$ is discussed in appendix 7.C.

where $\beta_f = (1 - 4m_f^2/M_{\varphi_i^0}^2)^{1/2}$. The one-loop functions are given by

$$
C_{gg}^{\varphi_i^0} \;=\; \frac{\sigma(gg \to \varphi_i^0)}{\sigma(gg \to h)_{\mathrm{SM}}} \;=\; \frac{\left| \sum_q \mathrm{Re}(y_q^{\varphi_i^0})\, \mathcal{F}(x_q) \right|^2 + \left| \sum_q \mathrm{Im}(y_q^{\varphi_i^0})\, \mathcal{K}(x_q) \right|^2}{\left| \sum_q \mathcal{F}(x_q) \right|^2} \tag{7.15}
$$

and

$$
C_{\gamma\gamma}^{\varphi_i^0} \;=\; \frac{\Gamma(\varphi_i^0 \to \gamma\gamma)}{\Gamma(h \to \gamma\gamma)_{\mathrm{SM}}} \tag{7.16}
$$

$$
\;=\; \frac{\left| \sum_f \mathrm{Re}(y_f^{\varphi_i^0})\, N_C^f\, Q_f^2\, \mathcal{F}(x_f) + \mathcal{G}(x_W)\mathcal{R}_{i1} + \mathcal{C}_{H^\pm}^{\varphi_i^0} \right|^2 + \left| \sum_f \mathrm{Im}(y_f^{\varphi_i^0})\, N_C^f\, Q_f^2\, \mathcal{K}(x_f) \right|^2}{\left| \sum_f N_C^f\, Q_f^2\, \mathcal{F}(x_f) + \mathcal{G}(x_W) \right|^2} ,
$$

with N_C^f and Q_f the number of colours and the electric charge of the fermion f, $x_f = 4m_f^2/M_{\varphi_i^0}^2$ and $x_W = 4M_W^2/M_{\varphi_i^0}^2$. Notice that the ratios (7.11) are defined for $M_{\varphi_i^0} = M_{h_{\mathrm{SM}}}$. The two separate terms in the numerators of eqs. (7.15) and (7.16) correspond to the CP-even and CP-odd structures $\varphi_i^0 X_{\mu\nu} X^{\mu\nu}$ and $\varphi_i^0 X_{\mu\nu} \widetilde{X}^{\mu\nu}$, with $X_{\mu\nu} = G_{\mu\nu}$ $(F_{\mu\nu})$ in the gluon (photon) case and $\widetilde{X}^{\mu\nu} = \epsilon^{\mu\nu\sigma\rho} X_{\sigma\rho}$. The functions $\mathcal{F}(x_f)$, $\mathcal{K}(x_f)$ and $\mathcal{G}(x_W)$ contain the triangular 1-loop contributions from fermions and $W^\pm$ bosons. We will neglect the masses of the first two fermion generations. Since $\mathcal{F}(x_f)$ and $\mathcal{K}(x_f)$ vanish for massless fermions, we only need to consider the top, bottom and tau contributions; the last two are negligible in the SM, but in the A2HDM could be enhanced by the alignment factors ς_d and ς_l. In $C_{\gamma\gamma}^{\varphi_i^0}$ we have also considered the contribution from a charged-scalar loop parametrized by

$$
\mathcal{C}_{H^\pm}^{\varphi_i^0} \;=\; \frac{v^2}{2M_{H^\pm}^2}\, \lambda_{\varphi_i^0 H^+ H^-}\, \mathcal{A}(x_{H^\pm})\,, \tag{7.17}
$$

with $x_{H^\pm} = 4M_{H^\pm}^2/M_{\varphi_i^0}^2$. The explicit expressions of the different loop functions are:

$$
\mathcal{F}(x) \;=\; \frac{x}{2}[4 + (x-1)f(x)]\,, \qquad\qquad \mathcal{G}(x) \;=\; -2 - 3x + \left(\frac{3}{2}x - \frac{3}{4}x^2\right)f(x)\,,
$$

$$
\mathcal{A}(x) \;=\; -x - \frac{x^2}{4}f(x)\,, \qquad\qquad\qquad \mathcal{K}(x) \;=\; -\frac{x}{2}f(x)\,, \tag{7.18}
$$

with

$$
f(x) \;=\; \begin{cases} -4\arcsin^2(1/\sqrt{x})\,, & x \geqslant 1 \\[2mm] \left[\ln\left(\frac{1+\sqrt{1-x}}{1-\sqrt{1-x}} \right) - i\pi \right]^2\,, & x < 1 \end{cases}. \tag{7.19}
$$

7.4 Phenomenological Analysis

We are interested in analyzing the current LHC and Tevatron data within the A2HDM. The experimental information on the new neutral boson is certainly in early stages; some decay channels have very big uncertainties while some others have not even been seen yet. Nevertheless, while more precise information on all possible production and decay channels is necessary in order to make a detailed study, present data already allow us to extract significant constraints on the parameter space of the model.

The deviations from the SM expectations originate from several sources. The three neutral scalars of the A2HDM have couplings to the gauge bosons which are different (smaller in absolute value) than the ones of the SM Higgs: in SM units they are given by $\mathcal{R}_{i1}$. The Yukawa couplings get also multiplied by the factors $y_f^{\varphi_i^0}$, which are functions of $\mathcal{R}_{ij}$ and the parameters ς_f. Moreover, the presence of a charged scalar manifests in one additional one-loop contribution to the $\varphi_i^0 \to 2\gamma$ decay amplitudes, parametrized through the constants $\mathcal{C}_{H^\pm}^{\varphi_i^0}$. In the limit of CP conservation, there are two clear candidates for the new scalar, the CP-even fields h and H (we will nevertheless analyze later the unlikely A possibility). The A2HDM allows in addition for physical CP-violating phases, both in the scalar potential and the Yukawa couplings, generating mixings among the three neutral scalars and CP-odd contributions to the Higgs-like signal strength parameters. Being quadratic in the CP-violating parameters, this last type of corrections could be expected to be small. However, the current bounds on the A2HDM couplings still allow for sizeable effects [25–30].

Sensitivity to the top-quark Yukawa coupling and to a lesser extent to the bottom coupling appears through the one-loop production mechanism of gluon fusion and in the $\gamma\gamma$ decay channel. Neutral scalar production via $pp \to t\varphi_i^0 j(b)$ could provide complementary information on the top Yukawa coupling when more data becomes available [66,67]. The most important constraints on the bottom Yukawa coupling come indirectly from the total decay width, which is in general dominated by $\varphi_i^0 \to b\bar{b}$, and the measurement of scalar production with an associated vector boson ($q\bar{q}' \to \varphi_i^0 V \to (b\bar{b})V$). Neutral boson production via top-quark fusion with subsequent decay into a pair of b quarks, $q\bar{q}/gg \to t\bar{t}\varphi_i^0 \to t\bar{t}(\bar{b}b)$, in which the bottom and top Yukawa couplings appear at tree level will also play an important role; the current experimental sensitivities in this channel are still low [68,69]. The τ Yukawa coupling is directly tested through $\varphi_i^0 \to \tau^+\tau^-$, the

most accessible production mechanisms at the LHC being in this case vector-boson fusion, associated production with a vector boson and gluon fusion.

For a given choice of neutral scalar-field candidate φ_i^0 and its couplings, we define the χ^2 function as

$$\chi^2(\varphi_i^0) \;=\; \sum_k \frac{\left(\mu_k^{\varphi_i^0} - \hat{\mu}_k\right)^2}{\sigma_k^2}\,, \tag{7.20}$$

where k runs over the different production/decay channels considered, $\hat{\mu}_k$ and σ_k are the measured Higgs signal strengths and their one-sigma errors, respectively, and $\mu_k^{\varphi_i^0}$ the corresponding theoretical predictions in terms of the A2HDM parameters, as given in eqs. (7.11) and (7.14). Scanning over the allowed parameter space, we then look for those sets of couplings minimizing the χ^2 and their corresponding uncertainties. The details about the statistical treatment and data used in this work are presented in appendix 7.C.

We will first analyze the CP-conserving limit in section 7.4.1, where we will also study some particular scenarios often adopted in previous works. In section 7.4.2 we will discuss the most general case, without making any assumption about the scalar potential, and analyze the present constraints on the complex Yukawa couplings of the assumed 126 GeV scalar boson.

7.4.1   The A2HDM in the CP-conserving limit

Assuming that the Lagrangian preserves the CP symmetry, the two CP-even neutral scalars h and H couple to the gauge bosons with reduced couplings $\mathcal{R}_{11} = \cos\tilde{\alpha}$ and $\mathcal{R}_{21} = -\sin\tilde{\alpha}$, respectively, and their Yukawa couplings are real:

$$y_f^h \;=\; \cos\tilde{\alpha} + \varsigma_f \sin\tilde{\alpha}\,, \qquad\qquad y_f^H \;=\; -\sin\tilde{\alpha} + \varsigma_f \cos\tilde{\alpha}\,. \tag{7.21}$$

The CP-odd boson A does not couple at tree-level to W^+W^- and ZZ ($\mathcal{R}_{31} = 0$), while its fermionic couplings are purely imaginary (pseudoscalar interaction):

$$y_{d,l}^A \;=\; i\,\varsigma_{d,l}\,, \qquad\qquad y_u^A \;=\; -i\,\varsigma_u\,. \tag{7.22}$$

A light CP-even Higgs at 126 GeV

We will first focus in the most plausible possibility that the lightest scalar h corresponds to the observed neutral boson with $M_h = 126$ GeV. The alternative choice of the heavier field

H can be easily recovered through an appropriate change of the mixing angle, $\tilde{\alpha} \to \tilde{\alpha} - \pi/2$, and will be further discussed in section 7.4.1. We will also consider later, in section 7.4.1, the more exotic case of a CP-odd Higgs A. In this first analysis we assume that the charged scalar is either very heavy or its coupling to the neutral Higgs is very small, so that its contribution $\mathcal{C}_{H^\pm}^h$ to the $h \to \gamma\gamma$ decay width is negligible. We also assume that the bounds from flavour physics are naturally evaded, as it is the case at large values of the charged scalar mass. The $H^\pm$ contribution to the diphoton decay width as well as the flavour constraints will be considered later in section 7.4.1.

The minimization of $\chi^2(h)$ leads to two different solutions, differing in the sign of the top Yukawa coupling. The central values of the corresponding A2HDM parameters and their statistical one-sigma errors obtained from the global fit are:

$$\cos\tilde{\alpha} = 0.99^{+0.01}_{-0.06}\,, \qquad y_u^h = 0.8^{+0.1}_{-0.2}\,, \qquad \left|y_d^h\right| = 0.7 \pm 0.3\,, \qquad \left|y_l^h\right| = 0.8 \pm 0.5\,, \qquad (7.23)$$

and

$$\cos\tilde{\alpha} = 0.99^{+0.01}_{-0.04}\,, \qquad y_u^h = -0.8^{+0.1}_{-0.3}\,, \qquad \left|y_d^h\right| = 1.1 \pm 0.3\,, \qquad \left|y_l^h\right| = 0.9 \pm 0.5\,. \qquad (7.24)$$

In both cases, the gauge coupling g_{hVV} is very close to the SM one. Changing simultaneously the signs of $\cos\tilde{\alpha}$ and y_f^h leads obviously to identical Higgs signal strengths and, therefore, to two equivalent solutions.

In the first solution the $W^\pm$ and top-quark loops contribute with different signs to the $h \to \gamma\gamma$ amplitude, giving a destructive interference as in the SM. The needed enhancement of the 2γ branching ratio is obtained through a smaller total decay width, $\rho(h) \approx 0.6$. This pushes upward the ratios $\mu_{\gamma\gamma}^h$ and $\mu_{\gamma\gamma jj}^h$, allowing to explain part of the excess experimentally observed in these two channels. However, the gluon-fusion production channel has a smaller cross section than in the SM. The combined effect results in a small increase of the $\gamma\gamma$ channel, $\mu_{\gamma\gamma}^h \approx 1.1$, while a much larger enhancement remains in the $\gamma\gamma jj$ case, $\mu_{\gamma\gamma jj}^h \approx 1.5$.

The second solution corresponds to a top-quark contribution to $h \to \gamma\gamma$ with the opposite sign, so that it interferes constructively with the $W^\pm$ amplitude. This allows one to explain the 2γ excess without hardly modifying the total decay rate, $\rho(h) \approx 1.1$ and providing a slightly better fit.

In both solutions there is a sign degeneracy in the bottom and tau Yukawa couplings. Although the tree-level decays $h \to \bar{b}b$ and $h \to \tau^+\tau^-$ are insensitive to these signs, the

loop-induced processes $gg \to h$ and $h \to \gamma\gamma$ receive contributions from the bottom and tau (only the $\gamma\gamma$ process) Yukawas, which interfere with the leading top and $W^\pm$ (in the $\gamma\gamma$ decay) amplitudes as shown in eqs. (7.15) and (7.16). In the SM the bottom and tau contributions are negligible, but their effect could be relevant in the A2HDM if the top Yukawa coupling is considerably suppressed or if the parameters $\varsigma_{d,l}$ are large. However, this is not the case for the fitted Yukawa values in eqs. (7.23) and (7.24), which are of $\mathcal{O}(1)$ for both solutions, leaving the sign of the bottom and tau Yukawas undetermined. The relevance of the $\tau^+\tau^-$ and $\bar{b}b$ channels to determine possible deviations from the SM and within the different $\mathcal{Z}_2$ versions of the 2HDM, which could be pointing to a more general Yukawa structure as provided by the A2HDM, has been emphasized recently in ref. [53].
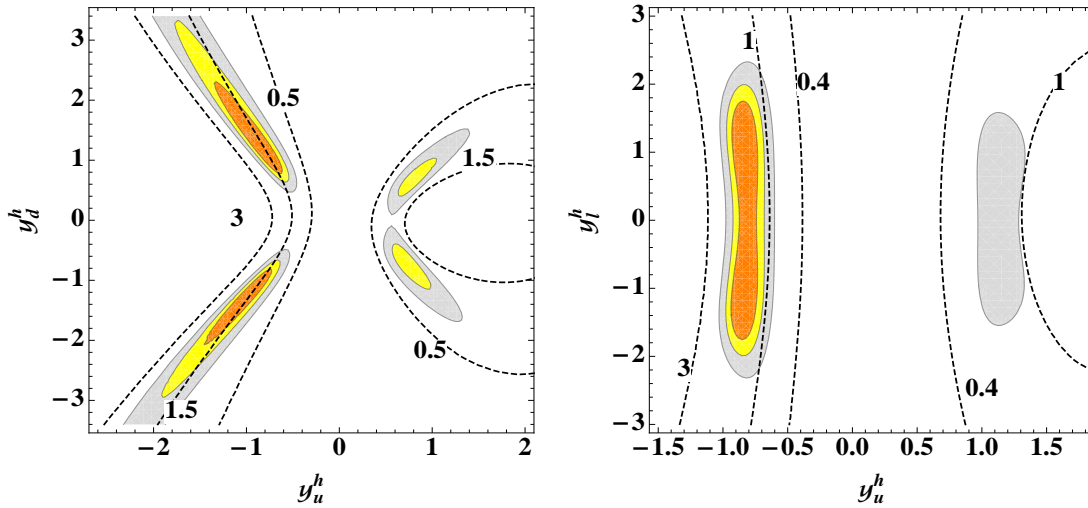

Figure 7.1: *Global fit to the A2HDM, in the CP-conserving case, in the planes $y_u^h - y_d^h$ (left) and $y_u^h - y_l^h$ (right). The parameters not shown in each case are fixed to the best global-fit point. The orange, yellow and gray areas denote 68%, 90% and 99% CL regions. The dashed lines correspond to fixed values of $\mu_{\gamma\gamma}^h$.*

In figure 7.1 we show graphically the results of this global fit, giving the allowed regions in the $y_u^h - y_d^h$ (left) and $y_u^h - y_l^h$ (right) planes at 68%, 90% and 99% CL. The parameters that are not shown are, in each case, set to the best global-fit point. The sign degeneracy in the τ and b Yukawa couplings is clearly observed. Moreover, the right

panel shows a somewhat reduced sensitivity to the leptonic coupling y_l^h. The SM-like solution $(y_u^h, y_{d,l}^h) = (1, 1)$ lies inside the 90% CL allowed region; however, at 68% CL the top Yukawa has the sign flipped with respect to the SM, *i.e.*, only the solution (7.24) remains. Similar results have also been obtained in ref. [24, 53].

The allowed ranges, at the 1σ and 2σ level, for the different Higgs signal strengths in the fit (7.24) are compared in figure 7.2 with the experimental values. A good agreement with data is obtained in all cases. Previous analyses within the CP-conserving A2HDM have been performed in refs. [53, 54], using a different notation, also finding good agreement with the data.
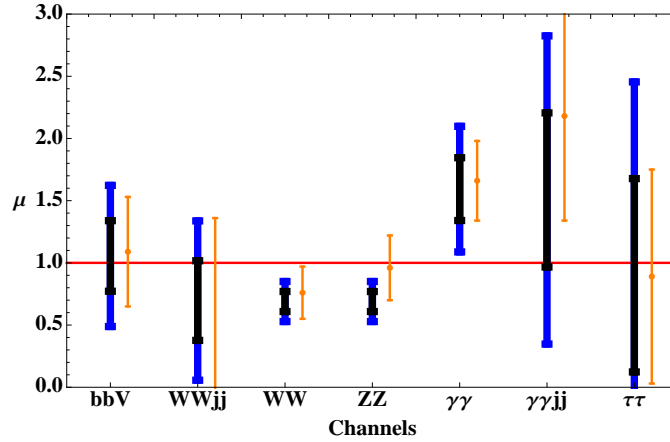

Figure 7.2:   *Allowed ranges for the Higgs signal strengths obtained from the fit* (7.24) *at* 1σ *(black, dark) and* 2σ *(blue, dark), together with the averaged experimental data from the ATLAS, CMS, CDF and DØ collaborations with the corresponding* 1σ *errors (orange, light).*

Using the sum rules in eqs. (7.7) and (7.9), we can extract constraints on the heavy CP-even Higgs couplings from our global fit with $M_h = 126$ GeV. For the solution (7.24) we find at 68% CL that the coupling of H to vector bosons is suppressed, $\sin\tilde{\alpha} < 0.37$, while its coupling to top quarks is very large, $|y_u^H| > 4.6$. This region of parameter space requires a very large value of $|\varsigma_u|$ in order to flip the sign of y_u^h, which is the top Yukawa of h. Such large values of $|\varsigma_u|$ would then imply a significant enhancement of the production of H via gluon fusion and can give rise to non-perturbative $H^+\bar{t}b$, $H\bar{t}t$ and $A\bar{t}t$ couplings. This was noted previously within the same context in ref. [53].
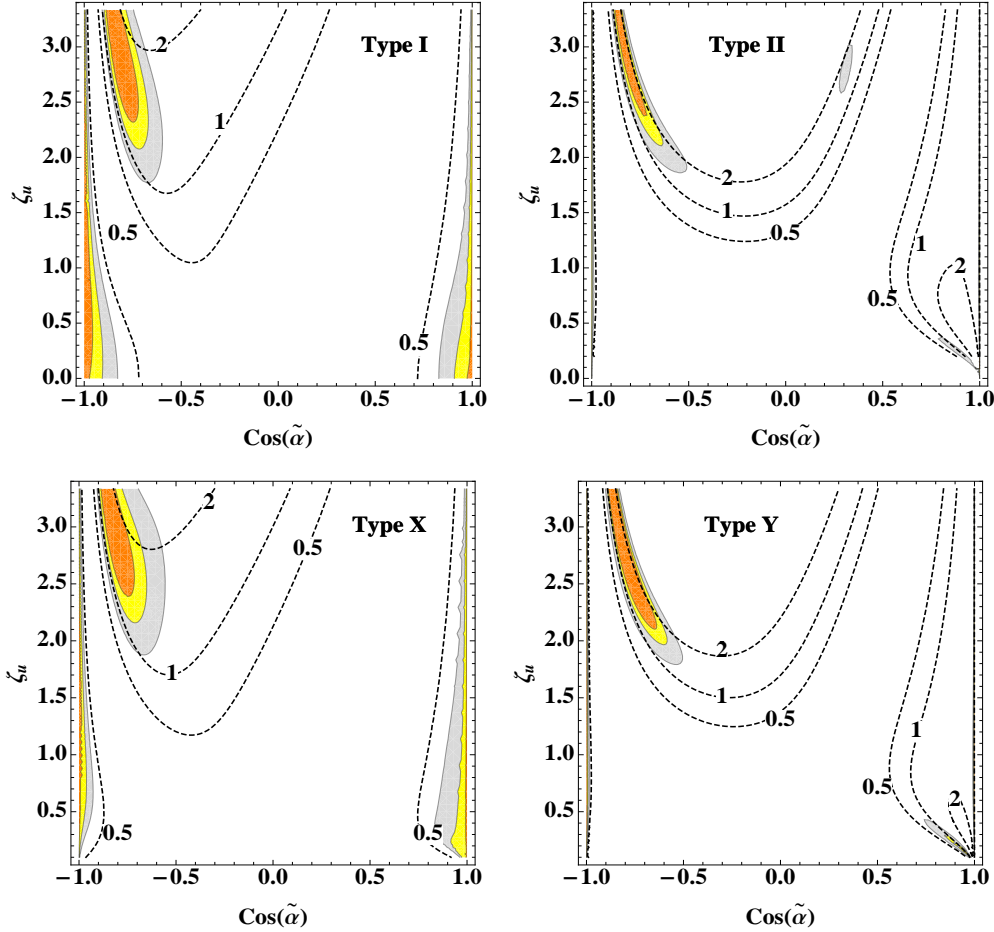
Global fit within $\mathcal{Z}_2$ models

Figure 7.3: *Global fit within 2HDMs of types I (upper left), II (upper right), X (lower left) and Y (lower right), at 68% (orange), 90% (yellow) and 99% (gray) CL. The dashed lines correspond to constant values of $\mu_{\gamma\gamma}^h$.*

The usual 2HDMs with natural flavour conservation, based on discrete $\mathcal{Z}_2$ symmetries, are particular cases of the CP-conserving A2HDM, with ς_f taking the values given in table 7.1. Thus, the three alignment factors are determined by a single parameter through the constraints $\varsigma_u = \varsigma_d = \varsigma_l = \cot\beta$ (type I), $\varsigma_u = -\varsigma_d^{-1} = -\varsigma_l^{-1} = \cot\beta$ (type II), $\varsigma_u = \varsigma_d = -\varsigma_l^{-1} = \cot\beta$ (type X) and $\varsigma_u = -\varsigma_d^{-1} = \varsigma_l = \cot\beta$ (type Y), with $\cot\beta = v_1/v_2 \geq 0$.

This leads to specific relations among the production cross sections and decay rates for the Higgs bosons that can be tested with the LHC data. The separate measurement of the various Higgs signal strengths should allow to disentangle the different scalings of the three Yukawa couplings. In particular, exclusive Higgs production measurements in the final states $\tau^+\tau^-$ and $b\bar{b}$ will be crucial to test the different $\mathcal{Z}_2$ versions of the 2HDM [33, 43, 53].

Figure 7.3 shows the results of the global fit for the 2HDMs of types I, II, X and Y, assuming that the lightest neutral Higgs h is the boson observed around 126 GeV. Allowed regions at 68%, 90% and 99% CL are shown, together with lines of constant $\mu_{\gamma\gamma}^h$. The relevance of the diphoton channel is evident from the figure. In models I and X, an allowed region around $\cos\tilde{\alpha} \approx 1$ appears, where there is no sensitivity to ς_u since its contribution to the neutral Yukawa couplings is suppressed by $\sin\tilde{\alpha}$; in this region the couplings of h to vector bosons and fermions are close to the SM ones. Another allowed region appears for negative values of $\cos\tilde{\alpha}$, in which the $W^\pm$ and top-quark loops contribute with the same sign to the $h \to \gamma\gamma$ decay amplitude, thus allowing for a constructive interference. Both solutions with $\cos\tilde{\alpha} \approx \pm 1$ are present for the inert model (type I with $\varsigma_u = 0$). There is a third allowed region at large values of the top Yukawa and negative $\cos\tilde{\alpha}$, which approaches $\cos\tilde{\alpha} = -1$ as ς_u increases.
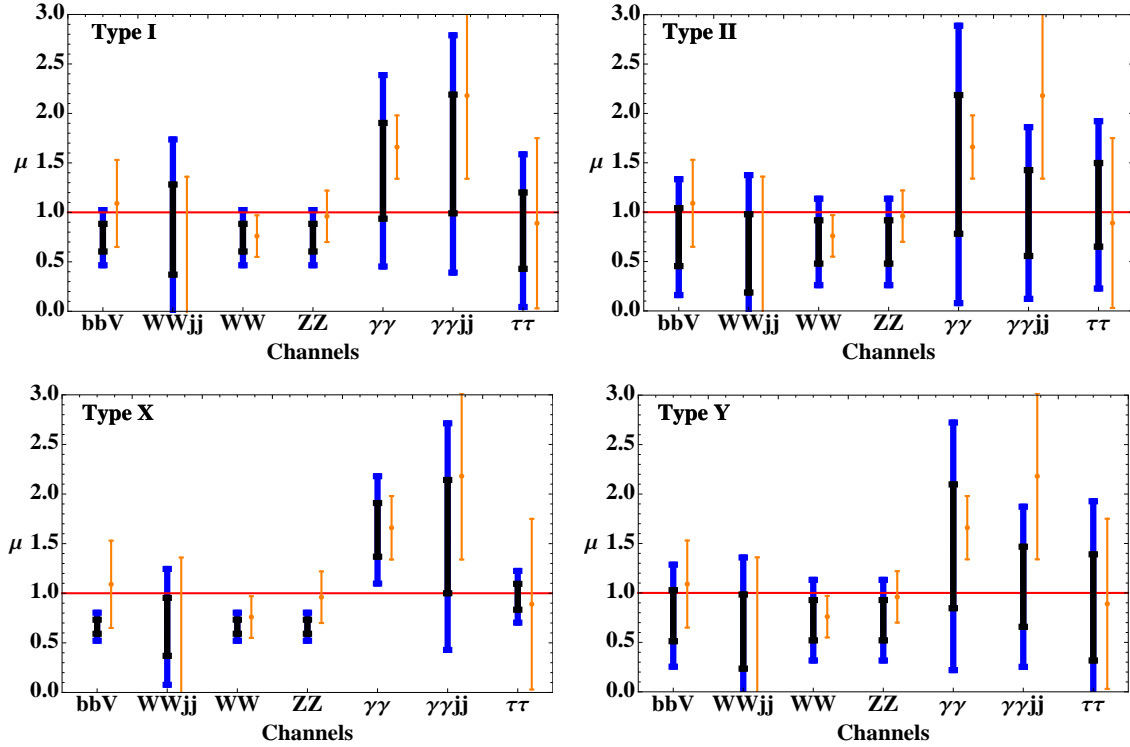
Figure 7.4: *Allowed ranges for the Higgs signal strengths in 2HDMs of type I, II, X and Y, at 1σ (black, dark) and 2σ (blue, dark). Other captions as in figure 7.2.*

In models II and Y the solutions around $\cos\tilde\alpha \approx \pm 1$ reduce to two extremely narrow vertical lines and one small region at low ς_u and positive $\cos\tilde\alpha$, which remain allowed at 99% CL but are not present at 90%. The solution at large values of the top Yukawa and negative $\cos\tilde\alpha$ is also present, but in a region much smaller than in models I and X.

Figure 7.4 shows the allowed ranges for the Higgs signal strengths obtained in these four types of 2HDMs (I, II, X and Y). The agreement with the data is good; however, as already noted in ref. [43], the preferred region has large values of $|\varsigma_u|$, which are ruled out from flavour physics constraints for a charged Higgs boson below the TeV scale. Large values of $|\varsigma_u|$ can also make some top-quark Yukawa couplings non-perturbative, as commented in the previous section.

A charged Higgs and the diphoton excess

One of the most distinctive features of 2HDMs with respect to other alternative scenarios of electroweak symmetry breaking is the presence of a charged scalar boson in the spectrum. The present experimental lower bound on the $H^\pm$ mass is $M_{H^\pm} \gtrsim 80$ GeV (95% CL) [70], assuming that the charged scalar H^+ only decays into the fermionic channels $H^+ \to c\bar{s}$ and $H^+ \to \tau^+ \nu_\tau$. A slightly softer limit $M_{H^\pm} \gtrsim 72.5$ GeV is obtained, allowing for the decay $H^+ \to W^+ A \to W^+ b\bar{b}$, with $M_A > 12$ GeV, and assuming a type-I fermionic structure [70]. A model-independent bound can be extracted from the measured Z width which constraints the Z decays into non-SM modes, and in particular $Z \to H^+ H^-$, to be below $\Gamma_Z^{\text{non-SM}} < 2.9$ MeV (95% CL); this implies $M_{H^\pm} \gtrsim 39.6$ GeV (95% CL) [70].

Direct searches for charged Higgs bosons at the Tevatron [71] and the LHC [72] have also been performed with null results so far.

Current LHC data are sensitive to such charged scalar through the $h \to \gamma\gamma$ decay channel. The one-loop $H^\pm$ contribution can interfere with the $W^\pm$ and fermionic amplitudes, thus being able to enhance or suppress the decay rate. The exact value of the charged Higgs contribution $C_{H^\pm}^h$ depends on the cubic Higgs coupling $\lambda_{hH^+H^-}$ and the charged Higgs mass $M_{H^\pm}$. One expects however that $|C_{H^\pm}^h| \lesssim O(1)$ based on perturbativity arguments (see appendix 7.D).

When considering a relatively light charged Higgs boson, one must take into account constraints from electroweak precision tests and the flavour sector; a light $H^\pm$ would contribute sizably to loop-induced processes, such as $Z \to \bar{b}b$, $b \to s\gamma$ or B^0–$\bar{B}^0$ mixing. These phenomenological constraints have been analyzed in detail within the framework of the A2HDM in refs. [27–30], where it has been found that a charged Higgs below the TeV scale would require $|\varsigma_u| \lesssim 2$ to be compatible with present data. This rules out the hypothetical scenario of a top Yukawa coupling with flipped sign, as found in (7.24) and also favoured by the fits shown in figure 7.3 within the four types of $\mathcal{Z}_2$ models. The reason is that current $h \to WW, ZZ, \gamma\gamma(jj)$ data require $|\cos\tilde{\alpha}| \sim 1$ (*i.e.*, the gauge coupling of the new neutral scalar should be close to the SM one). Since the top Yukawa coupling is given by $y_u^h = \cos\tilde{\alpha} + \varsigma_u \sin\tilde{\alpha}$, in order to flip the sign of y_u^h one needs then a large value for $|\varsigma_u|$, which is excluded by the previous bound.

Including the charged-Higgs contribution, it is no longer necessary to flip the sign of the top Yukawa in order to enhance the $h \to \gamma\gamma$ decay width. The best fit region is now

obtained for Yukawa and gauge couplings close to the SM limit:

$$\cos\tilde{\alpha} \;=\; 0.98^{+0.02}_{-0.06}\,, \qquad\qquad C^h_{H^\pm} \;=\; (-2.8\pm1.3)\,\cup\,(16.0\pm1.3)\,,$$

$$y^h_u \;=\; 1.0\pm0.2\,, \qquad \left|y^h_d\right| \;=\; 1.1\pm0.3\,, \qquad \left|y^h_l\right| \;=\; 0.8\pm0.5\,. \qquad (7.25)$$

The two disjoint $C^h_{H^\pm}$ solutions correspond to either a constructive interference of the $H^\pm$ and $W^\pm$ amplitudes or a destructive one but with a charged-Higgs contribution so large that it reverses the sign of the total $h \to 2\gamma$ amplitude. In both cases, one obtains a better fit than in the SM and also better than the previous A2HDM fits (except for (7.24) which is comparable to this one). The presence of the charged Higgs allows one to easily explain the $h \to \gamma\gamma(jj)$ excess without large modifications of the total decay rate (*i.e.*, $\rho(h) \approx 1.1$). The fit predictions for the μ_k ratios and their one and two-sigma statistical errors are shown in figure 7.5. In all cases, good agreement with the data is obtained.
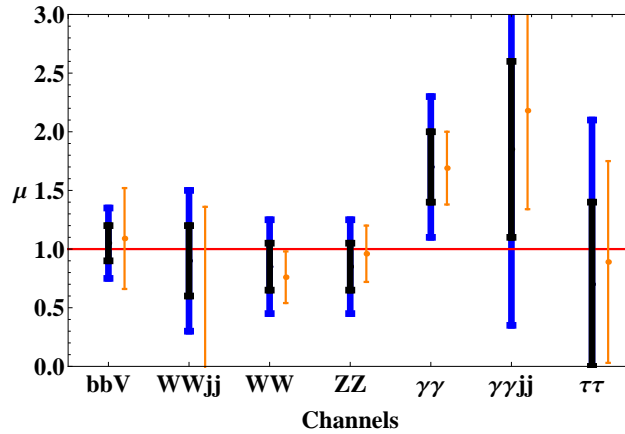
Figure 7.5:   *Allowed ranges for the Higgs signal strengths from the global fit within the CP-conserving A2HDM, including the charged Higgs contribution to $h \to \gamma\gamma$, at 1σ (black, dark) and 2σ (blue, dark). Other captions as in figure 7.2.*

In figure 7.6 we show the allowed regions of the $(|\lambda_{hH^+H^-}|, M_{H^\pm})$ plane, corresponding to the two possible fitted values of $C^h_{H^\pm}$, at 68% and 90% CL, together with the perturbativity bounds discussed in appendix 7.D. Clearly, the solution with a very large contribution to $h \to \gamma\gamma$ from the charged Higgs ($C^h_{H^\pm} \approx 16$) is excluded if one requires the theory to be perturbative. We obtain an upper bound for the mass of the charged

Higgs around 300 GeV, at the one-sigma level. However, the bound disappears at the two-sigma level because the charged-Higgs contribution becomes compatible with zero.

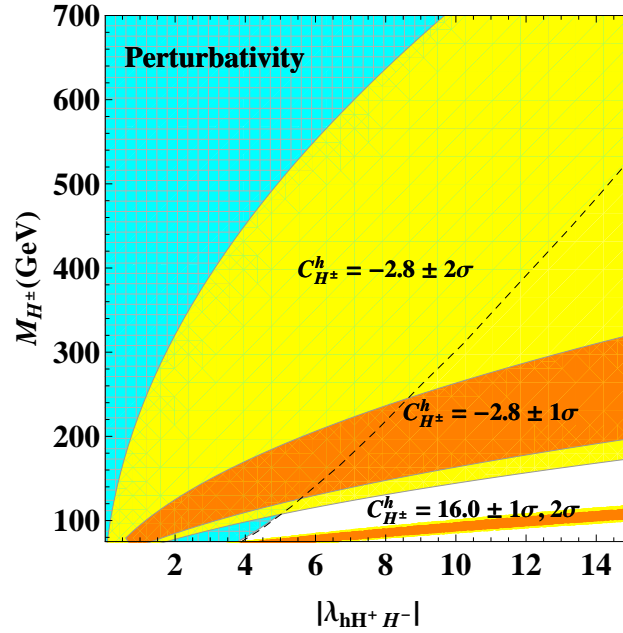Figure 7.6: *Allowed regions of the* $(|\lambda_{hH^+H^-}|, M_{H^\pm})$ *plane, corresponding to the two possible fitted values of* $C_{H^\pm}^h$, *at 68% (orange, dark) and 90% CL (yellow, light). The blue (hashed) area, between the left vertical axis and the dashed line, is the domain where the theory remains perturbative.*

Inert 2HDM

In the inert 2HDM a $\mathcal{Z}_2$ symmetry is imposed, in the Higgs basis (7.2), under which all SM fields and Φ_1 are even while $\Phi_2 \to -\Phi_2$. Terms with an odd number of Φ_2 fields in the scalar potential (7.31) are then forbidden by the $\mathcal{Z}_2$ symmetry, therefore $\mu_3 = \lambda_6 = \lambda_7 = 0$. In this case there is no mixing between the CP-even neutral states h and H, and the scalars H, A and $H^\pm$ decouple from the fermions. The couplings of the remaining Higgs field h to fermions and to vector bosons are the same than in the SM (*i.e.*, $\cos\tilde{\alpha} = 1$ and $y_f^h = 1$). Thus, only the diphoton channels can show a deviation from the SM prediction (assuming that there are no open decay channels other than the SM ones). From the global fit of this scenario, we find a charged-Higgs contribution to the

$h \to \gamma\gamma$ amplitude in the range $C_{H^\pm}^h \in [-1.7, -0.89]$ at 68% CL and $C_{H^\pm}^h \in [-2.4, -0.1]$ at 90% CL. We have assumed that $M_{H^\pm}$ is greater than $M_h/2 \approx 63$ GeV so that $C_{H^\pm}^h$ is real; for lower charged-Higgs masses, it would develop and imaginary absorptive part. The fitted negative sign of $C_{H^\pm}^h$ causes a constructive interference with the $W^\pm$ amplitude in the $h \to \gamma\gamma$ decay width.

Note that in the limit $\varsigma_f = 0$, the charged Higgs does not couple to fermions independently of any assumption on the scalar potential, see eq. (7.4). The implications of this more general case for the neutral Higgs boson phenomenology as well as the possibility of a very light charged Higgs boson are discussed in section 7.4.2. Detailed analyses of the inert 2HDM and the possibility of a Dark Matter candidate within this model, in light of the LHC data, can be found in refs. [39, 73]. An enhancement of the $h \to \gamma\gamma$ decay rate has also been discussed in ref. [74] within the Quasi-Inert 2HDM in connection with the top forward-backward asymmetry observed at the Tevatron; the limit on $C_{H^\pm}^h$ obtained in this section also applies to this scenario.

A heavy CP-even Higgs at 126 GeV

We have discussed so far the phenomenology of the lightest Higgs boson, but there is nothing a priori preventing the boson discovered by ATLAS and CMS to be identified with the heaviest CP-even state H or with the CP-odd Higgs A. These possibilities have been already discussed in refs. [35, 37, 53]. An analysis in terms of the more general CP-violating scalar potential, setting limits on the scalar-pseudoscalar mixing, has been done in ref. [36].

Using the previous fits for h, it is straightforward to analyze the possibility of having a heavy Higgs with $M_H = 126$ GeV. Assuming that non-SM decays like $H \to hh$ are kinematically forbidden or very suppressed, the constraints on the heavy Higgs boson couplings can be easily obtained from those of h through an appropriate change of the mixing angle: $\tilde{\alpha} \to \tilde{\alpha} - \pi/2$. In this case the coupling of the heavy Higgs to vector bosons is close to the SM limit ($\sin\tilde{\alpha} \approx 1$), while the light-scalar g_{hVV} couplings are suppressed by $\cos\tilde{\alpha} \approx 0$. The absolute values of the Yukawa couplings and all the other parameters remain unchanged. A solution analogous to the one in eq. (7.24), where a large value of $|\varsigma_u|$ is required to flip the sign of the top Yukawa coupling, is excluded by low energy flavour constraints for a charged Higgs below the TeV scale ($Z \to \bar{b}b$, $B^0 - \bar{B}^0$ mixing and

neutral Kaon mixing [27]).

The LEP searches for neutral Higgs particles could have missed the light scalar h, since the associated production with a vector boson would be strongly suppressed. Moreover, $\left|y_d^h\right| \sim \left|\varsigma_d\right|$ could be small enough to avoid the constraints from the usual $h \to b\bar{b}$ search mode. The OPAL collaboration performed a decay-mode-independent search for a light neutral scalar and found upper limits for the Higgs-strahlung cross section in units of the SM: $(\mathcal{R}_{11})^2 \equiv (g_{hVV}/g_{hVV}^{\mathrm{SM}})^2 < 0.1$ for $M_h < 19$ GeV, and $(\mathcal{R}_{11})^2 < 1$ for $M_h < 81$ GeV [75]. Together with the constraints from electroweak precision tests at the Z peak, this provides useful information on the allowed mass spectrum for the remaining scalars. Using the current bounds from the oblique parameters S, T and U [76,77] (the corresponding A2HDM formulae are given in appendix 7.E), we show in the left panel of figure 7.7 the allowed regions in the $(M_{H^\pm}, M_A)$ plane. We have set $M_H = 126$ GeV and $\sin\tilde{\alpha} \in [0.7, 1]$. The constraints shown in the figure turn out to be determined by the T parameter, since S and U give weaker restrictions. The charged scalar mass is of course constrained by the direct experimental lower bound discussed before, but its exact value depends on the assumed decay channels. The region where both $M_{H^\pm}$ and M_A become very heavy corresponds to uncomfortably large values of the quartic couplings λ_i of the scalar potential and the theory is no longer perturbative.
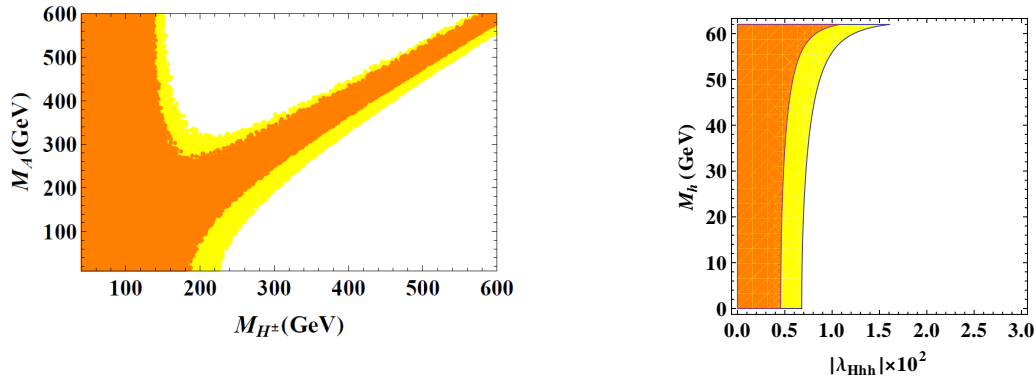

Figure 7.7: *Left-panel: Constraint in the $(M_{H^\pm}, M_A)$ plane from the oblique parameters S, T and U. Right-panel: Constraints from the invisible Higgs decay width in the $(|\lambda_{Hhh}|, M_h)$ plane, assuming SM couplings of H to fermions and vector bosons. The orange (dark) and yellow (light) regions are allowed at 68% and 90% CL.*

A light neutral boson h or A below the kinematical threshold of $M_H/2 \approx 63$ GeV would have important phenomenological consequences, because the 126 GeV Higgs could decay into lighter scalars. These decay channels can be included in our fit in terms of an invisible decay width as long as we neglect possible contributions from cascade decays into the observed final states.[4] In general one would expect in this case a suppression of the measured Higgs decay rates compared with the SM, due to the larger total width of the scalar H. Current data for the $\gamma\gamma$ channel, however, shows a slight enhancement over the SM prediction, thus placing strong bounds on possible invisible decays of the 126 GeV Higgs boson. Assuming that the heavy-Higgs couplings to fermions and vector bosons are SM-like (*i.e.*, $y_f^H = 1$ and $\sin\tilde\alpha = 1$), the best fit point is obtained for a null invisible H decay width; at 68% CL (90% CL) we obtain an upper bound of 9% (20%) on the invisible H decay width (in units of the SM total decay width).

Considering the scenario of a very light CP-even Higgs h, the decay width of the heavier CP-even scalar into hh is given by

$$\Gamma(H \to hh) \;=\; \frac{v^2 \lambda_{Hhh}^2}{8\pi M_H} \left(1 - \frac{4M_h^2}{M_H^2}\right)^{1/2}, \tag{7.26}$$

where the cubic scalar coupling λ_{Hhh} is expressed in units of v and can be obtained from eq. (7.43). In the right panel of figure 7.7 we show the constraints from our $\Gamma(H \to hh)$ fit in the $(|\lambda_{Hhh}|, M_h)$ plane. Strong bounds are obtained for the cubic Higgs coupling, $|\lambda_{Hhh}| \lesssim 10^{-2}$, as expected.

Recent updates from the ATLAS collaboration in the high-resolution channels report a significant difference in the mass of the neutral boson as determined from $H \to ZZ^{(*)} \to 4\ell$ ($123.5 \pm 0.8 \pm 0.3$ GeV) and $H \to \gamma\gamma$ ($126.6 \pm 0.3 \pm 0.7$ GeV) events [1]. Here we do not consider as a possible explanation for this discrepancy, the possibility of having two quasi-degenerate Higgs bosons, since the current mass value in the $H \to ZZ^{(*)} \to 4\ell$ channel obtained by CMS, $126.2 \pm 0.6 \pm 0.2$ GeV [3], does not support this hypothesis.

Degenerate CP-even and CP-odd Higgs bosons at 126 GeV

A CP-odd scalar does not couple at tree level to two vector bosons; its decay to gauge bosons starts at the one-loop level and it is therefore very suppressed. For this reason, a

---

[4]These effects are beyond the scope of the present work, but they could be relevant. For example, $H \to AA \to \gamma\gamma + \gamma\gamma$ could be mistaken by a two-photon signal when the photon pairs are very collimated [78]

pure CP-odd Higgs boson is already strongly disfavoured by present data as a candidate for the 126 GeV boson. However, the observed signal could result from two Higgs bosons with quasi-degenerate masses; this could explain the excess of $\gamma\gamma$ events observed by ATLAS and CMS. This possibility was proposed in ref. [79] within the non-minimal supersymmetric extension of the SM, and has also been considered within the context of 2HDMs, both for $\mathcal{Z}_2$ versions [80–82] and with a more general Yukawa structure [53, 55]. Model-independent methods to test experimentally for such possibility have also been proposed recently in refs. [83, 84].

We consider in this section the possibility of two Higgs bosons with quasi-degenerate masses around 126 GeV, one of them being CP-even and the other one CP-odd. We perform a global fit of the data with $M_h = M_A \approx 126$ GeV, and comment on the alternative possibility of quasi-degenerate H and A. The observed Higgs signals strengths will then receive contributions from both particles:

$$\mu_k^{(h+A)} = \mu_k^h + \mu_k^A. \tag{7.27}$$

Given the presently large experimental uncertainties, we neglect the small AVV coupling generated at one loop. Therefore, among all the channels considered in this work, the CP-odd Higgs will only contribute to $A \to \tau\tau$ and $A \to \gamma\gamma$. In both cases the dominant production channel is the gluon-fusion one. The loop-induced decay $A \to \gamma\gamma$ is only mediated by fermions. In figure 7.8 (left) we show the constraints on $M_{H^\pm}$ and M_H obtained from the oblique parameters. These masses are varied in the ranges $M_{H^\pm} \in [50, 600]$ GeV and $M_H \in [126, 600]$ GeV, while the coupling of h to vector bosons is kept close to the SM limit (*i.e.*, $|\cos\tilde{\alpha}| \in [0.8, 1]$), as suggested by the current experimental data. In the right panel of figure 7.8 we show similar bounds on the plane $(M_{H^\pm}, M_h)$, keeping the light scalar mass below $M_H = M_A = 126$ GeV and taking $\sin\tilde{\alpha} \in [0.8, 1]$; in this case the oblique parameters require the existence of a charged Higgs below the electroweak symmetry breaking scale $v = 246$ GeV.
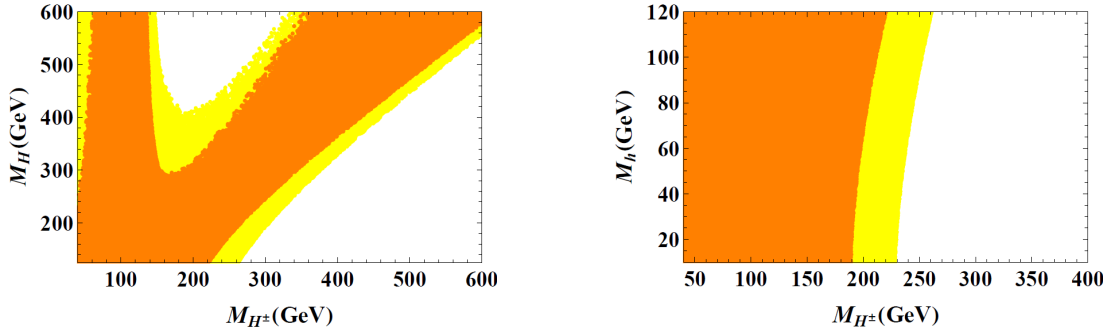
Figure 7.8: *Constraints in the* $(M_{H^\pm}, M_H)$ *plane for the case* $M_h = M_A = 126$ *GeV (left) and in the* $(M_{H^\pm}, M_h)$ *plane for the case* $M_H = M_A = 126$ *GeV (right), from the oblique parameters* S, T *and* U. *The orange (dark) and yellow (light) regions are allowed at 68% and 90% CL.*

In the scenario $M_h = M_A = 126$ GeV, the best fit region in the A2HDM parameter space, assuming the charged Higgs contribution to the 2γ channel to be negligible, is given by:

$$\cos\tilde{\alpha} = 0.98 \pm 0.2\,, \qquad \varsigma_u = -1.1\,^{+0.5}_{-0.4}\,, \qquad |\varsigma_d| = 1.2 \pm 1.2\,, \qquad \varsigma_l = -0.2\,^{+0.6}_{-0.4}\,.$$
(7.28)

The corresponding allowed ranges for the Higgs signal strengths, at 1σ and 2σ, are shown in figure 7.9. We obtain a smaller total decay width of the CP-even boson, $\rho(h) \approx 0.7$, which produces a sizeable enhancement of the $\mu^h_{\gamma\gamma jj}$ signal strength (the CP-odd boson A does not contribute to this channel). On the other hand, the excess in the two photon channel comes from the decays of both A and h, which give contributions of similar size ($\mu^h_{\gamma\gamma} \approx \mu^A_{\gamma\gamma} \approx 0.7$). The remaining contribution of A is to the $\tau^+\tau^-$ decay channel, which is small (ς_l is small). We must also notice that solutions with a flipped relative sign between the W and top contributions to $h \to \gamma\gamma$ are not allowed because they would require large values of ς_u; this would increase C^A_{gg} and $C^A_{\gamma\gamma}$ generating a large excess in the $\tau^+\tau^-$ and $\gamma\gamma$ channels, exceeding the current experimental bounds.

It is important to note that for a light charged Higgs boson, very strong flavour constraints in the $\varsigma_u - \varsigma_d$ plane can be obtained from $\bar{B} \to X_s\gamma$ [27]. The allowed ranges at 68% CL shown in eq. (7.28) were obtained assuming that the charged Higgs contribution to the diphoton channel is negligible (this is true even for a light charged Higgs if $\lambda_{hH^+H^-} \simeq$

0). Including the charged Higgs contribution to the 2γ channel in the fit one obtains at 68% CL that $C_{H^\pm}^h = -3.0 \pm 1.4$, while the alignment parameters ς_f remain weakly constrained and compatible with zero. In the limit $\varsigma_f = 0$, the stringent flavour constraints for a light charged Higgs, in particular $\bar{B} \to X_s \gamma$, are avoided since the charged Higgs decouples from the fermions. These constraints would be particularly relevant in the scenario $M_H = M_A = 126$ GeV for which the charged Higgs mass is bounded to lie below the electroweak scale, see figure 7.8 (right).
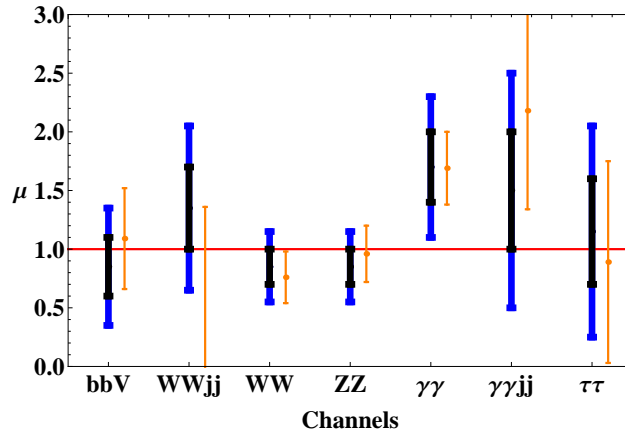
Figure 7.9:   *Allowed ranges for the Higgs signal strengths from the global fit within the CP-conserving A2HDM for the case of degenerate Higgs bosons with $M_h = M_A = 126$ GeV, at 1σ (black, dark) and 2σ (blue, dark). Other captions as in figure 7.2.*

7.4.2   The CP-violating A2HDM

In the A2HDM the up and down-quark as well as the leptonic Yukawa couplings are all independent complex parameters. Thus, one can expect a very rich phenomenology associated to the Higgs sector responsible for the breaking of the electroweak symmetry. Moreover, if one considers the most general scalar potential, the neutral scalars h, H and A are not CP eigenstates but rather a mixture of CP-even and CP-odd fields, parametrized by the general orthogonal matrix $\mathcal{R}$ introduced in section 7.2. Thus, there are new sources of CP violation, both from the Yukawa sector and the scalar potential, which could lead to interesting phenomenological predictions.

The study of CP-violating observables is beyond the scope of the present work and we

will defer it to future publications.[5] Nevertheless, we shall investigate next, the sensitivity of the different (CP-conserving) Higgs signal strengths to the CP-violating phases. Since the present data are consistent with the SM within rather large uncertainties, we will consider separately the different CP-odd possibilities, by fitting some complex coupling constants to the Higgs-signal-strength data while setting the remaining parameters to their SM-like values. A similar analysis has also been performed within a model independent framework in ref. [24].

Complex Yukawa couplings

Let us consider φ_i^0 to be the observed boson with a mass of 126 GeV. We will analyze three simple scenarios that will serve to determine the sensitivity to its complex Yukawa couplings and to what extent the SM limit is preferred by present data. We will set two Yukawa couplings to their SM values ($y_f^{\varphi_i^0} = 1$), and find the preferred values for the remaining Yukawa coupling by minimizing the χ^2 function. Figure 7.10 shows the resulting allowed regions for the top, bottom and tau Yukawa couplings when the coupling of φ_i^0 to vector bosons is fixed to $\mathcal{R}_{i1} = 0.95$; this value lies well within the 90% CL allowed band obtained from our previous fits.

Since all the observables considered are CP-even, the bounds obtained are symmetric under $\mathrm{Im}(y_f^{\varphi_i^0}) \to -\mathrm{Im}(y_f^{\varphi_i^0})$. Moreover, the real and imaginary parts of the Yukawa couplings do not interfere. The sensitivity to $\mathrm{Im}(y_f^{\varphi_i^0})$ is similar to that obtained previously, when considering only real couplings. For tree-level decays this is obvious from eq. (7.14), given that the parameter β_f is very close to one for $f = b, \tau$. For loop-induced decays this can be understood by observing that the loop functions (7.18) are closely related, $\mathcal{F}(\tau) = 2\tau + \frac{\tau^2}{2}f(\tau) + \mathcal{K}(\tau)$. For b quarks and τ leptons, $\mathcal{F}(\tau_f) \approx \mathcal{K}(\tau_f)$; for the top quark there is a small but sizable difference between the contributions of its real and imaginary Yukawa parts. Note that in the limit $\mathcal{R}_{i1} = 1$ the Yukawa couplings of φ_i^0 become SM-like ($y_f^{\varphi_i^0} = 1$) due to the orthogonality of $\mathcal{R}$; thus, there is no sensitivity to the ς_f parameters when considering the neutral Higgs couplings. The charged Higgs couplings on the other hand are proportional to ς_f and do not depend on the mixing matrix $\mathcal{R}$.

In the left upper panel of figure 7.10 we show the results of the fit for a complex

---

[5] For theoretical studies about the CP-properties of extended Higgs sectors at the LHC and in possible future colliders see ref. [85] and references therein.

top Yukawa coupling, while setting $y_d^{\varphi_i^0} = y_l^{\varphi_i^0} = 1$. The dashed lines show contours of constant value for $\mu_{\gamma\gamma}^{\varphi_i^0}$. The SM-like point $(\mathrm{Re}(y_u^{\varphi_i^0}), \mathrm{Im}(y_u^{\varphi_i^0})) = (1,0)$ lies outside the 90% CL region, but becomes allowed at 99% CL.
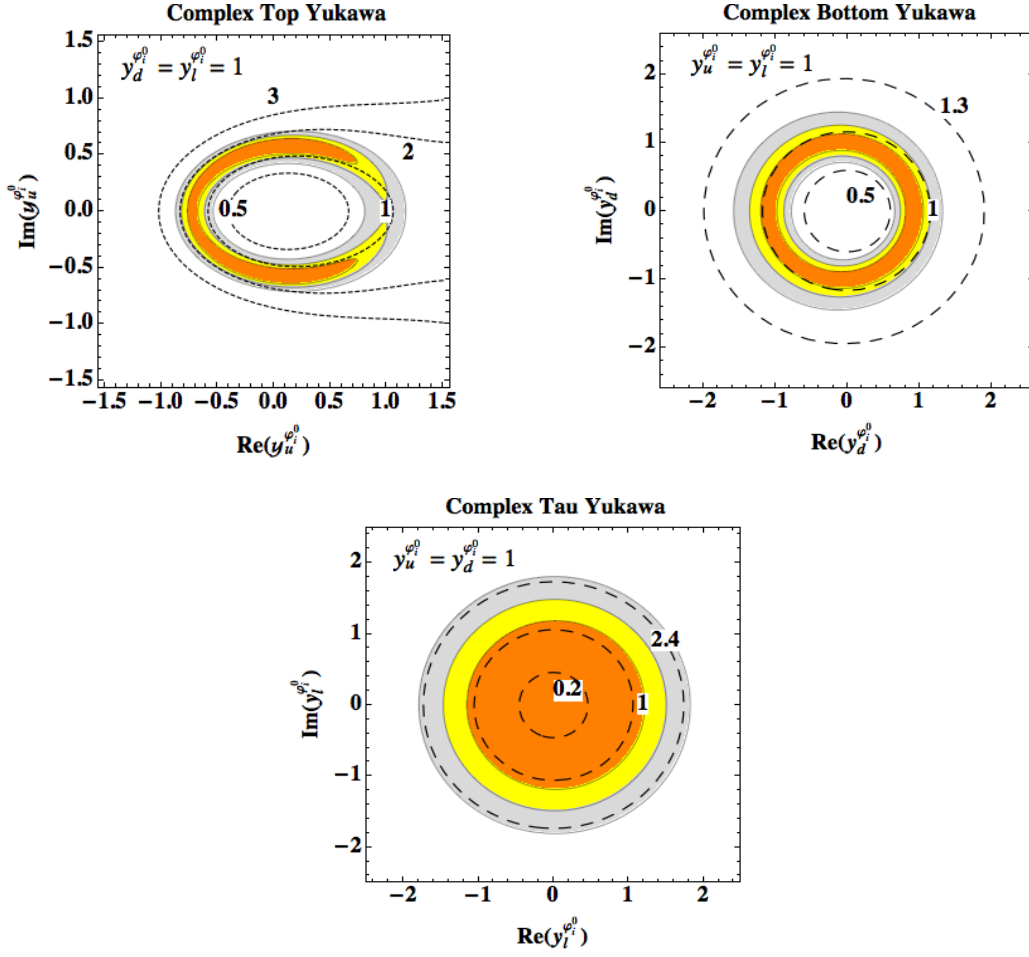
Figure 7.10:   *Allowed regions at 68% (orange), 90% (yellow) and 99% (grey) CL for the complex top (upper-left), bottom (upper-right) and tau (lower) Yukawa couplings. In each plot the two Yukawa couplings not shown are set to their SM value and the coupling to vector bosons is taken to be $\mathcal{R}_{i1} = 0.95$. The dashed lines show contours of constant values for $\mu_{\gamma\gamma}^{\varphi_i^0}$ (top plot), $\mu_{bbV}^{\varphi_i^0}$ (bottom plot) and $\mu_{\tau\tau V}^{\varphi_i^0}$ (tau plot).*

It can be seen that the allowed region at 90% CL accommodates an enhanced $\gamma\gamma$ rate between one and two times that of the SM. Within this 90% CL region, $\rho(\varphi_i^0) = 1.00 \pm 0.03$

as expected, since the dominant decay channel is $\bar{b}b$; the gluon fusion cross section is slightly reduced compared with the SM ($C_{gg}^{\varphi_i^0} = 0.87 \pm 0.28$), while the $\gamma\gamma$ partial decay width is enhanced ($C_{\gamma\gamma}^{\varphi_i^0} = 1.67 \pm 0.56$). The preferred allowed region is that for which the top Yukawa coupling has opposite sign to $\mathcal{R}_{i1}$, thus, creating a constructive interference with the vector boson contribution for the $\varphi_i^0 \to \gamma\gamma$ amplitude. The other option would be to have a significant imaginary component $\mathrm{Im}(y_u^{\varphi_i^0})$, which would also enhance the $\gamma\gamma$ rate. Similar results were obtained in ref. [24].

The right upper panel of figure 7.10 shows the fitted values for the complex bottom coupling, with the top and tau Yukawa couplings set to their SM values. The dashed lines indicate contours of constant value for $\mu_{bbV}^{\varphi_i^0}$. In this case the SM limit $(\mathrm{Re}(y_d^{\varphi_i^0}), \mathrm{Im}(y_d^{\varphi_i^0})) = (1, 0)$ lies inside the 90% CL allowed region, which accommodates $0.7 < \mu_{bbV}^{\varphi_i^0} < 1.2$. In this 90% CL region, the total decay width is rescaled by $\rho(\varphi_i^0) = 1.11 \pm 0.67$; the gluon-fusion cross section ratio is $C_{gg}^{\varphi_i^0} = 1.15 \pm 0.10$, while the $\gamma\gamma$ partial decay width turns out to be slightly suppressed with respect to the SM, $C_{\gamma\gamma}^{\varphi_i^0} = 0.89 \pm 0.10$. Since the total decay width depends strongly on the value of $|y_d^{\varphi_i^0}|^2$, a large variation range is obtained for $\rho(\varphi_i^0)$.

In the lower panel of figure 7.10, we show the fitted values of the complex τ Yukawa coupling assuming $y_u^{\varphi_i^0} = y_d^{\varphi_i^0} = 1$. Contours of constant value for $\mu_{\tau\tau V}^{\varphi_i^0}$ are also shown as dashed lines. We obtain that the signal strength $\mu_{\tau\tau V}^{\varphi_i^0} < 1.5$ lies within the 68% CL allowed region. The total Higgs decay width and the gluon-fusion cross section are equal in this case to the SM ones, while some suppression is observed in the $\gamma\gamma$ partial decay width: at 90% CL, $C_{\gamma\gamma}^{\varphi_i^0} = 0.90 \pm 0.11$ is obtained. This scenario is therefore disfavoured by the observed excess in the two-photon channel.

A fermiophobic charged Higgs

In the limit $\varsigma_f \to 0$ the charged Higgs does not couple to fermions, independently of any assumption about the scalar potential. Such *fermiophobic* charged Higgs could have avoided detection at LEP while being very light. Current LHC searches, as well as searches at the Tevatron, would have also missed such particle since it can neither be produced via top decay nor decay into fermions. Flavour constraints on this charged Higgs are also avoided trivially. Detecting such particle in an experiment is therefore quite challenging, since it can only be produced in processes involving vector bosons and/or neutral Higgs

particles; the same occurs for its decay channels.

The case of a fermiophobic charged Higgs is however highly predictive in the neutral Higgs sector, since all the channels which do not involve the $\gamma\gamma$ (γZ) final state only depend on one free parameter, $\mathcal{R}_{i1}$. The rescaling of the Higgs coupling to vector bosons in this case is the same as that of the neutral Yukawa ones, $y_f^{\varphi_i^0} = g_{\varphi_i^0 VV}/g_{\varphi_i^0 VV}^{\mathrm{SM}} = \mathcal{R}_{i1}$, which implies that all Higgs signal strengths are rescaled by a factor $\mathcal{R}_{i1}^2$ with respect to the SM, meaning that $\mu_{bb}^{\varphi_i^0} = \mu_{\tau\tau}^{\varphi_i^0} = \mu_{WW,ZZ}^{\varphi_i^0} = \rho(\varphi_i^0)^{-1}\mathcal{R}_{i1}^4 = \mathcal{R}_{i1}^2$, in any of the relevant production mechanisms. Therefore, in this scenario the signal strengths of the three neutral scalars are correlated:

$$\sum_{\varphi_i^0 = h,H,A} \mu_{ff}^{\varphi_i^0} = \sum_{\varphi_i^0 = h,H,A} \mu_{WW,ZZ}^{\varphi_i^0} = 1 \,. \tag{7.29}$$

Present data on the neutral Higgs boson are sensitive to a fermiophobic charged Higgs through the loop-induced decay $\varphi_i^0 \to \gamma\gamma$. The charged-scalar contribution to this decay can be sizeable for a light $H^\pm$, and this is a quite interesting situation in view of the possibility to detect such particle in the future. Assuming that the scalar with a mass of 126 GeV does not decay into lighter scalars, we show in figure 7.11 the allowed region in the parameter space $(\mathcal{R}_{i1}, \mathcal{C}_{H^\pm}^{\varphi_i^0})$. For the χ^2 fit we have only considered real values of $\mathcal{C}_{H^\pm}^{\varphi_i^0}$, which is true above the kinematical threshold $M_{H^\pm} > M_{\varphi_i^0}/2 \approx 63$ GeV, as we have mentioned before. In the figure we also show dashed contour lines of constant $\mu_{\gamma\gamma}^{\varphi_i^0}$. It can be observed that the preferred relative sign between the charged Higgs and the $W^\pm$ contributions to the $\gamma\gamma$ decay rate is such that it causes a constructive interference, thus enhancing slightly the $\gamma\gamma$ decay rate. The fit prefers a gauge coupling close to the SM one ($\chi^2_{\min}$ is obtained for $\mathcal{R}_{i1} \approx 0.95$) and puts the 90% CL lower bound $|\mathcal{R}_{i1}| > 0.79$. The SM-like point $(\mathcal{R}_{i1}, \mathcal{C}_{H^\pm}^{\varphi_i^0}) = (1,0)$ lies outside the 68% CL region, but is allowed at 90% CL (although close to the boundary). The presence of a non-zero (and negative) $\mathcal{C}_{H^\pm}^{\varphi_i^0}$ contribution is clearly favoured, while the preference for a slightly reduced gauge coupling implies a small suppression of the total decay width compared with the SM (*i.e.*, $\rho(\varphi_i^0) = 0.85 \pm 0.19$, at 90% CL). From the global fit, $\mu_{\gamma\gamma}^{\varphi_i^0} = \mu_{\gamma\gamma jj}^{\varphi_i^0} = 1.45 \pm 0.49$ is obtained at 90% CL; all the other Higgs signal strengths that are not affected by the charged Higgs contribution are equal to $\mu = 0.8 \pm 0.2$.
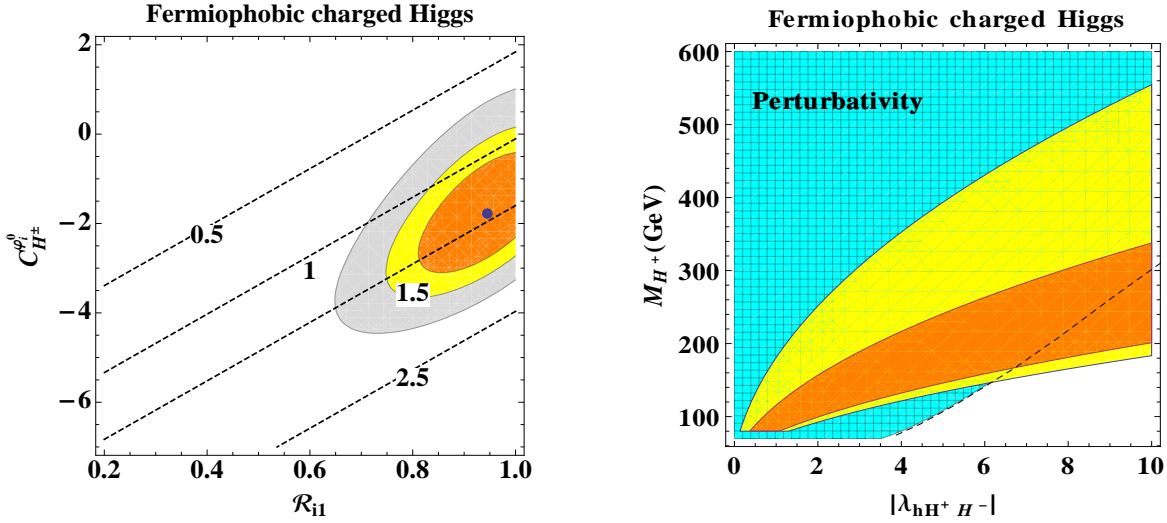
Figure 7.11: *Allowed regions at 68% (orange), 90% (yellow) and 99% CL (gray) for a fermio-phobic charged Higgs on the parameter space $(\mathcal{R}_{i1}, \mathcal{C}_{H^\pm}^{\varphi_i^0})$; dashed lines denote contours of constant $\mu_{\gamma\gamma}^{\varphi_i^0}$ (left). The right plot shows the corresponding 68% and 90% CL regions in the parameters $\lambda_{\varphi_i^0 H^+ H^-}$ and $M_{H^\pm}$, setting the value of $\mathcal{R}_{i1}$ at its best fit point. The region where perturbation theory remains valid is indicated in blue (hashed).*

The right panel in figure 7.11 shows the corresponding allowed regions in terms of the variables $\lambda_{\varphi_i^0 H^+ H^-}$ and $M_{H^\pm}$. The value of $\mathcal{R}_{i1}$ has been set to its best fit point. Also shown in the figure, is the region satisfying the perturbativity constraints discussed in appendix 7.D.

For the previous discussion we have not made any assumptions on the quantum numbers of the scalar field φ_i^0; we have only assumed that $M_{\varphi_i^0} = 126$ GeV and that its decay into lighter scalars is not allowed. Thus, the obtained results are general and apply both to a CP-conserving and to a CP-violating scalar potential. It must be noted that in the limit $|\mathcal{R}_{i1}| = 1$ the phenomenology of φ_i^0 becomes identical to that of the SM in every channel, except for $\gamma\gamma$ and γZ which are affected by the $H^\pm$ contribution. For a fermiophobic charged Higgs lighter than $M_{\varphi_i^0}/2 \approx 63$ GeV, $\mathcal{C}_{H^\pm}^{\varphi_i^0}$ develops an imaginary absorptive part. If kinematically open, the channel $\varphi_i^0 \to H^+ H^-$ would increase the total width of the Higgs boson; furthermore, in this scenario the production cross section is always less or equal to the SM. Therefore, the signal strengths would be reduced in every channel, with respect to the SM. This is in clear contradiction with the data, specially

with the measurements for the two-photon channel.

CP-even and CP-odd neutral scalar mixing

A CP-violating scalar potential generates mixings among the three neutral scalars, which are no longer CP eigenstates. Here, we are interested in exploring the possibility that the observed 126 GeV state could be the CP-odd scalar with a small CP admixture of the CP-even ones. A similar analysis within 2HDMs of types I and II, with explicit CP violation and soft breaking of the $\mathcal{Z}_2$ symmetry has been done in ref. [36], placing numerical bounds on the size of a possible CP-odd component for the scalar particle with 126 GeV of mass.

In the presence of CP violation, the admixture between the three neutral scalar fields is described by the 3-dimensional orthogonal matrix $\mathcal{R}$ which diagonalizes their mass matrix. This diagonalization can be done numerically, once the parameters of the scalar potential are known, but a simple analytical solution is not available for the most general case. It is well known, on the other hand, that in the CP-conserving limit the mass-matrix simplifies and it is possible to give explicit expressions for the masses and physical states in terms of the scalar potential parameters. A reasonable assumption when dealing with the general 2HDM scalar potential, is that the CP-violating terms are small; this makes a perturbative expansion in these parameters a valid approximation in principle. In appendix 7.A we provide explicit analytical expressions for the neutral scalar masses and the corresponding eigenstates to leading order in the CP-violating parameters of the scalar potential $\lambda_{5,6}^{\mathrm{I}}$. The corrections to the masses are quadratic in $\lambda_{5,6}^{\mathrm{I}}$, while the mixing between the CP-even and CP-odd states is only suppressed by one power of $\lambda_{5,6}^{\mathrm{I}}$, making this effect the dominant one.

Let us assume that the discovered boson is the state $A = S_3 + \mathcal{R}_{31} S_1 + \mathcal{R}_{32} S_2$, with $\mathcal{R}_{31}$ and $\mathcal{R}_{32}$ the small CP-even admixture coefficients. To simplify the discussion, we consider a simple scenario in which we set the parameters $\varsigma_{u,d,l} = 0$. The Yukawa couplings, as well as the coupling to vector bosons, are equal in this case, $y_f^A = \mathcal{R}_{31}$. From a global fit to the data, we find a lower bound on the admixture coefficient: $\mathcal{R}_{31} > 0.83$, at 99% CL. This result is mainly driven by the measurements in the W^+W^-, ZZ and $\gamma\gamma$ channels, which are SM-like to a good degree.

We can analyze whether such large values for the correction $\mathcal{R}_{31}$ can be obtained for

natural values of the scalar potential parameters. From eq. (7.48), one has:

$$\mathcal{R}_{31} \approx \frac{v^4 \left(2\lambda_5^{\mathrm{R}}\lambda_6^{\mathrm{I}} - \lambda_6^{\mathrm{R}}\lambda_5^{\mathrm{I}}\right)}{\left(\bar{M}_A^2 - \bar{M}_h^2\right)\left(\bar{M}_A^2 - \bar{M}_H^2\right)} \, . \tag{7.30}$$

Thus, large mass differences between the scalar states suppress the effect of mixing due to CP violation in the scalar potential; on the other hand if the scalar bosons have very similar masses these effects could be considerably enhanced. Assuming that $|\lambda_{5,6}^{I,R}| \lesssim 10^{-1}$ we obtain $\mathcal{R}_{31} \lesssim \left[\left(\bar{M}_A^2 - \bar{M}_H^2\right)\left(\bar{M}_A^2 - \bar{M}_h^2\right)\right]^{-1} 10^8 \text{ GeV}^4$, which implies that $|\mathcal{R}_{31}| \lesssim 10^{-2}$ for $\bar{M}_H > \bar{M}_h \gtrsim 300$ GeV. Of course, when either $\bar{M}_h \sim \bar{M}_A$ or $\bar{M}_H \sim \bar{M}_A$ the coefficient $\mathcal{R}_{31}$ diverges and the approximations used in appendix 7.A are no longer valid. The general formalism to describe the dynamics of CP violation near degenerate neutral Higgs bosons has been developed in refs. [86,87]. In ref. [88] the effect of resonant enhancement of H and A mixing was studied for the CP-violating 2HDM in the decoupling limit, $\bar{M}_A^2 \gg |\lambda_i| v^2$. In this case the heavy states H, $H^\pm$ and A are nearly mass degenerate and decouple from the light state h.

In figure 7.12 we show the allowed values at 90% CL for $(\mathcal{R}_{i1}, \mathcal{R}_{i2}, \mathcal{R}_{i3})$ for a general scalar state φ_i^0 with $m_{\varphi_i^0} = 126$ GeV, assuming that the alignment parameters ς_f ($f = u, d, l$) are real. We have imposed $|\varsigma_u| < 2$, in order to satisfy the flavour constraints for a charged Higgs below the TeV scale, and moreover we have set $|\varsigma_{d,l}| < 10$. It is seen that the CP-odd admixture in the 126 GeV state has an upper bound $\mathcal{R}_{i3} \lesssim 0.7$, similar to that obtained in ref. [36] within 2HDMs of types I and II, with explicit CP violation and soft breaking of the $\mathcal{Z}_2$ symmetry.
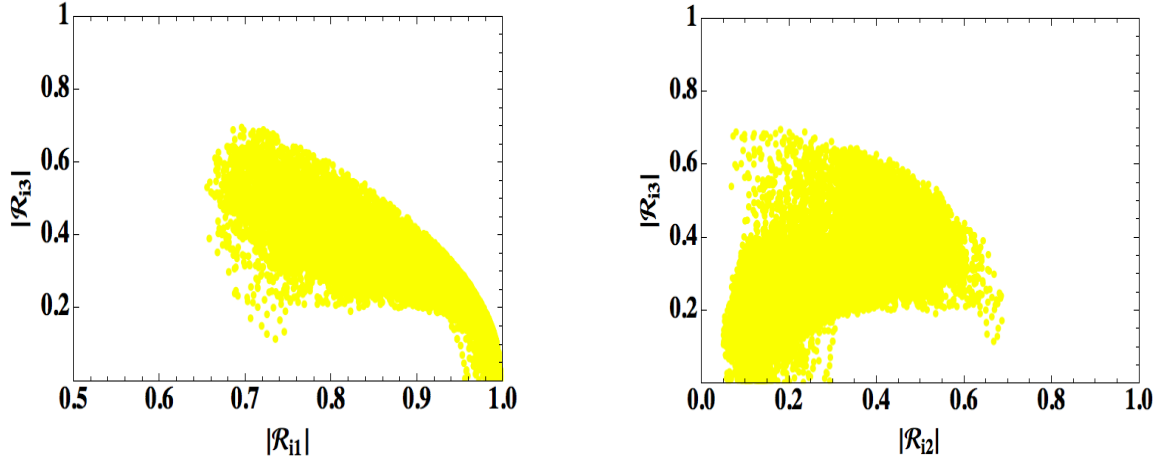
Figure 7.12:   *Allowed regions at 90% CL (yellow) on the parameter space $(\mathcal{R}_{i1}, \mathcal{R}_{i3})$, for real alignment parameters in the ranges $|\varsigma_u| < 2$ and $|\varsigma_{d,l}| < 10$ (left). The right plot shows the corresponding 90% CL region for the parameters $(\mathcal{R}_{i2}, \mathcal{R}_{i3})$.*

7.5   Summary

The recent LHC discovery of a new neutral boson, with mass close to 126 GeV, provides for the first time direct information on the electroweak symmetry breaking mechanism. The current data are so far compatible with the SM Higgs hypothesis, although a slight excess in the diphoton channel has been observed by the ATLAS and CMS collaborations. This channel is particularly interesting since the decay of the Higgs into two photons occurs at the one-loop level and is therefore sensitive to new charged particles that couple directly to the Higgs.

As new and more precise data become available, we shall test whether the properties of the 126 GeV particle correspond indeed to the SM Higgs boson or they manifest evidences for new phenomena, perhaps signalling the existence of a much richer scalar sector. Present experimental errors are still large but, nevertheless, they already allow us to extract useful constraints on alternative scenarios of electroweak symmetry breaking.

2HDMs constitute the simplest extension of the SM scalar sector, satisfying the electroweak precision tests, and give rise to interesting new phenomena through their enlarged scalar spectrum containing five physical scalars. In order to avoid dangerous FCNCs, the

2HDM phenomenology has been usually particularized to a few specific implementations, based on discrete $\mathcal{Z}_2$ symmetries, which severely restrict the fermionic couplings of the scalar bosons. The most widely used scenario is the so-called type II 2HDM, since it corresponds to the tree-level scalar sector of the minimal supersymmetric SM. However, the phenomenological FCNC requirements can be easily satisfied imposing a much softer alignment condition on the Yukawa couplings. The resulting A2HDM provides a general framework to describe an extended scalar sector with two Higgs doublets and no FCNCs at tree level, which includes as particular cases all previously considered 2HDM variants. It has a much larger parameter space with plenty of new phenomenological possibilities, such as new sources of CP violation and tunable strengths of the (family universal) Yukawas. Thus, it is the appropriate framework to perform an unbiased phenomenological analysis of the Higgs data.

In this paper, we have analyzed the present data on the Higgs signal strengths from the ATLAS, CMS, CDF and DØ collaborations, within the framework of the A2HDM. Even with the currently large experimental uncertainties, interesting conclusions can be obtained regarding the preferred regions in the parameter space of the model. We have considered a variety of possible departures from the SM predictions, within this framework, including the effects from new CP-violating phases. In particular, we have searched for possible ways to enhance the diphoton channel while being compatible with the rest of the data.

The measured WW, ZZ and $\gamma\gamma$ decay channels of the new boson suggest that its coupling to the weak vector bosons (W^+W^-, ZZ) is close to the SM one. This rules out the possibility of a pure CP-odd assignment for the quantum numbers of the new Higgs-like boson. A CP-even scalar, either pure or with a CP-odd admixture arising from CP-violating terms in the scalar potential, however, can accommodate the data rather well.

By flipping the relative sign of the top Yukawa coupling, the top-quark contribution to the Higgs decay amplitude into 2γ interferes constructively with the dominant $W^\pm$ contribution. This can only be realized in the A2HDM for large values of $|\varsigma_u|$, given that $g_{\varphi_i^0 VV} \approx g_{hVV}^{\mathrm{SM}}$. However, flavour constraints on a charged Higgs below the TeV scale (from $Z \to \bar{b}b$, $b \to s\gamma$ and B^0–$\bar{B}^0$ mixing) require that $|\varsigma_u| < 2$, even in the most general CP-violating A2HDM. Thus, a 2γ enhancement through a constructive interference of the top and $W^\pm$ contributions could only be possible in a decoupling scenario with an

enormously large $H^\pm$ mass.

Including the charged scalar contribution to the Higgs decay amplitude into two photons, one can explain the observed excess without significant deviations of the neutral scalar couplings from the SM limit, and satisfying at the same time the flavour constraints. This appears to be the most natural and likely possibility to accommodate current data within the A2HDM framework. The confirmation by future data of a significatively enhanced 2γ decay width could be a strong indication that a light charged scalar is around the corner, within the LHC reach.

The possibility that a CP-even and a CP-odd Higgs bosons have quasi-degenerate masses near 126 GeV was also analyzed. An excess in the $\gamma\gamma$ channel can occur in this case due to the contributions from both scalars (when signal strengths are added incoherently). We have also considered the most general A2HDM with complex Yukawa couplings. Since the Higgs signal strengths are CP-even observables, there is no interference between the contributions from the real and imaginary parts of the Yukawa couplings. It is then possible to enhance the $\gamma\gamma$ decay rate with a complex Yukawa coupling which has its real part close to the SM-like limit.

Future improvements of the present bounds on neutral and charged Higgs bosons, or perhaps their direct discovery, as well as more precise measurements of the current Higgs signal strengths are expected from the LHC in the next years. The complementarity between flavour constraints and collider searches for new scalar resonances will be crucial for the understanding of the mechanism of electroweak symmetry breaking. We have shown different alternative scenarios within the A2HDM that can accommodate present data very well, placing bounds on the relevant parameter space and discussing possible consequences that could be tested in the near future.

Note added: After the submission of this work for publication, updated experimental analyses of the LHC data have been made public [89,90]. While an enhanced diphoton rate is still present in the ATLAS results, the CMS collaboration finds now a 2γ rate compatible with the SM prediction. The new CMS results would favour a SM-like scenario, similar to that obtained in eq. (7.23), without any need for a charged scalar contribution to the 2γ decay mode. More data are needed to clarify this issue.

Acknowledgements

Appendix

7.A   Scalar Potential

In the Higgs basis, the most general scalar potential takes the form

$$
\begin{aligned}
V \;=\;& \mu_1\,\Phi_1^\dagger\Phi_1 + \mu_2\,\Phi_2^\dagger\Phi_2 + \left[\mu_3\,\Phi_1^\dagger\Phi_2 + \mu_3^*\,\Phi_2^\dagger\Phi_1\right] \\
& + \lambda_1\left(\Phi_1^\dagger\Phi_1\right)^2 + \lambda_2\left(\Phi_2^\dagger\Phi_2\right)^2 + \lambda_3\left(\Phi_1^\dagger\Phi_1\right)\left(\Phi_2^\dagger\Phi_2\right) + \lambda_4\left(\Phi_1^\dagger\Phi_2\right)\left(\Phi_2^\dagger\Phi_1\right) \\
& + \left[\left(\lambda_5\,\Phi_1^\dagger\Phi_2 + \lambda_6\,\Phi_1^\dagger\Phi_1 + \lambda_7\,\Phi_2^\dagger\Phi_2\right)\left(\Phi_1^\dagger\Phi_2\right) + \text{h.c.}\right].
\end{aligned}
\tag{7.31}
$$

The Hermiticity of the potential requires all parameters to be real except μ_3, λ_5, λ_6 and λ_7; thus, there are 14 real parameters.

The minimization conditions $\langle 0|\Phi_1^T(x)|0\rangle = \frac{1}{\sqrt{2}}\,(0,v)$ and $\langle 0|\Phi_2^T(x)|0\rangle = \frac{1}{\sqrt{2}}\,(0,0)$ impose the relations

$$
\mu_1 \;=\; -\lambda_1\,v^2\,, \qquad\qquad \mu_3 \;=\; -\frac{1}{2}\,\lambda_6\,v^2\,.
\tag{7.32}
$$

The potential can then be decomposed into a quadratic term plus cubic and quartic interactions

$$
V \;=\; -\frac{1}{4}\,\lambda_1\,v^4 + V_2 + V_3 + V_4\,.
\tag{7.33}
$$

The mass terms take the form

$$
\begin{aligned}
V_2 \;=\;& M_{H^\pm}^2\,H^+H^- + \frac{1}{2}\,(S_1,S_2,S_3)\,\mathcal{M}\begin{pmatrix} S_1 \\ S_2 \\ S_3 \end{pmatrix} \\[2mm]
\;=\;& M_{H^\pm}^2\,H^+H^- + \frac{1}{2}\,M_h^2\,h^2 + \frac{1}{2}\,M_H^2\,H^2 + \frac{1}{2}\,M_A^2\,A^2\,,
\end{aligned}
\tag{7.34}
$$

with

$$M_{H^\pm}^2 \;=\; \mu_2 + \frac{1}{2}\,\lambda_3\,v^2 \tag{7.35}$$

and

$$\mathcal{M} \;=\; \begin{pmatrix} 2\lambda_1 v^2 & v^2\,\lambda_6^{\mathrm{R}} & -v^2\,\lambda_6^{\mathrm{I}} \\[4pt] v^2\,\lambda_6^{\mathrm{R}} & M_{H^\pm}^2 + v^2\left(\frac{\lambda_4}{2}+\lambda_5^{\mathrm{R}}\right) & -v^2\,\lambda_5^{\mathrm{I}} \\[4pt] -v^2\,\lambda_6^{\mathrm{I}} & -v^2\,\lambda_5^{\mathrm{I}} & M_{H^\pm}^2 + v^2\left(\frac{\lambda_4}{2}-\lambda_5^{\mathrm{R}}\right) \end{pmatrix}, \tag{7.36}$$

where $\lambda_i^{\mathrm{R}} \equiv \mathrm{Re}(\lambda_i)$ and $\lambda_i^{\mathrm{I}} \equiv \mathrm{Im}(\lambda_i)$. The symmetric mass matrix $\mathcal{M}$ is diagonalized by an orthogonal matrix $\mathcal{R}$, which defines the neutral mass eigenstates:

$$\mathcal{M} \;=\; \mathcal{R}^T \begin{pmatrix} M_h^2 & 0 & 0 \\ 0 & M_H^2 & 0 \\ 0 & 0 & M_A^2 \end{pmatrix} \mathcal{R}\,, \qquad\qquad \begin{pmatrix} h \\ H \\ A \end{pmatrix} = \mathcal{R} \begin{pmatrix} S_1 \\ S_2 \\ S_3 \end{pmatrix}. \tag{7.37}$$

Since the trace remains invariant, the masses satisfy the relation

$$M_h^2 \;+\; M_H^2 \;+\; M_A^2 \;=\; 2\,M_{H^\pm}^2 \;+\; v^2\,(2\,\lambda_1 + \lambda_4)\,. \tag{7.38}$$

The minimization conditions allow us to trade the parameters μ_1 and μ_3 by v and λ_6. The freedom to rephase the field Φ_2 implies, moreover, that only the relative phases among λ_5, λ_6 and λ_7 are physical; but only two of them are independent. Therefore, we can fully characterize the potential with 11 parameters: v, μ_2, $|\lambda_{1,\ldots,7}|$, $\arg(\lambda_5\lambda_6^*)$ and $\arg(\lambda_5\lambda_7^*)$. Four parameters can be determined through the physical scalar masses.

In the CP conserving limit $\lambda_5^{\mathrm{I}} = \lambda_6^{\mathrm{I}} = \lambda_7^{\mathrm{I}} = 0$ and S_3 does not mix with the other neutral fields. The scalar spectrum contains then a CP-odd field $A = S_3$ and two CP-even scalars h and H which mix through the rotation matrix (7.3). In this case, the scalar masses are given by

$$\bar{M}_h^2 \;=\; \frac{1}{2}\,(\Sigma - \Delta)\,, \qquad \bar{M}_H^2 \;=\; \frac{1}{2}\,(\Sigma + \Delta)\,, \qquad \bar{M}_A^2 \;=\; M_{H^\pm}^2 + v^2\left(\frac{\lambda_4}{2} - \lambda_5^{\mathrm{R}}\right), \tag{7.39}$$

where

$$\Sigma \;=\; M_{H^\pm}^2 \;+\; v^2\left(2\,\lambda_1 + \frac{\lambda_4}{2} + \lambda_5^{\mathrm{R}}\right), \tag{7.40}$$

$$\Delta \;=\; \sqrt{\left[M_{H^\pm}^2 + v^2\left(-2\,\lambda_1 + \frac{\lambda_4}{2} + \lambda_5^{\mathrm{R}}\right)\right]^2 + 4v^4(\lambda_6^{\mathrm{R}})^2}\,, \tag{7.41}$$

and the mixing angle is determined through

$$\tan \tilde{\alpha} \;=\; \frac{\bar{M}_h^2 - 2\lambda_1 v^2}{v^2 \lambda_6^{\mathrm{R}}}\,. \tag{7.42}$$

We use the notation $\bar{M}_{\varphi_i^0}$ to emphasize that these are the neutral scalar masses in the CP-conserving limit. The cubic and quartic Higgs couplings involving the charged and the neutral physical scalars (without Goldstone boson couplings) take the form,

$$
\begin{aligned}
V_3 \;=\;& v\, H^+ H^- \left(\lambda_3\, S_1 + \lambda_7^{\mathrm{R}}\, S_2 - \lambda_7^{\mathrm{I}}\, S_3\right) - \frac{1}{2}\, v\, \lambda_7^{\mathrm{I}}\, S_3^3 - \frac{1}{2}\, v\, \lambda_7^{\mathrm{I}}\, S_2^2 S_3 - \frac{3}{2}\, v\, \lambda_6^{\mathrm{I}}\, S_1^2 S_3 \\
&+ \lambda_1\, v\, S_1^3 + \frac{1}{2}\, v\, \lambda_7^{\mathrm{R}}\, S_2^3 + \frac{3}{2}\, v\, \lambda_6^{\mathrm{R}}\, S_1^2 S_2 + \frac{1}{2}\, v\, \left(2\lambda_5^{\mathrm{R}} + \lambda_3 + \lambda_4\right) S_1 S_2^2 \\
&- \frac{1}{2}\, v\, \left(2\lambda_5^{\mathrm{R}} - \lambda_3 - \lambda_4\right) S_1 S_3^2 + \frac{1}{2}\, v\, \lambda_7^{\mathrm{R}}\, S_2 S_3^2 - 2\, v\, \lambda_5^{\mathrm{I}}\, S_1 S_2 S_3\,,
\end{aligned}
\tag{7.43}
$$

$$
\begin{aligned}
V_4 \;=\;& H^+ H^- \left(\lambda_2\, H^+ H^- + \frac{\lambda_3}{2}\, S_1^2 + \lambda_2\, S_3^2 + \lambda_2\, S_2^2 - \lambda_7^{\mathrm{I}}\, S_1 S_3 + \lambda_7^{\mathrm{R}}\, S_1 S_2\right) \\
&+ \frac{1}{4}\left(\lambda_3 + \lambda_4 + 2\lambda_5^{\mathrm{R}}\right)(S_1 S_2)^2 + \frac{1}{4}\left(\lambda_3 + \lambda_4 - 2\lambda_5^{\mathrm{R}}\right)(S_1 S_3)^2 + \frac{\lambda_2}{2}\,(S_2 S_3)^2 \\
&- \frac{1}{2}\,\lambda_6^{\mathrm{I}}\, S_1^3 S_3 - \lambda_5^{I}\, S_1^2 S_2 S_3 - \frac{\lambda_7^{\mathrm{I}}}{2}\, S_1 S_2^2 S_3 - \frac{\lambda_7^{\mathrm{I}}}{2}\, S_1 S_3^3 + \frac{\lambda_6^{\mathrm{R}}}{2}\, S_1^3 S_2 + \frac{\lambda_7^{\mathrm{R}}}{2}\, S_1 S_3^3 + \frac{\lambda_7^{\mathrm{R}}}{2}\, S_1 S_2 S_3^2 \\
&+ \frac{\lambda_1}{4}\, S_1^4 + \frac{\lambda_2}{4}\, S_2^4 + \frac{\lambda_2}{4}\, S_3^4\,.
\end{aligned}
\tag{7.44}
$$

In the CP-conserving limit all vertices involving an odd number of S_3 fields vanish. A basis-independent discussion of the 2HDM scalar sector can be found in ref. [91].

7.A.1 Neutral scalar mass matrix to lowest order in CP violation

Assuming that λ_5^{I} and λ_6^{I} are small, we can diagonalize the mass matrix (7.36) perturbatively as an expansion in powers of these CP-violating parameters. The leading corrections to the neutral scalar masses are quadratic in $\lambda_{5,6}^{\mathrm{I}}$:

$$M_{\varphi_i^0}^2 \;=\; \bar{M}_{\varphi_i^0}^2 + \alpha_1^{\varphi_i^0}\,(\lambda_5^{I})^2 + \alpha_2^{\varphi_i^0}\,(\lambda_6^{I})^2 + \alpha_3^{\varphi_i^0}\,(\lambda_5^{I}\lambda_6^{I})\,, \tag{7.45}$$

where $\bar{M}_{\varphi_i^0}$ denote the corresponding masses in the CP-conserving limit given in (7.39) and

$$\alpha_1^{\varphi_i^0} = \frac{v^4 \left(\bar{M}_{\varphi_i^0}^2 - 2\lambda_1 v^2 \right)}{\prod_{j \neq i} \left(\bar{M}_{\varphi_j^0}^2 - \bar{M}_{\varphi_i^0}^2 \right)} ,$$

$$\alpha_2^{\varphi_i^0} = \frac{v^4 \left(2\lambda_1 v^2 + \bar{M}_{\varphi_i^0}^2 - \bar{M}_H^2 - \bar{M}_h^2 \right)}{\prod_{j \neq i} \left(\bar{M}_{\varphi_j^0}^2 - \bar{M}_{\varphi_i^0}^2 \right)} ,$$

$$\alpha_3^{\varphi_i^0} = \frac{2v^6 \lambda_6^R}{\prod_{j \neq i} \left(\bar{M}_{\varphi_j^0}^2 - \bar{M}_{\varphi_i^0}^2 \right)} . \tag{7.46}$$

The physical states $\varphi_i^0 = \{h, H, A\}$ receive corrections at first order in $\lambda_{5,6}^{\mathrm{I}}$, which are given by

$$\begin{pmatrix} h \\ H \\ A \end{pmatrix} = \begin{pmatrix} \cos\tilde{\alpha} & \sin\tilde{\alpha} & \epsilon_{13} \\ -\sin\tilde{\alpha} & \cos\tilde{\alpha} & \epsilon_{23} \\ \epsilon_{31} & \epsilon_{32} & 1 \end{pmatrix} \begin{pmatrix} S_1 \\ S_2 \\ S_3 \end{pmatrix} , \tag{7.47}$$

where

$$\epsilon_{13} = \frac{v^2}{\left(\bar{M}_A^2 - \bar{M}_h^2 \right)} \left(\sin\tilde{\alpha}\,\lambda_5^{\mathrm{I}} + \cos\tilde{\alpha}\,\lambda_6^{\mathrm{I}} \right) , \qquad \epsilon_{23} = \frac{v^2}{\left(\bar{M}_A^2 - \bar{M}_H^2 \right)} \left(\cos\tilde{\alpha}\,\lambda_5^{\mathrm{I}} - \sin\tilde{\alpha}\,\lambda_6^{\mathrm{I}} \right) ,$$

$$\epsilon_{31} = -\frac{1}{2v^2} \left(\alpha_3^A \lambda_5^{\mathrm{I}} + 2\,\alpha_2^A \lambda_6^{\mathrm{I}} \right) , \qquad \epsilon_{32} = -\frac{1}{2v^2} \left(2\,\alpha_1^A \lambda_5^{\mathrm{I}} + \alpha_3^A \lambda_6^{\mathrm{I}} \right) . \tag{7.48}$$

Note that for the case of a scalar potential with a softly-broken $\mathcal{Z}_2$ symmetry in the Higgs basis we have $\lambda_6 = \lambda_7 = 0$ and, therefore, $\epsilon_{31} = 0$.

7.B   Scalar Couplings to the Gauge Bosons

The scalar doublets couple to the gauge bosons through the covariant derivative and gauge-fixing terms:

$$\mathcal{L}_K + \sum_{i=1}^{2} (D_\mu \Phi_a)^\dagger D^\mu \Phi_a + \mathcal{L}_{\mathrm{GF}} = \mathcal{L}_{V^2} + \mathcal{L}_{\phi^2} + \mathcal{L}_{\phi V} + \mathcal{L}_{\phi^2 V} + \mathcal{L}_{\phi V^2} + \mathcal{L}_{\phi^2 V^2} , \tag{7.49}$$

where $\mathcal{L}_K$ is the usual gauge-boson kinetic term and the covariant derivative is given by[6] $D_\mu = \partial_\mu + ieQA_\mu + i\dfrac{g}{\cos\theta_W} Z_\mu(T_3 - Q\sin^2\theta_W) + ig\left[T_+ W_\mu^\dagger + T_- W_\mu\right]$. It is convenient to adopt the following R_ξ gauge-fixing term ($\xi = 1$),

$$\mathcal{L}_{\text{GF}} = -\frac{1}{2}\left(\partial_\mu A^\mu\right)^2 - \frac{1}{2}\left(\partial_\mu Z^\mu + M_Z G^0\right)^2 - \left(\partial^\mu W_\mu^\dagger + iM_W G^+\right)\left(\partial_\nu W^\nu - iM_W G^-\right),$$
(7.50)

which cancels exactly the quadratic mixing terms between the gauge and Goldstone bosons generated by the covariant derivatives, so that $\mathcal{L}_{\phi V} = 0$, and provides the Goldstone bosons with the masses $M_{G^\pm} = M_W = gv/2$ and $M_{G^0} = M_Z = M_W/\cos\theta_W$. Then,

$$\mathcal{L}_{V^2} = -\frac{1}{2}\left(\partial_\mu A^\mu\right)^2 - \frac{1}{2}\left(\partial_\mu Z^\mu\right)^2 + \frac{1}{2} M_Z^2 Z_\mu Z^\mu - \left(\partial^\mu W_\mu^\dagger\right)\left(\partial_\nu W^\nu\right) + M_W^2 W_\mu^\dagger W^\mu, \quad (7.51)$$

while

$$\begin{aligned}
\mathcal{L}_{\phi^2} &= \frac{1}{2}\left[\partial_\mu h\, \partial^\mu h + \partial_\mu H\, \partial^\mu H + \partial_\mu A\, \partial^\mu A\right] + \partial_\mu H^+ \partial^\mu H^- \\
&+ \frac{1}{2}\partial_\mu G^0\, \partial^\mu G^0 - \frac{1}{2} M_Z^2 (G^0)^2 + \partial_\mu G^+ \partial^\mu G^- - M_W^2 G^+ G^- .
\end{aligned}$$
(7.52)

The interaction terms between the scalar and gauge bosons are given by:

$$\begin{aligned}
\mathcal{L}_{\phi^2 V} &= ie\left[A^\mu + \cot(2\theta_W)\, Z^\mu\right]\left[(H^+ \overset{\leftrightarrow}{\partial}_\mu H^-) + (G^+ \overset{\leftrightarrow}{\partial}_\mu G^-)\right] \\
&+ \frac{e}{\sin(2\theta_W)}\, Z^\mu \left[(G^0 \overset{\leftrightarrow}{\partial}_\mu S_1) + (S_3 \overset{\leftrightarrow}{\partial}_\mu S_2)\right] \\
&+ \frac{g}{2}\, W^{\mu\dagger}\left[(H^- \overset{\leftrightarrow}{\partial}_\mu S_3) - i(H^- \overset{\leftrightarrow}{\partial}_\mu S_2) + (G^- \overset{\leftrightarrow}{\partial}_\mu G^0) - i(G^- \overset{\leftrightarrow}{\partial}_\mu S_1)\right] \\
&+ \frac{g}{2}\, W^{\mu}\left[(H^+ \overset{\leftrightarrow}{\partial}_\mu S_3) + i(H^+ \overset{\leftrightarrow}{\partial}_\mu S_2) + (G^+ \overset{\leftrightarrow}{\partial}_\mu G^0) + i(G^+ \overset{\leftrightarrow}{\partial}_\mu S_1)\right], \quad (7.53)
\end{aligned}$$

$$\begin{aligned}
\mathcal{L}_{\phi V^2} &= \frac{2}{v}\, S_1 \left[\frac{1}{2} M_Z^2 Z_\mu Z^\mu + M_W^2 W_\mu^\dagger W^\mu\right] \\
&+ \left(eM_W A^\mu - gM_Z \sin^2\theta_W Z^\mu\right)\left(G^+ W_\mu + G^- W_\mu^\dagger\right), \quad (7.54)
\end{aligned}$$

---

[6]The weak mixing angle θ_W is defined through the relation $g\sin\theta_W = g'\cos\theta_W = e$. The operators $T_\pm = \frac{1}{\sqrt{2}}(T_1 \pm T_2)$ and T_3 can be expressed in terms of the Pauli matrices by $T_i = \dfrac{\sigma_i}{2}$.

$$
\begin{aligned}
\mathcal{L}_{\phi^2 V^2} &= \frac{1}{v^2}\left[\frac{1}{2}M_Z^2\,Z_\mu Z^\mu + M_W^2\,W_\mu^\dagger W^\mu\right]\left[H^2 + h^2 + A^2 + (G^0)^2\right] \\
&+ \left\{e^2\left[A^\mu + \cot\left(2\theta_W\right)Z^\mu\right]^2 + \frac{g^2}{2}\,W_\mu^\dagger W^\mu\right\}\left(G^+G^- + H^+H^-\right) \\
&+ \frac{eg}{2}\left(A^\mu - \tan\theta_W\,Z^\mu\right)\left[S_1\left(G^+W_\mu + G^-W_\mu^\dagger\right) + S_2\left(H^+W_\mu + H^-W_\mu^\dagger\right)\right. \\
&\qquad\qquad\left. +\; i\,S_3\left(H^-W_\mu^\dagger - H^+W_\mu\right) + i\,G^0\left(G^-W_\mu^\dagger - G^+W_\mu\right)\right],
\end{aligned}
$$

$$(7.55)$$

with $S_i = \mathcal{R}_{ji}\varphi_j^0$ ($\varphi_j^0 = \{h, H, A\}$) and the usual notation $A\overset{\leftrightarrow}{\partial}_\mu B \equiv A(\partial_\mu B) - (\partial_\mu A)B$.

7.C   Statistical treatment and data

To obtain the preferred values for the parameters of the A2HDM we build a global χ^2 function

$$
\chi^2 \;=\; \sum_k \frac{(\mu_k - \hat{\mu}_k)^2}{\sigma_k^2}\,,
\tag{7.56}
$$

where σ_i is the experimental error extracted from the data at $1\,\sigma$. Errors on the reported Higgs signal strengths $\hat{\mu}_k$ are symmetrized using

$$
\delta\hat{\mu}_k \;=\; \sqrt{\frac{(\delta\hat{\mu}_+)^2 + (\delta\hat{\mu}_-)^2}{2}}\,,
\tag{7.57}
$$

where $\delta\hat{\mu}_\pm$ are the one-sided errors given by the experimental collaborations. We use the latest data available after the "Hadron Collider Physics Symposium 2012 (HCP2012)", including the latest update from ATLAS of the high-resolution channels $\gamma\gamma$, $ZZ^{(*)}$ [1]. For the diphoton channels we use the data given by ATLAS and CMS at 7 and 8 TeV, provided in refs. [1, 2, 13, 14]. For the rest of the channels we use the averages listed in table 7.2, which include the $7 \oplus 8$ TeV data reported by ATLAS and CMS together with CDF and DØ data [10–12] at $\sqrt{s} = 1.96$ TeV.

For a general channel with inclusive production we have (neglecting the subdominant production channels)

$$
\mu_k^{\varphi_i^0} \;=\; \frac{\sigma_{gg}}{\sigma_{gg}^{\rm SM}}\cdot\frac{\mathrm{Br}(\varphi_i^0 \to k)}{\mathrm{Br}(\varphi_i^0 \to k)_{\rm SM}}\,.
\tag{7.58}
$$

Table 7.2: *Higgs signal strengths in each of the channels considered in this work. Averages obtained from ATLAS and CMS data at $7 \oplus 8$ TeV together with CDF and DØ data at $\sqrt{s} = 1.96$ TeV. (*) We do not consider non-inclusive measurements in the $\tau\tau$ channel. Due to the large current errors associated with these measurements, our conclusions would not be modified at this level.*

Channel	$\hat{\mu}_k$	Comment
$b\bar{b}V$	1.1 ± 0.44	ATLAS, CMS, CDF and DØ [1, 2, 11, 12] (our average)
$WWjj$	-0.2 ± 1.56	ATLAS and CMS [1, 2, 14] (our average)
WW	0.76 ± 0.21	ATLAS, CMS, CDF and DØ [1, 2, 10, 11, 13] (our average)
ZZ	0.96 ± 0.26	ATLAS and CMS [1, 2] (our average)
$\tau\tau$ (incl.) (*)	0.89 ± 0.86	ATLAS and CMS [1, 2] (our average)
$\gamma\gamma$	1.66 ± 0.32	ATLAS and CMS [1, 2] (our average)
$\gamma\gamma jj$	2.18 ± 0.84	ATLAS and CMS [1, 2] (our average)

For the Higgs searches in the $\gamma\gamma$ channel, the ATLAS and CMS collaborations have established different categories. To take this into account, we write the Higgs signal strength in a given $\gamma\gamma$ channel as

$$\mu_{\gamma\gamma}^{\varphi_i^0} = \frac{\epsilon_{ggF}\,\sigma_{ggF} + \epsilon_{\text{VBF}}\,\sigma_{VBF} + \epsilon_{\text{VH}}\,\sigma_{\text{VH}}}{\epsilon_{ggF}\,\sigma_{ggF}^{\text{SM}} + \epsilon_{\text{VBF}}\,\sigma_{\text{VBF}}^{\text{SM}} + \epsilon_{\text{VH}}\,\sigma_{\text{VH}}^{\text{SM}}} \cdot \frac{\text{Br}(\varphi_i^0 \to \gamma\gamma)}{\text{Br}(\varphi_i^0 \to \gamma\gamma)_{\text{SM}}}, \qquad (7.59)$$

where the coefficients $\epsilon_{(ggF,\text{VBF},\text{VH})}$ accounting for the relative weight of each production channel have been provided by ATLAS and CMS [5,6]. The top-quark-fusion contribution could be added in a similar way. In eq. (7.59), the SM production cross sections and decay widths are taken from the web page of the LHC Higgs Cross Section Working Group [92]. For the gluon-fusion production mechanism we have

$$\sigma(gg \to \varphi_i^0) \equiv \sigma_{ggF} = C_{gg}^{\varphi_i^0} \sigma_{ggF}^{\text{SM}}, \qquad (7.60)$$

where the scaling of the gluon-fusion cross section $C_{gg}^{\varphi_i^0}$ was defined in section 7.3. Vector-boson fusion scales with the coefficient $\mathcal{R}_{i1}$ as

$$\sigma(qq' \to qq'\varphi_i^0) \equiv \sigma_{\text{VBF}} = (\mathcal{R}_{i1})^2 \sigma_{\text{VBF}}^{\text{SM}}, \qquad (7.61)$$

and similarly for the associated production with a vector boson

$$\sigma(q\bar{q} \to V\varphi_i^0) \;\equiv\; \sigma_{\mathrm{VH}} \;=\; (\mathcal{R}_{i1})^2\, \sigma_{\mathrm{VH}}^{\mathrm{SM}}\,. \tag{7.62}$$

7.D   Perturbativity Constraints

The charged Higgs boson contribution to $\varphi_i^0 \to \gamma\gamma$ depends crucially on the value of the neutral scalar coupling to a pair of charged Higgs bosons. To assure the validity of perturbation theory, upper bounds on the quartic Higgs self-couplings are usually imposed requiring these to be smaller than 8π (see [31, 32] and references therein). The cubic Higgs self-couplings are also bounded indirectly in this way. In this work we consider an alternative perturbativity bound on the relevant Higgs cubic coupling which is more restrictive for light charged Higgs masses. Consider the $\varphi_i^0 H^+ H^-$ one-loop vertex correction given by figure 7.13. The contribution of this diagram is finite and can give us an idea about the allowed magnitude of the cubic coupling in order not to spoil the perturbative convergence.
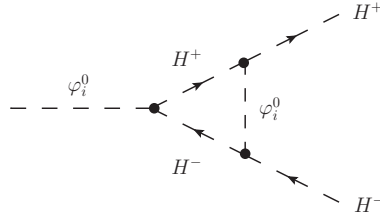

Figure 7.13: *Diagram contributing to the one-loop $\varphi_i^0 H^+ H^-$ vertex correction.*

We obtain:

$$(\lambda_{\varphi_i^0 H^+ H^-})_{\mathrm{eff}} \;=\; \lambda_{\varphi_i^0 H^+ H^-} \left[1 + \frac{v^2 \lambda_{\varphi_i^0 H^+ H^-}^2}{16\pi^2 M_{H^\pm}^2}\, \mathcal{Z}\!\left(\frac{M_{\varphi_i^0}^2}{M_{H^\pm}^2} \right) \right] \;\equiv\; \lambda_{\varphi_i^0 H^+ H^-}\, (1 + \Delta)\,, \tag{7.63}$$

where

$$\mathcal{Z}(X) \;=\; \int_0^1 dy \int_0^{1-y} dz \left[(y+z)^2 + X\,(1 - y - z - yz) \right]^{-1}\,. \tag{7.64}$$

Allowing the correction to be at most 50% ($\Delta \leqslant 0.5$) constraints the allowed parameter space in the $(\lambda_{\varphi_i^0 H^+ H^-}, M_{H^\pm})$ plane to be within the blue (hashed) region indicated in figure 7.6.

7.E Oblique Parameters

Possible deviations from the SM in the gauge-boson self-energies are usually characterized through the oblique parameters S, T and U [93]. Taking as a reference SM Higgs mass $M_{h,\text{ref}} = 126$ GeV, the most recent global fit to electroweak precision observables quotes the values [76, 77]:

$$S = 0.03 \pm 0.10\,, \qquad T = 0.05 \pm 0.12\,, \qquad U = 0.03 \pm 0.10\,. \qquad (7.65)$$

The expressions for the oblique parameters in the CP conserving A2HDM are adapted from ref. [94]:

$$
\begin{aligned}
S = \frac{1}{\pi M_Z^2} \Bigg\{ &\cos^2 \tilde{\alpha} \left[\mathcal{B}_{22}(M_Z^2; M_Z^2, M_h^2) - M_Z^2\, \mathcal{B}_0(M_Z^2; M_Z^2, M_h^2) + \mathcal{B}_{22}(M_Z^2; M_H^2, M_A^2) \right] \\
&+ \sin^2 \tilde{\alpha} \left[\mathcal{B}_{22}(M_Z^2; M_Z^2, M_H^2) - M_Z^2\, \mathcal{B}_0(M_Z^2; M_Z^2, M_H^2) + \mathcal{B}_{22}(M_Z^2; M_h^2, M_A^2) \right] \\
&- \mathcal{B}_{22}(M_Z^2; M_{H^\pm}^2, M_{H^\pm}^2) - \mathcal{B}_{22}(M_Z^2; M_Z^2, M_{h,\text{ref}}^2) + M_Z^2\, \mathcal{B}_0(M_Z^2; M_Z^2, M_{h,\text{ref}}^2) \Bigg\}\,,
\end{aligned}
$$

$$(7.66)$$

$$
\begin{aligned}
T = \frac{1}{16\pi M_W^2 s_W^2} \Bigg\{ &\cos^2 \tilde{\alpha} \left[\mathcal{F}(M_{H^\pm}^2, M_H^2) - \mathcal{F}(M_H^2, M_A^2) + 3\, \mathcal{F}(M_Z^2, M_h^2) - 3\, \mathcal{F}(M_W^2, M_h^2) \right] \\
&+ \sin^2 \tilde{\alpha} \left[\mathcal{F}(M_{H^\pm}^2, M_h^2) - \mathcal{F}(M_h^2, M_A^2) + 3\, \mathcal{F}(M_Z^2, M_H^2) - 3\, \mathcal{F}(M_W^2, M_H^2) \right] \\
&+ \mathcal{F}(M_{H^\pm}^2, M_A^2) - 3\, \mathcal{F}(M_Z^2, M_{h,\text{ref}}^2) + 3\, \mathcal{F}(M_W^2, M_{h,\text{ref}}^2) \Bigg\}\,, \qquad (7.67)
\end{aligned}
$$

$$U \; = \; \mathcal{H}(M_W^2) - \mathcal{H}(M_Z^2) + \frac{1}{\pi M_W^2} \left\{ \sin^2 \tilde{\alpha} \; \mathcal{B}_{22}(M_W^2; M_{H^\pm}^2, M_h^2) + \cos^2 \tilde{\alpha} \; \mathcal{B}_{22}(M_W^2; M_{H^\pm}^2, M_H^2) \right.$$

$$\left. + \; \mathcal{B}_{22}(M_W^2; M_{H^\pm}^2, M_A^2) - 2 \, \mathcal{B}_{22}(M_W^2; M_{H^\pm}^2, M_{H^\pm}^2) \right\}$$

$$- \frac{1}{\pi M_Z^2} \left\{ \sin^2 \tilde{\alpha} \; \mathcal{B}_{22}(M_Z^2; M_h^2, M_A^2) + \cos^2 \tilde{\alpha} \; \mathcal{B}_{22}(M_Z^2; M_H^2, M_A^2) \right.$$

$$\left. - \; \mathcal{B}_{22}(M_Z^2; M_{H^\pm}^2, M_{H^\pm}^2) \right\}, \tag{7.68}$$

where

$$\mathcal{H}(M_V^2) \; \equiv \; \frac{1}{\pi M_V^2} \left\{ \cos^2 \tilde{\alpha} \left[\mathcal{B}_{22}(M_V^2; M_V^2, M_h^2) - M_V^2 \, \mathcal{B}_0(M_V^2; M_V^2, M_h^2) \right] \right.$$

$$+ \; \sin^2 \tilde{\alpha} \left[\mathcal{B}_{22}(M_V^2; M_V^2, M_H^2) - M_V^2 \, \mathcal{B}_0(M_V^2; M_V^2, M_H^2) \right]$$

$$\left. - \; \mathcal{B}_{22}(M_V^2; M_V^2, M_{h,\text{ref}}^2) + M_V^2 \, \mathcal{B}_0(M_V^2; M_V^2, M_{h,\text{ref}}^2) \right\}. \tag{7.69}$$

The loop functions are given by

$$B_{22}(q^2; m_1^2, m_2^2) \; = \; \frac{1}{4} \left(\Delta + 1 \right) \left[m_1^2 + m_2^2 - \frac{1}{3} q^2 \right] - \frac{1}{2} \int_0^1 dx \; X \; \log\left(X - i\epsilon \right), \tag{7.70}$$

$$B_0(q^2; m_1^2, m_2^2) \; = \; \Delta - \int_0^1 dx \; \log\left(X - i\epsilon \right), \tag{7.71}$$

$$\mathcal{F}(m_1^2, m_2^2) \; = \; \frac{1}{2} \left(m_1^2 + m_2^2 \right) - \frac{m_1^2 m_2^2}{m_1^2 - m_2^2} \; \log\left(\frac{m_1^2}{m_2^2} \right), \tag{7.72}$$

with

$$X \; \equiv \; m_1^2 \, x + m_2^2 \left(1 - x \right) - q^2 \, x(1-x), \qquad \Delta \; \equiv \; \frac{2}{4-d} + \ln 4\pi - \gamma_E, \tag{7.73}$$

in d space-time dimensions, where γ_E is the Euler-Mascheroni constant, and where we have defined:

$$\mathcal{B}_{22}(q^2; m_1^2, m_2^2) \; \equiv \; B_{22}(q^2; m_1^2, m_2^2) - B_{22}(0; m_1^2, m_2^2), \tag{7.74}$$

$$\mathcal{B}_0(q^2; m_1^2, m_2^2) \; \equiv \; B_0(q^2; m_1^2, m_2^2) - B_0(0; m_1^2, m_2^2). \tag{7.75}$$

Bibliography

[1] G. Aad *et al.* [ATLAS Collaboration], Phys. Lett. B **716** (2012) 1 [arXiv:1207.7214 [hep-ex]]; ATLAS-CONF-2012-170 (December 13, 2012).

[2] S. Chatrchyan *et al.* [CMS Collaboration], Phys. Lett. B **716** (2012) 30 [arXiv:1207.7235 [hep-ex]]; CMS-PAS-HIG-12-045 (November 16, 2012).

[3] S. Chatrchyan *et al.* [CMS Collaboration], Phys. Rev. Lett. **108** (2012) 111804 [arXiv:1202.1997 [hep-ex]]; Phys. Rev. Lett. **110** (2013) 081803 [arXiv:1212.6639 [hep-ex]].

[4] G. Aad *et al.* [ATLAS Collaboration], Phys. Lett. B **710** (2012) 383 [arXiv:1202.1415 [hep-ex]]; ATLAS-CONF-2012-169 (December 13, 2012).

[5] G. Aad *et al.* [ATLAS Collaboration], Phys. Rev. Lett. **108** (2012) 111803 [arXiv:1202.1414 [hep-ex]]; ATLAS-CONF-2012-168 (December 13, 2012).

[6] S. Chatrchyan *et al.* [CMS Collaboration], Phys. Lett. B **710** (2012) 403 [arXiv:1202.1487 [hep-ex]]; CMS-PAS-HIG-12-015 (July 8, 2012).

[7] T. Aaltonen *et al.* [CDF and D0 Collaborations], Phys. Rev. Lett. **109** (2012) 071804 [arXiv:1207.6436 [hep-ex]].

[8] R. Barate *et al.* [LEP Working Group for Higgs boson searches and ALEPH and DELPHI and L3 and OPAL Collaborations], Phys. Lett. B **565** (2003) 61 [hep-ex/0306033].

[9] T. Aaltonen *et al.* [CDF and D0 Collaboration], Phys. Rev. Lett. **104** (2010) 061802 [arXiv:1001.4162 [hep-ex]]; V. M. Abazov *et al.* [D0 Collaboration], arXiv:1301.6122 [hep-ex].

[10] Tevatron New Physics Higgs Working Group and CDF and D0 Collaborations, arXiv:1207.0449 [hep-ex]. V. M. Abazov *et al.* [D0 Collaboration], arXiv:1301.5358 [hep-ex].

[11] T. Aaltonen *et al.* [CDF Collaboration], Phys. Rev. Lett. **109** (2012) 111802 [arXiv:1207.1707 [hep-ex]]; arXiv:1301.4440 [hep-ex]; arXiv:1301.6668 [hep-ex].

[12] V. M. Abazov *et al.* [D0 Collaboration], Phys. Rev. Lett. **109** (2012) 121802 [arXiv:1207.6631 [hep-ex]]. Yuji Enari talk at the Hadron Collider Physics Symposium, Kyoto (November, 2012).

[13] G. Aad *et al.* [ATLAS Collaboration], Phys. Rev. D **86** (2012) 032003 [arXiv:1207.0319 [hep-ex]].

[14] S. Chatrchyan *et al.* [CMS Collaboration], Phys. Lett. B **710** (2012) 26 [arXiv:1202.1488 [hep-ex]].

[15] J. R. Espinosa, C. Grojean, M. Muhlleitner and M. Trott, JHEP **1212** (2012) 045 [arXiv:1207.1717 [hep-ph]]; JHEP **1205** (2012) 097 [arXiv:1202.3697 [hep-ph]]; JHEP **1209** (2012) 126 [arXiv:1205.6790 [hep-ph]].

[16] M. Klute, R. Lafaye, T. Plehn, M. Rauch and D. Zerwas, Phys. Rev. Lett. **109** (2012) 101801 [arXiv:1205.2699 [hep-ph]].

[17] D. Carmi, A. Falkowski, E. Kuflik and T. Volansky, JHEP **1207** (2012) 136 [arXiv:1202.3144 [hep-ph]].

[18] A. Azatov, R. Contino and J. Galloway, JHEP **1204** (2012) 127 [arXiv:1202.3415 [hep-ph]].

[19] A. Azatov *et. al.*, JHEP **1206** (2012) 134 [arXiv:1204.4817 [hep-ph]].

[20] P. P. Giardino, K. Kannike, M. Raidal and A. Strumia, Phys. Lett. B **718** (2012) 469 [arXiv:1207.1347 [hep-ph]].

[21] T. Corbett, O. J. P. Eboli, J. González-Fraile and M. C. González-García, Phys. Rev. D **86** (2012) 075013 [arXiv:1207.1344 [hep-ph]]; Phys. Rev. D **87** (2013) 015022 [arXiv:1211.4580 [hep-ph]].

[22] E. Masso and V. Sanz, Phys. Rev. D **87** (2013) 033001 [arXiv:1211.1320 [hep-ph]].

[23] J. Ellis and T. You, JHEP **1209** (2012) 123 [arXiv:1207.1693 [hep-ph]].

[24] K. Cheung, J. S. Lee and P. -Y. Tseng, arXiv:1302.3794 [hep-ph].

[25] A. Pich, Nucl. Phys. Proc. Suppl. **209** (2010) 182 [arXiv:1010.5217 [hep-ph]].

[26] A. Pich and P. Tuzón, Phys. Rev. D **80** (2009) 091702 [arXiv:0908.1554 [hep-ph]].

[27] M. Jung, A. Pich and P. Tuzón, JHEP **1011** (2010) 003 [arXiv:1006.0470 [hep-ph]].

[28] M. Jung, A. Pich and P. Tuzón, Phys. Rev. D **83** (2011) 074011 [arXiv:1011.5154 [hep-ph]].

[29] M. Jung, X. -Q. Li and A. Pich, JHEP **1210** (2012) 063 [arXiv:1208.1251 [hep-ph]].

[30] A. Celis, M. Jung, X. -Q. Li and A. Pich, JHEP **1301** (2013) 054 [arXiv:1210.8443 [hep-ph]].

[31] G. C. Branco *et. al.*, Phys. Rept. **516** (2012) 1 [arXiv:1106.0034 [hep-ph]].

[32] J. F. Gunion, H. E. Haber, G. L. Kane and S. Dawson, Front. Phys. **80** (2000) 1.

[33] N. Craig and S. Thomas, JHEP **1211** (2012) 083 [arXiv:1207.4835 [hep-ph]].

[34] P. M. Ferreira, R. Santos, M. Sher and J. P. Silva, Phys. Rev. D **85** (2012) 077703 [arXiv:1112.3277 [hep-ph]].

[35] P. M. Ferreira, R. Santos, M. Sher and J. P. Silva, Phys. Rev. D **85** (2012) 035020 [arXiv:1201.0019 [hep-ph]].

[36] A. Barroso, P. M. Ferreira, R. Santos and J. P. Silva, Phys. Rev. D **86** (2012) 015022 [arXiv:1205.4247 [hep-ph]].

[37] G. Burdman, C. E. F. Haluch and R. D. Matheus, Phys. Rev. D **85** (2012) 095016 [arXiv:1112.3961 [hep-ph]].

[38] A. Arhrib, C. -W. Chiang, D. K. Ghosh and R. Santos, Phys. Rev. D **85** (2012) 115003 [arXiv:1112.5527 [hep-ph]].

[39] A. Arhrib, R. Benbrik and N. Gaur, Phys. Rev. D **85** (2012) 095021 [arXiv:1201.2644 [hep-ph]].

[40] E. Gabrielli, B. Mele and M. Raidal, Phys. Lett. B **716** (2012) 322 [arXiv:1202.1796 [hep-ph]].

[41] K. Blum and R. T. D'Agnolo, Phys. Lett. B **714** (2012) 66 [arXiv:1202.2364 [hep-ph]].

[42] G. Belanger, B. Dumont, U. Ellwanger, J. F. Gunion and S. Kraml, JHEP **1302** (2013) 053 [arXiv:1212.5244 [hep-ph]].

[43] C. -Y. Chen and S. Dawson, Phys. Rev. D **87** (2013) 055016 [arXiv:1301.0309 [hep-ph]].

[44] S. L. Glashow and S. Weinberg, Phys. Rev. D **15** (1977) 1958.

[45] H. E. Haber, G. L. Kane and T. Sterling, Nucl. Phys. B **161** (1979) 493.

[46] L. J. Hall and M. B. Wise, Nucl. Phys. B **187** (1981) 397.

[47] J. F. Donoghue and L. F. Li, Phys. Rev. D **19** (1979) 945.

[48] V. D. Barger, J. L. Hewett and R. J. N. Phillips, Phys. Rev. D **41** (1990) 3421.

[49] Y. Grossman, Nucl. Phys. B **426** (1994) 355 [hep-ph/9401311].

[50] A. G. Akeroyd and W. J. Stirling, Nucl. Phys. B **447** (1995) 3. A. G. Akeroyd, Phys. Lett. B **377** (1996) 95 [hep-ph/9603445]; J. Phys. G **24** (1998) 1983 [hep-ph/9803324].

[51] M. Aoki, S. Kanemura, K. Tsumura and K. Yagyu, Phys. Rev. D **80** (2009) 015017 [arXiv:0902.4665 [hep-ph]].

[52] N. G. Deshpande and E. Ma, Phys. Rev. D **18** (1978) 2574. E. Ma, Mod. Phys. Lett. A **23** (2008) 647 [arXiv:0802.2917 [hep-ph]]; Phys. Rev. D **73** (2006) 077301 [hep-ph/0601225].

[53] W. Altmannshofer, S. Gori and G. D. Kribs, Phys. Rev. D **86** (2012) 115009 [arXiv:1210.2465 [hep-ph]].

[54] Y. Bai, V. Barger, L. L. Everett and G. Shaughnessy, arXiv:1210.4922 [hep-ph].

[55] E. Cervero and J. -M. Gerard, Phys. Lett. B **712** (2012) 255 [arXiv:1202.1973 [hep-ph]].

[56] G. C. Branco, W. Grimus and L. Lavoura, Phys. Lett. B **380** (1996) 119 [hep-ph/9601383].

[57] F. J. Botella, G. C. Branco and M. N. Rebelo, Phys. Lett. B **687** (2010) 194 [arXiv:0911.1753 [hep-ph]].

[58] F. J. Botella, G. C. Branco, M. Nebot and M. N. Rebelo, JHEP **1110** (2011) 037 [arXiv:1102.0520 [hep-ph]].

[59] N. Cabibbo, Phys. Rev. Lett. **10** (1963) 531; M. Kobayashi, T. Maskawa, Prog. Theor. Phys. **49** (1973) 652.

[60] P. M. Ferreira, L. Lavoura and J. P. Silva, Phys. Lett. B **688** (2010) 341 [arXiv:1001.2561 [hep-ph]].

[61] C. B. Braeuninger, A. Ibarra and C. Simonetto, Phys. Lett. B **692** (2010) 189 [arXiv:1005.5706 [hep-ph]].

[62] H. Serodio, Phys. Lett. B **700** (2011) 133 [arXiv:1104.2545 [hep-ph]].

[63] I. de Medeiros Varzielas, Phys. Lett. B **701** (2011) 597 [arXiv:1104.2601 [hep-ph]].

[64] G. Cree and H. E. Logan, Phys. Rev. D **84** (2011) 055021 [arXiv:1106.4039 [hep-ph]].

[65] M. Farina, C. Grojean and E. Salvioni, JHEP **1207** (2012) 012 [arXiv:1205.0011 [hep-ph]].

[66] M. Farina, C. Grojean, F. Maltoni, E. Salvioni and A. Thamm, arXiv:1211.3736 [hep-ph].

[67] S. Biswas, E. Gabrielli and B. Mele, JHEP **1301** (2013) 088 [arXiv:1211.0499 [hep-ph]].

[68] CMS Collaboration, CMS-PAS-HIG-12-025 (July 8, 2012).

[69] ATLAS Collaboration, ATLAS-CONF-2012-135 (September 28, 2012).

[70] LEP Higgs Working Group for Higgs boson searches and ALEPH and DELPHI and L3 and OPAL Collaborations, hep-ex/0107031; arXiv:1301.6065 [hep-ex].

[71] A. Abulencia *et al.* [CDF Collaboration], Phys. Rev. Lett. **96** (2006) 042003 [hep-ex/0510065]. V. M. Abazov *et al.* [D0 Collaboration], Phys. Lett. B **682** (2009) 278 [arXiv:0908.1811 [hep-ex]].

[72] G. Aad *et al.* [ATLAS Collaboration], JHEP **1206** (2012) 039 [arXiv:1204.2760 [hep-ex]]. S. Chatrchyan *et al.* [CMS Collaboration], JHEP **1207** (2012) 143 [arXiv:1205.5736 [hep-ex]].

[73] M. Gustafsson, S. Rydbeck, L. Lopez-Honorez and E. Lundstrom, Phys. Rev. D **86** (2012) 075019 [arXiv:1206.6316 [hep-ph]]; B. Swiezewska and M. Krawczyk, arXiv:1212.4100 [hep-ph].

[74] L. Wang and X. -F. Han, JHEP **1205** (2012) 088 [arXiv:1203.4477 [hep-ph]].

[75] G. Abbiendi *et al.* [OPAL Collaboration], Eur. Phys. J. C **27** (2003) 311 [hep-ex/0206022].

[76] M. Baak *et al.*, Eur. Phys. J. C **72** (2012) 2205 [arXiv:1209.2716 [hep-ph]]; http://gfitter.desy.de/.

[77] LEP Electroweak Working Group, http://lepewwg.web.cern.ch/LEPEWWG/.

[78] ATLAS Collaboration, ATLAS-CONF-2012-079 (June 28, 2012).

[79] J. F. Gunion, Y. Jiang and S. Kraml, Phys. Rev. D **86** (2012) 071702 [arXiv:1207.1545 [hep-ph]].

[80] A. Drozd, B. Grzadkowski, J. F. Gunion and Y. Jiang, arXiv:1211.3580 [hep-ph].

[81] S. Chang, S. K. Kang, J. -P. Lee, K. Y. Lee, S. C. Park and J. Song, arXiv:1210.3439 [hep-ph].

[82] P. M. Ferreira, H. E. Haber, R. Santos and J. P. Silva, Phys. Rev. D **87** (2013) 055009 [arXiv:1211.3131 [hep-ph]].

[83] J. F. Gunion, Y. Jiang and S. Kraml, Phys. Rev. Lett. **110** (2013) 051801 [arXiv:1208.1817 [hep-ph]].

[84] Y. Grossman, Z. 'e. Surujon and J. Zupan, JHEP **1303** (2013) 176 [arXiv:1301.0328 [hep-ph]].

[85] E. Accomando *et al.*, hep-ph/0608079.

[86] A. Pilaftsis, Nucl. Phys. B **504** (1997) 61 [hep-ph/9702393].

[87] J. R. Ellis, J. S. Lee and A. Pilaftsis, Phys. Rev. D **70** (2004) 075010 [hep-ph/0404167].

[88] S. Y. Choi, J. Kalinowski, Y. Liao and P. M. Zerwas, Eur. Phys. J. C **40** (2005) 555 [hep-ph/0407347].

[89] ATLAS Collaboration, ATLAS-CONF-2013-034 (March 14, 2013).

[90] CMS Collaboration, CMS-PAS-HIG-13-005 (April 18, 2013).

[91] H. E. Haber and D. O'Neil, Phys. Rev. D **74** (2006) 015018 [hep-ph/0602242].

[92] S. Dittmaier *et al.* [LHC Higgs Cross Section Working Group Collaboration], arXiv:1101.0593 [hep-ph].

[93] M. E. Peskin and T. Takeuchi, Phys. Rev. D **46** (1992) 381; Phys. Rev. Lett. **65** (1990) 964.

[94] H. E. Haber and D. O'Neil, Phys. Rev. D **83** (2011) 055017 [arXiv:1011.6188 [hep-ph]].

Towards a general analysis of LHC data within two-Higgs-doublet models

Alejandro Celis, Victor Ilisie and Antonio Pich

IFIC, Universitat de València – CSIC, Apt. Correus 22085, E-46071 València, Spain

The data accumulated so far confirm the Higgs-like nature of the new boson discovered at the LHC. The Standard Model Higgs hypothesis is compatible with the collider results and no significant deviations from the Standard Model have been observed neither in the flavour sector nor in electroweak precision observables. We update the LHC and Tevatron constraints on CP-conserving two-Higgs-doublet models without tree-level flavour-changing neutral currents. While the relative sign between the top Yukawa and the gauge coupling of the 126 GeV Higgs is found be the same as in the SM, at 90% CL, there is a sign degeneracy in the determination of its bottom and tau Yukawa couplings. This results in several disjoint allowed regions in the parameter space. We show how generic sum rules governing the scalar couplings determine the properties of the additional Higgs bosons in the different allowed regions. The role of electroweak precision observables, low-energy flavour constraints and LHC searches for additional scalars to further restrict the available parameter space is also discussed.

8.1   Introduction

Experimental data from the ATLAS [1, 2], CMS [3, 4], DØ and CDF [5] collaborations confirm that the new boson discovered at the LHC is related to the mechanism of electroweak symmetry breaking. The masses of the new boson measured by ATLAS ($125.5 \pm 0.2 \, ^{+0.5}_{-0.6}$ GeV) and CMS ($125.7 \pm 0.3 \pm 0.3$ GeV) are in good agreement, giving the average value $M_h = 125.64 \pm 0.35$ GeV, and its spin/parity is compatible with the Standard Model (SM) Higgs boson hypothesis, $J^P = 0^+$ [6–8]. Global analyses of current data find to a good accuracy that the new $h(126)$ boson couples to the vector bosons $(W^\pm, Z)$ with the required strength to restore perturbative unitarity in vector boson scattering amplitudes. The $h(126)$ couplings to fermions of the third generation are also found to be compatible with the SM Higgs scenario [9, 10].

A complex scalar field transforming as a doublet under $SU(2)_L$ seems at present the most elegant and simple explanation for elementary particle masses. None of the fundamental principles of the SM, however, forbids the possibility that a richer scalar sector is responsible for the electroweak symmetry breaking. Unlike the addition of new fermion generations or new gauge bosons, an enlarged scalar sector remains in general much more elusive to experimental constraints. Two-Higgs-doublet models (2HDMs) provide a minimal extension of the SM scalar sector that naturally accommodates the electroweak precision tests, giving rise at the same time to many interesting phenomenological effects [11]. The scalar spectrum of a two-Higgs-doublet model consists of three neutral and one charged Higgs bosons. The direct search for additional scalar states at the LHC or indirectly via precision flavour experiments will therefore continue being an important task in the following years.

Many analyses of LHC and Tevatron data have been performed recently within the framework of CP-conserving 2HDMs with natural flavour conservation (NFC) [12–27]. These works have focused on different versions of the 2HDM in which a discrete $\mathcal{Z}_2$ symmetry is imposed in the Lagrangian to eliminate tree-level flavour-changing neutral currents (FCNCs). A more general alternative is to assume the alignment in flavour space of the Yukawa matrices for each type of right-handed fermion [28]. The so-called aligned two-Higgs-doublet model (A2HDM) contains as particular cases the different versions of the 2HDM with NFC, while at the same time introduces new sources of CP violation beyond the CKM phase. First studies of the $h(126)$ boson data within the A2HDM, in

the CP-conserving limit, were performed in refs. [29–32] and more recently in refs. [33–35]. The implications of new sources of CP violation within this model for the $h(126)$ phenomenology were also analyzed in ref. [32].

In this work we extend the analysis of ref. [32] and update the bounds that current LHC and Tevatron data impose on the CP-conserving A2HDM, taking into account the latest results released by the experimental collaborations after the first LHC shutdown. We also discuss the role of electroweak precision observables and flavour constraints to further restrict the parameter space. The allowed regions are classified according to the sign of the bottom and tau Yukawa couplings of the $h(126)$ boson, relative to its coupling to vector bosons. Due to generic sum rules governing the scalar couplings [32, 36–38], the properties of the additional scalar fields of the model are very different in each of these allowed regions. We consider also current limits from the search of additional scalars at the LHC and its impact on our knowledge of the $h(126)$ properties. The possibility of a fermiophobic charged Higgs [32] is also analyzed in light of the latest LHC data. A study of CP-violating effects in the 2HDM along the lines of ref. [32] will be deferred to a future work.

This paper is organized as follows. The present bounds from LHC and Tevatron data are analyzed in section 8.2, discussing also the role of the loop-induced processes $Z \to \bar{b}b$ and $\bar{B} \to X_s\gamma$ to further constrain the available parameter space. In section 8.3 we consider the search for additional Higgs bosons at the LHC. The particular case of a fermiophobic charged Higgs is analyzed in section 8.4. A comparison of our findings with those of related works is done in section 8.5 and a summary of our results is finally given in section 8.6.

8.2   A2HDM fit in the CP-conserving limit

Let us consider the scalar sector of the CP-conserving 2HDM. In the so-called Higgs basis where only one of the doublets acquires a vacuum expectation value, the two doublets are parametrized as [32]

$$\Phi_1 = \begin{bmatrix} G^+ \\ \frac{1}{\sqrt{2}}\left(v + S_1 + iG^0\right) \end{bmatrix}, \qquad \Phi_2 = \begin{bmatrix} H^+ \\ \frac{1}{\sqrt{2}}\left(S_2 + iS_3\right) \end{bmatrix}. \qquad (8.1)$$

Thus, Φ_1 plays the role of the SM scalar doublet with $v = (\sqrt{2}\,G_F)^{-1/2} \simeq 246$ GeV. The physical scalar spectrum consists of five degrees of freedom: two charged fields $H^{\pm}(x)$ and three neutral scalars $\varphi_i^0(x) = \{h(x), H(x), A(x)\}$. The later are related with the S_i fields through an orthogonal transformation $\varphi_i^0(x) = \mathcal{R}_{ij}S_j(x)$, which is determined by the scalar potential [32]. In the most general case, the CP-odd component S_3 mixes with the CP-even fields $S_{1,2}$ and the resulting mass eigenstates do not have definite CP quantum numbers. For a CP-conserving potential this admixture disappears, giving $A(x) = S_3(x)$ and[1]

$$
\begin{pmatrix} h \\ H \end{pmatrix} = \begin{bmatrix} \cos\tilde{\alpha} & \sin\tilde{\alpha} \\ -\sin\tilde{\alpha} & \cos\tilde{\alpha} \end{bmatrix} \begin{pmatrix} S_1 \\ S_2 \end{pmatrix}. \tag{8.2}
$$

Performing a phase redefinition of the neutral CP-even fields, it is possible to fix the sign of $\sin\tilde{\alpha}$. In this work we adopt the conventions $M_h \leq M_H$ and $0 \leq \tilde{\alpha} \leq \pi$, so that $\sin\tilde{\alpha}$ is always positive. To avoid FCNCs, we assume the alignment in flavour space of the Yukawa matrices. In terms of the fermion mass-eigenstate fields, the Yukawa interactions of the A2HDM read [28]

$$
\begin{aligned}
\mathcal{L}_Y &= -\frac{\sqrt{2}}{v}\,H^+\left\{\bar{u}\left[\varsigma_d\,V M_d \mathcal{P}_R - \varsigma_u\,M_u V \mathcal{P}_L\right] d + \varsigma_l\,\bar{\nu} M_l \mathcal{P}_R l\right\} \\
&\quad -\frac{1}{v}\sum_{\varphi_i^0, f} y_f^{\varphi_i^0}\,\varphi_i^0\,\left[\bar{f}\,M_f \mathcal{P}_R f\right] + \text{h.c.},
\end{aligned} \tag{8.3}
$$

where $\mathcal{P}_{R,L} \equiv \frac{1 \pm \gamma_5}{2}$ are the right-handed and left-handed chirality projectors, M_f the diagonal fermion mass matrices and ς_f ($f = u, d, l$) the family-universal alignment parameters. The only source of flavour-changing phenomena is the CKM matrix V. The well-known versions of the 2HDM with NFC are recovered as particular limits of this parametrization, given in table 8.1.

In the present analysis we neglect possible CP-violating effects; i.e., we consider a CP-conserving scalar potential and real alignment parameters ς_f. The couplings of the

---

[1]In a generic scalar basis $\phi_a(x)$ ($a = 1, 2$) in which both doublets acquire vacuum expectation values: $\langle 0|\phi_a^T(x)|0\rangle = \frac{1}{\sqrt{2}}\,(0, v_a\,\mathrm{e}^{i\theta_a})$, we have $\tilde{\alpha} = \alpha - \beta$ in the usually adopted notation. The angle α determines h and H in terms of the CP-even fields and $\tan\beta = v_2/v_1$ is the ratio of vacuum expectation values. Given that the choice of basis is arbitrary, the parameters α and β are in general unphysical. These angles are meaningful only in particular models in which a specific basis is singled out (through a symmetry for example) [39].

Table 8.1: *CP-conserving 2HDMs based on discrete $\mathcal{Z}_2$ symmetries.*

Model	ς_d	ς_u	ς_l
Type I	$\cot\beta$	$\cot\beta$	$\cot\beta$
Type II	$-\tan\beta$	$\cot\beta$	$-\tan\beta$
Type X (lepton-specific)	$\cot\beta$	$\cot\beta$	$-\tan\beta$
Type Y (flipped)	$-\tan\beta$	$\cot\beta$	$\cot\beta$
Inert	0	0	0

neutral scalar fields are then given, in units of the SM Higgs couplings, by

$$
\begin{aligned}
y_f^h &= \cos\tilde\alpha + \varsigma_f \sin\tilde\alpha\,, & y_{d,l}^A &= i\,\varsigma_{d,l}\,,\\
y_f^H &= -\sin\tilde\alpha + \varsigma_f \cos\tilde\alpha\,, & y_u^A &= -i\,\varsigma_u\,,
\end{aligned}
\tag{8.4}
$$

for the fermionic couplings and $(\kappa_V^{\varphi_i^0} \equiv g_{\varphi_i^0 VV}/g_{hVV}^{\mathrm{SM}},\ V = W, Z)$

$$
\kappa_V^h \;=\; \cos\tilde\alpha\,, \qquad \kappa_V^H \;=\; -\sin\tilde\alpha\,, \qquad \kappa_V^A \;=\; 0\,,
\tag{8.5}
$$

for the gauge couplings. The CP symmetry implies a vanishing gauge coupling of the CP-odd scalar. In the limit $\tilde\alpha \to 0$, the h couplings are identical to those of the SM Higgs field and the heavy CP-even scalar H decouples from the gauge bosons.[2]

8.2.1 Implications of LHC and Tevatron data for the h(126) boson

We assume that the $h(126)$ boson corresponds to the lightest CP-even scalar h of the CP-conserving A2HDM. Current experimental data require its gauge coupling to have a magnitude close to the SM one; *i.e.*, $|\cos\tilde\alpha| \sim 1$ [32]. A global fit of the parameters $(\cos\tilde\alpha, \varsigma_u, \varsigma_d, \varsigma_l)$ to the latest LHC and Tevatron data gives $(\chi^2_{\min}/\mathrm{dof} \simeq 0.73)$

$$
|\cos\tilde\alpha| \;>\; 0.90 \quad (0.80)\,,
\tag{8.6}
$$

---

[2] The scalar mixing is often parametrized in terms of $\alpha' = \tilde\alpha + \frac{\pi}{2}$, so that $\kappa_V^h = \sin\alpha'$ and the SM limit corresponds to $\alpha' = \pi/2$ [11]. We prefer to describe small deviations from the SM limit with $\tilde\alpha \simeq 0$.
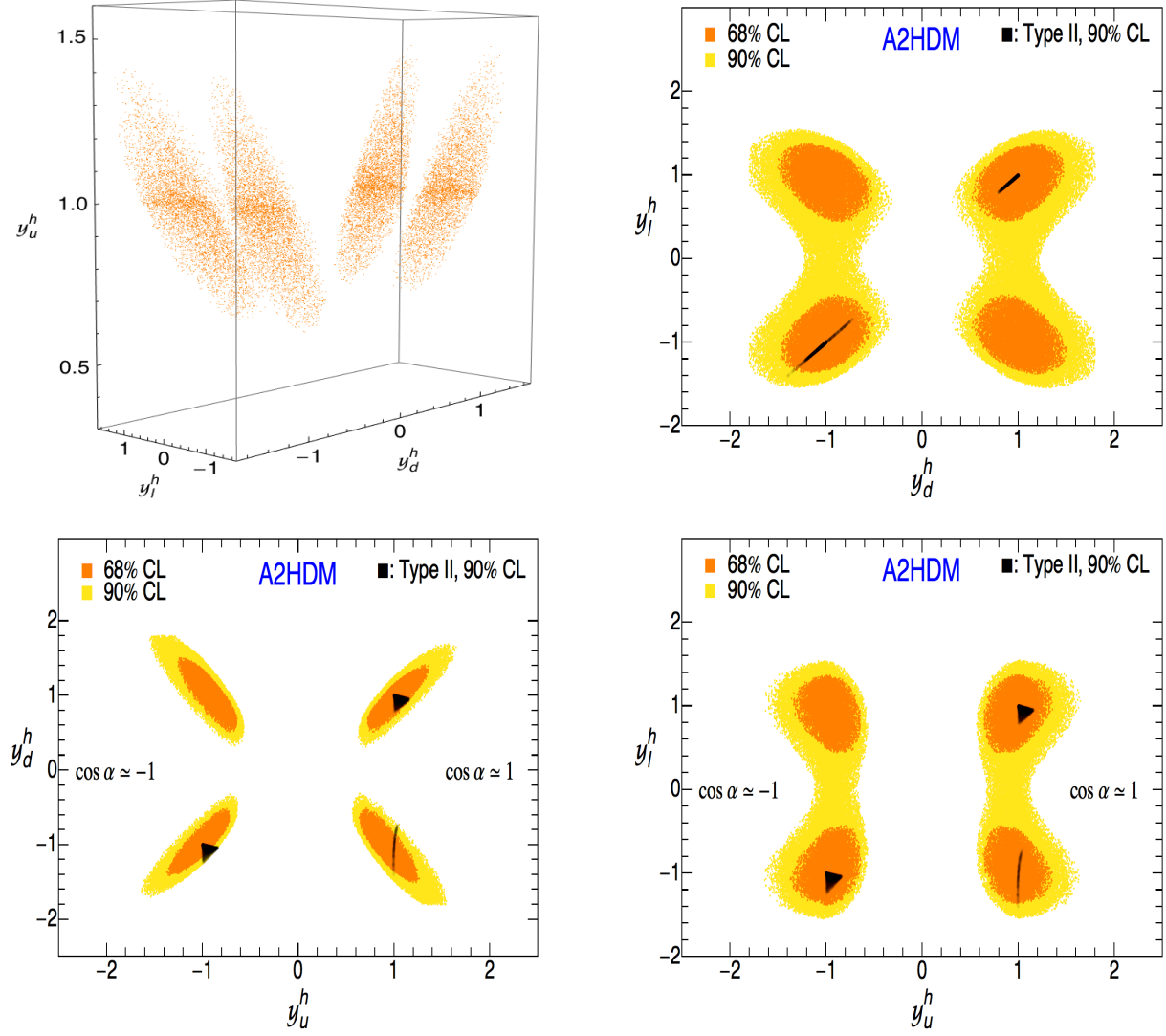
Figure 8.1: *Allowed regions in the planes $y_d^h - y_l^h$ (top-right), $y_u^h - y_d^h$ (bottom-left) and $y_u^h - y_l^h$ (bottom-right) at 68% (orange, dark) and 90% (yellow, light) CL from a global fit of LHC and Tevatron data, within the CP-conserving A2HDM. The particular case of the discrete $\mathcal{Z}_2$ model of type II is also indicated at 90% CL (black). Top-left panel: Allowed region in the space (y_u^h, y_d^h, y_l^h) with $\cos \tilde{\alpha} > 0$ at 68% CL (orange).*

or equivalently $\sin \tilde{\alpha} < 0.44$ (0.60), at 68% CL (90% CL). The resulting constraints on the Yukawa couplings of h are shown in figure 8.1. The charged Higgs contribution to the

$h \to \gamma\gamma$ amplitude has been assumed to be negligible in this fit. The global fit determines the relative sign between y_u^h and g_{hVV} to be the same as in the SM. The flipped sign solution for the top Yukawa coupling, which was preferred before Moriond 2013 due to the observed excess in the $\gamma\gamma$ channel [32], is ruled out by current data at 90% CL.

The partial decay widths of the Higgs decaying into a pair of fermions are not sensitive to the sign of the Yukawa couplings, $\Gamma(h \to \bar{f}f) \propto |y_f^h|^2$. The loop-induced processes $h \to \gamma\gamma$ and $gg \to h$, on the other hand, are sensitive in principle to the $y_{f=u,d,l}^h$ signs. The decay widths, normalized to the SM prediction, can be written in terms of the modified Higgs couplings as,

$$\frac{\Gamma(h \to \gamma\gamma)}{\Gamma(h \to \gamma\gamma)^{\text{SM}}} \simeq \left(0.28\,y_u^h - 0.004\,y_d^h - 0.0035\,y_l^h - 1.27\,\kappa_V^h\right)^2 + \left(0.006\,y_d^h + 0.003\,y_l^h\right)^2 ,$$

$$(8.7)$$

where we have neglected a possible charged Higgs contribution to $h \to 2\gamma$, and

$$\frac{\Gamma(h \to gg)}{\Gamma(h \to gg)^{\text{SM}}} \simeq \left(1.06\,y_u^h - 0.06\,y_d^h\right)^2 + \left(0.09\,y_d^h\right)^2 . \qquad (8.8)$$

The last terms in (8.7) and (8.8) are the absorptive contributions from $\tau^+\tau^-$ and $b\bar{b}$ loops. Neglecting the charged Higgs contribution to $h \to \gamma\gamma$ is well justified if the charged Higgs is very heavy and/or if the cubic Higgs self-coupling hH^+H^- is very small. Due to their small masses, the tau and bottom contributions are very suppressed and, therefore, flipping the sign of $y_{d,l}^h$ has only a very small effect on the relevant partial widths.

The top-left panel in figure 8.1 shows the 68% CL allowed regions in the space (y_u^h, y_d^h, y_l^h) with $\cos\tilde{\alpha} > 0$. Four disjoint possibilities can be observed, which can be characterized by the relative signs of $y_{d,l}^h$ to that of κ_V^h; four additional, equivalent, solutions are found flipping simultaneously the signs of y_f^h and $\cos\tilde{\alpha}$. We restrict in the rest of this work to the solutions with $\cos\tilde{\alpha} > 0$. The other panels show the projections in the planes $y_d^h - y_l^h$ (top-right), $y_u^h - y_d^h$ (bottom-left) and $y_u^h - y_l^h$ (bottom-right), at 68% (orange, dark) and 90% (yellow, light) CL. The sign degeneracy in the determination of the bottom and tau Yukawa couplings from current data is clearly observed. At 90% CL, the leptonic Yukawa coupling y_l^h is found to be compatible with zero and therefore only two disjoint islands remain ($y_d^h < 0$ and $y_d^h > 0$).

Figure 8.1 shows also (small black areas, $\chi^2_{\text{min}}/\text{dof} \simeq 0.65$) the constraints in the particular case of the type II model ($\varsigma_{d,l} = -1/\varsigma_u = -\tan\beta$), usually assumed in the

literature and realized in minimal supersymmetric scenarios. The allowed regions get considerably reduced in this case. This illustrates that there is a much wider range of open phenomenological possibilities waiting to be explored. The only allowed regions in the type II model are those with identical y_d^h and y_l^h couplings, making a straight line with slope $+1$ in the $y_d^h - y_l^h$ plane. The $y_{d,l}^h < 0$ region with $\cos\tilde\alpha > 0$ requires a relatively large value of $\tan\beta$ to flip the sign of $y_{d,l}^h$. Similar arguments can be made for the other types of 2HDMs with NFC. For instance, in the type I model $(\varsigma_{u,d,l} = \cot\beta)$ the allowed regions are straight lines with slope $+1$ in the three $y_f^h - y_{f'}^h$ planes.

In the following we will keep the discussion within the more general framework provided by the A2HDM. In case any of the versions of the 2HDM with NFC turns out to be (approximately) realized in Nature, an analysis of experimental data within the A2HDM would reveal it.

Figures 8.2, 8.3 and 8.4 show the allowed values for the alignment parameters ς_f, at 68% (orange, dark) and 90% (yellow, light) CL, as function of $\sin\tilde\alpha$. Since y_u^h has the same positive sign as $\cos\tilde\alpha$ and a similar magnitude, the product $|\varsigma_u|\sin\tilde\alpha$ cannot be large. Therefore, $|\varsigma_u|$ gets tightly bounded at large values of $\sin\tilde\alpha$ as indicated in figure 8.2. On the other hand, as $\sin\tilde\alpha$ approaches zero, all information on ς_u is lost since in this limit the h couplings are SM-like. The same behaviour is observed in figure 8.3, which shows the allowed values for the alignment parameters ς_d (left panel) and ς_l (right panel), in the regions with $y_d^h > 0$ or $y_l^h > 0$, respectively. Important bounds on the magnitudes of ς_d and ς_l are obtained, again, as long as $\sin\tilde\alpha \neq 0$.

A quite different result is obtained in those regions where the Yukawa couplings are negative (again, with $\cos\tilde\alpha > 0$). Figure 8.4 shows the allowed values for the alignment parameters $\varsigma_{d,l}$ when $y_d^h < 0$ (left panel) or $y_l^h < 0$ (right panel). A relatively large and negative value for $\varsigma_{d,l}$ is needed to flip the sign in $y_{d,l}^h$, given that $\cos\tilde\alpha \simeq 1$. Within the 90% CL allowed region, $y_d^h < 0$ requires $\varsigma_d \lesssim -2.3$, while $y_l^h < 0$ implies $\varsigma_l \lesssim -2.7$. When $\sin\tilde\alpha \lesssim 0.1$, the corresponding values for $|\varsigma_{d,l}|$ become very large: $\varsigma_{d,l} \lesssim -24$.

8.2.2 SM-like gauge coupling, $\kappa_V^h \sim 1$, without decoupling

If it is the case that Nature posses an elementary scalar sector composed of two-Higgs doublets, the fact that no large deviations of the $h(126)$ boson properties from the SM have been observed could be pointing towards a decoupling scenario. In the decoupling limit
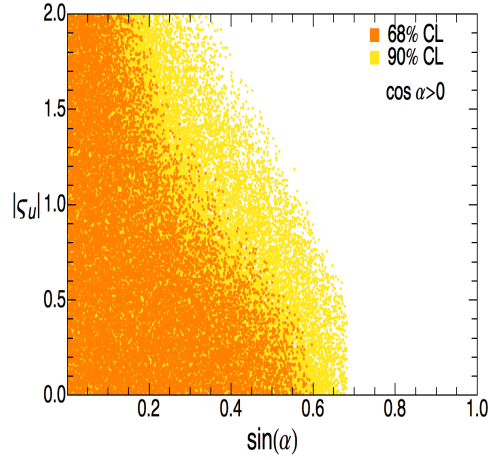
Figure 8.2: *Allowed values for ς_u, at 68% CL (orange) and 90% CL (yellow) CL, when $\cos \tilde{\alpha} > 0$.*

one of the Higgs doublets can be integrated out, leaving an effective low-energy theory with a SM-like Higgs doublet. The lightest CP-even Higgs appears with a mass around the electroweak scale and SM-like couplings, while the other scalars are much heavier and degenerate, up to corrections of $\mathcal{O}(v^2)$, $M_H^2 \simeq M_A^2 \simeq M_{H^\pm}^2 \gg v^2$. The decoupling limit implies that $|\kappa_V^h| \to 1$, the opposite however is not true. In the limit $|\kappa_V^h| \to 1$, the masses of the additional scalars, H, A and $H^\pm$, can still be of the order of the electroweak scale [40].[3]

The decoupling regime is very elusive to experimental tests, leaving a low-energy theory with a light SM-like Higgs, while putting the additional scalars beyond the reach of direct searches at colliders. Flavour physics constraints are naturally evaded in this case also due to the heaviness of the additional scalars. Distinguishing signatures of a 2HDM near the decoupling limit would require high-precision measurements of the $h(126)$ boson properties, for example at a future Higgs factory [40]. In this work, we are interested in the more testable case in which the scalar sector is not in the decoupling regime and all the additional scalars lie around the electroweak scale. We will assume in particular that

---

[3] In the Higgs basis [32], the decoupling limit occurs for $\mu_2 \gg v^2$, where μ_2 is the coefficient of the quadratic $\Phi_2^\dagger \Phi_2$ term in the scalar potential, while keeping perturbative quartic scalar couplings $|\lambda_i/4\pi| \lesssim 1$. The limit $|\kappa_V^h| \to 1$ without decoupling arises when $\mu_3, \lambda_6 \to 0$; *i.e.*, for vanishing $\Phi_1^\dagger \Phi_2$ and $\Phi_1^\dagger \Phi_1 \Phi_1^\dagger \Phi_2$ terms. For a recent discussion see also refs. [34, 41, 42].
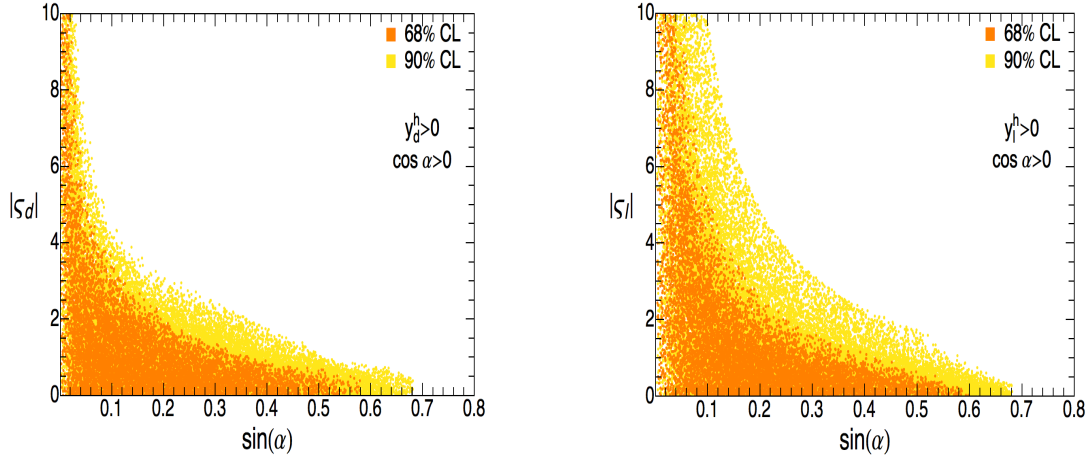
Figure 8.3:   *Allowed values for $\varsigma_{d,l}$ at 68% CL (orange, dark) and 90% CL (yellow, light) in the regions where $y_d^h > 0$ (left) or $y_l^h > 0$ (right), keeping only solutions with $\cos\tilde{\alpha} > 0$.*

the charged Higgs lies in the mass range $M_{H^\pm} \in [80, 500]$ GeV.

Deviations from the SM in the gauge-boson self-energies constrain the mass splittings between the additional physical scalars of the 2HDM. The induced corrections to the oblique parameters have been calculated in ref. [43] and summarized for the conventions adopted here in ref. [32]. To satisfy the precision electroweak constraints, the mass differences $|M_{H^\pm} - M_H|$ and $|M_{H^\pm} - M_A|$ cannot be both large ($\gg v$) at the same time. If there is a light charged Higgs below the TeV scale, an additional neutral boson should be around and vice versa. Figure 8.5 shows the 1σ oblique constraints on the $M_H - M_A$ plane, taking $M_{H^\pm} = 200$ GeV (yellow, light) and 500 GeV (orange, dark), while varying $\cos\tilde{\alpha} \in [0.9, 1]$. The bounds on the mass splittings from the oblique parameters, together with the perturbativity and perturbative unitarity bounds on the quartic-Higgs couplings [44], imply that both H and A should have masses below the TeV if $M_{H^\pm} < 500$ GeV. This is the scenario we will be interested in the following, where a rich interplay between precision flavour physics and direct Higgs searches at the LHC can be explored.

Interesting constraints are obtained in this case from flavour physics, specially from loop-induced processes with virtual charged Higgs and top quark contributions. The measured $\bar{B}^0 - B^0$ mixing and the $Z \to \bar{b}b$ decay width require for example that $|\varsigma_u| \lesssim 1.5$,
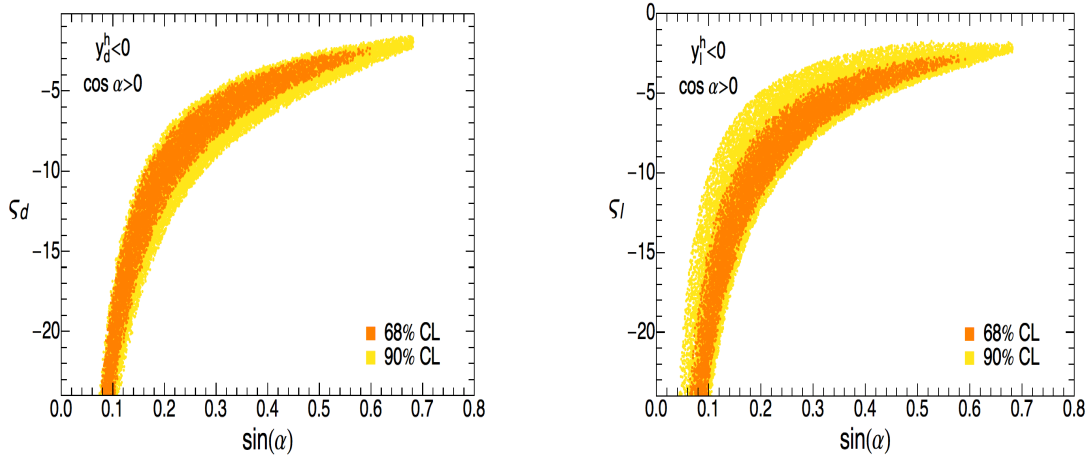
Figure 8.4:   *Allowed values for the alignment parameters $\varsigma_{d,l}$, at 68% CL (orange) and 90% CL (yellow), in the regions where $y_d^h < 0$ (left) or $y_l^h < 0$ (right), keeping only solutions with $\cos \tilde{\alpha} > 0$.*

for a charged Higgs below 500 GeV [45]. A more subtle condition can be derived from the radiative decay $\bar{B} \to X_s \gamma$. The relevant Wilson coefficients for this process take the form $C_i^{\text{eff}} = C_{i,SM} + |\varsigma_u|^2 C_{i,uu} - (\varsigma_u^* \varsigma_d) C_{i,ud}$, where $C_{i,uu}$ and $C_{i,ud}$ contain the dominant virtual top contributions. Thus, their combined effect can be very different for different values of the ratio ς_d/ς_u [45–47]. For real values of the alignment parameters, this provides a very strong bound. For instance, in the type II model, where the two terms interfere constructively, the $\bar{B} \to X_s \gamma$ rate excludes a charged Higgs mass below 380 GeV [48] at 95% CL for any value of $\tan \beta$. In the more general A2HDM framework, a much lighter charged Higgs is still allowed, but in a very restricted region of the parameter space $\varsigma_u - \varsigma_d$ [45–47].

Semileptonic and leptonic meson decays $(B \to \tau \nu_\tau, D_{(s)} \to \tau \nu_\tau (\mu \nu_\mu), B \to D^{(*)} \tau \nu_\tau)$, have been analyzed in detail within the A2HDM in refs. [45, 49]. These processes put bounds on the combinations $\varsigma_u \varsigma_l / M_{H^\pm}^2$ and $\varsigma_d \varsigma_l / M_{H^\pm}^2$, but the (tree-level) charged Higgs contribution decouples very fast. Given that we allow the possibility of a relatively heavy charged Higgs, $M_{H^\pm} < 500$ GeV, semileptonic and leptonic decays will not provide complementary information in our analysis. If one were to focus the discussion to a very light charged Higgs boson, these processes would certainly need to be taken into account.[4]

---

[4]The current excess observed by the BaBar collaboration in exclusive $b \to c \tau \nu$ transitions can only be
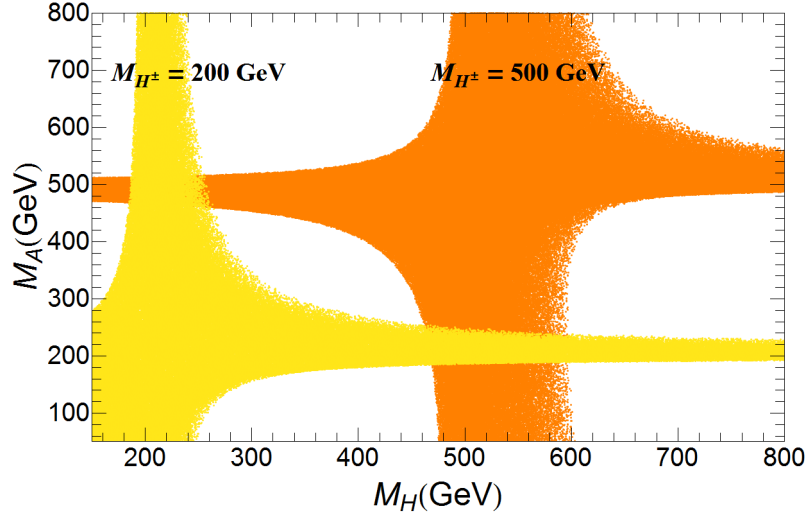
Figure 8.5:   *Constraints (68% CL) on the masses of the H and A bosons from the oblique parameters while varying* $\cos \tilde{\alpha} \in [0.9, 1]$. *The charged Higgs mass is fixed at* $M_{H^\pm} = 200$ *GeV (yellow, light) and* 500 *GeV (orange, dark).*

In figure 8.6 we show the effect of including $\bar{B} \to X_s \gamma$ and $R_b = \Gamma(Z \to \bar{b}b)/\Gamma(Z \to$ hadrons) in the fit of $(\cos \tilde{\alpha}, \varsigma_u, \varsigma_d, \varsigma_l)$ while varying $M_{H^\pm} \in [80, 500]$ GeV and, as usual, keeping only solutions with $\cos \tilde{\alpha} > 0$. The down-quark and leptonic alignment parameters are varied within $|\varsigma_{d,l}| \leq 50$ to maintain perturbative scalar interactions for bottom quarks and tau leptons. The charged Higgs contribution to the 2γ channel is also neglected in this fit; therefore, $M_{H^\pm}$ only enters in the fit through the flavour observables considered. Strictly, the analysis is then only valid in those regions of the parameter space in which the charged Higgs is reasonably heavy and/or the cubic Higgs self-coupling hH^+H^- is very small. The results, however, would not change significantly if the $H^\pm$ contribution to $h \to 2\gamma$ were included in the fit, since it would be compatible with zero, see section 8.4. In the $y_u^h - y_d^h$ plane, it can be observed that a significant part of the previously allowed region is excluded by flavour observables when compared to figure 8.1. This is due to the effect of $\mathrm{Br}(\bar{B} \to X_s \gamma)$ which induces severe constraints in the plane $\varsigma_u - \varsigma_d$, as shown in

accommodated within the framework of 2HDMs if one allows for a departure of the Yukawa alignment hypothesis [49, 50]. More theoretical studies on the relevant hadronic matrix elements as well as an update of these modes from the Belle collaboration using the full dataset, are needed to further asses the significance of this excess.
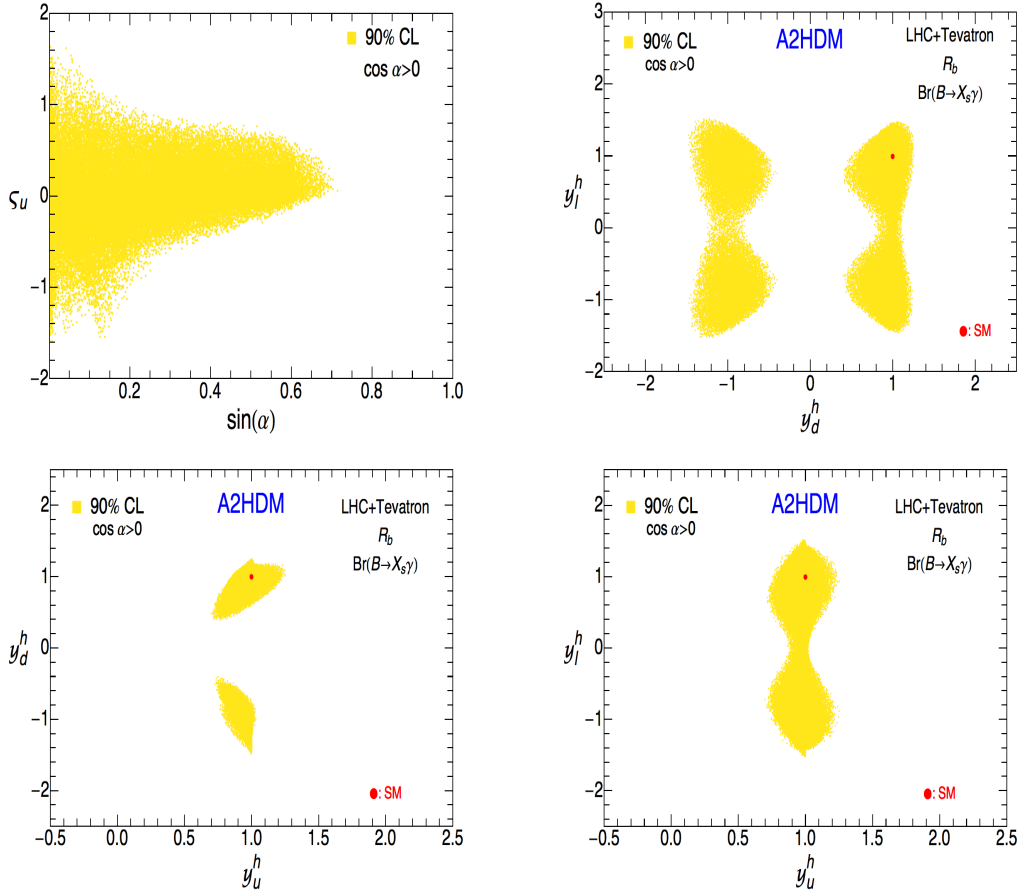
Figure 8.6:   *Allowed 90% CL regions in the planes* $\sin\tilde{\alpha} - \varsigma_u$ *(top-left),* $y_d^h - y_l^h$ *(top-right),* $y_u^h - y_d^h$ *(bottom-left), and* $y_u^h - y_l^h$ *(bottom-right), from a global fit of LHC and Tevatron data together with* R_b *and* $\mathrm{Br}(\bar{B} \to X_s\gamma)$, *within the CP-conserving A2HDM. The mass of the charged Higgs is varied within* $M_{H^\pm} \in [80, 500]$ *GeV and* $\cos\tilde{\alpha} > 0$.

figure 8.7.

For the case $y_d^h > 0$, collider data do not put any bound on $\varsigma_{u,d}$ in the limit $\sin\tilde{\alpha} \to 0$; the only constraint that appears in figure 8.7 (right-panel) is therefore coming from $Z \to \bar{b}b$ and $\bar{B} \to X_s\gamma$. For $y_d^h < 0$, LHC and Tevatron data determine that $\varsigma_d \lesssim -2$ in order to flip the Yukawa sign, thus excluding a large region that would otherwise be allowed by flavour observables alone. Compared with figure 8.2, the value of $|\varsigma_u|$ is slightly more constrained by R_b; when $M_{H^\pm} < 500$ GeV, one finds $|\varsigma_u| \lesssim 1.5$ for $\sin\tilde{\alpha} \simeq 0$ while a
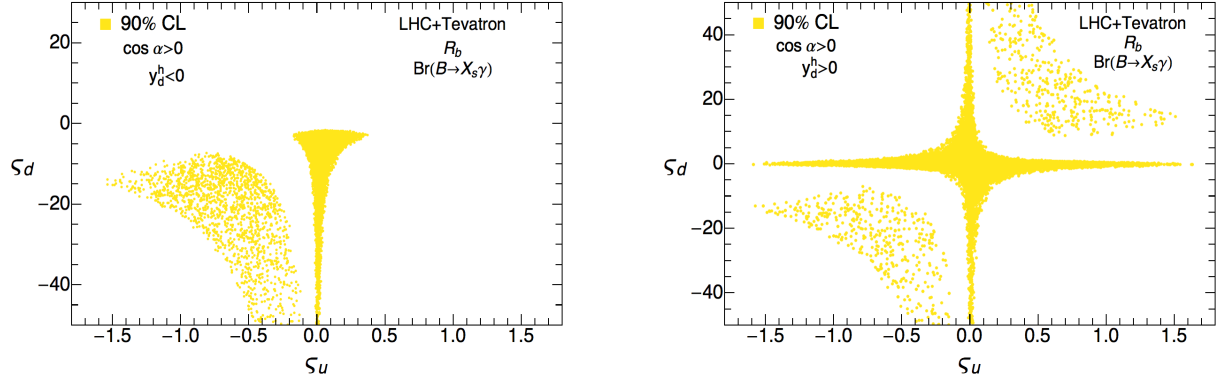
Figure 8.7: *Allowed* 90% *CL region in the plane* $\varsigma_u - \varsigma_d$, *from LHC and Tevatron data together with* R_b *and* $\mathrm{Br}(\bar{B} \to X_s \gamma)$, *for* $y_d^h < 0$ *(left) or* $y_d^h > 0$ *(right), with* $M_{H^\pm} \in [80, 500]$ *GeV and* $\cos \tilde{\alpha} > 0$.

stronger limit is obtained for larger values of $\sin \tilde{\alpha}$ due to LHC and Tevatron data. The corresponding allowed regions shown in figures 8.3 and 8.4 remain almost identical after adding the flavour observables and, therefore, are not shown here.

8.3 Searches for additional Higgs bosons

The search for additional Higgs bosons is one of the most important tasks for the next LHC run. The current information on the $h(126)$ properties puts relevant constraints on the couplings of the other scalars. In particular, eqs. (8.4) and (8.5) imply the sum rules

$$\left| \kappa_V^H \right|^2 \;\; = \;\; 1 - \left| \kappa_V^h \right|^2 , \tag{8.9}$$

$$\left| y_f^H \right|^2 - \left| y_f^A \right|^2 \;\; = \;\; 1 - \left| y_f^h \right|^2 , \tag{8.10}$$

$$\kappa_V^H \, y_f^H \;\; = \;\; 1 - \kappa_V^h \, y_f^h . \tag{8.11}$$

The first one is just the trivial trigonometric relation between $\sin \tilde{\alpha}$ and $\cos \tilde{\alpha}$, which implies that the gauge coupling g_{HVV} goes to zero when g_{hVV} approaches the SM value. The lower bound on $|\cos \tilde{\alpha}|$ in eq. (8.6) gives a direct limit on the coupling of the heavy CP-even scalar H to two gauge bosons, with important implications for searches in the $H \to VV$ channels. The relation (8.10) constrains the difference of the magnitudes of

the H and A Yukawa couplings. When the mixing angle $\tilde{\alpha}$ becomes zero, $y_f^h = 1$ and $\left|y_f^H\right| = \left|y_f^A\right| = \varsigma_f$. Relation (8.11) shows that whenever h has a flipped sign Yukawa ($\kappa_V^h \sim 1, y_f^h \sim -1$), the corresponding Yukawa coupling of H must be very large $y_f^H \kappa_V^H \sim 2$. This sum rule plays a crucial rule in the restoration of perturbative unitarity in $W_L^+ W_L^- \to f\bar{f}$ scattering and is behind the particular shape of the allowed regions in figure 8.4. The allowed values for κ_V^h and y_f^h, obtained in section 8.2.2 from $h(126)$ collider data and flavour constraints, imply, due to the sum rules, the following 90% CL bounds:

$$
\begin{aligned}
|y_u^H|^2 - |y_u^A|^2 &\in [-0.6, 0.5]\,, & \kappa_V^H\, y_u^H &\in [-0.17, 0.5]\,, \\
|y_d^H|^2 - |y_d^A|^2 &\in [-1.2, 0.9]\,, & \kappa_V^H\, y_d^H &\in [-0.3, 0.7] \cup [1.3, 2.5]\,, \\
|y_l^H|^2 - |y_l^A|^2 &\in [-1.3, 1.0]\,, & \kappa_V^H\, y_l^H &\in [-0.5, 2.5]\,.
\end{aligned}
\tag{8.12}
$$

A generic $h(126)$ boson with modified couplings to fermions and gauge bosons would violate perturbative unitarity at high energies, in certain physical processes. Partial-wave unitarity bounds would be violated for example in $W_L^+ W_L^- \to f\bar{f}$ inelastic scattering at a scale $\sqrt{s} \simeq \Lambda = 16\pi v^2/(m_f\,|1 - y_f^h\,\kappa_V^h|)$ [51]. For flipped-sign Yukawa couplings, $\kappa_V^h \simeq 1$ and $y_f^h \simeq -1$, we obtain an approximate value of $\Lambda \sim 9$ TeV for the top quark, while $\Lambda \sim 400$ TeV is obtained for the bottom quark and tau lepton due to the fact that they have smaller masses. A modified hVV coupling would also lead to a violation of perturbative unitarity in $W_L^- W_L^+ \to W_L^- W_L^+$ elastic scattering; for $\kappa_V^h = 0.89$ (0.95) this occurs at a scale $\sqrt{s} = 2.7$ (3.8) TeV respectively [52]. The scalar couplings in the 2HDM satisfy generic sum rules which ensure that perturbative unitarity is restored, provided the additional scalar states are light enough. In the processes considered previously, $W_L^+ W_L^- \to f\bar{f}$ and $W_L^- W_L^+ \to W_L^- W_L^+$, the heavier CP-even Higgs enters with the required couplings to cancel the bad high-energy behavior of the amplitudes. It must be noted that a given physical state needed to restore perturbative unitarity can appear well below the scale at which the partial-wave unitarity bounds are violated. This is well known in the SM where the Higgs mass is only weekly bounded by perturbative unitarity: $M_h \lesssim 1$ TeV [53].

The possibility of flipped-sign bottom and/or tau Yukawa couplings has important implications for the properties of the additional Higgs bosons but only subtle effects in the $h(126)$ phenomenology. Relatively large values for the alignment parameters $\varsigma_{d,l}$ are needed to flip the sign of $y_{d,l}^h$ given that $|\kappa_V^h| \simeq 1$, implying that the additional Higgs bosons $H^\pm, H$ and A should posses very large couplings to bottom and/or tau leptons.

The couplings of the missing Higgs bosons $H^{\pm}$, H and A, and therefore their phenomenology, are very different in each of the allowed regions shown in figure 8.1. It thus seems appropriate to discuss the search strategy for additional scalar states and the experimental constraints in each allowed island separately. An obvious question to address is how future Higgs searches at the LHC, combined with low-energy precision experiments at the intensity frontier, can be used to exclude some of the allowed islands and/or determine the right solution chosen by Nature.

The SM-like region with $y_f^h > 0$ ($f = u, d, l$) includes the trivial solution $\varsigma_f = 0$. Moreover, the Yukawa couplings y_f^H are also compatible with zero. Therefore, one has to face the possibility of a SM-like scalar h plus a fermiophobic scalar doublet including the H, A and $H^{\pm}$ fields. This is a very difficult experimental scenario where the missing scalars decouple from the fermionic sector and also the coupling $g_{HVV} = 0$. In this case, the production of the additional scalars can occur for example through the ZHA, $ZH^{\pm}H^{\mp}$, $W^{\pm}H^{\mp}H$ and $W^{\pm}H^{\mp}A$ couplings or through the scalar potential. In the limit $\sin\tilde{\alpha} = 0$, the $h(126)$ data does not provide any constraints on the alignment parameters ς_f (see figures 8.2 and 8.3). This opens a more interesting possibility with $\left|y_f^H\right| = \left|y_f^A\right| = \varsigma_f$; the H and A bosons could then be produced through the gluon-fusion mechanism or in associated production with a heavy-quark pair. Moreover, since ς_d and ς_l are only weakly constrained by flavour observables, the couplings to bottom quarks and tau leptons could be very sizeable, generating interesting phenomenological signals. For a very large $|\varsigma_d|$ for example, b-quark associated Higgs production $b\bar{b} \to \Phi$ or $gb \to \Phi b$ can become the dominant production mechanism of the heavy scalars H and A at the LHC. Similarly, charged Higgs production in association with top and bottom quarks, $gg \to t\bar{b}H^-$ or $q\bar{q} \to t\bar{b}H^-$, can be considerably enhanced in this case. If on the other hand $|\varsigma_l|$ is very large, heavy neutral scalars would probably decay dominantly into leptons, opening the interesting possibility of discovery in the very clean $\Phi \to \mu^+\mu^-$ channel. The charged Higgs also, would be expected to decay dominantly into a $\tau\nu_\tau$ pair in this case.

The situation is rather different in the other three regions with flipped-sign Yukawas: (a) $y_d^h < 0$ and $y_l^h > 0$, (b) $y_d^h > 0$ and $y_l^h < 0$, and (c) $y_{d,l}^h < 0$. As shown in figure 8.4, the alignment parameters are tightly constrained in these regions and the missing Higgs bosons could have a relatively large coupling to the bottom and/or tau fermions. In all four allowed regions the alignment parameter ς_u is compatible with zero, therefore there exists the possibility that all production mechanisms of the remaining scalars involving

the coupling with top-quarks could be greatly suppressed.

8.3.1   Charged Higgs searches

There are already important exclusion limits coming from charged Higgs searches at colliders, but most of them depend on the assumed Yukawa structure or some hypothesis about the scalar spectrum. In some cases, however, it is possible to set more general limits. For instance, a very light charged Higgs would modify the Z boson decay width if the channel $Z \to H^+ H^-$ is open. Since the coupling $ZH^+ H^-$ is completely fixed by the gauge symmetry and does not depend on any free parameter of the model, the constraint $\Gamma_Z^{\text{non-SM}} < 2.9$ MeV (95% CL) on non-SM decays of the Z boson implies $M_{H^\pm} \gtrsim 39.6$ GeV (95% CL) [54]. A much stronger lower bound on the $H^\pm$ mass, $M_{H^\pm} \gtrsim 80$ GeV (95% CL) [54], was set at LEP, assuming that the charged Higgs only decays into $\tau\nu$ or cs final states. A softer limit would be obtained on the other hand if the $H^+ \to W^+ A$ decay is kinematically allowed. Assuming that $M_A > 12$ GeV and a type-I Yukawa structure, the limit $M_{H^\pm} \gtrsim 72.5$ GeV was obtained in $H^+ \to W^+ A \to W^+ b\bar{b}$ searches [54].

In this section, we consider the LHC searches for a light charged Higgs produced via $t \to H^+ b$, in the decay channels $H^+ \to \tau^+ \nu_\tau$ [55, 56] and $H^+ \to c\bar{s}$ [57], which are kinematically limited to $M_{H^\pm} < m_t - m_b$. We focus on the constraints that can be extracted on the A2HDM from direct charged Higgs searches and flavour observables; the only parameters entering in this analysis are therefore $(M_{H^\pm}, \varsigma_u, \varsigma_d, \varsigma_l)$. A full scan of the A2HDM parameter space, taking into account electroweak precision data, perturbativity and perturbative unitarity bounds, would give as a result that the neutral scalars H and A cannot be arbitrarily heavy and strong correlations in the $M_H - M_A$ plane will appear as those shown in figure 8.5. We refer the reader to appendix 8.A for relevant formulae used here. To a good approximation, the branching ratio for $t \to H^+ b$ is given by

$$\text{Br}(t \to H^+ b) \simeq \frac{\Gamma(t \to H^+ b)}{\Gamma(t \to W^+ b) + \Gamma(t \to H^+ b)}, \qquad (8.13)$$

where we have neglected CKM-suppressed channels in the total top width. We do not consider the possibility of a very light CP-odd Higgs boson which could open decay channels like $H^+ \to W^+ A$; therefore, the charged Higgs decays only into fermions. Searches into the final state $\tau^+ \nu_\tau$ put bounds on the combination $\text{Br}(t \to H^+ b) \times \text{Br}(H^+ \to \tau^+ \nu)$, while current searches for quark decay modes are usually interpreted as limits on $\text{Br}(t \to$

$H^+b) \times \mathrm{Br}(H^+ \to c\bar{s})$. This is due to the expected dominant decay modes of the charged Higgs in the MSSM scenario or in the type-II 2HDM. In general, these searches really put bounds on $\mathrm{Br}(t \to H^+b) \times \left[\mathrm{Br}(H^+ \to c\bar{s}) + \mathrm{Br}(H^+ \to c\bar{b})\right]$. Other final states involving light quarks are neglected as they bring much smaller contributions.

For the next discussion it is useful to write down the following approximate formulae

$$\frac{\Gamma(H^+ \to c\bar{b})}{\Gamma(H^+ \to c\bar{s})} \simeq \frac{|V_{cb}|^2 \left(|\varsigma_d|^2 m_b^2 + |\varsigma_u|^2 m_c^2\right)}{|V_{cs}|^2 \left(|\varsigma_d|^2 m_s^2 + |\varsigma_u|^2 m_c^2\right)},$$

$$\frac{\Gamma(H^+ \to c\bar{b})}{\Gamma(H^+ \to \tau^+\nu_\tau)} \simeq \frac{N_C|V_{cb}|^2 \left(|\varsigma_d|^2 m_b^2 + |\varsigma_u|^2 m_c^2\right)}{m_\tau^2|\varsigma_l|^2}. \tag{8.14}$$

We can observe that the decay channel $H^+ \to c\bar{b}$ can be important, compared with $H^+ \to c\bar{s}$, in certain regions of the A2HDM parameter space in which the strong CKM suppression ($|V_{cb}| \ll |V_{cs}|$) is compensated by a hierarchy of the alignment parameters [58]. Indeed, for $|\varsigma_d| \gg |\varsigma_u|, |\varsigma_l|$ the decay channel $H^+ \to c\bar{b}$ becomes significant compared with $H^+ \to c\bar{s}, \tau^+\nu_\tau$, as shown in eq. (8.14). This does not occur in the 2HDMs of types I, II and X, due to correlations between the parameters $\varsigma_{f=u,d,l}$, see table 8.1. In the type-Y 2HDM, on the other hand, the limit $|\varsigma_d| \gg |\varsigma_u|, |\varsigma_l|$ is achieved for large $\tan\beta$; in this case, however, the $\mathrm{Br}(\bar{B} \to X_s\gamma)$ constraints forbid a light charged Higgs because $\varsigma_u = -1/\varsigma_d$ [58]. It has been shown in ref. [58] that a dedicated search for $H^+ \to c\bar{b}$ decays, implementing a b tag on one of the jets coming from $H^\pm$, could provide important constraints on the parameter space region with $|\varsigma_d| \gg |\varsigma_u|, |\varsigma_l|$ where this channel becomes important.

In figure 8.8 we show the bounds on the A2HDM parameter space from direct searches of a light charged Higgs at the LHC. Note that the present upper bounds on $\mathrm{Br}(t \to H^+b) \times \left[\mathrm{Br}(H^+ \to c\bar{s}) + \mathrm{Br}(H^+ \to c\bar{b})\right]$ and $\mathrm{Br}(t \to H^+b) \times \mathrm{Br}(H^+ \to \tau^+\nu)$ set an upper limit on $|\varsigma_u\varsigma_l|/M_{H^\pm}^2$ of $\mathcal{O}(\lesssim 10^{-3})\,\mathrm{GeV}^{-2}$. Leptonic B, D and D_s meson decays put weaker constraints on this combination, $\varsigma_u\varsigma_l/M_{H^\pm}^2 \in [-0.006, 0.037] \cup [0.511, 0.535]\,\mathrm{GeV}^{-2}$ at 95% CL [45]. Moreover an upper bound on the combination $|\varsigma_u\varsigma_d|$ is obtained from direct charged Higgs searches. Semileptonic and leptonic meson decays, on the other hand, only constrain the combinations $\varsigma_u\varsigma_l$ and $\varsigma_d\varsigma_l$ [45]. For both decay rates: $\Gamma(t \to H^+b)$ and $\Gamma(H^+ \to u_i\bar{d}_j, \tau^+\nu)$, see eqs. (8.18) and (8.19), terms proportional to $\varsigma_u\varsigma_d$ or $\varsigma_u\varsigma_l$ are negligible. Thus, no information on the relative sign between ς_u and $\varsigma_{d,l}$ is obtained.

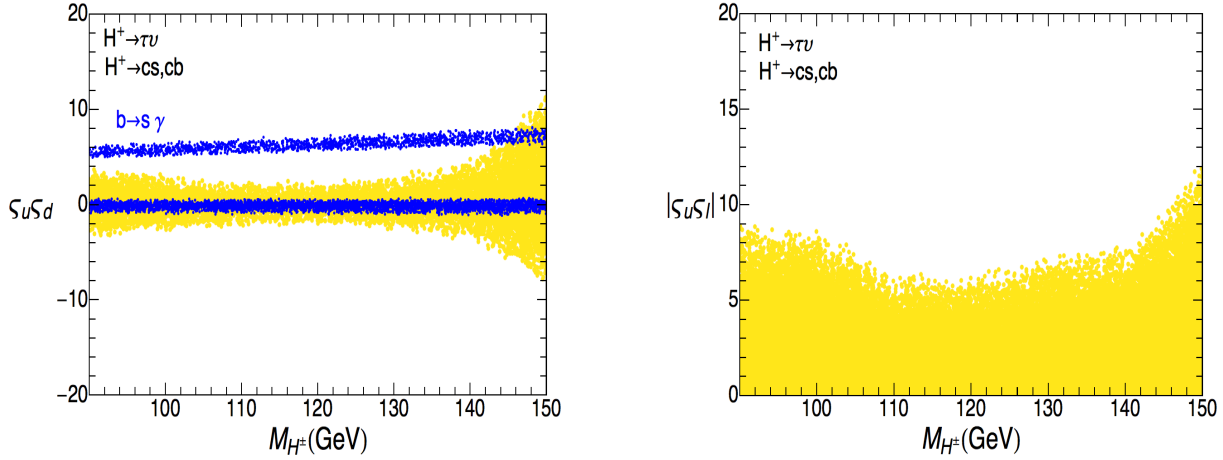Allowed values at 90% CL from the loop-induced process $\bar{B} \to X_s\gamma$ [46, 47] on the

Figure 8.8:   *Left-panel: Allowed values for $\varsigma_u \varsigma_d$ as a function of the charged Higgs mass (yellow-light) obtained from the experimental 95% CL upper bounds on $\mathrm{Br}(t \rightarrow H^+ b) \times \left[\mathrm{Br}(H^+ \rightarrow c\bar{s}) + \mathrm{Br}(H^+ \rightarrow c\bar{b})\right]$ and $\mathrm{Br}(t \rightarrow H^+ b) \times \mathrm{Br}(H^+ \rightarrow \tau^+ \nu)$. Allowed values for $\varsigma_u \varsigma_d$ from $\mathrm{Br}(\bar{B} \rightarrow X_s \gamma)$ are shown in blue-dark. Right-panel: Similar constraints on the combination $|\varsigma_u \varsigma_l|$ from direct charged Higgs searches. The alignment parameters have been varied in the range $|\varsigma_u| \leq 1$ and $|\varsigma_{d,l}| \leq 50$.*

$(M_{H^\pm}, \varsigma_u \varsigma_d)$ plane are also shown in figure 8.8. They are given by the two narrow (blue, dark) horizontal strips. We observe that, with the exception of the small region for which $M_{H^\pm} \sim [140, 150]$ GeV, the upper strip is already excluded by direct $H^\pm$ searches. $\bar{B} \rightarrow X_s \gamma$ impose no additional constraints on the combination $(M_{H^\pm}, |\varsigma_u \varsigma_l|)$. For all given points in figure 8.8 we find that $|\varsigma_u| \leq 0.5$, which is fully compatible with the flavour constraints given by R_b and neutral meson mixing [45].

In the A2HDM, the three-body decay $H^+ \rightarrow t^* \bar{b} \rightarrow W^+ b\bar{b}$ can also play an important role for a light charged Higgs when $M_{H^\pm} > M_W + 2m_b$, see appendix 8.A. This decay is normally very suppressed for a large region of the parameter space. It has been previously analyzed in refs. [59–63] and it was found that it can bring a sizeable contribution to the total charged Higgs decay rate in the $\mathcal{Z}_2$ models or in the MSSM when $M_{H^\pm} > 135$–145 GeV, depending on the model and on the chosen value of $\tan \beta$. In the A2HDM it can bring sizeable contributions to the branching fraction, of the order of 10–20%, already when $M_{H^\pm} \gtrsim 110$ GeV. Figure 8.9 shows the regions satisfying the condition
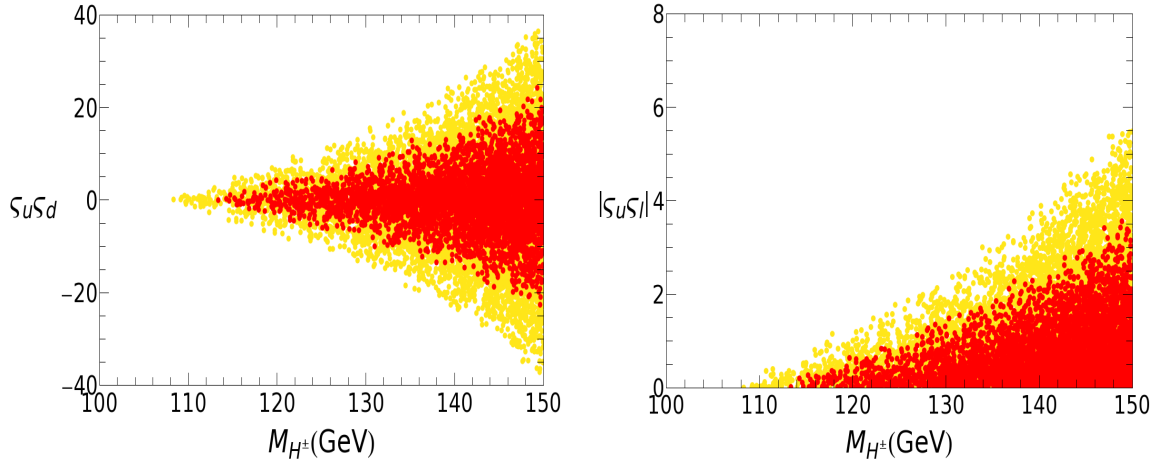
Figure 8.9: *Region in the $M_{H^\pm} - \varsigma_u\varsigma_d$ (left) and $M_{H^\pm} - |\varsigma_u\varsigma_l|$ (right) planes which satisfy the condition $\mathrm{Br}(H^+ \to W^+ b\bar{b}) > 10\%$ (yellow, light) and $\mathrm{Br}(H^+ \to W^+ b\bar{b}) > 20\%$ (red, dark). The alignment parameters have been varied in the range $|\varsigma_u| \leq 1$ and $|\varsigma_{d,l}| \leq 50$.*

$\mathrm{Br}(H^+ \to W^+ b\bar{b}) > 10\%$ (20%), in the planes $M_{H^\pm} - \varsigma_u\varsigma_d$ and $M_{H^\pm} - |\varsigma_u\varsigma_l|$. There are wide regions that can bring potentially large contributions to the decay rate, and that partially overlap with the allowed regions shown in figure 8.8. If we reanalyze the previous experimental constraints from the direct charged Higgs searches by adding this channel to the total decay rate, the allowed regions stay roughly the same, however, the allowed points concentrate in the region $|\varsigma_u\varsigma_d| \lesssim 1.5$. Thus, we conclude that experimental direct searches for a charged Higgs should be enlarged by also including this channel.

It is also worth noticing that for a fermiophobic charged Higgs, for which $\varsigma_{f=u,d,l} = 0$ and hence, $H^\pm$ does not couple to fermions at tree-level, all experimental constraints are trivially satisfied. Other production mechanisms and decay channels would have to be considered in this case to experimentally probe such scenario.

8.3.2   Neutral Higgs searches

The ATLAS and CMS collaborations have searched for additional neutral Higgs bosons up to masses of 1 TeV in the $\varphi \to ZZ$ and $\varphi \to WW$ channels [64,65]. These searches are sensitive in principle to the heavy CP-even Higgs H, given that the CP-odd Higgs does not couple at tree-level with vector bosons. Having observed no signal, they have set upper

bounds on the relevant cross section $\sigma(pp \to \varphi \to VV)$, using ~ 5 fb^{-1} and ~ 20 fb^{-1} of collected data at $\sqrt{s} = 7$ TeV and $\sqrt{s} = 8$ TeV respectively. Searches for neutral bosons in the leptonic final state $\tau^+\tau^-$ with masses up to 500 GeV have been performed by the ATLAS collaboration, using ~ 5 fb^{-1} of collected data at $\sqrt{s} = 7$ TeV [66]. Bounds in the $\tau^+\tau^-$ channel have also been presented recently by the CMS collaboration, using the full $2011 + 2012$ dataset, for Higgs masses up to 1 TeV [67]. These searches are sensitive to both CP-even and CP-odd Higgs bosons. Since the CP-odd Higgs does not couple at tree-level with vector bosons, its decay branching ratios into fermions are expected to be large. We assume in this section that the heavy scalars H and A cannot decay in non-SM decay channels like $H/A \to hh$; the bounds obtained here would be weaker if these decay channels were relevant. This assumption is well justified only in certain regions of the parameter space, namely, when $M_H < 2M_h$ or if the relevant cubic Higgs self-couplings are very small.

At present, searches for heavy scalars in the $H \to ZZ$ channel are the most sensitive, reaching $\sigma(pp \to H \to ZZ)/\sigma(pp \to H \to ZZ)_{\mathrm{SM}} \sim 10^{-1}$ for $M_H \lesssim 600$ GeV. Generic constraints on the properties of the missing 2HDM scalars can also be obtained from $h(126)$ collider data and flavour observables due to the sum rules governing the scalar couplings. Bounds on the combination $\kappa_V^H y_u^H$, as determined in eq. (8.12), are shown in figure 8.10 (yellow-light). Current experimental limits on $\sigma(pp \to H \to ZZ)$ are also included in figure 8.10, reducing the allowed parameter space to the purple-dark area. It can be observed that for heavier Higgs masses the bounds become weaker as expected.

To assess the impact of direct searches for additional scalars to further restrict the available parameter space of the 2HDM, we take the heavy CP-even and CP-odd Higgses to lie in the mass ranges: $M_H \in [200, 600]$ GeV and $M_A \in [150, 600]$ GeV. Of course, a similar analysis could be performed in any other mass ranges for H and A, or by also including constraints from collider searches of a charged Higgs. Here, we have varied the masses of the CP-even and CP-odd scalars independently. Electroweak precision data gives rise to correlations in the $M_H - M_A$ plane depending on the value of the charged Higgs mass, as shown in figure 8.5. At this point however, this does not have any impact on the allowed regions found in figures 8.10 and 8.11.

In figure 8.11 we show the allowed regions (yellow-light) obtained in section 8.2.2, considering the $h(126)$ collider data together with the flavour observables R_b and $\mathrm{Br}(\bar{B} \to X_s\gamma)$. The allowed regions get reduced when taking into account the limits from direct
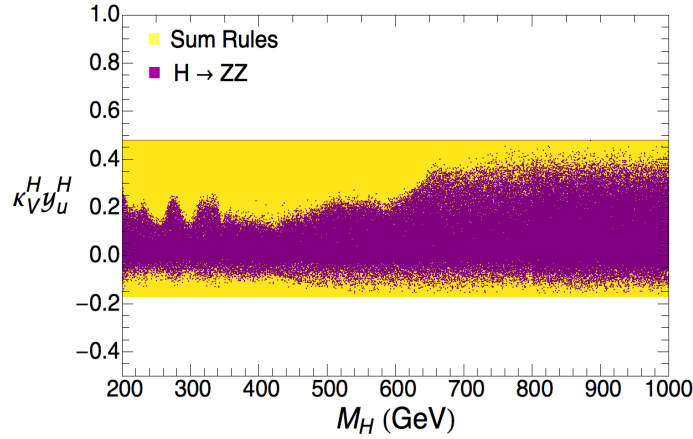
Figure 8.10: *Allowed values (90% CL) for the combination $\kappa_V^H y_u^H$ due to generic sum rules, taking into account $h(126)$ collider data and flavour constraints (yellow-light). Experimental limits on $\sigma(pp \to H \to ZZ)$ are also included, shrinking the allowed region to the purple-dark area.*

searches of additional scalars at the LHC (purple-dark). The most important effects are a lower bound on y_u^h and a smaller allowed area in the $\varsigma_u - \sin\tilde{\alpha}$ plane, which are mainly due to the present experimental upper limits on $\sigma(pp \to H \to ZZ)$; current searches in the $\tau^+\tau^-$ and W^+W^- channels put weaker constraints. The production cross section via gluon fusion scales as $\sigma(gg \to H) \propto |y_u^H|^2 = |\sin\tilde{\alpha} - \varsigma_u \cos\tilde{\alpha}|^2$ (neglecting the contributions from other quarks which are in general subdominant). When $\sin\tilde{\alpha}$ is far from zero, the decay channels $H \to VV$ ($V = ZZ, W^+W^-$) are the dominating ones, given that the fermionic couplings are not very large as the LHC and Tevatron data seem to suggest. The production cross section $\sigma(gg \to H)$ will then grow for negative values of ς_u, giving rise to a significant total cross section that becomes excluded by the present upper limits on $\sigma(pp \to H \to ZZ)$.

8.4   The fermiophobic charged Higgs scenario

In the limit $\varsigma_{f=u,d,l} = 0$ the charged Higgs does not couple to fermions at tree level. A very light fermiophobic charged Higgs, even below 80 GeV, is perfectly allowed by data. All bounds coming from flavour physics or direct charged Higgs searches that involve
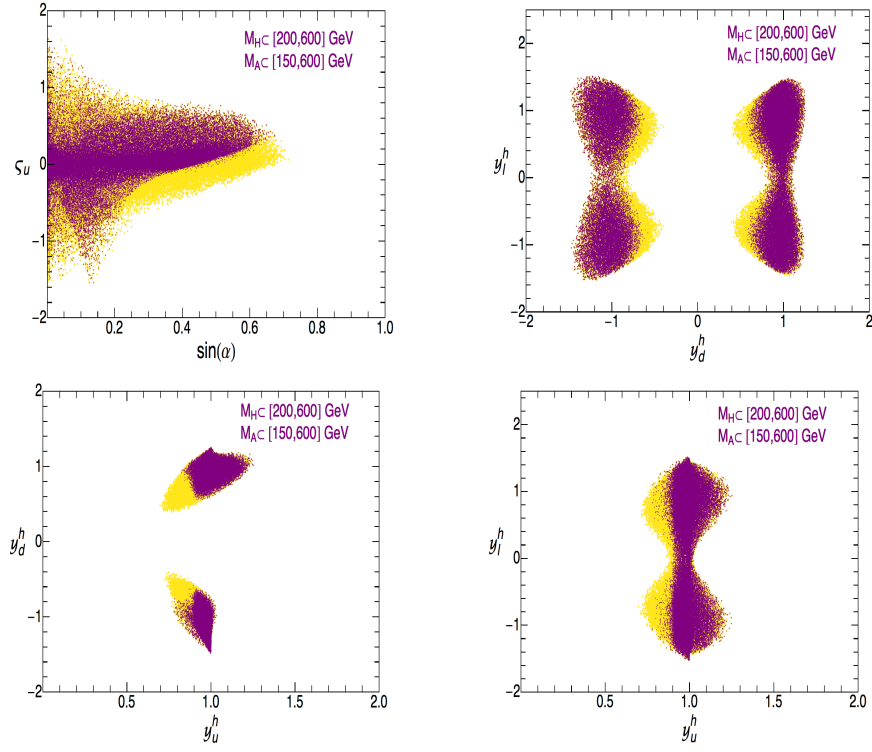
Figure 8.11:   *Allowed regions in the planes* $\sin\tilde\alpha - \varsigma_u$ *(top-left),* $y_d^h - y_l^h$ *(top-right),* $y_u^h - y_d^h$ *(bottom-left), and* $y_u^h - y_l^h$ *(bottom-right) at 90% CL, from a global fit of* $h(126)$ *collider data together with* R_b *and* $\mathrm{Br}(\bar{B} \to X_s\gamma)$*, within the CP-conserving A2HDM, are shown in yellow-light. Constraints from neutral Higgs searches at the LHC have also been included taking* $M_H \in [200, 600]$ *GeV and* $M_A \in [150, 600]$ *GeV, shrinking the allowed region to the purple-dark area, see text for details.*

the $H^\pm$ couplings to fermions are naturally evaded in this case. It is also known that when $|\kappa_V^h| = |\cos\tilde\alpha| \simeq 1$ (which is presently favoured by LHC and Tevatron data), the process $h \to 2\gamma$ provides a unique place were non-decoupling effects can be manifest if $M_{H^\pm} \sim \mathcal{O}(v)$ [40]. This motivates a dedicated analysis of this scenario in light of the latest collider data. Here we assume that the lightest CP-even state h is the 126 GeV boson and that CP is a good symmetry of the scalar sector, as in the previous section. The scaling of the neutral Higgs couplings to vector bosons and fermions becomes equal in this limit, $y_f^h = \kappa_V^h$, which makes this scenario very predictive in the neutral scalar

sector. The $h \to 2\gamma$ decay width is approximately given in this case by

$$\frac{\Gamma(h \to \gamma\gamma)}{\Gamma(h \to \gamma\gamma)^{\text{SM}}} \simeq \left(\kappa_V^h - 0.15\, C_{H^\pm}^h \right)^2 , \tag{8.15}$$

where $C_{H^\pm}^h$ encodes the charged Higgs contribution to the $h \to 2\gamma$ decay width. More specifically, $C_{H^\pm}^h = v^2/(2M_{H^\pm}^2)\, \lambda_{hH^+H^-}\, \mathcal{A}(x_{H^\pm})$ with $x_{H^\pm} = 4M_{H^\pm}^2/M_h^2$, the cubic Higgs coupling is defined through $\mathcal{L}_{hH^+H^-} = -v\, \lambda_{hH^+H^-}\, hH^+H^-$ and the loop function $\mathcal{A}(x)$ is given by

$$\mathcal{A}(x) = -x - \frac{x^2}{4}f(x), \qquad f(x) = -4\arcsin^2(1/\sqrt{x}). \tag{8.16}$$

Here we have assumed that $M_{H^\pm} > M_h/2 \simeq 63$ GeV so that $C_{H^\pm}^h$ does not contain an imaginary absorptive part. The cubic Higgs self coupling $\lambda_{hH^+H^-}$ can be expressed as a linear combination of quartic couplings of the scalar potential in the Higgs basis, see for example ref. [32]. To reduce the number of parameters to a minimal set, we perform a fit to $(\cos\tilde\alpha, C_{H^\pm}^h)$, treating $C_{H^\pm}^h$ as a free real variable. A full scan of the scalar parameter space, taking into account electroweak precision data, vacuum stability of the potential, perturbativity and perturbative unitarity bounds, would of course give rise to non-trivial correlations between the relevant Higgs self couplings and the scalar masses.

The best fit to the data is obtained for $(\cos\tilde\alpha, C_{H^\pm}^h) = (0.99, -0.58)$ with $\chi_{\text{min}}^2/\text{dof} \simeq 0.65$. In figure 8.12 (left) we show the allowed regions at 68% (orange), 90% (yellow) and 99% (gray) CL in the variables $(\sin\tilde\alpha, C_{H^\pm}^h)$. In the right panel of figure 8.12, the resulting constraint on $C_{H^\pm}^h$ at 68% CL is shown in terms of the cubic Higgs coupling $\lambda_{hH^+H^-}$ and the charged Higgs mass $M_{H^\pm}$. The perturbativity limits on the cubic Higgs coupling hH^+H^-, discussed in ref. [32], are also indicated (light-blue). The allowed region in the plane $(\lambda_{hH^+H^-}, M_{H^\pm})$ is slightly tilted towards negative $\lambda_{hH^+H^-}$ values, since the best fit point prefers a small negative charged Higgs contribution to the $h \to 2\gamma$ decay amplitude.

At 90% CL, we find for the Higgs signal strengths:[5] $\mu_{b\bar b}^h = \mu_{\bar\tau\tau}^h = \mu_{WW,ZZ}^h = \cos^2\tilde\alpha \in [0.74, 1]$ and $\mu_{\gamma\gamma}^h = 1.13 \pm 0.48$. These relations between the Higgs signal strengths hold in any of the relevant Higgs production mechanisms [32].

Heavy Higgs boson searches in the channels W^+W^- and ZZ are sensitive to the gauge coupling κ_V^H and to cubic scalar couplings relevant to describe possible non-SM decay

---

[5]Higgs signal strengths refer to Higgs cross sections normalized by the SM prediction, $\mu_X^\varphi = \sigma(pp \to \varphi \to X)/\sigma(pp \to \varphi \to X)_{\text{SM}}$.
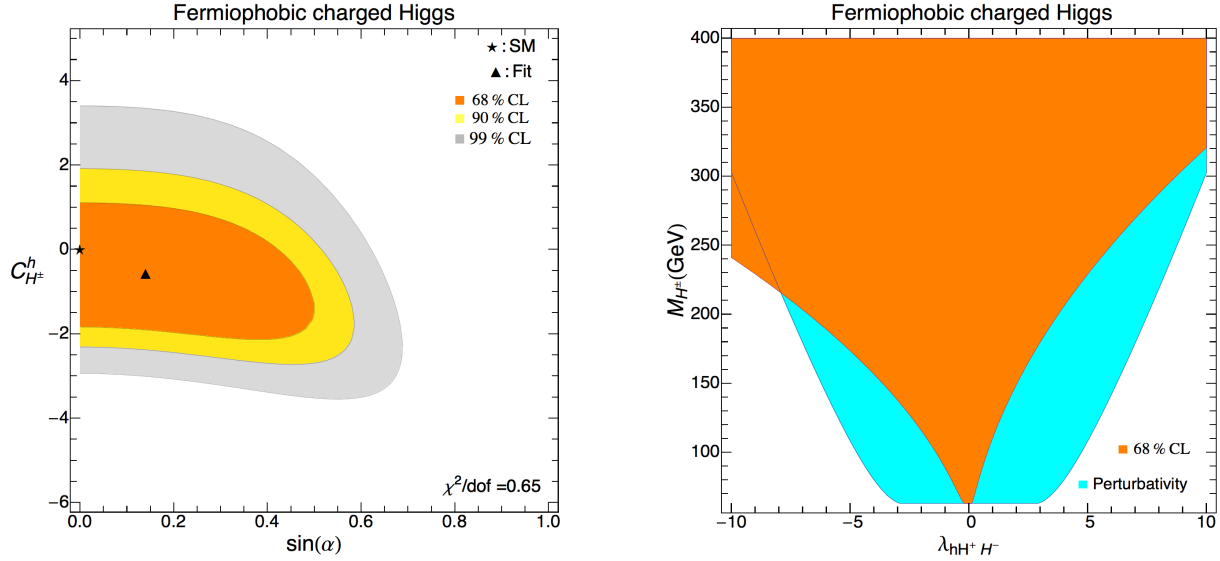
Figure 8.12: *Allowed regions at 68% (orange), 90% (yellow) and 99% CL (grey) for a fermio-phobic charged Higgs in the plane $\sin\tilde\alpha - \mathcal{C}_{H^\pm}^h$ (left). The right plot shows the corresponding 68% CL (orange) region in the parameters $\lambda_{hH^+H^-}$ and $M_{H^\pm}$. The region where perturbation theory remains valid is indicated in light-blue.*

channels like $H \to hh$. In the following we assume that the later can be neglected, this implies that the analysis presented here is only valid in certain regions of the parameter space. We find then that $\mu_{WW,ZZ}^H = \sin^2\tilde\alpha \leq 0.26$ at 90% CL. Considering the current experimental limits on $\mu_{WW,ZZ}^H$ [64,65], one can rule out a heavy CP-even Higgs in the mass range $M_H \in [130, 630]$ GeV when $\sin^2\tilde\alpha = 0.26$; this bound disappears of course when $\sin\tilde\alpha \to 0$, since H decouples from the vector bosons and the fermions. Associated charged Higgs production with a $W^\pm$ boson via neutral Higgs decays, $\varphi_j^0 \to H^\pm W^\mp$, with the charged Higgs decaying later to lighter neutral Higgs bosons, is a possible channel to probe the fermiophobic charged Higgs scenario. Sum rules among the couplings $g_{\varphi_j^0 H^\pm W^\mp}$ imply that $|g_{hH^\pm W^\mp}/g_{HH^\pm W^\mp}| = |\sin\tilde\alpha/\cos\tilde\alpha| < 0.6$ at 90% CL, while $g_{AH^\pm W^\mp}$ is completely fixed by the gauge symmetry [32]. Since the charged Higgs does not decay into fermions at tree level, branching fractions for $H^\pm \to \varphi_j^0 W^\pm$ decays can be particularly large.

An even more restricted scenario in which the charged Higgs decouples from the fermions is given by the Inert 2HDM. In this case a $\mathcal{Z}_2$ symmetry is imposed in the

Higgs basis so that all SM fields and Φ_1 are even under this symmetry while $\Phi_2 \rightarrow -\Phi_2$. Therefore, there is no mixing between the CP-even neutral Higgs bosons h and H. Assuming that the $h(126)$ boson corresponds to the lightest CP-even Higgs, we then have that $y_f^h = 1$ and $\cos\tilde{\alpha} = 1$. If furthermore one assumes that there are no open decay channels other than the SM ones, only the diphoton channel can show a deviation from the SM due to the charged Higgs contribution. From a global fit of this scenario to LHC and Tevatron data we obtain $C_{H^\pm}^h \in [-1.9, 1.2]$ at 90% CL ($\chi^2_{\min}/\mathrm{dof} \simeq 0.6$). This can be compared with the situation before Moriond 2013 in which $C_{H^\pm}^h \in [-2.4, -0.1]$ at 90% CL, driven by the excess in the diphoton signal observed at the moment [32]. Detailed studies of the Inert 2HDM, discussing the possibility to account for the Dark Matter in the Universe, can be found in refs. [20–22] and references therein.

8.5   Comparison with other works

Following the discovery of the $h(126)$ boson, a large number of works have appeared, analyzing the implications of collider data within the framework of 2HDMs. The majority of these analyses have been performed assuming NFC [12–27], thus restricting considerably the Yukawa structure of the model and the phenomenological possibilities. The ATLAS and CMS collaborations were initially observing a significant excess in the diphoton channel. The most natural explanation for such excess was a large charged Higgs contribution to the $h \rightarrow \gamma\gamma$ decay amplitude, other alternatives being usually in conflict with flavour constraints or perturbativity bounds, see ref. [32] and references therein. The situation has changed drastically after Moriond 2013, given that the CMS collaboration now reports a diphoton signal that is no longer enhanced. The main message that can be extracted from recent analyses is that current collider data can be accommodated very well in the SM; the addition of a second Higgs doublet does not improve in a significant way the agreement with the data. Important constraints start to appear for 2HDMs with NFC, restricting them to lie closer to the SM-limit.

Considerable work has also been done recently to analyze the future prospects at the LHC, as well as in possible future machines, to detect additional Higgs bosons within 2HDMs. Compared with the vast literature on the subject before the $h(126)$ discovery, information about the $h(126)$ boson properties is now being included in these analyses.

Phenomenological studies within 2HDMs with NFC, relevant for the search of additional scalars, have been done in refs. [13–16, 19, 24, 25, 41, 68–70]. Promising production mechanisms and decay channels have been pointed out in these works. In particular, if the $h(126)$ couplings are found to be very close to those of the SM, searches for heavy neutral Higgs bosons in the channels $\gamma\gamma$ or $\tau^+\tau^-$ become particularly relevant [16]. It could also be possible that heavy Higgs bosons decay mostly into the lightest state h, assumed to be the $h(126)$ boson. In this case, h production via heavy Higgs decays could be the way to detect these heavy states [70]. Some possibilities for this scenario are $H \to hh$, $A \to Zh$, and $H^\pm \to W^\pm h$. In any case, the non-observation of additional Higgs bosons will provide complementary information, together with direct measurements of the $h(126)$ boson properties, to restrict the parameter space of 2HDMs.

The experimental collaborations have also shown interest to search for signatures of extended Higgs sectors at the LHC, beyond the usually tested minimal supersymmetric scenarios. The ATLAS collaboration, for example, has released a search for a heavy CP-even Higgs boson in the $H \to WW \to e\nu\mu\nu$ channel within the types I and II 2HDMs, in the mass range $[135, 300]$ GeV, using 13 fb^{-1} of data at $\sqrt{s} = 8$ TeV center of mass energy [71]. The CMS collaboration, on the other hand, has analyzed the future prospects in the search for heavy neutral Higgs bosons at the LHC. The analysis was performed in the channels $H \to ZZ \to 4\ell$ ($\ell = e, \mu$) and $A \to Zh \to \ell\ell bb$, assuming an integrated luminosity of 3000 fb^{-1} at $\sqrt{s} = 14$ TeV center of mass energy [72]. On the experimental side, the main challenge seems to account for the large number of free parameters present in the 2HDM, even in the more restricted versions with NFC. On the theoretical side there is still a lot of work to be done to be able to start a precision study of these more general extended Higgs sectors. Theoretical predictions for cross-sections and branching ratios, taking into account relevant electroweak and QCD corrections, as well as its implementation in standard tools will be of utmost importance as experimental data becomes more precise, see for example refs. [73–76] for some relevant works in this direction.

In this work, we have focused on the possibility of performing a more general analysis of collider data within the framework of 2HDMs, without resorting to any symmetry in the Yukawa sector as is done in the different scenarios with NFC. The A2HDM provides a rich Yukawa structure that includes all the different 2HDMs with a $\mathcal{Z}_2$ symmetry as particular limits while, at the same time, suppresses flavour changing transitions in low-

energy systems to acceptable levels [28, 45–47]. First studies of the $h(126)$ boson data within the A2HDM, in the CP-conserving limit, were performed in refs. [29–32] and more recently in refs. [33, 34]. The role of new sources of CP-violation beyond the CKM-phase present in the A2HDM were also discussed in ref. [32]; we will consider this possibility in more detail in a future work. The main problem one has to face in this approach is the larger number of free parameters, compared with the NFC models. On the other hand, one is able to perform in this way non-biased analyses of the scalar sector of the 2HDM, without imposing symmetries which at first hand might seem ad-hoc. We have shown for example how generic sum-rules governing the scalar couplings provide a direct connection between the $h(126)$ properties and those of the missing scalars, see eq. (8.12).

A comprehensive analysis of current $h(126)$ data within extended Higgs sectors has been recently performed in ref. [34], including comparisons between the A2HDM and different $\mathcal{Z}_2$ 2HDMs. Also of relevance in this work, is a discussion of the effect of quantum corrections in relation to high-precision studies of the Higgs sector. In ref. [33], emphasis was given on an estimation of the future sensitivity that can be achieved at a high-luminosity LHC, a linear electron-positron collider and a muon collider, making the relevant comparisons between the A2HDM and the different NFC scenarios. A discussion of possible phenomenological strategies to test the 2HDM has been done recently in the Higgs basis [41], following the basis independent methods developed in ref. [39].

Information about the $h(126)$ boson properties is crucial for making simplifying assumptions and reducing the number of relevant variables, in order to perform a viable scan of the 2HDM parameter space at the LHC or at future colliders. In this work, we have analyzed the current data, keeping only a minimal set of parameters that are of relevance while capturing the rich phenomenology provided by the Yukawa structure of the A2HDM.

8.6 Summary

We have studied the implications of LHC and Tevatron data, after the first LHC shutdown, for CP-conserving 2HDMs, assuming that the $h(126)$ boson corresponds to the lightest CP-even state of the scalar spectrum. The phenomenological analysis has been done within the general framework of the A2HDM, which contains as particular limits all

different 2HDMs based on $\mathcal{Z}_2$ symmetries. Interesting bounds on the properties of the additional Higgs bosons of the model can be extracted, due to the existence of sum rules relating the different scalar couplings.

The $h(126)$ coupling to vector bosons is found to be very close to the SM limit, implying an upper bound on the heavy CP-even Higgs coupling to vector bosons: $|\kappa_V^H| <$ 0.6 at 90% CL. Other bounds on the couplings of the missing neutral scalars have been summarized in eq. (8.12). The flipped-sign solution for the top-quark Yukawa coupling, which was preferred by the fit before Moriond 2013 in order to explain the excess in the 2γ channel [32], is now found to be excluded at 90% CL. A sign degeneracy in the determination of the bottom and tau Yukawa couplings however remains.

We have discussed the role of flavour physics constraints, electroweak precision observables and LHC searches for additional scalars to further restrict the parameter space. Some results of our analysis can be pointed out. Loop-induced processes ($Z \to \bar{b}b$ and $\bar{B} \to X_s\gamma$) set important constraints on the quark Yukawa couplings, y_u^h and y_d^h, for charged Higgs masses below 500 GeV. Also, heavy Higgs searches in the ZZ channel put significant limits on the up-type quark Yukawa coupling y_u^h. Regarding direct charged Higgs searches at colliders, decays of the charged Higgs into a $c\bar{b}$ pair and three-body decays $H^+ \to t^*\bar{b} \to W^+b\bar{b}$, can have sizable decay rates in some regions of the allowed parameter space. Future searches for a light charged Higgs at the LHC in hadronic final states should take these possibilities into account, perhaps through the implementation of b-tagging techniques as suggested in ref. [58].

The fermiophobic charged-Higgs scenario has been discussed in light of current experimental data. Though this is a particular limit of the A2HDM, it deserved a separate analysis for different reasons. A very light fermiophobic charged Higgs boson can give unusually large contributions to the $h \to \gamma\gamma$ amplitude. Another reason is that in this case many simple relations arise between the properties of the neutral Higgs bosons, making this scenario particularly predictive when analyzing the searches for additional Higgs bosons at the LHC. We find that current data still allow for very light charged scalars and sizable contributions from a charged Higgs to the $h \to 2\gamma$ amplitude.

Appendix

8.A   Useful formulae for a light charged Higgs

A light charged Higgs with $M_{H^\pm} < m_t + m_b$ can be produced at the LHC via top-quark decays. The relevant partial decay widths are given by

$$\Gamma(t \to W^+ b) \; = \; \frac{g^2 \, |V_{tb}|^2}{64 \, \pi \, m_t^3} \; \lambda^{1/2}(m_t^2, m_b^2, M_W^2) \, \left(m_t^2 + m_b^2 + \frac{(m_t^2 - m_b^2)^2}{M_W^2} - 2M_W^2 \right) , \tag{8.17}$$

$$\Gamma(t \to H^+ b) \; = \; \frac{|V_{tb}|^2}{16\pi m_t^3 v^2} \; \lambda^{1/2}(m_t^2, m_b^2, M_{H^\pm}^2) \, \Big[(m_t^2 + m_b^2 - M_{H^\pm}^2)(m_b^2|\varsigma_d|^2 + m_t^2|\varsigma_u|^2)$$
$$- 4m_b^2 m_t^2 \, \mathrm{Re}(\varsigma_d \varsigma_u^*) \Big] , \tag{8.18}$$

with $\lambda(x, y, z) = x^2 + y^2 + z^2 - 2(xy + xz + yz)$ and $g = 2M_W/v$. QCD vertex corrections to $t \to H^\pm b$ and $t \to W^\pm b$ cancel to a large extent in $\mathrm{Br}(t \to H^\pm b)$ [77]. The charged Higgs decays into quarks and leptons are described in the A2HDM by the following expressions:

$$\Gamma(H^+ \to l^+ \nu_l) \; = \; \frac{m_l^2}{8\pi v^2} \left(1 - \frac{m_l^2}{M_{H^\pm}^2} \right)^2 M_{H^\pm} \, |\varsigma_l|^2 ,$$

$$\Gamma(H^+ \to u_i \bar{d}_j) \; = \; \frac{N_C \, |V_{ij}|^2}{8\pi v^2 M_{H^\pm}^3} \; \lambda^{1/2}(M_{H^\pm}^2, m_{u_i}^2, m_{d_j}^2) \left(1 + \frac{17}{3} \frac{\alpha_s(M_{H^\pm})}{\pi} \right)$$
$$\times \; \Big[(M_{H^\pm}^2 - m_{u_i}^2 - m_{d_j}^2)(|\varsigma_d|^2 m_{d_j}^2 + |\varsigma_u|^2 m_{u_i}^2) + 4m_{u_i}^2 \, m_{d_j}^2 \, \mathrm{Re}(\varsigma_d \varsigma_u^*) \Big] , \tag{8.19}$$

where N_C is the number of colours. Running $\overline{\mathrm{MS}}$ quark masses entering in these expressions are evaluated at the scale $M_{H^\pm}$, and the leading QCD vertex correction to $H^+ \to u\bar{d}$ has been taken into account [78].

When the charged Higgs mass satisfies $M_{H^\pm} > M_W + 2m_b$, three-body decays of the charged Higgs mediated by a virtual top quark can be relevant, see figure 8.13. The decay width for $H^+ \to t^* \bar{b} \to W^+ b \bar{b}$ is given in the A2HDM by

$$\Gamma(H^\pm \to t^* \bar{b} \to W^+ b \bar{b}) \; = \; \frac{N_C \, g^2 |V_{tb}|^4}{128\pi^3 M_{H^\pm}^3 M_W^2 v^2} \int ds_{23} \int ds_{13} \, \frac{G(s_{23}, s_{13})}{[s_{23} - m_t^2]^2} , \tag{8.20}$$
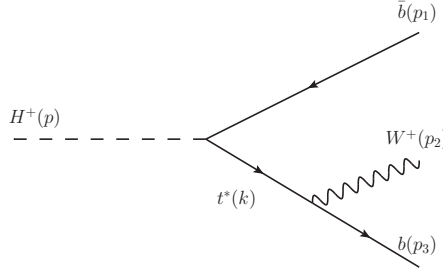
Figure 8.13:   *Feynman diagram for the three-body charged Higgs decay $H^+ \to t^*\bar{b} \to W^+ b\bar{b}$.*

where

$$
\begin{aligned}
G(s_{23}, s_{13}) &= \left[M_W^2 (p_1 p_3) + 2 (p_2 p_3)(p_1 p_2)\right] \left[|\varsigma_u|^2 m_t^4 - |\varsigma_d|^2 m_b^2 k^2\right] \\
&+ \left[M_W^2 m_b^2 (p_3 k) + 2 m_b^2 (p_2 p_3)(p_2 k)\right] \left[2 |\varsigma_d|^2 (p_1 k) + 2 m_t^2 \,\mathrm{Re}(\varsigma_u \varsigma_d^*)\right] ,
\end{aligned}
\tag{8.21}
$$

with:

$$
k = p_2 + p_3 , \qquad k^2 = s_{23} , \qquad (p_1 p_3) = \frac{1}{2}(s_{13} - 2 m_b^2) ,
$$

$$
(p_2 p_3) = \frac{1}{2}(s_{23} - M_W^2 - m_b^2) , \qquad (p_1 p_2) = \frac{1}{2}(M_{H^\pm}^2 + m_b^2 - s_{23} - s_{13}) .
\tag{8.22}
$$

The integration limits are:

$$
s_{23}^{\min} = \frac{1}{4 s_{13}} \left\{ (M_{H^\pm}^2 - M_W^2)^2 - \left[\lambda^{1/2}(M_{H^\pm}^2, s_{13}, M_W^2) + \lambda^{1/2}(s_{13}, m_b^2, m_b^2)\right]^2 \right\} ,
$$

$$
s_{23}^{\max} = \frac{1}{4 s_{13}} \left\{ (M_{H^\pm}^2 - M_W^2)^2 - \left[\lambda^{1/2}(M_{H^\pm}^2, s_{13}, M_W^2) - \lambda^{1/2}(s_{13}, m_b^2, m_b^2)\right]^2 \right\} ,
\tag{8.23}
$$

with

$$
4 m_b^2 \leqslant s_{13} \leqslant (M_{H^\pm} - M_W)^2 .
\tag{8.24}
$$

8.B   Statistical treatment and experimental data

The experimental $h(126)$ data used in the fit can be found in tables 8.2 and 8.3; experimental uncertainties are assumed to be Gaussian. To obtain the preferred values for the parameters of the A2HDM we build a global χ^2 function. For some channels the correlation coefficient ρ between different production modes can be estimated from the 68% CL

Table 8.2: *Experimental data from the ATLAS and CMS collaborations at $\sqrt{s} = 7 + 8$ TeV.*

Channel	$\hat{\mu}$ (ATLAS)	Comment	$\hat{\mu}$ (CMS)	Comment
bb(VH)	0.25 ± 0.65	ref. [2]	1.0 ± 0.5	ref. [4]
$\tau\tau$(ggF)	2.19 ± 2.2	$\rho = -0.50$	0.68 ± 1.05	$\rho = -0.5$
$\tau\tau$(VBF + VH)	-0.31 ± 1.25	ref. [2]	1.57 ± 1.13	ref. [4]
WW(ggF)	0.79 ± 0.52	$\rho = -0.2$	0.76 ± 0.35	$\rho = -0.3$
WW(VBF+VH)	1.6 ± 1.25	ref. [2]	0.24 ± 1.14	ref. [4]
ZZ(incl.)	1.5 ± 0.4	ref. [2]	0.92 ± 0.28	ref. [4]
$\gamma\gamma$(ggF)	1.6 ± 0.6	$\rho = -0.3$	0.47 ± 0.49	$\rho = -0.6$
$\gamma\gamma$(VBF+VH)	1.76 ± 1.28	ref. [2]	1.6 ± 1.14	ref. [4]

Table 8.3: *Experimental data from CDF and DØ at $\sqrt{s} = 1.96$ TeV.*

Channel	$\hat{\mu}$	Comment
bb(VH)	1.59 ± 0.71	ref. [5]
$\tau\tau$(incl.)	1.7 ± 2.0	ref. [5]
WW(incl.)	0.94 ± 0.84	ref. [5]
$\gamma\gamma$(incl.)	5.97 ± 3.25	ref. [5]

contours provided by the experimental collaborations, assuming that the $\Delta\chi^2 = \chi^2 - \chi^2_{\min}$ is well described by a bivariate normal distribution. This information is taken into account in the fit. The 68% and 90% one-dimensional confidence level (CL) intervals are given by $\Delta\chi^2 = 1$ and 2.71, respectively. Two-dimensional 68% and 90% CL intervals are given by $\Delta\chi^2 = 2.30$ and 4.31, respectively.

Regarding the flavour observables considered in this work, we use the latest $\bar{B} \to X_s\gamma$ experimental measurement, $\mathrm{Br}(\bar{B} \to X_s\gamma)_{E_0 > 1.6 \text{ GeV}} = (3.41 \pm 0.22) \times 10^{-4}$ [79]. The theoretical prediction of this quantity is obtained following ref. [80]. The calculation of R_b within 2HDMs was detailed in ref. [81]; the experimental value is $R_b = \Gamma(Z \to \bar{b}b)/\Gamma(Z \to \text{hadrons}) = 0.21629 \pm 0.00066$ [82].

Acknowledgements

Bibliography

[1] ATLAS Collaboration, Phys. Lett. B **716** (2012) 1 [arXiv:1207.7214 [hep-ex]].

[2] ATLAS Collaboration, Phys. Lett. B **726** (2013) 88 [arXiv:1307.1427 [hep-ex]]; ATLAS-CONF-2013-079 (July 19, 2013); ATLAS-CONF-2013-034 (March 13, 2013); David López Mateos talk at EPS 2013 for the ATLAS collaboration.

[3] CMS Collaboration, Phys. Lett. B **716** (2012) 30 [arXiv:1207.7235 [hep-ex]].

[4] CMS Collaboration, JHEP **06** (2013) 081 [arXiv:1303.4571 [hep-ex]]; CMS-PAS-HIG-13-005 (April 17, 2013).

[5] CDF and D0 Collaborations, Phys. Rev. Lett. **109** (2012) 071804 [arXiv:1207.6436 [hep-ex]]; Phys. Rev. D **88** (2013) 052014 [arXiv:1303.6346 [hep-ex]].

[6] ATLAS Collaboration, Phys. Lett. B **726** (2013) 120 [arXiv:1307.1432 [hep-ex]].

[7] CMS Collaboration, Phys. Rev. Lett. **110** (2013) 081803 [arXiv:1212.6639 [hep-ex]].

[8] D0 Collaboration, D0 Note 6387-CONF (July 22, 2013).

[9] K. Cheung, J. S. Lee and P. -Y. Tseng, JHEP **1305** (2013) 134 [arXiv:1302.3794 [hep-ph]]; J. Ellis and T. You, JHEP **1306** (2013) 103 [arXiv:1303.3879 [hep-ph]]; A. Falkowski, F. Riva and A. Urbano, JHEP **1311** (2013) 111 [arXiv:1303.1812 [hep-ph]]; P. P. Giardino, K. Kannike, I. Masina, M. Raidal and A. Strumia, arXiv:1303.3570 [hep-ph].

[10] A. Pich, arXiv:1307.7700.

[11] J. F. Gunion, H. E. Haber, G. L. Kane and S. Dawson, Front. Phys. **80** (2000) 1; G. C. Branco, P. M. Ferreira, L. Lavoura, M. N. Rebelo, M. Sher and J. P. Silva, Phys. Rept. **516** (2012) 1 [arXiv:1106.0034 [hep-ph]].

[12] A. Barroso, P. M. Ferreira, R. Santos, M. Sher and J. P. Silva, arXiv:1304.5225 [hep-ph].

[13] B. Grinstein and P. Uttayarat, JHEP **1306** (2013) 094 [arXiv:1304.0028 [hep-ph]].

[14] O. Eberhardt, U. Nierste and M. Wiebusch, JHEP **1307** (2013) 118 [arXiv:1305.1649 [hep-ph]].

[15] C. -Y. Chen, S. Dawson and M. Sher, Phys. Rev. D **88** (2013) 015018 [arXiv:1305.1624 [hep-ph]].

[16] N. Craig, J. Galloway and S. Thomas, arXiv:1305.2424 [hep-ph].

[17] B. Coleppa, F. Kling and S. Su, arXiv:1305.0002 [hep-ph].

[18] J. Shu and Y. Zhang, Phys. Rev. Lett. **111** (2013) 091801 [arXiv:1304.0773 [hep-ph]].

[19] C. -W. Chiang and K. Yagyu, JHEP **1307** (2013) 160 [arXiv:1303.0168 [hep-ph]].

[20] M. Krawczyk, D. Sokolowska, P. Swaczyna and B. Swiezewska, JHEP **1309** (2013) 055 [arXiv:1305.6266 [hep-ph]].

[21] A. Goudelis, B. Herrmann and O. Stål, JHEP **1309** (2013) 106 [arXiv:1303.3010 [hep-ph]].

[22] A. Arhrib, Y. -L. S. Tsai, Q. Yuan and T. -C. Yuan, arXiv:1310.0358 [hep-ph].

[23] G. Belanger, B. Dumont, U. Ellwanger, J. F. Gunion and S. Kraml, Phys. Rev. D **88** (2013) 075008 [arXiv:1306.2941 [hep-ph]].

[24] R. Enberg, J. Rathsman and G. Wouda, JHEP **1308** (2013) 079 [arXiv:1304.1714 [hep-ph]].

[25] R. Enberg, J. Rathsman and G. Wouda, arXiv:1311.4367 [hep-ph].

[26] S. Chang, S. K. Kang, J. -P. Lee, K. Y. Lee, S. C. Park and J. Song, arXiv:1310.3374 [hep-ph].

[27] K. Cheung, J. S. Lee and P. -Y. Tseng, arXiv:1310.3937 [hep-ph].

[28] A. Pich and P. Tuzón, Phys. Rev. D **80** (2009) 091702 [arXiv:0908.1554 [hep-ph]].

[29] E. Cervero and J. -M. Gerard, Phys. Lett. B **712** (2012) 255 [arXiv:1202.1973 [hep-ph]].

[30] W. Altmannshofer, S. Gori and G. D. Kribs, Phys. Rev. D **86** (2012) 115009 [arXiv:1210.2465 [hep-ph]].

[31] Y. Bai, V. Barger, L. L. Everett and G. Shaughnessy, Phys. Rev. D **87** (2013) 115013 [arXiv:1210.4922 [hep-ph]].

[32] A. Celis, V. Ilisie and A. Pich, JHEP **1307** (2013) 053 [arXiv:1302.4022 [hep-ph]].

[33] V. Barger, L. L. Everett, H. E. Logan and G. Shaughnessy, arXiv:1308.0052 [hep-ph].

[34] D. Lopez-Val, T. Plehn and M. Rauch, JHEP **1310** (2013) 134 [arXiv:1308.1979 [hep-ph]].

[35] V. Ilisie, arXiv:1310.0931 [hep-ph].

[36] J. F. Gunion, H. E. Haber and J. Wudka, Phys. Rev. D **43** (1991) 904.

[37] B. Grzadkowski, J. F. Gunion and J. Kalinowski, Phys. Lett. B **480** (2000) 287 [hep-ph/0001093].

[38] I. F. Ginzburg and M. Krawczyk, Phys. Rev. D **72** (2005) 115013 [hep-ph/0408011].

[39] S. Davidson and H. E. Haber, Phys. Rev. D **72**, 035004 (2005) [Erratum-ibid. D **72**, 099902 (2005)] [hep-ph/0504050]; H. E. Haber and D. O'Neil, Phys. Rev. D **74** (2006) 015018 [hep-ph/0602242].

[40] J. F. Gunion and H. E. Haber, Phys. Rev. D **67** (2003) 075019 [hep-ph/0207010].

[41] D. M. Asner, T. Barklow, C. Calancha, K. Fujii, N. Graf, H. E. Haber, A. Ishikawa and S. Kanemura *et al.*, arXiv:1310.0763 [hep-ph].

[42] M. Carena, I. Low, N. R. Shah and C. E. M. Wagner, arXiv:1310.2248 [hep-ph].

[43] H. -J. He, N. Polonsky and S. -f. Su, Phys. Rev. D **64** (2001) 053004 [hep-ph/0102144]; W. Grimus, L. Lavoura, O. M. Ogreid and P. Osland, Nucl. Phys. B **801** (2008) 81 [arXiv:0802.4353 [hep-ph]]; H. E. Haber and D. O'Neil, Phys. Rev. D **83** (2011) 055017 [arXiv:1011.6188 [hep-ph]].

[44] J. Maalampi, J. Sirkka and I. Vilja, Phys. Lett. B **265** (1991) 371; S. Kanemura, T. Kubota and E. Takasugi, Phys. Lett. B **313** (1993) 155 [hep-ph/9303263]; A. G. Akeroyd, A. Arhrib and E. -M. Naimi, Phys. Lett. B **490** (2000) 119 [hep-ph/0006035]; I. F. Ginzburg and I. P. Ivanov, Phys. Rev. D **72** (2005) 115010 [hep-ph/0508020]; P. Osland, P. N. Pandita and L. Selbuz, Phys. Rev. D **78** (2008) 015003 [arXiv:0802.0060 [hep-ph]].

[45] M. Jung, A. Pich and P. Tuzón, JHEP **1011** (2010) 003 [arXiv:1006.0470 [hep-ph]].

[46] M. Jung, A. Pich and P. Tuzón, Phys. Rev. D **83** (2011) 074011 [arXiv:1011.5154 [hep-ph]].

[47] M. Jung, X. -Q. Li and A. Pich, JHEP **1210** (2012) 063 [arXiv:1208.1251 [hep-ph]].

[48] T. Hermann, M. Misiak and M. Steinhauser, JHEP **1211** (2012) 036 [arXiv:1208.2788 [hep-ph]].

[49] A. Celis, M. Jung, X. -Q. Li and A. Pich, JHEP **1301** (2013) 054 [arXiv:1210.8443 [hep-ph]].

[50] J. P. Lees *et al.* [BaBar Collaboration], Phys. Rev. Lett. **109** (2012) 101802 [arXiv:1205.5442 [hep-ex]].

[51] M. Farina, C. Grojean, F. Maltoni, E. Salvioni and A. Thamm, JHEP **1305** (2013) 022 [arXiv:1211.3736 [hep-ph]].

[52] K. Cheung, C. -W. Chiang and T. -C. Yuan, Phys. Rev. D **78** (2008) 051701 [arXiv:0803.2661 [hep-ph]].

[53] B. W. Lee, C. Quigg and H. B. Thacker, Phys. Rev. D **16** (1977) 1519.

[54] ALEPH, DELPHI, L3 and OPAL Collaborations, Eur. Phys. J. C **73** (2013) 2463 [arXiv:1301.6065 [hep-ex]].

[55] ATLAS Collaboration, JHEP **1206** (2012) 039 [arXiv:1204.2760 [hep-ex]]; ATLAS-CONF-2013-090 (August 25, 2013).

[56] CMS Collaboration, JHEP **1207** (2012) 143 [arXiv:1205.5736 [hep-ex]].

[57] ATLAS Collaboration, Eur. Phys. J. C **73** (2013) 2465 [arXiv:1302.3694 [hep-ex]].

[58] A. G. Akeroyd, S. Moretti and J. Hernández-Sánchez, Phys. Rev. D **85** (2012) 115002 [arXiv:1203.5769 [hep-ph]].

[59] A. Djouadi, J. Kalinowski and P. M. Zerwas, Z. Phys. C **70** (1996) 435 [hep-ph/9511342].

[60] E. Ma, D. P. Roy and J. Wudka, Phys. Rev. Lett. **80** (1998) 1162 [hep-ph/9710447].

[61] F. Borzumati and A. Djouadi, Phys. Lett. B **549** (2002) 170 [hep-ph/9806301].

[62] S. Moretti and W. J. Stirling, Phys. Lett. B **347** (1995) 291 [Erratum-ibid. B **366** (1996) 451] [hep-ph/9412209, hep-ph/9511351].

[63] X. -J. Bi, Y. -B. Dai and X. -Y. Qi, Phys. Rev. D **61** (2000) 015002 [hep-ph/9907326].

[64] ATLAS Collaboration, ATLAS-CONF-2013-013; ATLAS-CONF-2013-067.

[65] CMS Collaboration, Eur. Phys. J. C **73** (2013) 2469 [arXiv:1304.0213 [hep-ex]]; CMS-HIG-12-024 (July 24, 2013).

[66] ATLAS Collaboration, JHEP **1302** (2013) 095 [arXiv:1211.6956 [hep-ex]].

[67] CMS Collaboration, CMS-PAS-HIG-13-021 (November 1, 2013).

[68] C. -Y. Chen, arXiv:1308.3487 [hep-ph].

[69] E. Brownson, N. Craig, U. Heintz, G. Kukartsev, M. Narain, N. Parashar and J. Stupak, arXiv:1308.6334 [hep-ex].

[70] A. Arhrib, P. M. Ferreira and R. Santos, arXiv:1311.1520 [hep-ph].

[71] ATLAS Collaboration, ATLAS-CONF-2013-027 (March 10, 2013).

[72] CMS Collaboration, CMS-PAS-FTR-13-024 (October 9, 2013).

[73] D. Eriksson, J. Rathsman and O. Stål, Comput. Phys. Commun. **181** (2010) 189 [arXiv:0902.0851 [hep-ph]].

[74] R. V. Harlander, S. Liebler and H. Mantler, Computer Physics Communications **184** (2013) 1605 [arXiv:1212.3249 [hep-ph]].

[75] R. V. Harlander, S. Liebler and T. Zirke, arXiv:1307.8122 [hep-ph].

[76] C. Englert, M. McCullough and M. Spannowsky, arXiv:1310.4828 [hep-ph].

[77] C. S. Li and T. C. Yuan, Phys. Rev. D **42** (1990) 3088 [Erratum-ibid. D **47** (1993) 2156]; A. Czarnecki and S. Davidson, Phys. Rev. D **48** (1993) 4183 [hep-ph/9301237].

[78] E. Braaten and J. P. Leveille, Phys. Rev. D **22** (1980) 715; M. Drees and K. -i. Hikasa, Phys. Lett. B **240** (1990) 455 [Erratum-ibid. B **262** (1991) 497].

[79] BaBar Collaboration, Phys. Rev. Lett. **109** (2012) 191801 [arXiv:1207.2690 [hep-ex]]; Phys. Rev. D **86** (2012) 112008 [arXiv:1207.5772 [hep-ex]].

[80] M. Misiak and M. Steinhauser, Nucl. Phys. B **764** (2007) 62 [hep-ph/0609241].

[81] G. Degrassi and P. Slavich, Phys. Rev. D **81** (2010) 075001 [arXiv:1002.1071 [hep-ph]].

[82] ALEPH, CDF, D0, DELPHI, L3, OPAL and SLD Collaborations, arXiv:0911.2604 [hep-ex].

Chapter 9

Conclusions

With the discovery of a new boson around 126 GeV with properties so far compatible with the SM Higgs boson, a new era for our understanding of the electroweak symmetry breaking mechanism has started. Many extensions of the SM electroweak sector involve extended scalar sectors, the 126 GeV boson could then be just one out of many scalar bosons present in Nature. Since the properties of the recently discovered Higgs boson are compatible with the SM Higgs, we already know that any viable alternative explanation for electroweak symmetry breaking should resemble the SM in some limit.

Adding additional scalar singlets and/or doublets to the SM field content is a minimal extension of the SM that gives rise to an interesting phenomenology. One can also be interested in studying such simple NP scenarios because they might represent a low-energy effective theory of a more fundamental NP theory. While scalar singlets do not couple to fermions directly due to gauge invariance, scalar doublets couple to fermions in the same way than the SM Higgs and lead to tree-level FCNCs in general. Low-energy constraints require the non-diagonal scalar couplings to be very small (specially for light quarks). To explain why non-diagonal Higgs couplings in flavour space are so suppressed or absent, one needs to postulate that some symmetry or unknown flavour dynamics is restricting the Yukawa structure. Another possibility is that the scalar sector of the multi-Higgs doublet model is close to the large-mass decoupling regime, in this case flavour violating phenomena are naturally suppressed by the large scalar masses. This last possibility is however less interesting from the phenomenological point of view since the additional scalars lie beyond the reach of high energy colliders and leave no imprint on low-energy

phenomena.

Within the scenario of the 2HDM without large-mass decoupling, that is, considering a rich scalar sector at the electroweak scale; we performed in this thesis different phenomenological analyses that can be summarized by:

- Possible violations of lepton flavour universality in B and D meson decays due to the presence of a charged scalar.

- Higgs mediated lepton flavour violating τ decays and interplay with searches at the LHC via Higgs decays.

- Analyses of LHC and Tevatron data for the 126 GeV boson and complementarity with electroweak precision data, flavour constraints, and, searches for additional scalars.

A very concise summary of the most relevant findings or results described in this thesis is:

- The excess observed recently by the BaBar collaboration in $B \to D^{(*)} \tau \nu$ transitions cannot be accommodated within the framework of the A2HDM because one encounters tensions with present limits on $B \to \tau \nu$ and $D_{(s)}$ leptonic decays.

- Improvements on the hadronic form factors relevant to describe Higgs mediated $\tau \to \ell \pi \pi$ ($\ell = e, \mu$) decays have a significant impact on the bounds that can be extracted on possible LFV Higgs couplings. Semileptonic τ decays offer an important handle to scrutinize any possible LFV signal at the LHC.

- Studies of the Higgs sector within the 2HDM can be performed without assuming a priori a Yukawa sector with natural flavour conservation, concrete results are obtained in this case despite the larger number of free parameters. Tree-level unitarity sum-rules encode the structure of the 2HDM scalar sector and provide a very useful way to frame the discussion of LHC Higgs data within the framework of 2HDMs.

Acknowledgments

I would like to thank all the IFIC members and people from the physics department which had made my stay in Valencia more pleasant during all these years. I am truly and deeply indebted to Victor Ilisie, Martin Jung, Xin-Qiang Li, Vincenzo Cirigliano and Emilie Passemar with which I had the pleasure to collaborate in several research projects; projects which have become the bulk of this thesis. I hope we continue having a fruitful collaboration in the following years. I should also add a special gratitude to V. Cirigliano and E. Passemar for hosting me at Los Alamos and to all the members of the T-2 Theory Division of Los Alamos National Laboratory for making my stay enjoyable. I thank Arantza Oyanguren for inviting me to present some of my research results at conferences and/or workshops, I enjoyed a lot those opportunities. I also thank Federico Mescia for the invitation to give a talk at the 2014 winter meeting in Benasque.

I thank all the members of our research group, with which I have enjoyed pleasant conversations, lunches, etc. in the day-to-day at IFIC. Among all the members of the group I have to add a special note to Jorge Portoles who has always been available to help me from the first day I arrived to Valencia, I sincerely appreciate this. Finally, I have to thank Toni for these wonderful years and the excellent mentor he is. Working with him has been a very rewarding experience for me.

"What is that you express in your eyes? It seems to me more than all the print I have read in my life."
Walt Whitman (1819-1892). Leaves of Grass.